A geodynamic model for continental breakup and sea-floor spreading initiation: Implications for post-breakup rifted margin hinterland uplift

UNIVERSITY OF LIVERPOOL

THESIS SUBMITTED IN ACCORDANCE WITH THE REQUIREMENTS OF THE UNIVERSITY OF LIVERPOOL FOR THE DEGREE OF DOCTOR IN PHILOSOPHY

BY ERICA GREENHALGH

SEPTEMBER 2010

Abstract

A geodynamic model for continental breakup and sea-floor spreading initiation: Implications for post-breakup rifted margin hinterland uplift

Erica Greenhalgh

Many, mainly volcanic, rifted margins exhibit uplifted hinterland regions which are asymmetrical in shape, and separated from a narrow coastal plain by a steep seaward-facing escarpment. It is now generally accepted that the uplift of these margins post-dates continental rifting and breakup; however, the mechanism behind it is yet to be established. Knowledge of the uplift history of a rifted margin is vital for correct interpretation of the offshore sedimentary record and to assess the reservoir potential of the marginal basins. Observations do not preclude that some common, underlying, mechanism has acted at every margin, a candidate for which could be a mechanism related to deformation of the lithosphere during continental breakup and sea-floor spreading initiation. A geodynamic model of continental lithosphere thinning leading to sea-floor spreading initiation coupled with erosion, sediment transport and deposition is presented, and its implications for post-breakup rifted margin hinterland uplift are considered. Prior to breakup, continental lithosphere thinning is assumed to occur by combined pure shear and buoyancy-driven upwelling. This produces an outward flow of asthenosphere material towards the young continental margin lithosphere, thickening the lithosphere beneath the continental hinterland. This may be further amplified if buoyancy-driven upwelling continues during the first few million years of sea-floor spreading at a young volcanic margin. The geothermal gradient is decreased over regions of thickened continental lithosphere and increased over regions of thinned continental lithosphere and oceanic lithosphere. As the geotherm re-equilibrates, the oceanic regions will subside due to cooling of the geotherm, and warming of the continental lithosphere geotherm will lead to gradual uplift of the hinterland. The resulting topography is determined from the sum of the flexural isostatic response to geotherm perturbation, crustal thinning and erosion. Significant amounts of post-breakup thermal uplift, up to 500 m, are predicted by the model due to thermal buoyancy-driven upwelling. Sensitivity testing shows that the dominant parameter in the model controlling the predicted thermal uplift is the magnitude of the buoyancy-driven upwelling during early sea-floor spreading. Flexural isostasy is the dominant control on the wavelength of the uplift and the flexural isostatic response to erosion amplifies the initial uplift. Erosion and sea-level changes are also important in shaping the topography at a rifted margin. The model can match the wavelength and shape of the observed uplift, but cannot match the observed timing and magnitude of uplift events. However, results from the model strongly suggest that the continental breakup process may provide some control on the onshore evolution of a rifted margin.

Acknowledgments

First and foremost, I would like to thank Nick Kusznir for giving me the opportunity to do this PhD, for his help, enthusiasm and patience over the last four years, and for sending me to conferences in nice places. Thanks also go to Tony Doré and Erik Lundin for sharing their vast knowledge about the observations of post-breakup uplift and for valuable feedback throughout the project. NERC and the Case studentship partner, Statoil, are thanked for providing financial support for this project. I would also like to thank Alan Mac for rescuing my computer, and my work, from the clutches of a virus on more than one occasion. David Hodgson and Richard England are gratefully acknowledged for agreeing to examine this thesis (and for passing me!).

Thanks to my parents, who have no idea what this project is about, but have supported me nonetheless, and to Mars, for always cheering me up. A massive thank-you goes to all my friends, who are ace, and who have made my time as a student so enjoyable. I would especially like to thank the members of the Geodynamics Research Group – Ricardo, John, Chris, Goz, Anna and Gilvan – for their enduring enthusiasm for cups of tea, ranting, and stimulating, occasionally scientific, discussions. An extra special mention goes to John and Gilvan, who cannot be thanked enough, for ensuring the on-time handing-in of this thesis. Chris is also thanked for giving me his Stokes flow code and explaining the physics behind it, without which significant sections of this thesis would not have been written. Thanks to Laura (my sister!) for accompanying me to see the lions and the uplift of South Africa. Also to Sheona, for sharing her FORTRAN expertise and for making mid-afternoons pass that little bit faster. Tusen, tusen takk to Lene and Ida, for being so supportive and feeding me. Lastly, I would like to thank Rosie, for meeting me in Hell and accompanying me back from there, for volunteering to read this thesis, and for her excellent words of advice.

Contents

List of figures

List of tables

Chapter 1

Introduction

1.1 Aims

The continental hinterlands of many, mainly volcanic, rifted margins appear to have experienced post-breakup uplift, the cause of which has not yet been established. The aims of this thesis are:

i) To test the hypothesis that post-breakup hinterland uplift of rifted margins could be a fundamental consequence of the continental breakup and sea-floor spreading initiation process.

ii) To investigate the effect erosion, sediment deposition and flexural coupling has on the evolution of a topographic profile across a rifted margin.

A geodynamic model for continental lithosphere thinning and breakup, coupled with erosion and flexural isostasy, is presented to determine whether significant hinterland uplift can arise from deformation to continental lithosphere during continental lithosphere thinning and breakup. This thesis can be divided into four sections:

i) A literature review of the observations of post-breakup hinterland uplift and mechanisms which have been proposed to explain it (Chapters 2 – 3).

ii) Development of a geodynamic model for continental rifting and breakup with particular application to post-breakup hinterland uplift (Chapters 4 – 6).

iii) Development of a model for erosion, sediment transport and deposition (Chapter 7).

iv) Presentation of the coupled model of geodynamic and surface processes and discussion of model application to global observations (Chapters 8 – 9).

1.2 Post-breakup rifted margin hinterland uplift

Many rifted margins exhibit a common topography consisting of an asymmetrical elevated plateau, up to 2 km or more above sea-level, separated from a coastal plain by a steep seaward-facing escarpment. The escarpments run near-parallel to the coastline and extend over hundreds of kilometres along strike. Locations where this characteristic topography is observed include Norway, East and West Greenland, Brazil, southern Africa, West India and South-East Australia. The existence of elevated topography at rifted margins long after continental breakup, and on timescales greater than the lithosphere thermal decay constant, has been the subject of many studies over the last few decades. It is now generally accepted that the uplift events forming the present-day topography at these margins, in most cases, post-date continental breakup; there remains, however, little consensus on the details of the uplift history and therefore the mechanism causing it (e.g. Doré et al., 2002b; Anell et al., 2009).

Key observations, including timing and magnitude, of the uplift are required to provide some controls on the uplift mechanism, yet these are often poorly constrained. Direct measurements are limited as there is generally no onshore depositional record of the uplift (e.g. van der Beek & Braun, 1999). Instead, techniques such as Apatite Fission Track (AFT) analysis, landform analysis and onshore-offshore correlation of the stratigraphic record are commonly used to determine the uplift history. The validity of the results from these techniques may still be called into question though, since their interpretation often requires several important assumptions for which there is sometimes little evidence, for example the palaeogeothermal gradient or age of stratigraphic layers. A successful mechanism needs to explain the timing, magnitude and wavelength of the uplift; it is therefore not surprising, given the lack of consensus in the observational data, that vastly differing viewpoints on the cause(s) of the uplift exist (e.g. Brown et al., 1990).

Numerous geodynamic and geomorphological processes may have played a part, in some way, in the onshore evolution of the uplifted rifted margins. The many postulated uplift mechanisms can be broadly classified into three groups:

i) mechanisms involving an increase of material, e.g. magmatic underplating (Cox, 1993).

ii) mechanisms related to thermal expansion, e.g. the asthenospheric diapir model of Rohrman & van der Beek (1996).

iii) mechanisms related to isostatic movements, e.g. post-glacial rebound (Riis & Fjeldskaar, 1992).

Numerical modelling has shown the importance of the flexural isostatic response to denudational unloading in maintaining the elevated topography (van der Beek et al., 2002, & references therein). It has been argued that this effect, considered alongside the apparent uplift observed with a fall in sea-level, and assuming some initial elevation at breakup, is sizeable enough to generate the present-day topography of the Norwegian margin (Nielsen et al., 2009), and therefore there may be no need to invoke a tectonic component of uplift. The observation remains, however, that the uplifted rifted margins exhibit similar structural characteristics, regardless of their age, lithology and the climates they have been subjected to. As Gallagher & Brown (1999) point out, the complexities of the relationship between the tectonic and geomorphological processes that have controlled the evolution of the rifted margins are such that it seems unlikely that a single mechanism for post-breakup hinterland uplift could satisfactorily account for the uplift histories of all the margins. Yet this does not preclude that some common, underlying, mechanism may have contributed to their formation. The most obvious tectonic event to have acted at each margin is continental lithosphere thinning, breakup and sea-floor spreading initiation, so could deformation to the continental lithosphere during those processes result in significant uplift of the continental hinterland?

1.3 Why is understanding post-breakup rifted margin hinterland uplift important?

A detailed knowledge of the onshore evolution of a rifted margin is important for two main reasons. Firstly, it is required for a thorough understanding of the superposition of tectonic and surface processes acting at a regional scale which control the structural and geomorphological development of a rifted margin. Secondly, it is the evolution of the onshore region of a margin which determines the

variation in sediment flux to the offshore basins; this information is vital for correct interpretation of the offshore sedimentary record, and to predict the thermal history of a margin. The timing, magnitude and mechanism of uplift events are of considerable interest to the petroleum industry, to determine the reservoir potential of exhumed basins. This has been the driving force behind much of the research on post-breakup uplift at rifted margins, especially for the margins bordering the North-East Atlantic (Doré et al., 2002a).

1.4 How will the work described in this thesis contribute to our understanding of the problem?

This thesis tests the hypothesis that post-breakup hinterland uplift may be a fundamental consequence of continental rifting, breakup and sea-floor spreading initiation. If this hypothesis is correct, this would be a mechanism acting globally, so in order to assess the model's validity, knowledge of the uplift histories of the margins is vital. To this end, a literature review covering the Norwegian, eastern and western Greenland, Brazilian, southern African, western Indian, and south-eastern Australian margins has been undertaken (Chapter 2) to determine if there are any similarities in the observations of post-breakup uplift at the margins. The mechanisms which have been previously proposed to explain the post-breakup uplift have also been reviewed (Chapter 3) in order to understand which observations they can account for, and also their limitations.

During rifting and early sea-floor spreading, buoyancy-driven upwelling may lead to thickening of the continental lithosphere inboard of the region of continental lithosphere thinning, and hence a cooling of the geotherm in the thickened region. As the geotherm re-equilibrates and warms, the continental hinterland will be gradually uplifted. A general model for continental lithosphere thinning and breakup is presented, and the predicted hinterland uplift arising from the geotherm perturbation is determined using local isostasy (Chapter 4). The question of how continental lithosphere is thinned, whether depth-uniform or depth-dependent, prior to breakup is, as yet, unanswered. Therefore, the model incorporates thinning by either pure shear (c.f. Mckenzie, 1978) or buoyancy-driven upwelling (c.f. Kusznir & Karner, 2007), or a combination of the two, with the buoyant upwelling being represented by

an upwelling-divergent flow field or by Stokes flow. The effect of lateral heat transfer at the margin is also considered (Chapter 5). The model is further developed by considering the flexural isostatic response to the geotherm perturbation and crustal thinning, coupled with water-loaded subsidence offshore (Chapter 6). Eustatic sea-level changes, according to the sea-level curve of Haq et al. (1987) are also incorporated into the model. Sensitivity testing has been carried out (Chapters 4, 5 & 6) to determine the relative importance of the various model input parameters.

Several studies have highlighted the importance that geomorphological processes play in shaping the topography of a rifted margin (e.g. van der Beek et al., 2002; Nielsen et al., 2009). Furthermore, the flexural response to onshore denudational unloading and offshore loading due to sediment deposition can give rise to significant topographic effects. Erosion, sediment transport, and deposition can be modelled using the diffusion equation (Culling, 1960); this is modelled first using a box profile to gain an understanding of the general model behaviour (Chapter 7). Erosion and the corresponding flexural response are then incorporated into the model for continental lithosphere thinning and breakup (Chapter 8). The combined model is then systematically tested to determine whether it can generate, and maintain, significant hinterland uplift (Chapter 8). The results are discussed and compared to observations, suggestions for further model development are given, and the main findings from this research are summarised (Chapter 9).

1.5 References

Anell, I., H. Thybo and I. M. Aftemieva (2009), Cenozoic uplift and subsidence in the North Atlantic region: Geological evidence revisited, *Tectonophysics*, vol. 474, no. 1-2, p. 78-105.

Brown, R. W., D. J. Rust, M. A. Summerfield, A. J. W. Gleadow and M. C. J. Dewit (1990), An Early Cretaceous Phase of Accelerated Erosion on the South-Western Margin of Africa - Evidence from Apatite Fission-Track Analysis and the Offshore Sedimentary Record, *Nuclear Tracks and Radiation Measurements*, vol. 17, no. 3, p. 339-350.

Cox, K. G. (1993), Continental Magmatic Underplating, *Philosophical Transactions of the Royal Society A - Mathematical, Physical & Engineering Sciences*, vol. 342, p. 155-166.

Culling, W. E. H. (1960), Analytical Theory of Erosion, *Journal of Geology*, vol. 68, no. 3, p. 336-344.

Doré, A. G., D. V. Corcoran and I. C. Scotchman (2002a) Prediction of the hydrocarbon system in exhumed basins, and application to the NW European margin, in Doré, A. G., J. A. Cartwright, M. S. Stoker, J. P. Turner and N. White (eds), *Exhumation of the North Atlantic Margin: Timing, Mechanisms and Implications for Petroleum Exploration*, Geological Society, London, Special Publications, vol. 196, p. 401-429.

Doré, A. G., J. A. Cartwright, M. S. Stoker, J. P. Turner and N. J. White (2002b) Exhumation of the North Atlantic margin: introduction and background, in Doré, A. G., J. A. Cartwright, M. S. Stoker, J. P. Turner and N. J. White (eds), *Exhumation of the North Atlantic Margin: Timing, Mechanisms and Implications for Petroleum Exploration*, Geological Society, London, Special Publications, vol. 196, p. 1-12.

Gallagher, K. and R. Brown (1999), Denudation and uplift at passive margins: the record on the Atlantic Margin of southern Africa, *Philosophical Transactions of the Royal Society of London Series a-Mathematical Physical and Engineering Sciences*, vol. 357, no. 1753, p. 835-857.

Haq, B. U., J. Hardenbol and P. R. Vail (1987), Chronology of Fluctuating Sea Levels since the Triassic, *Science*, vol. 235, no. 4793, p. 1156-1167.

Kusznir, N. J. and G. D. Karner (2007) Continental lithospheric thinning and breakup in response to upwelling divergent mantle flow: application to the Woodlark, Newfoundland and Iberia margins, in Karner, G. D., G. Manatschal and L. M. Pinheiro (eds), *Imaging, Mapping and Modelling Continental Lithosphere Extension and Breakup*, Geological Society, London, Special Publications, vol. 282, p. 389-419.

Mckenzie, D. (1978), Some Remarks on Development of Sedimentary Basins, *Earth and Planetary Science Letters*, vol. 40, no. 1, p. 25-32.

Nielsen, S. B., K. Gallagher, C. Leighton, N. Balling, L. Svenningsen, B. H. Jacobsen, E. Thomsen, O. B. Nielsen, C. Heilmann-Clausen, D. L. Egholm, M. A. Summerfield, O. R. Clausen, J. A. Piotrowski, M. R. Thorsen, M. Huuse, N. Abrahamsen, C. King and H. Lykke-Andersen (2009), The evolution of western Scandinavian topography: A review of Neogene uplift versus the ICE (isostasy-climate-erosion) hypothesis, *Journal of Geodynamics*, vol. 47, no. 2-3, p. 72-95.

Riis, F. and W. Fjeldskaar (1992) On the magnitude of the Late Tertiary and Quaternary erosion and its significance for the uplift of Scandinavia and the Barents Sea, in Larsen, R. M., H. Brekke, B. T. Larsen and E. Talleraas (eds), *Structural and Tectonic Modelling and its Application to Petroleum Geology*, NPF Special Publication, vol. 1, p. 163-185.

Rohrman, M. and P. van der Beek (1996), Cenozoic postrift domal uplift of North Atlantic margins: An asthenospheric diapirism model, *Geology*, vol. 24, no. 10, p. 901-904.

van der Beek, P. and J. Braun (1999), Controls on post-mid-Cretaceous landscape evolution in the southeastern highlands of Australia: Insights from numerical surface process models, *Journal of Geophysical Research-Solid Earth*, vol. 104, no. B3, p. 4945-4966.

van der Beek, P., M. A. Summerfield, J. Braun, R. W. Brown and A. Fleming (2002), Modeling postbreakup landscape development and denudational history across the southeast African (Drakensberg Escarpment) margin, *Journal of Geophysical Research-Solid Earth*, vol. 107, no. B12, p. 2351.

Chapter 2

Observations of post-breakup rifted margin hinterland uplift: a literature review

2.1 Introduction

Many, mainly magma-rich, rifted margins exhibit elevated hinterland regions, asymmetrical in shape, separated from a narrow coastal plain by a steep seaward-facing escarpment. This characteristic topography is observed at Norway, East and West Greenland, Brazil, southern Africa, western India and south-eastern Australia (Figure 2.1). The continued existence of elevated topography at rifted margins, long after continental breakup, has been something of an enigma to researchers for a number of decades. It is now generally accepted that the uplift of these margins post-dates continental rifting and breakup; this, however, is contrary to the classical notion that such margins are "passive". A comprehensive knowledge of the tectonic, morphological, climatic and eustatic events which have shaped the onshore evolution of the rifted margins is therefore required, in order to understand the superposition of mechanisms which are capable of producing large-scale uplift. This information is also vital for predicting the denudational and thermal history of the margin, to aid in the interpretation of the offshore sedimentary record and for assessing the likelihood of hydrocarbon productivity.

In 1985, C.F. Pain eloquently summed up the certainties of the south-eastern Australian uplift by stating "A survey of the evidence shows that very little positive can be said about uplift of the Eastern Highlands, except that it happened". More recent studies of post-breakup hinterland uplift have benefitted from advances in the methods for determining the timing and magnitude of uplift events (see Anell et al. (2009) for a succinct review of the various techniques), particularly regarding the application of apatite fission track (AFT) analysis. However, the key observations of

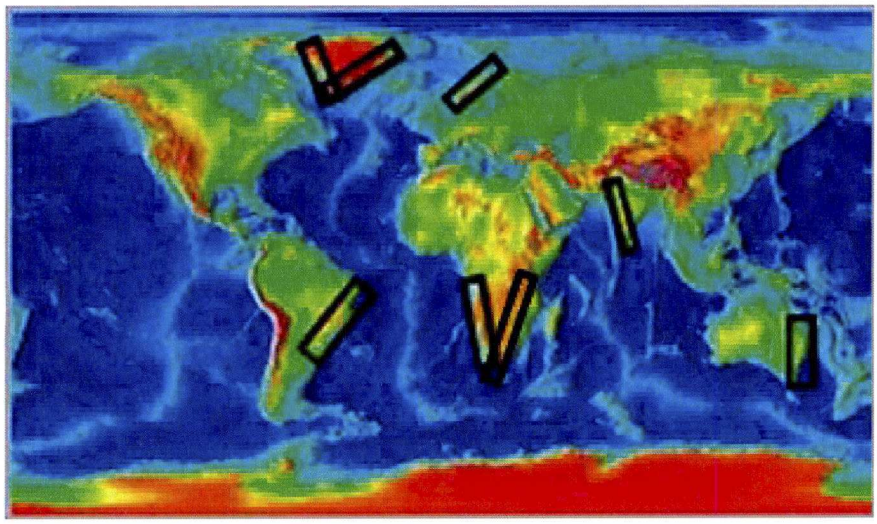

Figure 2.1: Global map showing the locations of the rifted margins which have experienced post-breakup hinterland uplift

the uplift events remain, for the most part, poorly constrained and there is often a lack of consensus on the uplift history of a margin (e.g. Anell et al., 2009). This chapter is a literature review of published studies of the observations of post-breakup uplift on the aforementioned rifted margins; it has been undertaken to determine any similarities between the uplift histories of the different margins. To what extent is Pain's quote still relevant, and could it be applicable to other locations besides south-eastern Australia?

2.2 Global climate and sea-level fluctuations

Climatic and eustatic sea-level changes have important implications for the uplift and denudational history of a rifted margin (Molnar & England, 1990; Huuse, 2002; Nielsen et al., 2002). A positive feedback exists between climate change, erosion, and isostatic rebound whereby an uplifted region may alter the climate, thus leading to enhanced erosion and further uplift due to isostatic compensation, which in turn may lead to further climatic deterioration, and so on. This can give a false impression of accelerated uplift (Molnar & England, 1990). The rifted margins that are the focus of this chapter have different climate histories; these are discussed for each area individually in the sections that follow.

Global sea-level fluctuates because of changes in the volume of water in the oceans, mainly due to the development or decay of ice caps, or because of changes in

the volume of the ocean basins (Miller et al., 2005). These fluctuations affect the distribution of sediment in the basins adjacent to the margins (Haq et al., 1987) and alter the erosional base level (Nielsen et al., 2002). A fall in sea-level gives rise to an apparent surface uplift of the same magnitude (Huuse, 2002). Furthermore, this would increase the area exposed above sea-level, resulting in uplift due to the isostatic response to the erosional unloading and the removal of water.

Eustatic sea-level curves for the Phanerozoic are given by Haq et al. (1987) and Miller et al. (2005). The sea-level curve of Haq et al. (1987) shows that throughout the Cretaceous, sea-level broadly increased, from +150 m (above the present level) in the Albian, reaching a high of approximately +250 m in the mid Cretaceous. Following this, the curve shows a very gradual decline, although sea-level remained relatively high until the Oligocene. Around the Palaeogene – Neogene transition, sea-level fell quite dramatically; this reflected a significant global climate cooling and the growth of ice caps (Stuevold & Eldholm, 1996). Sea-level in the late Pliocene and Quaternary is characterised by several short-term fluctuations, coinciding with major glacial events. A sea-level low of -120 m was attained during the last glacial maximum (Haq et al., 1987).

2.3 Uplift of the margins bordering the North Atlantic

Post-breakup uplift at most of the margins bordering the North Atlantic, including Norway, East and West Greenland (discussed below), as well as the British Isles, the Faeroe Islands and Svalbard, has been widely reported (e.g. Japsen & Chalmers, 2000; Doré et al., 2002, & references therein). Uplift of the basin margin areas appears to have been accompanied by accelerated subsidence of some of the basin centres (Figure 2.2). The NW European margins of the Norwegian-Greenland Sea have also experienced localised compressional deformation since breakup (Lundin & Doré, 2002).

2.3.1 Geological history

The opening of the North-East Atlantic, the region of the Atlantic Ocean north of the Charlie Gibbs Fracture Zone, began with rifting events throughout the late Permian to the late Cretaceous, with the extension broadly orientated WSW-ENE to

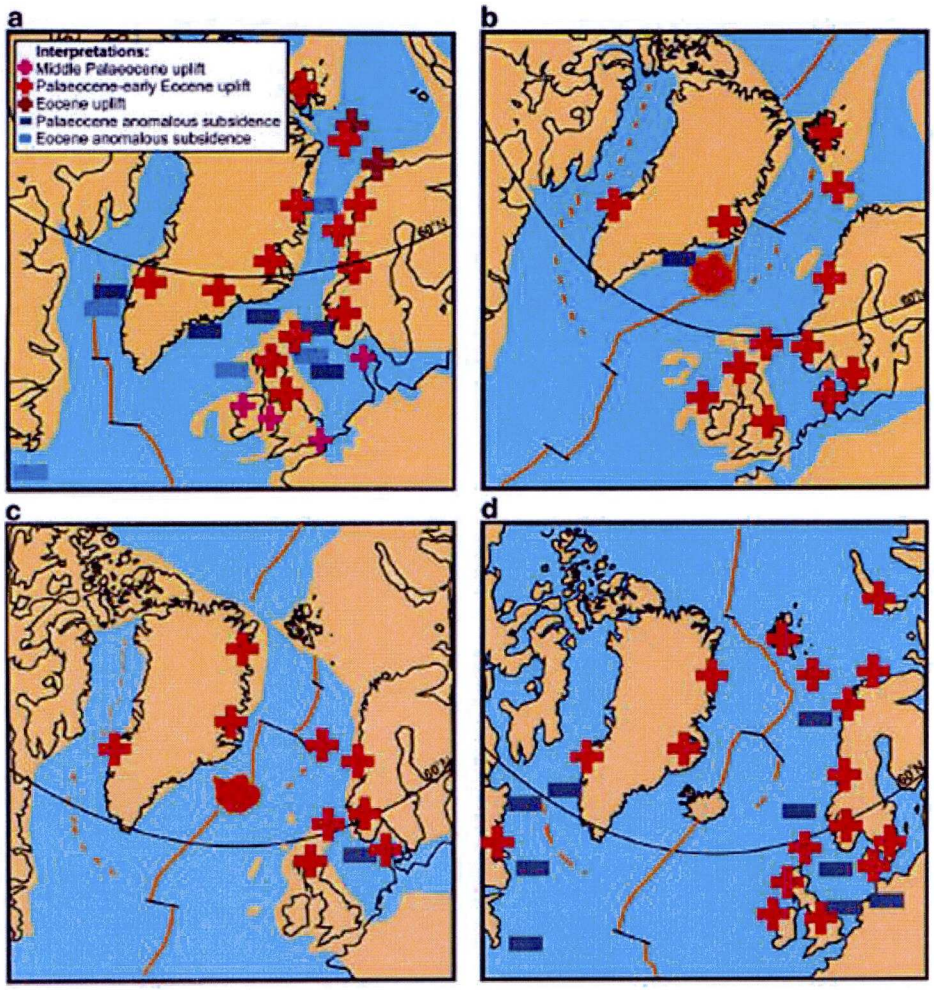

Figure 2.2: Locations of proposed Cenozoic uplift (red crosses) and subsidence (blue dashes) in the North Atlantic (from Anell et al., 2009); a) Palaeocene – Eocene; b) Oligocene; c) Miocene; d) Plio-Pleistocene.

W-E (Mosar et al., 2002a). Rifting continued during late Cretaceous to early Tertiary times but with a gradual rotation of the orientation of the extension to NNW-SSE. Continental breakup occurred in the Tertiary, with Greenland rifting off Norway and the onset of sea-floor spreading at 54 Ma, coincident with a major change in the stress field from extensional to weakly compressional. The present day stress field of Norway remains compressional, a significant component of which is perpendicular to the margin (Cloetingh et al., 1992). Continental breakup was accompanied by the emplacement of the basaltic magmas of the North Atlantic Igneous Province across most of the north-eastern Atlantic margins (Anell et al., 2009, & refs therein). The plate configuration at this time is shown in Figure 2.3a. Continued sea-floor spreading led to the development of the Reykjanes, Aegir and Mohns Ridges, which

were fully developed by ~ 47 Ma (Figure 2.3b). To the north, Svalbard and Greenland were separated by a broad strike-slip zone (Mosar et al., 2002b).

A rift developed between Jan Mayen and Greenland at 40 Ma; this rift propagated northwards and by 33 Ma (Figure 2.3c), fan-shaped sea-floor spreading was occurring on the west side of Jan Mayen (Muller et al., 2001), simultaneous with spreading on the Aegir Ridge. Around this time, the plate movement between Greenland and Svalbard changed to a divergent, strike-slip motion (Mosar et al., 2002b). Sea-floor spreading on the Aegir Ridge was abandoned by 21 Ma (Doré et al., 2008; Figure 2.3d). The Mohns and Reykjanes ridges were then connected by the Kolbeinsey Ridge, situated to the west of Jan Mayen. Figure 2.3e shows the plate configuration at ~ 20 Ma, when the Jan Mayen micro-continent had completely rifted off East Greenland. Rifting between the SW Barents Sea and NE Greenland led to the separation of Greenland and Svalbard and the formation of the Knipovitch Ridge (Lundin & Doré, 2002). By 16 Ma, a continuous ridge system connecting the North Atlantic and the Arctic Ocean had formed (Figure 2.3f), giving the present-day configuration of the plates (Engen et al., 2008).

West of Greenland, the Labrador Sea and Baffin Bay were formed by the north-westward propagation of sea-floor spreading in the North Atlantic, which is described in detail by Roest & Srivastava (1989) and Alvey (2010). Rifting began during the early Cretaceous, at ~125 Ma, culminating in plate separation in the Campanian (Doré et al., 2008). The initial separation was characterised by mantle exhumation; the onset of sea-floor spreading in the Labrador Sea was not until the late Mastrichtian. Sea-floor spreading began in Baffin Bay, which was connected to the Labrador Sea by a strike-slip fault system, at ~69 Ma. Between 84 – 59 Ma, the opening between Greenland and North America was orientated WSW-ENE, before changing to SSW-NNE between 59 – 56 Ma (Roest & Srivastava, 1989); this change in plate motion coincided with the onset of sea-floor spreading in the Norwegian-Greenland Sea. Sea-floor spreading in the Labrador Sea and Baffin Bay slowed significantly during the Eocene before terminating at ~33 Ma, contemporaneous with a regional shift in plate tectonics, as Greenland joined the North American plate.

2.3.2 Climate

It is thought that the North Atlantic climate was much warmer in the early Cenozoic, with temperatures peaking in the early Eocene (Zachos et al., 2001).

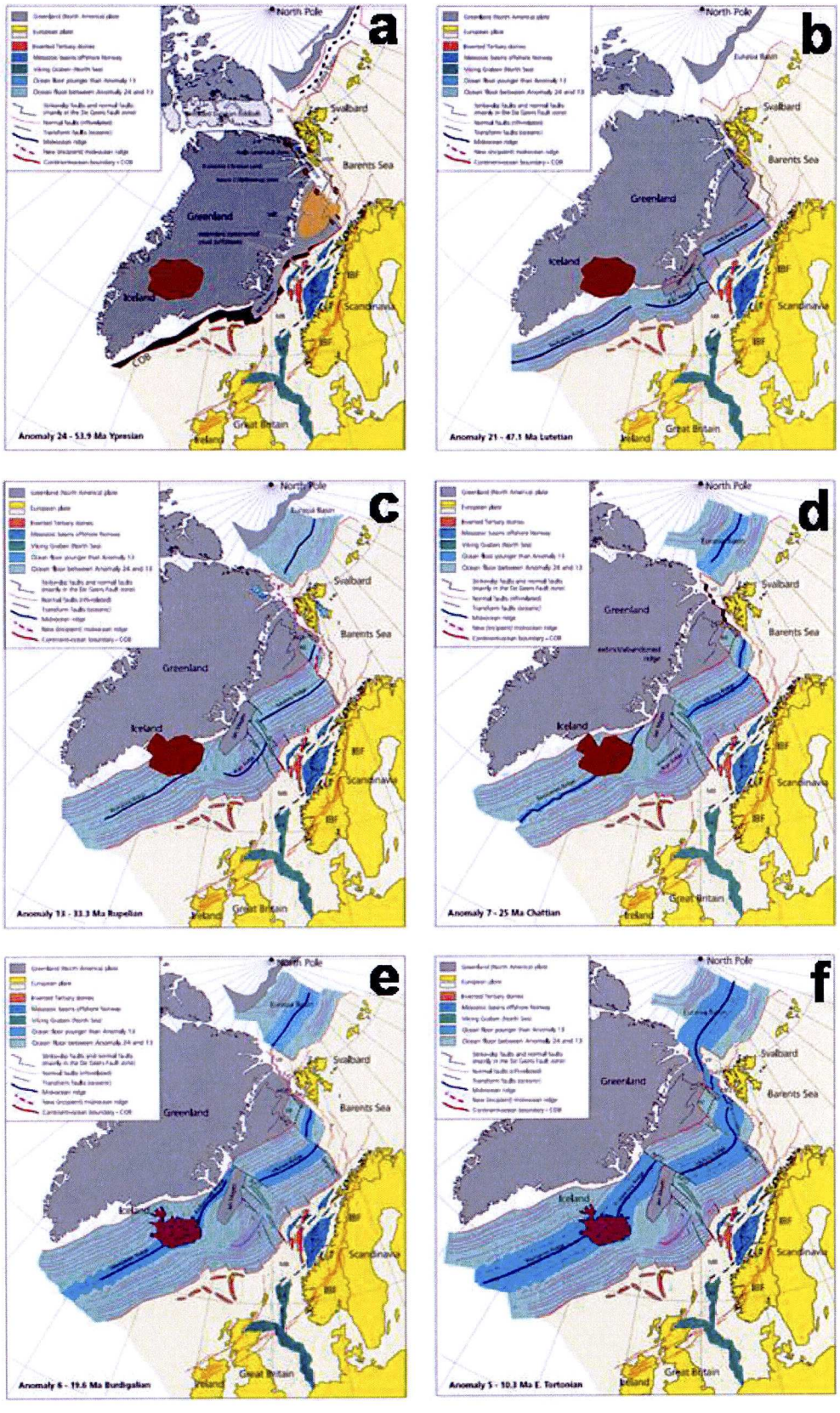

Figure 2.3: Plate reconstructions for the North Atlantic (from Mosar et al., 2002b).

Following this, the climate deteriorated, with a major fall in temperatures observed around the Eocene – Oligocene boundary. The climate warmed again throughout the late Oligocene to mid Miocene, before a long-term trend of gradual cooling from the late Miocene to present (Zachos et al., 2001). The first glaciations in Greenland occurred as early as 38 - 30 Ma, with the first Northern Hemisphere ice sheets being dated to the middle Miocene (Eldrett et al., 2007) and both Norway and Greenland experiencing major glaciations from the mid Pliocene onwards (Stuevold & Eldholm, 1996; Bonow et al., 2006b, & references therein).

2.4 Norway

The topography of Norway is defined by two asymmetric elevated regions, the Northern and Southern Scandes, separated by the relatively low-lying Trøndelag region of mid-Norway (Figures 2.4 & 2.5). The Northern Scandes are considered to be an elongated dome, ~1000 km long and ~200 km wide, with elevations up to 2100 m (Lidmar-Bergström & Näslund, 2002; Ebbing & Olesen, 2005; Rohrman & van der Beek, 1996). The Southern Scandes are higher, at up to 2500 m, and form a more oval dome, ~680 km long and up to 400 km wide. Several studies have suggested that these two regions have different uplift and denudational histories (Hendriks & Andriessen, 2002; Anell et al., 2009, & references therein).

The topographic highs of northern and southern Norway both coincide roughly with a Bouguer gravity anomaly low of around -100 mGal (Redfield et al., 2005; Rohrman & van der Beek, 1996; Ebbing, 2007). Gravity data suggest that the Scandes are largely isostatically compensated at depth, although a mass deficit below the domes is thought to indicate the presence of low-density material just below the Moho (Ebbing, 2007). This is supported by seismic tomography, which suggests a thermal anomaly exists at depth below the Southern Scandes (Rohrman et al., 2002).

Four major planation surfaces have been identified in southern Norway (Lidmar-Bergstrom et al., 2000). These surfaces cut across rocks of different lithology suggesting they were formed by erosion to some base level, commonly assumed to be controlled by sea-level. However Nielsen et al. (2009, & references therein) argue that these surfaces were instead formed at high altitude by glacial processes. Prior to uplift, it is thought that the topography of Norway was

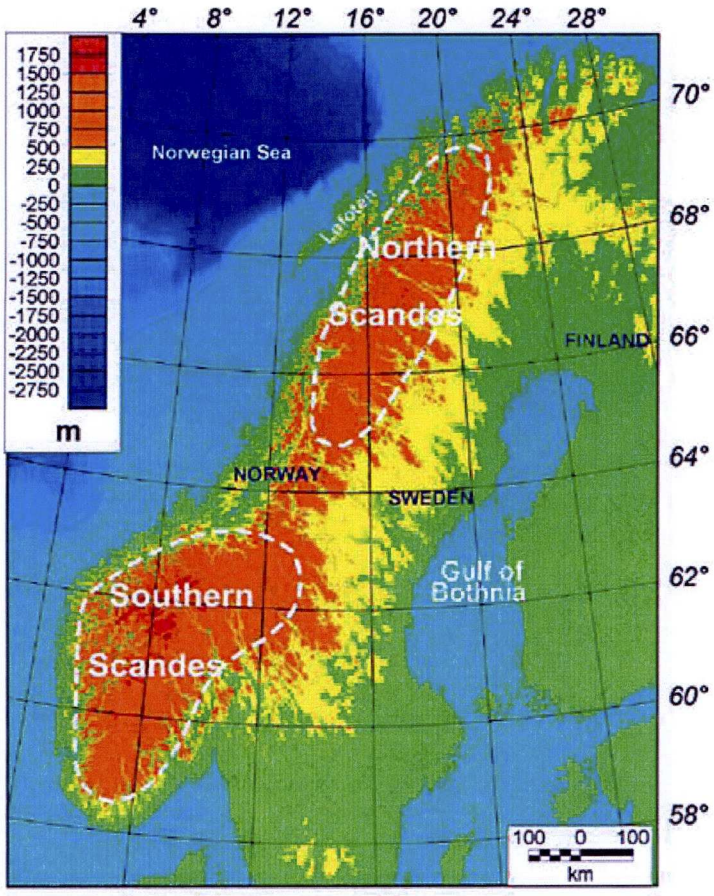

Figure 2.4: Topography of Norway (from Ebbing & Olsen, 2005). The white dotted lines correspond to 500 m above sea-level.

characterised by a low-elevation, low-relief surface, named the Palaeic surface, which now forms a deeply incised elevated plateau 1200 – 1400 m above sea-level (Stuevold & Eldholm, 1996). It is inferred that the Palaeic surface was formed in the Palaeogene, through correlation with the offshore Base Tertiary surface (Doré, 1992).

Norway is thought to have experienced two major phases of regional uplift in the Palaeogene and Neogene (Riis, 1996). In the Palaeogene phase, the uplift paralleled the margin whereas the Neogene phase is characterised by domal-style uplift (Praeg et al., 2005). Landform analysis indicates that the main uplift of the Northern Scandes is older than that of the Southern Scandes, as they are more heavily dissected by deep valleys (Lidmar-Bergström & Näslund, 2002). The Northern Scandes also show a more continuous cooling history since the Palaeogene, although possibly with an increase in the Neogene (Hendriks & Andriessen, 2002).

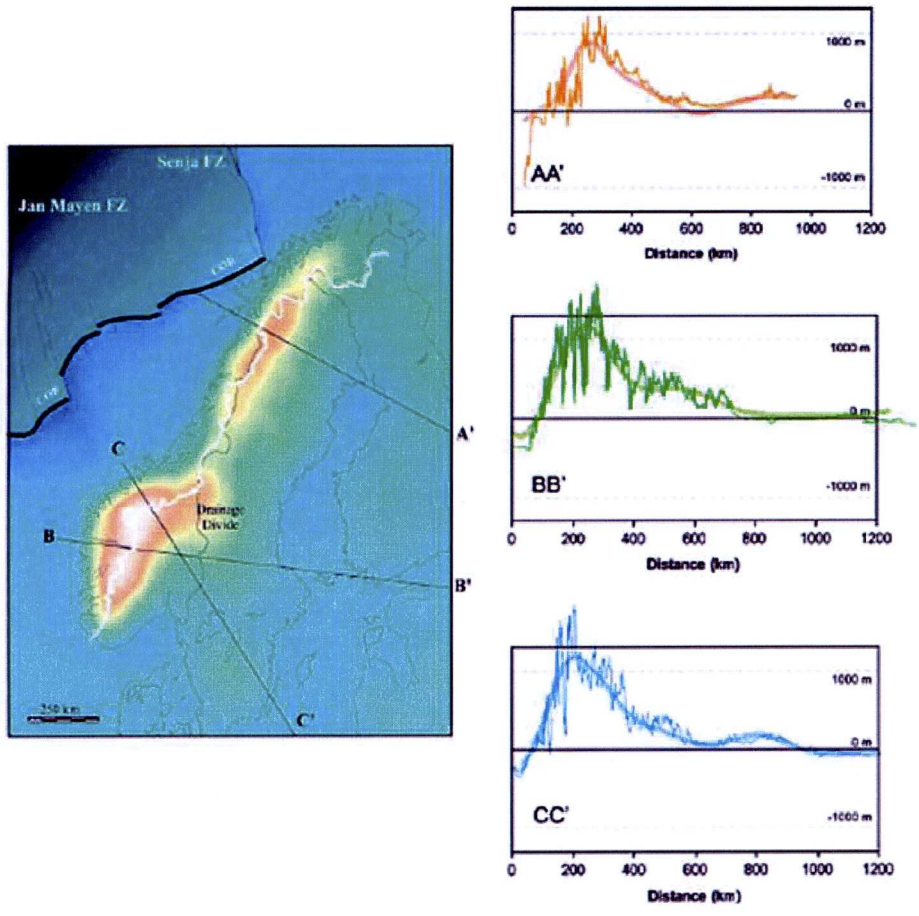

Figure 2.5: Topographic profiles across Scandinavia, taken from a smoothed digital elevation model (from Smelror et al., 2007).

Many studies have suggested a Norwegian uplift event, initiated in either the Oligocene or Neogene, and centred on the Southern Scandes (Anell et al., 2009, & references therein). Evidence for this includes AFT data which indicate enhanced denudation started at approximately 30 Ma and increased throughout the Neogene (Rohrman et al., 1995). Lidmar-Bergström et al. (2000) suggest that the Palaeic surface was uplifted mainly in the Neogene, although it may have been initiated as early as the late Eocene. The offshore sedimentary record is characterised by prograding clastic wedges that have been interpreted to reflect substantial uplift of the margin, starting in the late Oligocene – earliest Miocene (Stuevold & Eldholm, 1996). A large volume of Plio-Pleistocene sediments have also been deposited offshore, and are taken to indicate that the uplift was ongoing at that time (Evans et al., 2000; Riis, 1992). In contrast to this, Nielsen et al. (2009) argue that there has

been no Cenozoic uplift of Norway and that the Scandes are simply remnants of the Caledonides.

AFT data suggest that Norway has experienced 1.5 – 2.5 km of denudation, decreasing radially to less than 0.5 km near the coastline, as a result of domal uplift in the Neogene (Rohrman et al., 1995). Another fission track study, by Redfield et al. (2005), indicates up to 2 – 3 km of uplift of the continent. Riis (1996) suggested, from correlation of the onshore and offshore stratigraphy, that the Palaeogene uplift phase had a magnitude of ~1500 m and the Neogene phase a magnitude of ~1000 m, with the uplift centred on northern and southern Norway respectively. These estimates are in agreement with values of ~1000 m in the Palaeogene and up to 1200 m in the Neogene determined from geomorphological mapping by Lidmar-Bergström et al. (2000). Stuevold & Eldholm (1996) suggest a tectonic uplift of approximately 1 km since the Oligocene.

Numerous mechanisms have been proposed to explain the uplift of Norway, many of which are in some way connected to the Iceland plume. These include the asthenospheric diapir model of Rohrman & van der Beek (1996) and Rohrman et al. (2002), a model involving shallow convection or enhanced thermal flux (Stuevold & Eldholm, 1996), or lithospheric delamination (Nielsen et al., 2002). Alternatively, a mechanism involving intraplate stresses has been proposed (Cloetingh et al., 1992). Hendriks & Andriessen (2002) suggest that the denudational history of the Northern Scandes can be explained by a scarp retreat model. The uplift of Norway is thought to have a flexural component, with a coupling between the offshore subsidence and onshore uplift (Doré, 1992); southern Norway is considered to have a low elastic thickness of 10 – 20 km (Rohrman et al., 2002, & references therein).

It has also been argued that the majority of the Norwegian uplift can be accounted for by Plio-Pleistocene glacial rebound (Riis & Fjeldskaar, 1992), although it was shown that a tectonic component of uplift was still required to predict the present-day elevations. It is widely agreed, however, that any tectonic uplift was amplified during the late Pliocene and Pleistocene by the isostatic response to glacial unloading (Stuevold & Eldholm, 1996; Riis, 1992; Lidmar-Bergstrom et al., 2000, & references therein). A link between the uplift and sea-level fluctuations has also been suggested (Huuse, 2002; Nielsen et al., 2002; Nielsen et al., 2009).

2.5 East Greenland

Post-breakup uplift has been documented along the central part of the East Greenland margin; locations mentioned in the text are shown in Figure 2.6. The margin has experienced two phases of igneous activity: one associated with the emplacement of the flood basalts, coincident with the opening of the North Atlantic at 54 Ma, and a later, minor, phase in the mid Cenozoic (Thomson et al., 1999). At the time of continental breakup the margin appears to have been low-lying, as the Tertiary basalts were extruded at sea-level, but now average elevations in this region are ~1000 m near to the coastline, rising to > 2000 m inland, with maximum elevations of up to 4000 m (Hansen & Brooks, 2002, & references therein). A drainage divide is located along the top of the escarpment (Bonow et al., 2006a).

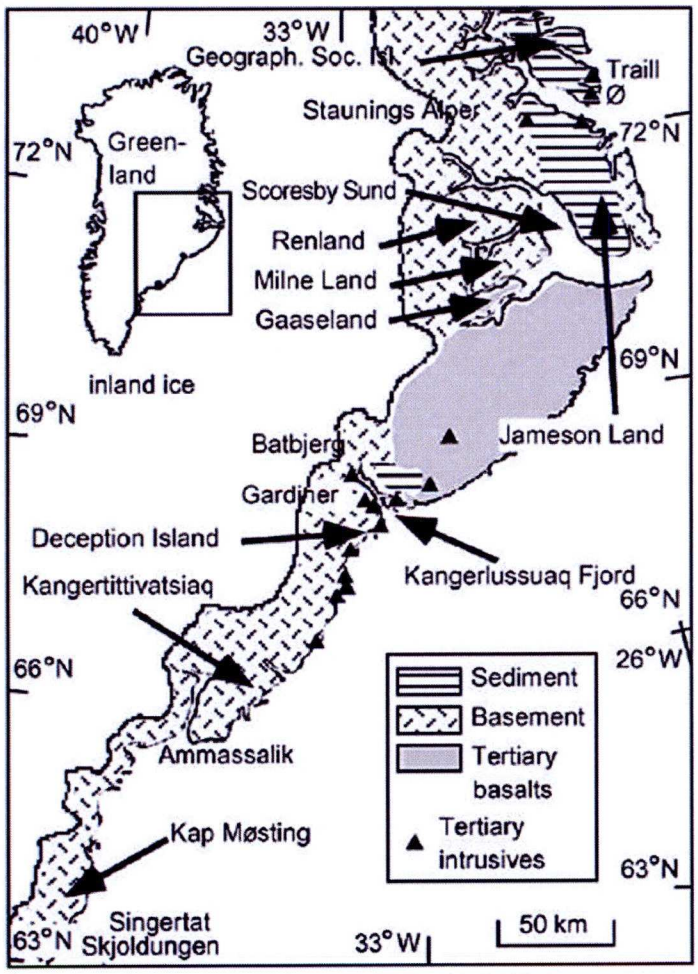

Figure 2.6: Geological map of East Greenland (from Hansen & Brooks, 2002).

It has been suggested that the East Greenland margin has experienced two distinct uplift events: a domal uplift, centred on Kangerdlugssuaq, and a regional plateau uplift (Brooks, 1985). In the Kangerdlugssuaq region, late Cretaceous – early Tertiary marine sediments are now at elevations of ~1500 m, indicating considerable Tertiary uplift (Hansen, 1996). Brooks (1985) dated the domal uplift to 55 – 50 Ma. Other published studies indicate that the margin experienced uplift and erosion during and after the magmatic event at 54 Ma (Thomson et al., 1999; Mathiesen et al., 2000, & refs therein), although Dam et al. (1998) suggest that this period of uplift was short, lasting less than 5 Myr. The regional uplift has been dated to ~35 Ma from geomorphological evidence (Brooks, 1985).

Several fission track studies (apatite, zircon and sphene) indicate accelerated erosion rates from the late Palaeocene to the present in the Jameson Land basin (Mathiesen et al., 2000), the Kangerdlugssuaq region (Hansen, 1996) and the Scoresby Sund region (Hansen, 1992). The erosion rates are particularly enhanced in the Jameson Land basin between 10 – 5 Ma (Mathiesen et al., 2000). This late Neogene cooling phase is supported by a study by Thomson et al. (1999) combining AFT and vitrinite reflectance data, which also indicated a cooling phase starting between 40 – 30 Ma. Further north, uplift events in the early Miocene and in the latest Miocene – earliest Pliocene are indicated by seismic data (Hamann et al., 2005).

On the East Greenland margin, the largest amount of Cenozoic denudation has occurred in the Kangerdlugssuaq region (Clift et al., 1996). In central Kangerdlugssuaq, since 25 – 30 Ma, there has been at least 4 km of erosion at the coast (Hansen & Brooks, 2002; Hansen, 1996); it has been suggested that the domal structure of this region originally had a height of 6 km (Brooks, 1985). In the hinterland, the maximum denudation is ~ 2 km (Hansen, 2000; Hansen & Brooks, 2002). AFT data indicate < 2 km of erosion in SE Greenland, at 63°N, and in the Scoresby Sund region (Clift et al., 1996). This is consistent with values of 1.5 – 3 km of erosion reported for the Jameson Land basin (Christiansen et al., 1992; Mathiesen et al., 2000), a region which Mathiesen et al. (2000) suggest has undergone a tectonic uplift of ~1 km. Brooks (1985) proposed that the plateau uplift had a magnitude of approximately 2.5 km.

The uplift of East Greenland has been suggested to be connected to igneous activity, either by magmatic underplating, or to dynamic uplift associated with the

passage of the Iceland plume beneath Greenland, particularly in reference to the domal uplift at Kangerdlugssauq (Brooks, 1985; Clift et al., 1996; Hansen & Brooks, 2002, & refs therein). Alternative mechanisms that have been proposed include a delayed phase change in the lower crust (Brooks, 1985), uplift resulting from compressive stress due to changes in the North Atlantic plate configuration (Thomson et al., 1999; Mathiesen et al., 2000) and flexural uplift of the margin due to the separation of Greenland and Jan Mayen (Thomson et al., 1999). Both Brooks (1985) and Clift et al. (1996) argue that there is no evidence of major tectonic uplift occurring on the East Greenland margin later than the Oligocene.

2.6 West Greenland

The central West Greenland margin is characterised by an elevated plateau, of low relief which cuts across rocks of different lithology (Figure 2.7; Japsen et al., 2009, & references therein). This margin differs from others that have experienced post-breakup uplift as a Cretaceous – Eocene sedimentary and volcanic record is exposed on the ~2 km high mountains of Nuussuaq and Disko (Japsen et al., 2006). Evidence from these mountains, as well as the offshore sedimentary record, indicate a Palaeocene regional uplift event, which occurred prior to the mid-Palaeocene magmatic event (Japsen et al., 2006, & references therein). This uplift event was short-lived and was followed immediately by rapid km-scale subsidence (Dam et al., 1998).

AFT and vitrinite reflectance data, and geomorphological analysis indicate that there have been three post-breakup uplift events (Japsen et al., 2005; Japsen et al., 2006; Bonow et al., 2006b); one event is proposed in the late Eocene – Oligocene and two events are proposed in the Neogene, starting between 40 – 30 Ma, 11 – 10 Ma and 7 – 2 Ma respectively. Planation surfaces have been identified in West Greenland by Bonow et al. (2006a; 2006b) which may correlate with the cooling events predicted by the AFT data, and unconformities in the offshore sedimentary record may be connected to the late Neogene events (Japsen et al., 2006; Chalmers, 2000).

Dam et al. (1998) estimated that the Palaeocene uplift event had a magnitude of up to 1.3 km, followed by a minimum of 1 km of subsidence. Palaeocene marine

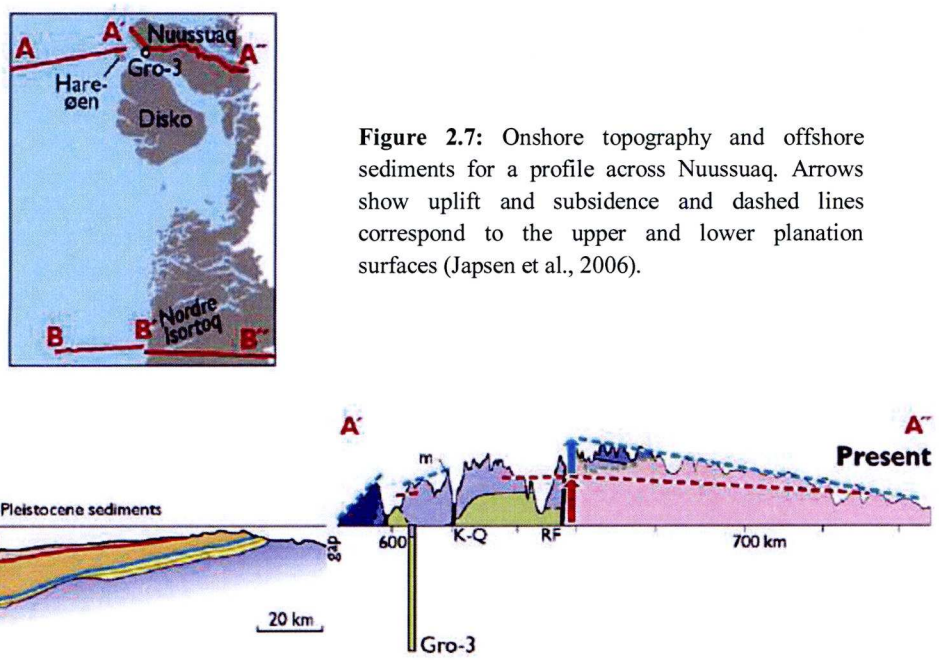

Figure 2.7: Onshore topography and offshore sediments for a profile across Nuussuaq. Arrows show uplift and subsidence and dashed lines correspond to the upper and lower planation surfaces (Japsen et al., 2006).

sediments are now found at elevations > 1 km above sea-level (Japsen et al., 2005; Japsen et al., 2006), indicating the minimum amount of Neogene uplift, which may have had a maximum of up to 2 – 3 km (Chalmers, 2000). The planation surface which formed during the Oligocene – Miocene, shown in Figure 2.8, is now situated at elevations of up to 2 km. This surface must have formed at some base-level; assuming this to be sea-level, it is inferred that the West Greenland margin has experienced approximately 2 km of uplift in the last ~ 10 Myr (Japsen et al., 2006; Japsen et al., 2005; Bonow et al., 2006b; Japsen et al., 2009). It is suggested that the late Neogene uplift events each had a magnitude of ~1 km (Bonow et al., 2006b).

Redfield (2010) argues that, whilst the geological evidence supports uplift of West Greenland since the early Eocene, the Neogene phases of uplift are unsupported by the AFT data. Young cooling events predicted by AFT data may instead be model artefacts, as the low temperature annealing of apatite is not accounted for in the model. Furthermore, it appears that Japsen et al. (2005) have been selective in the samples used for their analysis by excluding samples with older ages (Redfield, 2010), although it is possible that those samples are contaminated.

The Palaeocene uplift and subsequent rapid subsidence is thought to be related to plume activity (Dam et al., 1998). The cause of the later uplift events is, however, more enigmatic. There is a considerable time gap between the early Eocene

Figure 2.8: The upper planation surface at southern Disko, at ~ 900 m above sea-level (from Japsen et al., 2006).

magmatism and termination of sea-floor spreading in the Labrador Sea, and the Neogene uplift. This suggests that the uplift mechanism is not directly related to either process (Chalmers, 2000). The uplift may have been initiated by the isostatic response to increased erosion due to climatic deterioration. However, the interpretation of the evolution of West Greenland of Japsen et al. (2006) and Bonow et al. (2006b) suggests that prior to the Neogene uplift, the margin was near to sea-level and therefore there was no topography available to be eroded. Furthermore, the first late Neogene uplift event occurred ~3 Myr before the onset of glaciations in Greenland (Japsen et al., 2006). Instead, Japsen et al. (2005; 2006) and Bonow et al. (2006b) strongly advocate that a tectonic component is necessary to explain the Neogene uplift, although this will have been enhanced by the isostatic response to erosion and loading and unloading of the ice sheets.

2.7 Geological history of the South Atlantic

The formation of the South Atlantic, described in detail by Torsvik et al. (2009) and Moulin et al. (2010), began with the onset of rifting, preceding continental breakup, between South America and Africa at approximately 150 Ma. Sea-floor spreading began in the southernmost South Atlantic by 132 Ma, coinciding with the

eruption of the Paraná-Etendeka flood basalts on both sides of the Atlantic Ocean (Figure 2.9a). Rifting then propagated northwards, with sea-floor spreading established south of the Paraná-Etendeka fracture zone by the early Aptian (Figure 2.9b). The northwards propagation of sea-floor spreading continued throughout the Aptian (Figure 2.9c), connecting the South and Central Atlantic by ~100 Ma (Figure 2.9d).

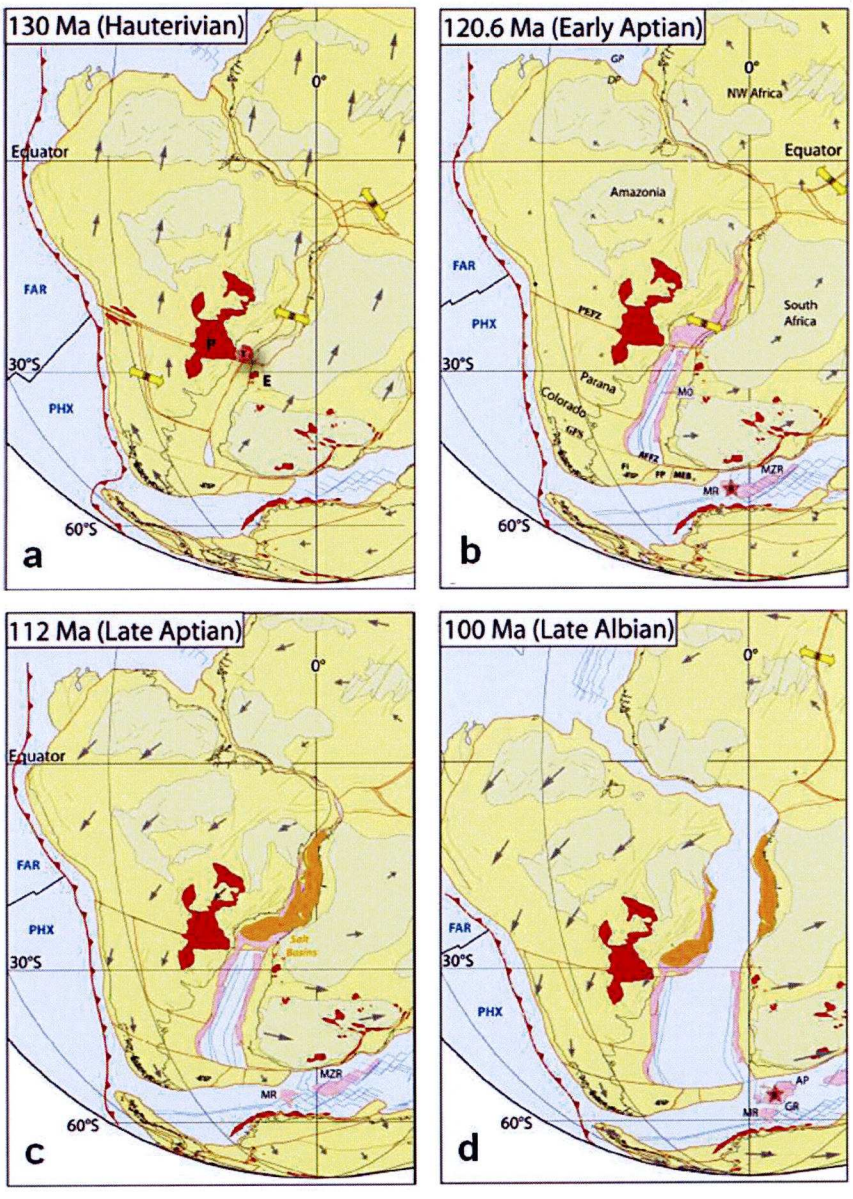

Figure 2.9: Plate reconstructions for the opening of the South Atlantic (from Torsvik et al., 2009). P = Paraná-Etendeka flood basalts.

2.8 Brazil

Both the south-eastern Brazilian rifted margin and the north-eastern Brazilian margin appear to have experienced post-breakup uplift of their continental hinterland. South-eastern Brazil has a well-developed escarpment, whereas in the north-east of Brazil, the escarpment is much less defined (Peulvast et al., 2008). The two regions are discussed separately below, as they are discussed independently in the literature.

2.8.1 North-eastern Brazil

The north-eastern Brazilian margin, between the Parnaiba Basin and the Borborema Plateau (Figure 2.10), is characterised by a stepped escarpment, parallel to the coast, leading up to elevated plateaus. Up to five main stepped surfaces, which form the escarpment, have been described, but a more recent study indicates there may only be two main surfaces (Peulvast & Claudino-Sales, 2004). A recent study by Bonow et al. (2009) identified two major planation surfaces which cut across rocks of varying age and lithology, which they suggest formed at sea-level.

The crest of the escarpment coincides with the drainage divide, and is located up to 300 km from the coast (Peulvast et al., 2008). The Ibiapabe – Araripe – Borborema plateaux form the highest part of the region with maximum elevations of 1000 – 1200 m (Figures 2.10 & 2.11); these elevated regions are mainly resistant Mesozoic sedimentary rocks. A positive geoid anomaly is observed across the whole of the Borborema Province (Morais Neto et al., 2008). The regional morphology of North-East Brazil is largely controlled by east – north-east trending structures which formed during continental breakup, and there is no evidence for any subsequent major faulting suggesting flexural deformation is dominant (Peulvast & Claudino-Sales, 2004). Estimates for the elastic thickness on the margin are 5 – 10 km (Peulvast et al., 2008; Magnavita et al., 1994).

The North-East Brazilian climate is presently semi-arid. It has been suggested that the development of the arid climate dates to the late Eocene/early Oligocene when pole-to-equator climatic gradients were established and the Antarctic ice sheet began to form (Morais Neto et al., 2008). Prior to this, a warm and humid climate had prevailed since at least the late Cretaceous (Peulvast et al., 2008).

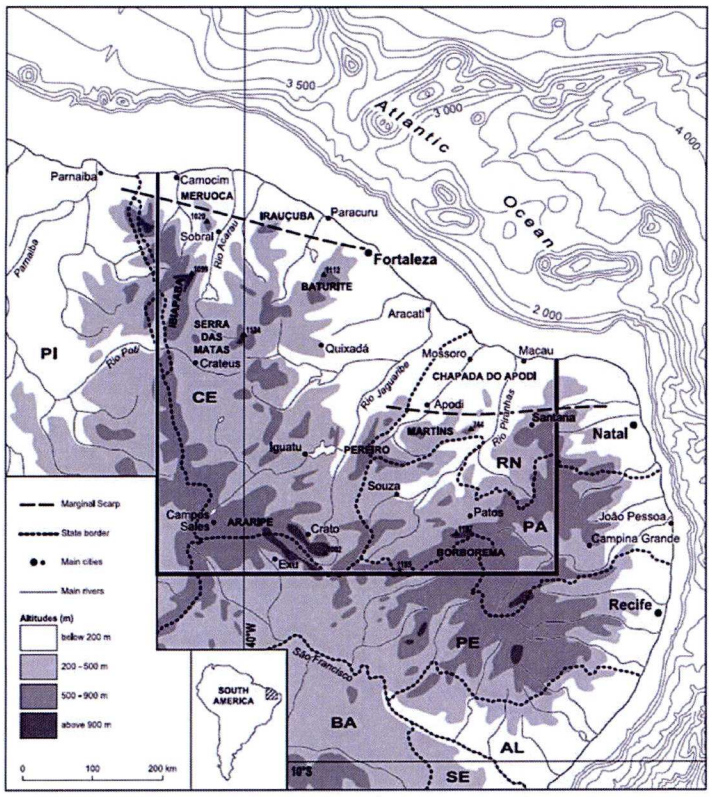

Figure 2.10: Topographic map of North-East Brazil (from Peulvast & Sales, 2004).

That the uplift of North-East Brazil occurred post-breakup is demonstrated by the Cretaceous marine basin of Araripe, which now forms an elevated plateau. It is thought that the end Cretaceous landscape was predominantly flat and low-lying, as the rift shoulders that formed during continental rifting and breakup had already been eroded away (Peulvast et al., 2008). The higher planation surface identified by Bonow et al. (2009) (Figure 2.12) is estimated to be of Palaeogene age, which implies that the landscape at that time was a peneplain close to sea-level. To the south-east of Araripe, two periods of uplift and erosion have been documented using vitrinite reflectance data (Magnavita et al., 1994); the first coincides with the end of rifting in the South Atlantic and a later event is dated to post-Albian, but before the Pliocene. In another study, AFT and vitrinite reflectance data indicate phases of accelerated denudation at 110 – 100 Ma and 40 – 10 Ma, and possibly another event at 80 – 60 Ma (Turner et al., 2008). This late Cretaceous – early Palaeocene event, which is thought to reflect plate reorganisation, corresponds to a widespread

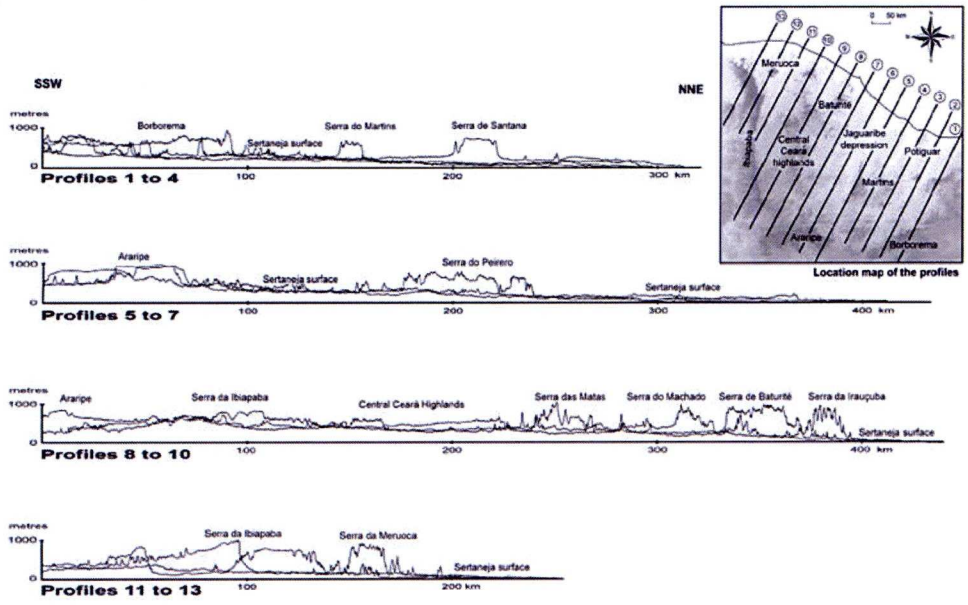

Figure 2.11: Topographic profiles taken normal to the NE Brazilian margin (from Peulvast et al., 2008).

unconformity in the Potiguar Basin which is dated at ~78 Ma. AFT data from the Borborema Plateau also show two main cooling events, with the first beginning around 100 – 90 Ma and a more recent event beginning in the Miocene, and another possible, less dominant, event at 65 – 50 Ma (Morais Neto et al., 2008).

There appears to be a consensus for a period of increased denudation in the late Cretaceous, contemporaneous with continental rifting and breakup; this event also corresponds to an increase in offshore sedimentation (Peulvast et al., 2008). A Neogene event is also supported by several studies, although it not known whether this event represents a discrete episode of uplift and erosion or is just part of a long-term trend (Morais Neto et al., 2008). It may be due to accelerated erosion as the climate increased in aridity, as indicated by the stratigraphic record of the Potiguar Basin which shows the clastic supply from the continental hinterland increased during the Miocene (Peulvast et al., 2008; Morais Neto et al., 2008).

Results from an AFT study indicate between 1 – 3 km of denudation since continental breakup on the Borborema plateau; the large degree of uncertainty arises because the palaeogeothermal gradient is assumed (Morais Neto et al., 2008). In the Araripe area, AFT data indicate that there has been 1.5 km of denudation in the last 30 Myr (Peulvast et al., 2008). Approximately 600 m of post-Albian tectonic uplift is

documented in Araripe and to the south-east in the Recôncavo-Tucano-Jatobá Rift (Peulvast et al., 2008; Morais Neto et al., 2008; Magnavita et al., 1994).

Various mechanisms have been proposed to explain the uplift of NE Brazil. Early work focussed on the idea of cyclic development (Peulvast & Claudino-Sales, 2004) but more recently-suggested mechanisms include plume-related uplift (Turner et al., 2008), magmatic underplating (Peulvast et al., 2008; Morais Neto et al., 2008; Magnavita et al., 1994), the flexural response to sediment loading of the margin (Peulvast et al., 2008), far-field stresses due to Andean convergence (Peulvast et al., 2008) and climate change (for the Neogene event only) (Morais Neto et al., 2008).

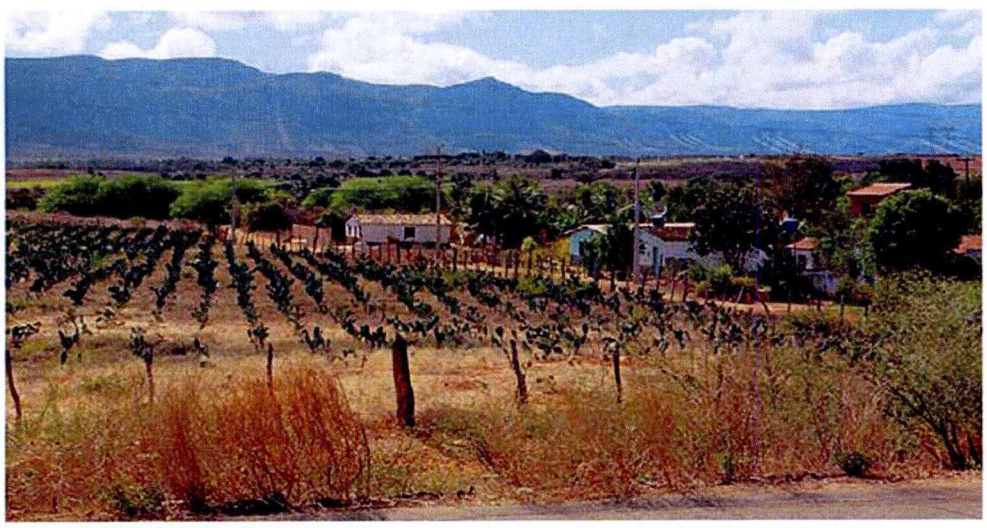

Figure 2.12: The lower planation with the escarpment leading up to the higher planation surface (from by Bonow et al., 2009).

2.8.2. South-eastern Brazil

South-eastern Brazil is characterised by two main elevated regions, forming plateaux > 1000 m above sea-level; these are the Ponta Grossa Arch, and the Serra da Mantiqueira, Serro do Mar and Serra dos Órgaos mountain ranges (Figures 2.13 & 2.14; Cobbold et al., 2001). The escarpment, which separates the high plateaus from the coastal plain, reaches a maximum elevation of 2000 m and is capped by Paraná basalts (Gallagher et al., 1995). In southern Brazil, south of Florianópolis, the escarpment is located 25 – 50 km from the coastline. To the north of Florianópolis,

the escarpment is less well defined and is located further inland, up to 80 km from the coast (van Balen et al., 1995; Gallagher et al., 1995). The initial escarpment of the Serra do Mar Mountain Range may have been fault bounded (Hackspacher et al., 2004) and surface process modelling results suggest the initial elevation of the rift shoulder was 1250 – 1850 m (Gallagher et al., 1995). The continental hinterland dips gently away from the escarpment, reaching sea-level approximately 600 km inland from the coast (Gallagher et al., 1994). The south-eastern Brazilian highlands correspond to a large negative Bouguer gravity anomaly of -80 mGal, and they appear to be isostatically compensated by a deep Moho, estimated to be at a depth of 38 – 43 km under the Serra do Mar to 42 – 47 km under the Paraná Basin (Cobbold et al., 2001).

It is thought, from AFT data, that a phase of accelerated denudation was experienced by the Serra do Mar and Higher Mantiqueira mountain ranges in the late Cretaceous – Palaeocene, and by the Lower Mantiqueira mountain range in the

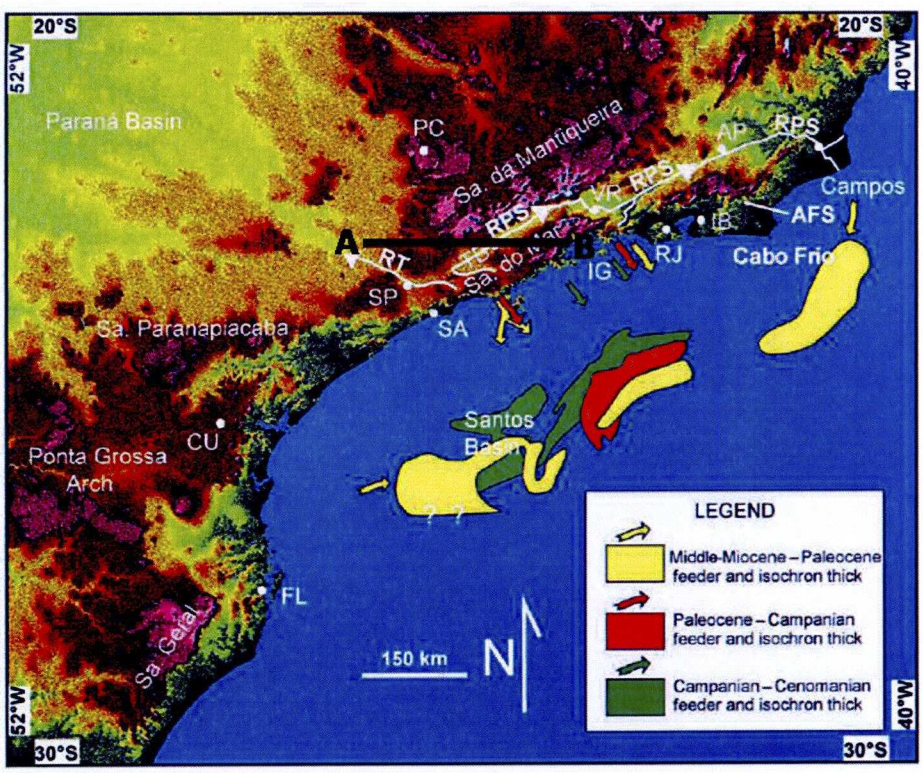

Figure 2.13: Topographic map of south-eastern Brazil (from Cobbold et al., 2001). Line shows the location of the cross section in Figure 2.14. FL = Florianópolis.

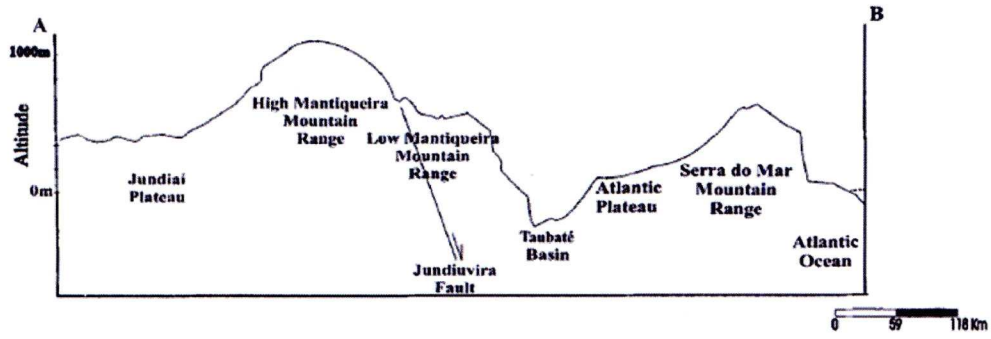

Figure 2.14: Topographic cross section across the south-eastern Brazilian margin (from Hackspacher et al., 2004).

Palaeocene (Saenz et al., 2003). Evidence suggests that the Japi surface, created by rapid Eocene erosion and which forms the top of the Serra do Mar and Mantiqueira mountain ranges, was partially uplifted and eroded during the late Miocene (Saenz et al., 2003). Other AFT studies indicate a phase of exhumation in south-eastern Brazil in the Cretaceous and a later phase beginning at 65 Ma and climaxing in the Eocene (Hackspacher et al., 2004; Cobbold et al., 2001). Gallagher et al. (1994) suggest up to 3 km and 1 km of denudation has occurred on the coastal plain and in the continental hinterland respectively, in keeping with the value of 2.5 – 4 km of denudation predicted by Hackspacher et al. (2004) on the coastal plain, and similar to values of denudation estimated in North-East Brazil.

The timing of the uplift on the south-eastern Brazilian margin suggests it must either be due to at least one permanent uplift mechanism or else by a mechanism which is unrelated to rifting. The distribution of the AFT ages, with younger ages on the coast and older ages in the hinterland regions, can be readily explained by protracted denudation since continental breakup (Gallagher et al., 1994), and are broadly consistent with a scarp retreat model (Gallagher et al., 1995; Hackspacher et al., 2004).

2.9 Southern Africa

The dominant feature of the landscape of southern Africa is the Great Escarpment (Figure 2.15), which has elevations generally in the range of 1500 – 2500 m, although it is higher in some places, and runs sub-parallel to much

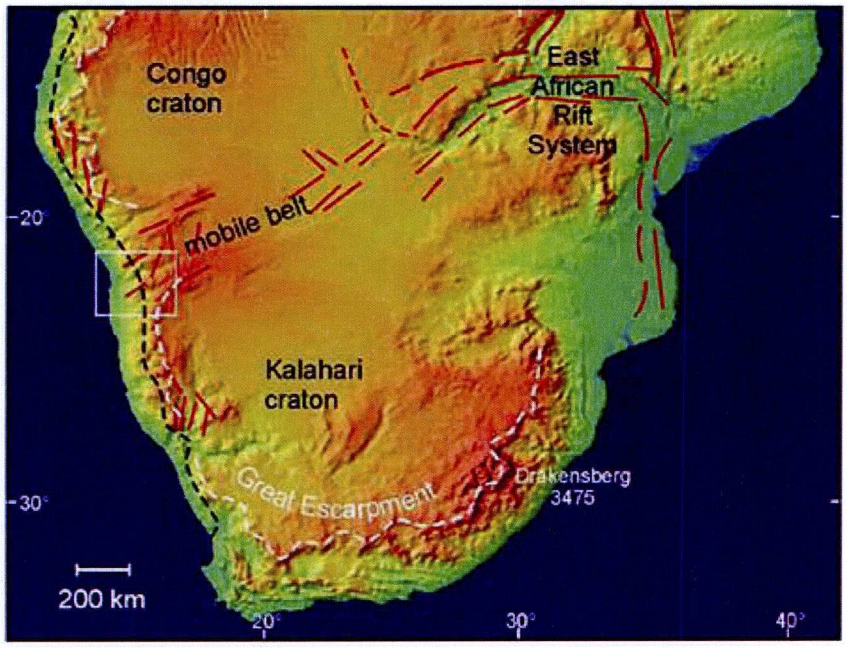

Figure 2.15: Shaded relief map of southern Africa (from van der Wateren & Dunai, 2001). The white dashed lines show the location of the Great Escarpment.

of the coastline (Tenbrink & Stern, 1992). It is located around 50 – 300 km inland of the coast (e.g. Tenbrink & Stern, 1992), where the escarpment summit is generally coincident with the continental drainage divide (Gilchrist et al., 1994; van der Beek et al., 2002). The location of the escarpment appears to be, at least partly, lithologically controlled (Gallagher & Brown, 1999), and as it is not, except locally, associated with faulting, it is considered a denudational feature (Gilchrist et al., 1994; Tenbrink & Stern, 1992). The mean elevation inland of the Great Escarpment is ~ 1000 m, with the elevated region covering nearly two-thirds of the interior of the southern African sub-continent (Brown et al., 1990; Nyblade & Sleep, 2003).

Southern Africa has experienced several large magmatic events in the Mesozoic. Karoo magmatism covered much of the sub-continent at 183 Ma, followed at 135 Ma by the emplacement of the Etendeka flood basalts, and two Kimberlite and alkaline volcanic activity events at 150 – 110 Ma and 90 – 60 Ma (Nyblade & Sleep, 2003; Raab et al., 2002). A widespread gravity low is observed over southern Africa (Hartley et al., 1996), which is perhaps caused by a considerable density decrease in the mantle (Artyushkov & Hofmann, 1998). There

are two main uplifted regions of focus in southern Africa: the south-western margin and the Drakensberg Mountains in the south-east; these areas have broadly similar uplift histories since the Mesozoic (Nyblade & Robinson, 1994), but are considered independently here, in-keeping with their separate treatment in the literature.

2.9.1 South-western Africa

The south-western African margin is the segment of the South Atlantic margin of Africa to the south of the Walvis Ridge. Its topography is dominated by a well-defined escarpment along much of the margin which separates the coastal regions from the elevated Kalahari Basin, which, although extensive, is quite shallow, with sediment thicknesses of up to 200 m (Tenbrink & Stern, 1992). High heat flow values are measured across the region (Nyblade & Sleep, 2003). Uplift of the south-western African margin was accompanied by tilting and rapid subsidence of the offshore regions (Janssen et al., 1995).

It is generally agreed that much of southern Africa was above sea-level at the time of breakup (Nyblade & Sleep, 2003). The last time large parts of the area are known to have been at sea-level was in the late Palaeozoic (Gilchrist et al., 1994), and there is little evidence to suggest the region was flooded after continental breakup. It has been suggested that southern Africa had an elevation of about 1000 m above sea-level at the time of breakup (Tenbrink & Stern, 1992 & references therein). The climate of south-western Africa changed from temperate to arid in the late Cretaceous – early Tertiary (Gallagher & Brown, 1999), supported by a change in the sediment discharge observed on the margin at this time (Brown et al., 1990). An increasing aridity of the climate since the early Oligocene is also indicated (e.g. Seranne & Anka, 2005; Gilchrist et al., 1994; Bierman & Caffee, 2001).

The whole of the south-western African margin experienced an episode of rapid denudation in the early Cretaceous, indicated by AFT data and offshore borehole data (Figure 2.16; Gallagher & Brown, 1999; Brown et al., 1990). This denudation event is thought to be associated with the breakup of Gondwana. AFT data indicate there has been two other phases of accelerated denudation since breakup: one in the latest Cretaceous (Figure 2.16; Gallagher & Brown, 1999; Raab et al., 2002) and another in the Eocene – late Miocene, which is also associated with accelerated subsidence offshore (Seranne & Anka, 2005, & references therein). The late Cretaceous event occurred at a time of global sea-level high and correlates with an

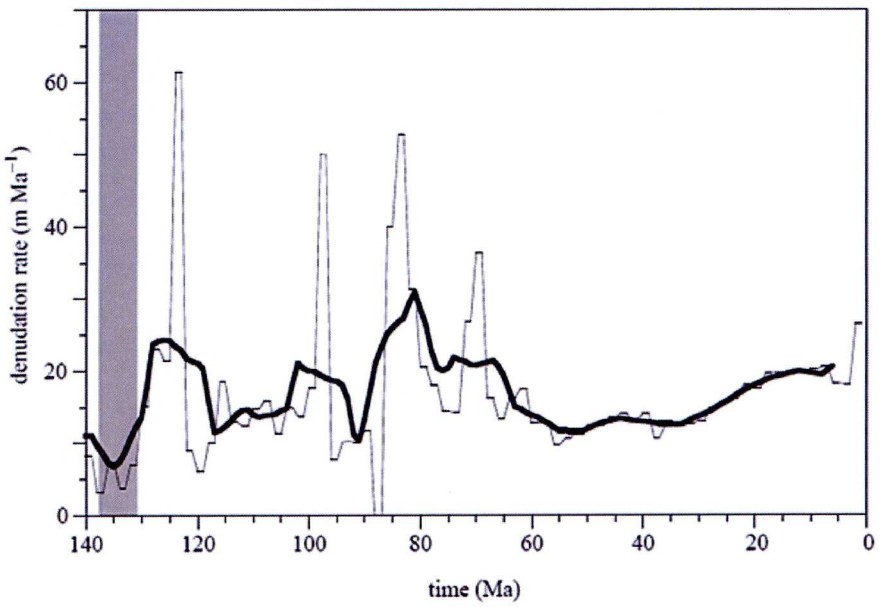

Figure 2.16: Denudation rate through time for the south-western African margin (from Gallagher & Brown, 1999). The lighter curve is the raw estimate of the denudation rate and the darker curve is the smoothed version. The shaded band corresponds to the time of continental breakup.

unconformity in the offshore stratigraphic record (Seranne & Anka, 2005). Lavier et al. (2001) suggested that a tectonic reactivation of the south-western African margin occurred in the Miocene, leading to uplift. It has also been suggested that uplift occurred in the early Miocene and late Pliocene and Pleistocene, with southern Africa being rapidly uplifted in the last 2.5 Myr (Artyushkov & Hofmann, 1998). However, van der Wateren & Dunai (2001) interpreted this late Neogene event as accelerated denudation in response to an increasingly wet climate associated with the Plio-Pleistocene global cooling.

It has been suggested that the south-western African margin, near to the escarpment, was uplifted by a total of 1200 m in the Miocene and Pliocene and just inland of the escarpment has been uplifted approximately 200 m (e.g. Artyushkov & Hofmann, 1998). The margin has experienced significant amounts of denudation since continental breakup, with much greater denudation in the coastal areas than in the elevated interior (Gilchrist et al., 1994). AFT data predict magnitudes of denudation of up to 3 – 5 km in the coastal regions and 1 km in the continental hinterland (van der Wateren & Dunai, 2001).

Various mechanisms have, again, been suggested as an explanation for the uplift of south-western Africa. These include magmatic underplating, a Mesozoic mantle plume, phase changes in the upper mantle, and dynamic rebound following the detachment of a subducting slab (Nyblade & Sleep, 2003, & references therein). The long wavelength of the uplift, the high heat flow measurements and a high geoid anomaly point to a mantle origin for the uplift; this has been termed the African Superswell and is thought to have been emplaced beneath southern Africa in the Miocene (Seranne & Anka, 2005; Nyblade & Robinson, 1994). The regional isostatic response to erosion has also been suggested to have played an important role in the topographic evolution of the south-western African margin (e.g. Gilchrist et al., 1994; Tenbrink & Stern, 1992).

2.9.2 South-eastern Africa

The south-eastern African margin formed by the opening of the Natal Basin and the shearing away of the Falkland Plateau along the Agulhas Fracture Zone at ~130 Ma (Fleming et al., 1999). The region experienced substantial volcanism between 198 – 173 Ma (Janssen et al., 1995). The Drakensberg Mountains form an elevated region of south-eastern Africa (Figure 2.17). The base of the Drakensberg Escarpment lies at around 2000 m and the escarpment summit, topped by Jurassic Drakensberg basalts which overlie the nearly-horizontal strata of the Karoo Supergroup, reaches a maximum of height of 3500 m (Figure 2.18; Brown et al., 2002). The terrain inland of the escarpment, forming the Lesotho Highlands (Figure 2.19), is the erosional remnant of the Karoo flood basalts (Fleming et al., 1999; Summerfield, 1991), which has a mean elevation of ~ 2700 m up to 300 km inland before decreasing very gradually to ~1000 m in the continental interior (van der Beek et al., 2002).

Geomorphological models for the landscape development of the Drakensberg Mountains indicate uplift events occurred in the earliest Oligocene (at ~ 30 Ma), in the early Miocene and in the late Pliocene (van der Beek et al., 2002, & references therein). However, this is based on the correlation of erosion surfaces, the allocated ages of which are questionable (Fleming et al., 1999). Moreover, AFT data and the offshore stratigraphic record do not support the occurrence of large-scale uplift events post-dating continental breakup on the south-eastern African margin (van der Beek et al., 2002). AFT data indicate a phase of rapid denudation near to the coast in

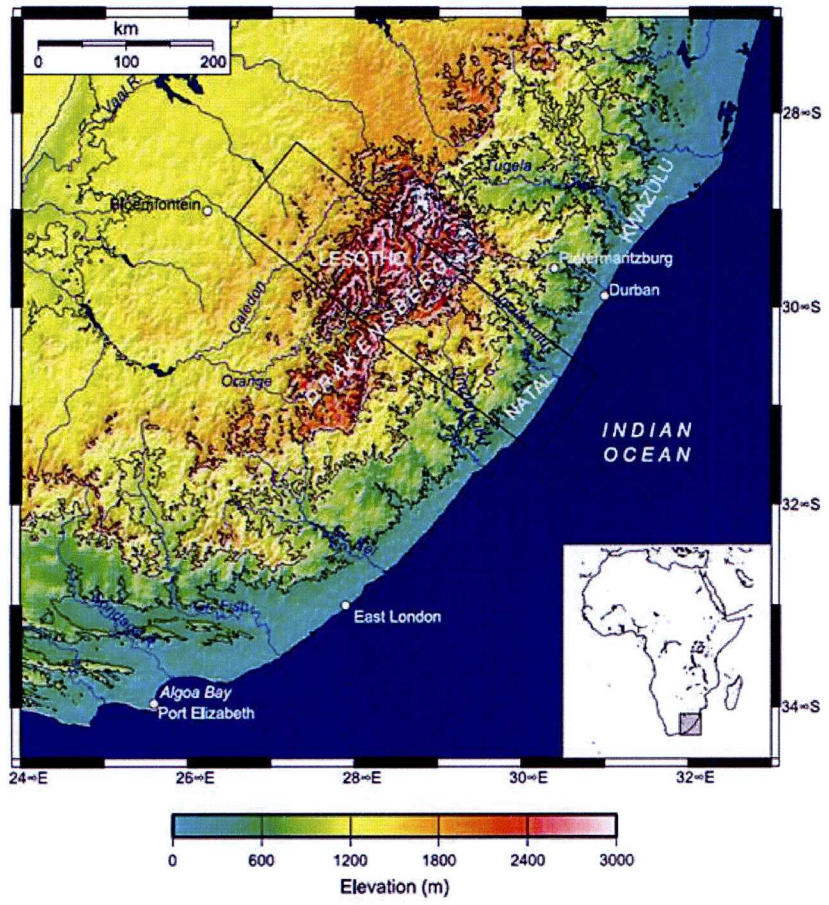

Figure 2.17: Shaded relief map of the south-eastern African margin (from van der Beek et al., 2002).

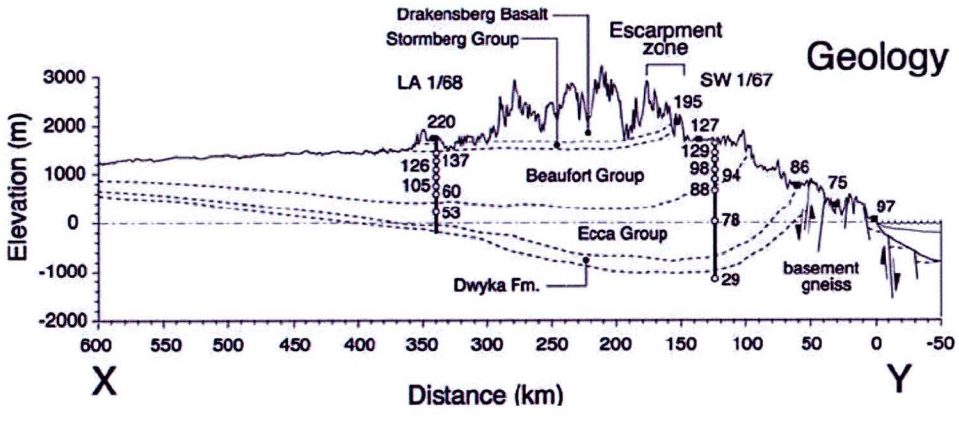

Figure 2.18: Topographic profile, geology and AFT ages along transect shown in Figure 2.17 (from Brown et al., 2002).

the early Cretaceous, which is broadly coincident with continental breakup (Brown et al., 2002). A later episode of accelerated denudation on the coastal plain is also documented at 90 – 70 Ma. The greatest amount of denudation has occurred on the coastal plain, with AFT data indicating a minimum of 4.5 km of denudation there since continental breakup; at approximately 200 km inland the estimated denudation is 1.7 ± 0.5 km and an estimated 0.5 – 1 km of denudation has occurred on the top of the Lesotho Highlands (Brown et al., 2002).

The Drakensberg Escarpment is a morphological feature which is thought to have originated at the coast at the time of continental breakup before, by parallel retreat or rapid incision, attaining its current position (Summerfield, 1991; Fleming et al., 1999). Van der Beek et al. (2002) suggest that no large-scale post-breakup tectonic uplift event is required to explain the morphological and denudational history of the south-eastern African margin; instead they propose, from numerical

Figure 2.19: Top: Peneplains at the Blyde River Canyon, capped by resistant quartzite; bottom left: the Sani Pass; bottom right: the low relief of the Lesotho Highlands.

models and flexural backstripping, that the margin was elevated prior to breakup by up to 2500 m. However, a mechanism is still needed to account for the initially high topography. Those suggested include magmatic underplating or the presence of large amounts of low-density melt residue in the lower mantle, both associated with the early Jurassic Karoo volcanism (van der Beek et al., 2002, & references therein), or dynamic support by a large, low-density body in the lower mantle, termed the "African superswell" (Lithgow-Bertelloni & Silver, 1998).

2.10 Western India

The formation of the western India margin began at ~ 180 Ma with major rifting events which preceded the breakup of eastern Gondwana. At 130 – 120 Ma, India and Madagascar rifted off eastern Africa and Antarctica, before India and Madagascar separated around 88 Ma. India and the Seychelles were separated by a ridge jump at 65 Ma which was followed by rapid sea-floor spreading, creating the Arabian Sea (see e.g. Gunnell et al., 2003; Widdowson, 1997; Campanile et al., 2008, & references therein). The separation of India from Seychelles coincided with the emplacement of the Deccan Traps. After the late Cretaceous, the Indian plate moved rapidly northwards before colliding with Eurasia in the Eocene – early Oligocene (Whiting et al., 1994).

On the western margin of India, the narrow, low-lying coastal plain (Konkan-Kanara lowlands) and the elevated plateau (Karnataka and Maharashtra uplands) are separated by the steep Western Ghats (a.k.a. Sahyadri) escarpment (Gunnell et al., 2003). The Karnataka plateau has a mean elevation of 0.6 – 0.9 km, with individual summits up to 1.9 km high (Figure 2.20). The escarpment extends over a distance of 1500 km, roughly parallel to the coast, regardless of the lithology or structure and forms the main drainage divide of India (Tiwari et al., 2006; Widdowson & Cox, 1996). Negative gravity anomalies are observed over the whole of India (Kailasam, 1979) and can be explained by the presence of a low density layer in the upper mantle extending 400 km laterally beneath the Ghats (Tiwari et al., 2006; Pandey et al., 1996). Published values of the elastic thickness of the western Indian margin range from 8 – 100 km; the lowest values are predicted by gravity studies

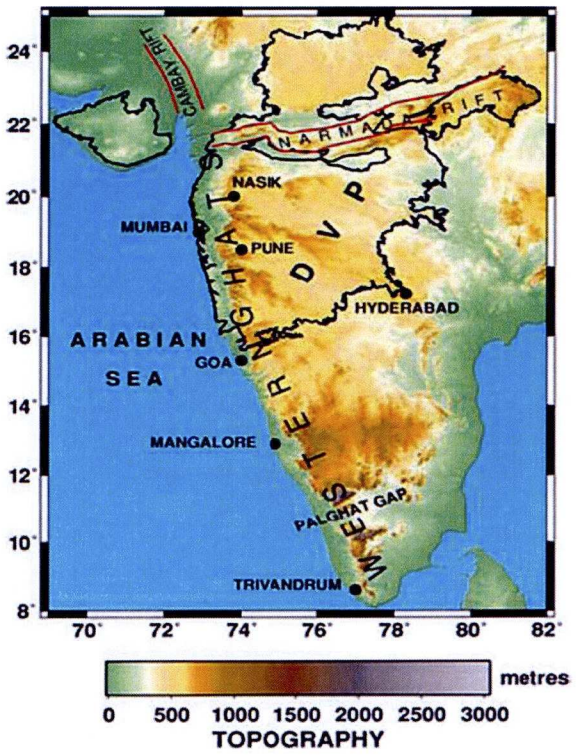

Figure 2.20: Topographic map of India (from Tiwari et al., 2006). DVP = Deccan Volcanic Province.

(Campanile et al., 2008) and the higher values are predicted by studies modelling denudation patterns (e.g. Gunnell & Fleitout, 1998; Widdowson & Cox, 1996).

The Deccan Traps cover a massive area with only slight changes in thickness, suggesting that the Indian margin was relatively flat when they were emplaced (Figure 2.21; Widdowson & Cox, 1996). It is thought that they dipped very gently to the east, therefore the surface adjacent to the rifted margin must have been above sea-level (Widdowson, 1997), although it is not known by how much. The formation of the escarpment post-dates the emplacement of the Deccan Traps (Gunnell et al., 2003). It has been suggested that the escarpment originated as a fault scarp and has retreated inland by an estimated 100 – 180 km since its formation (e.g. Widdowson, 1997). If this is the case, the fault line defining the escarpment would now be located seaward of the present coastline; several fault lines are identified offshore but none define the escarpment, so it is considered primarily an erosional feature (Gunnell et al., 2003; Widdowson & Cox, 1996; Campanile et al., 2008).

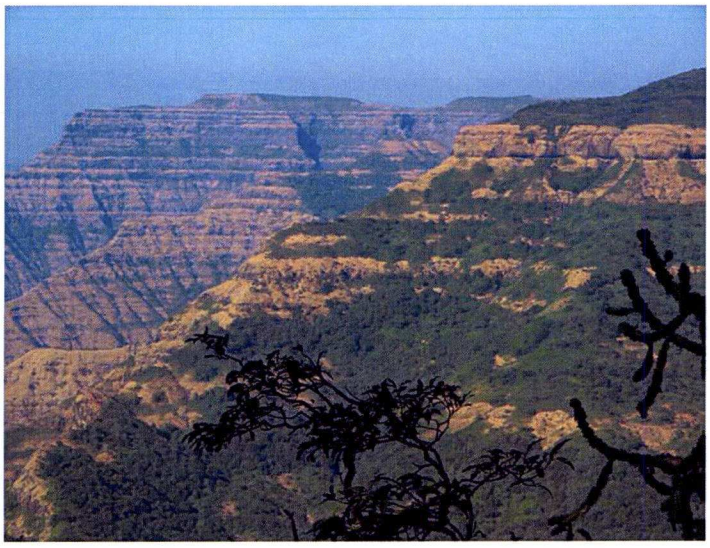

Figure 2.21: The Western Ghats escarpment (from Sheth, 2007). A late Cretaceous erosion surface tops the near-horizontal Deccan flood basalts.

India had a warm and humid climate throughout the Tertiary (Harbor & Gunnell, 2007; Gunnell, 1998). It is thought that the monsoon system, which developed at ~15 Ma, may have strengthened at 11 Ma, indicated by a change in the offshore sediment deposition, from carbonate to clastic sediments (Whiting et al., 1994).

AFT data indicate the uplift of western India has occurred since 60 – 70 Ma (Kalaswad et al., 1993). An alternative study of AFT data found denudation rates peaked at 130 Ma, 80 Ma, and 65 Ma, coincident with the rifting of India from Antarctica, Madagascar and Seychelles respectively (Gunnell et al., 2003). The phase of increased denudation observed at 65 Ma is supported by the offshore stratigraphic record of the Konkan and Kerala Basins, which shows a pulse of sedimentation in the Palaeocene (Campanile et al., 2008). A later phase of increased sedimentation beginning in the Pliocene is also observed (Campanile et al., 2008) but the cause of this is more enigmatic, although other studies suggest a climatic link (Whiting et al., 1994). The stratigraphic record of the Bay of Bengal, where material eroded to the east of the escarpment is deposited, indicates a period of increased erosion in the middle Eocene (Gunnell et al., 2003). Sheth (2007) suggested that tectonic uplift of the margin occurred in the Neogene.

AFT data predict that less than 1 km of denudation has occurred on the elevated regions of the western Indian margin since 50 Ma (Gunnell et al., 2003). This is consistent with a study of land surface correlation, which required at least 1.2 km of denudation on the plateau (Gunnell & Fleitout, 1998), and roughly equal to the magnitude of Neogene tectonic uplift (~1 km) proposed by Sheth (2007). A different AFT study suggests up to 2 – 4 km of material has been denuded in coastal areas and around 500 m inland of the escarpment since the early Palaeocene (Campanile et al., 2008). A relatively recent coast-parallel uplift of the northern part of India relative to the south, of approximately 100 m over a distance of 165 km, has also been documented (Widdowson & Cox, 1996).

Several mechanisms have been proposed to explain the uplift of India. Geodynamical mechanisms that have been investigated include mantle processes associated with a rising plume (e.g. Kailasam, 1979, & references therein), magmatic underplating (Gunnell & Fleitout, 1998), and buoyancy forces due to the shallow upper mantle low velocity zone beneath the Ghats (Tiwari et al., 2006). However, there is little support from the observations for such processes. A geomorphological cause for the uplift in the form of either denudational unloading or scarp retreat has also been suggested (e.g. Widdowson & Cox, 1996).

2.11 South-eastern Australia

The formation of the South-East Australian margin began with the onset of rifting at ~ 95 Ma which eventually lead to continental breakup between Australia and Antarctica, and the initiation of sea-floor spreading in the Tasman Sea at ~ 80 Ma (Ollier, 1995; van der Beek & Braun, 1999; van der Beek et al., 1999, & references therein). Throughout the Cenozoic, the margin was affected by widespread basaltic volcanism (van der Beek & Braun, 1999).

The South-East Australian Highlands are an uplifted area approximately 300 km wide (Stephenson & Lambeck, 1985; Wellman, 1979) with an elevation of 600 – 1000 m (Figures 2.22 & 2.23; van der Beek & Braun, 1999). They are separated from the coastal plain by the Great Escarpment which is up to 1 km high and stretches the entire ~ 2500 km length of the south-eastern Australian rifted margin (Braun & van der Beek, 2004). The escarpment of south-eastern Australia differs

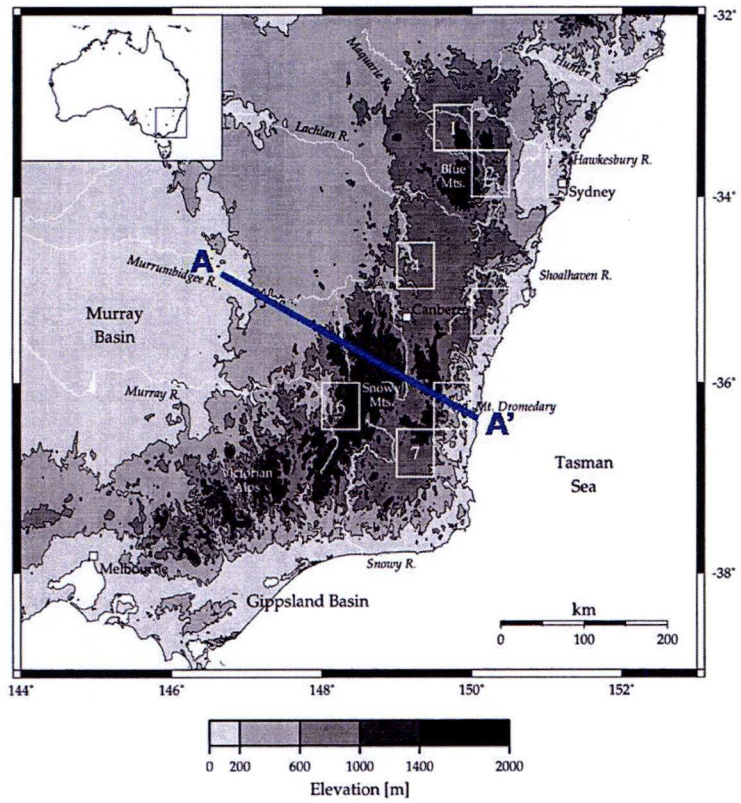

Figure 2.22: Topographic map of south-eastern Australia (from van der Beek & Braun, 1998). Line shows the location of the topographic profile in Figure 2.23.

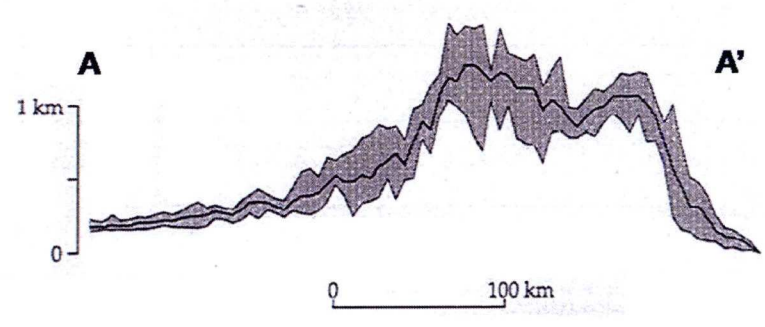

Figure 2.23: Topographic profile through the Snowy Mountains (from van der Beek & Braun, 1999). Lines correspond to average, minimum and maximum elevations.

from that at other rifted margins in that it is not broadly coincident with the drainage divide; instead, the drainage divide lies 50 – 100 km inland of the escarpment (Pain, 1985; Persano et al., 2005). There is no obvious relationship between the position of the escarpment and lithology or structures (Persano et al., 2005), except to the east of the Blue Mountains where it is defined by the Lapstone Structural Complex, a faulted monocline (van der Beek et al., 2001). It is thought, however, that the lithology may play a role in the development of the topography, with the horizontal bedding in the resistant Triassic sandstones controlling the flatness of the plateaux (Figure 2.24; van der Beek et al., 2001). The AFT data imply that the escarpment attained its current position by 10 – 20 Myr after continental breakup (Braun & van der Beek, 2004; Persano et al., 2002).

A strong negative Bouguer gravity anomaly runs the entire length of the highlands and they are located above a region of slow upper mantle seismic velocities (van der Beek & Braun, 1999). It is thought that the highlands are in isostatic equilibrium, suggesting they are not supported by high heat flow (Bishop, 1988). Gravity studies suggest that the lithosphere strength in the region is relatively low (Wellman, 1988) and estimates of the elastic thickness range from 5 – 50 km (Bishop & Brown, 1992).

The climate of south-eastern Australia is thought to have been fairly temperate, with widespread forests until the late Cenozoic giving rise to low denudation rates

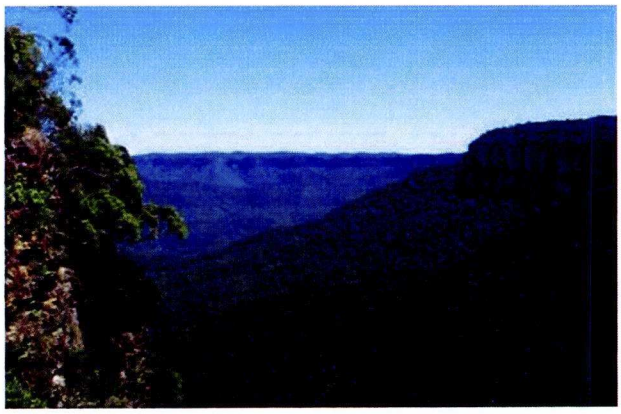

Figure 2.24: A peneplain at the Blue Mountains. Photograph courtesy of Sheona Masterton.

(van der Beek & Braun, 1998; Bishop, 1988). It is known that the highlands have been subaerial since the Cretaceous (van der Beek et al., 1999) and surface process models suggest the plateaux were initially a few hundred metres high (van der Beek & Braun, 1999).

Early geomorphological studies suggested the uplift of south-eastern Australia was a relatively recent phenomenon, occurring in the Late Pliocene or Pleistocene (Bishop, 1988; Stephenson & Lambeck, 1985, & references therein). However, this notion was discounted when the lavas in the highlands were dated, demonstrating that the peneplains were much older than this (Bishop, 1988). It has since been proposed that the uplift occurred during the Palaeozoic and early Mesozoic, with the highlands being simply an erosional remnant of a much larger mountain range (Stephenson & Lambeck, 1985). Brown (2000), however, argues against tectonic stability since that time; instead invoking a gentle seaward tilting of the margin in the late Cenozoic. Surface process models of the landscape evolution, which consider the drainage and denudational history of the margin, indicate there may be no need to invoke large-scale uplift events (van der Beek et al., 1999).

AFT data studies show a phase of increased denudation on the south-eastern Australian margin at 120 – 100 Ma (Persano et al., 2005), or alternatively at 100 – 80 Ma (van der Beek & Braun, 1999; Moore et al., 1986). This later phase coincides with rifting and the onset of sea-floor spreading in the Tasman Sea (Braun & van der Beek, 2004). Wellman (1988) suggested that uplift of the Highlands may have occurred between 160 – 80 Ma, or that there has been semi-continuous uplift since 70 Ma. A study of river bed heights indicates a constant uplift rate since at least 45 Ma (Wellman, 1979) although it has been argued that river incision is a standard process in landscape evolution and therefore cannot be used as an indicator for dynamic uplift (Bishop, 1988). Other researchers have inferred that the uplift began at 95 Ma, coinciding with a major change in sedimentation pattern and tectonics (van der Beek & Braun, 1999, & references therein).

There now seems to be a consensus that south-eastern Australia, with the exception of the Blue Mountains and the East Victoria Highlands has been relatively stable since the mid-Cenozoic (van der Beek et al., 2001; Bishop, 1998, & references therein). The uplift of the Blue Mountains is thought to have occurred before the basalts were emplaced in the Miocene, with palaeomagnetic data constraining the last movement on the Lapstone Structural Complex to be during the Palaeogene (van

der Beek et al., 2001). The depositional history of the East Victoria Highlands indicates post-Mesozoic uplift (Bishop, 1998, & references therein), with stratigraphic relationships in Southern Victoria implying a significant generation of topographic relief towards the end of the Miocene (Sandiford et al., 2004).

AFT studies indicate that since 100 Ma, a much greater amount of denudation has taken place on the coastal plain of South-East Australia than in the highlands (van der Beek & Braun, 1998). However, estimates of the magnitude of denudation vary between studies, in part because of the uncertainty in the palaeogeothermal gradient for the region. Moore (1986) gives values of 1.5 – 2.5 km of denudation in the coastal regions, whilst Persano et al. (2002) found 3 – 4 km of denudation along the coast within 28 Myr of breakup, and Ollier (1995) suggests less than 1 km of denudation has occurred at the Great Escarpment. From other techniques, less than 200 m of material is thought to have been removed from the Blue Mountain plateau since the Miocene (van der Beek et al., 2001). A landscape development model of the highlands predicts 1.5 – 2 km of denudation on the coastal plain since 100 Ma (van der Beek et al., 1999), whilst Wellman (1979) suggest there has been up to 1.5 km of uplift since the late Mesozoic.

As with the other uplifted rifted margins, several mechanisms have been suggested to explain the elevation of the south-eastern Australian margin. It has been proposed that the uplift is in some way related to late Cretaceous rifting, either by magmatic underplating or rift shoulder uplift, or to Tertiary volcanism, variations in intraplate stress due to plate reorganisation, or that the highlands are maintained by the isostatic response to denudational unloading (see e.g. van der Beek & Braun, 1999; van der Beek et al., 1999; van der Beek et al., 2001; Kohn et al., 2002; Gale, 1992). Alternatively, it has been hypothesised that the highlands are an erosional remnant of a pre-existing mountain belt (Lambeck & Stephenson, 1985). Specifically to the Blue Mountains, early Tertiary fault reactivation or a lithological control, or both, have been suggested (van der Beek et al., 2001).

2.12 Synthesis

Post-breakup tectonic uplift and/or phases of accelerated erosion have been suggested at all of the rifted margins discussed in this chapter. The margins appear to

have several similarities. Often, the elevated regions coincide with a large negative Bouguer gravity anomaly and several are suggested to have a thermal anomaly at depth. The escarpments which bound the uplifted plateaus are generally considered to be erosional features as they are not associated with major faulting. They are often capped by resistant rocks and coincident with a drainage divide. Some of the regions (e.g. southern Africa and south-eastern Australia) were elevated prior to breakup, whilst others (e.g. the North Atlantic margins) are thought to have been close to sea-level at some point after breakup. There are further differences between the margins regarding the observations of timing and magnitude of the uplift events, which are summarised in Figure 2.25 and Figure 2.26 respectively. Figure 2.26 also shows the timing of the events in Myr after breakup for each margin.

2.12.1 Timing of the hinterland uplift

Figure 2.25 is a summary of the proposed timing of the uplift events. All of the margins are suggested to have been uplifted or experienced a phase of accelerated erosion in the Neogene and many have events dated to around the time of continental breakup and between 30 – 50 Myr after breakup (Figure 2.26). Phases of increased erosion are often associated with climatic changes, rifting events, and reorganisation of the tectonic plates. In the North Atlantic, the Palaeogene uplift may coincide with the development of the Iceland plume but any link between the Neogene uplift and the Iceland plume is more tentative.

There is a consensus for two distinct uplift events on Norway in the Palaeogene and Neogene, although the exact timing of the events is still debated. East Greenland may have experienced up to four, relatively short-lived, Cenozoic uplift events, and West Greenland is thought to have experienced three phases of accelerated erosion (inferred to be related to uplift of the margin) since the late Eocene. Uplift of NE Brazil is dated to post-Albian. Both NE and SE Brazil show increased erosion in the late Cretaceous and in the Miocene. It is thought the uplift of southern Africa is a relatively recent phenomenon, dating from the Oligocene at the earliest. Two events have been suggested for western India – one in the early Palaeogene related to continental breakup, and one in the Neogene. Early geomorphological studies for South-East Australia suggested a semi-continuous uplift since continental breakup, but more recent AFT studies do not support post-breakup tectonic uplift of the margin.

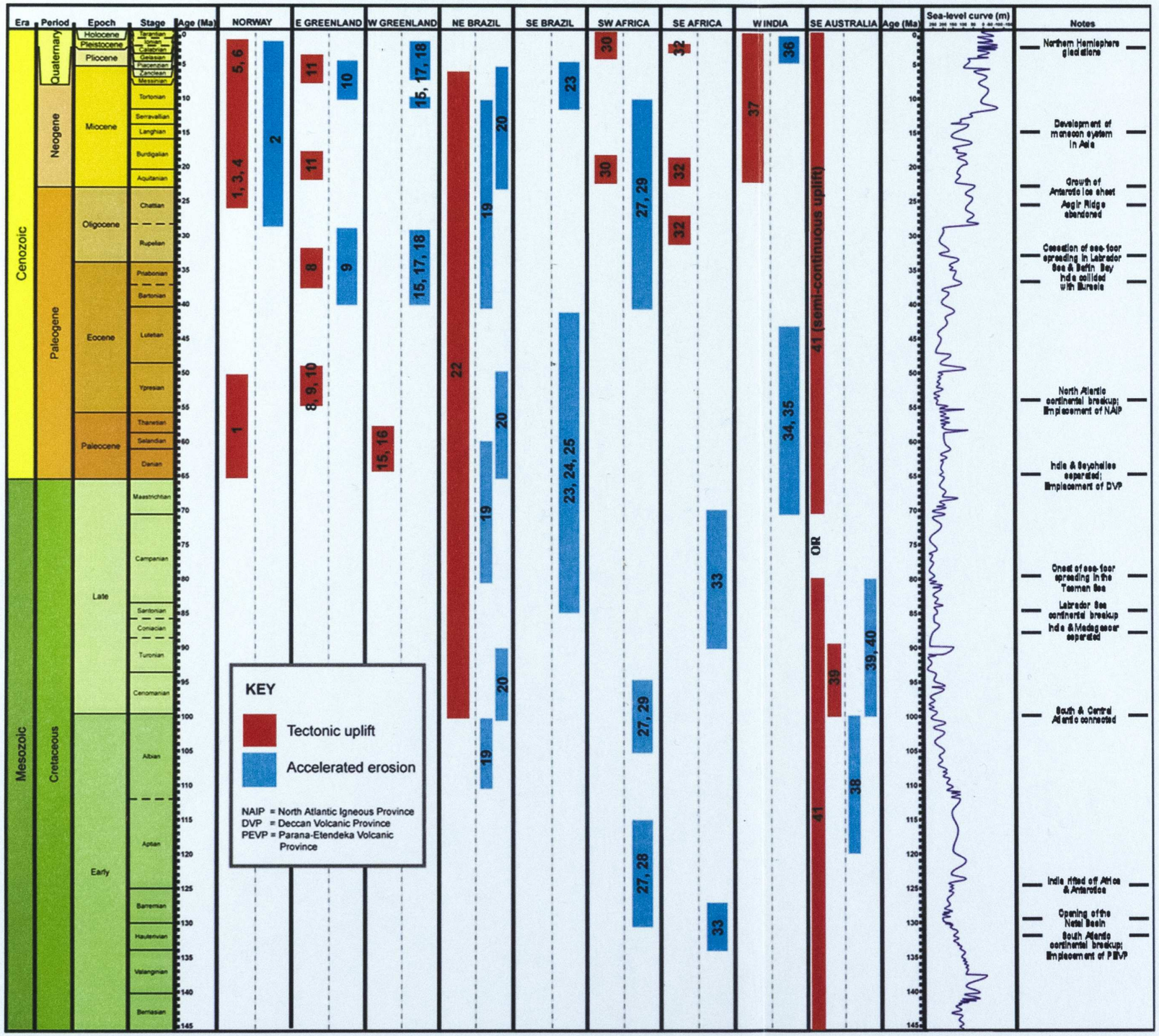

Figure 2.25: Timing of the proposed tectonic uplift and accelerated erosion events. The relation to sea-level height and major geological and climatic events is also shown. Numbers relate to references, given in Figure 2.26. Figure was created using Timescale Creator (TSCreator).

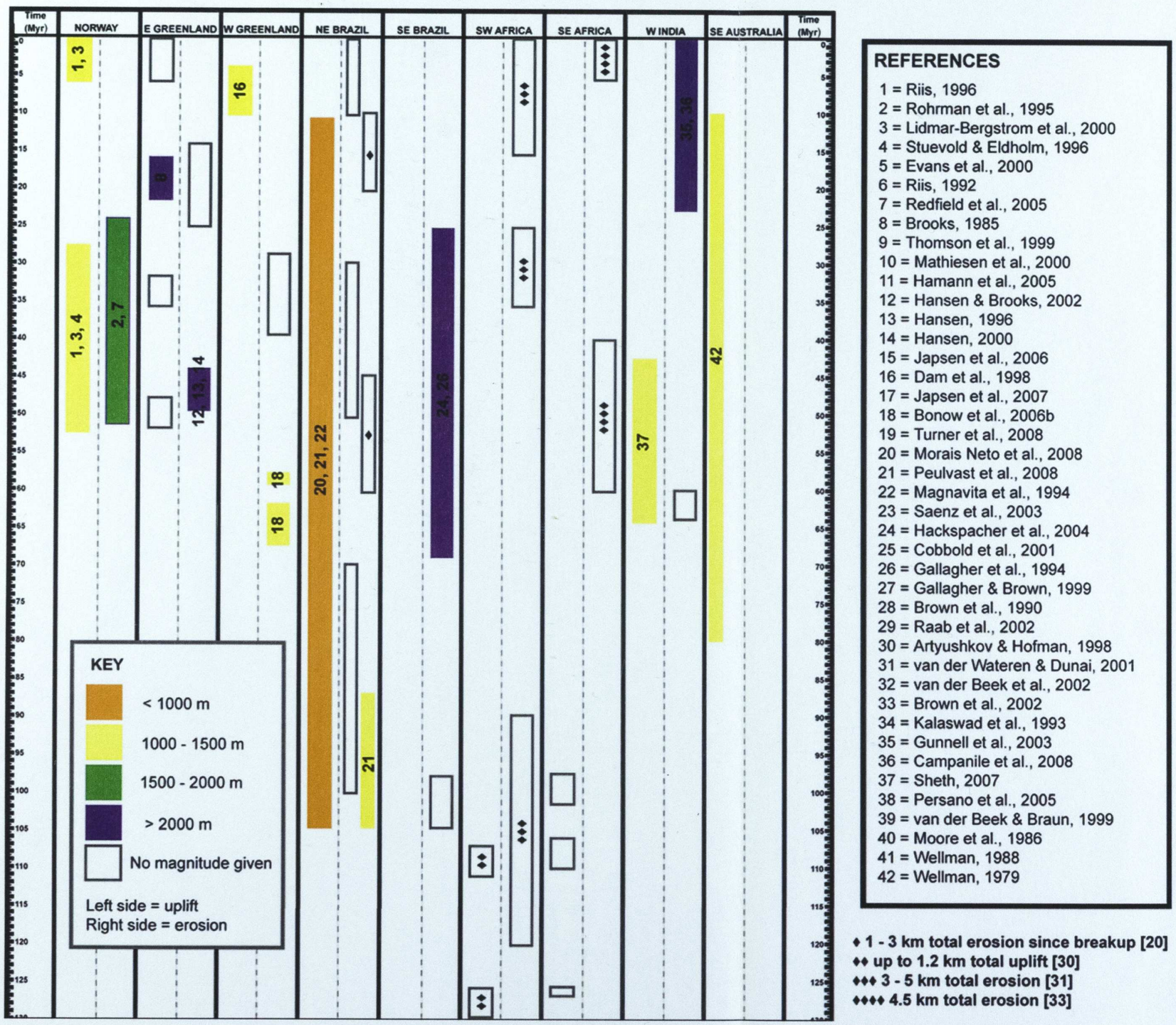

REFERENCES

1 = Riis, 1996
2 = Rohrman et al., 1995
3 = Lidmar-Bergstrom et al., 2000
4 = Stuevold & Eldholm, 1996
5 = Evans et al., 2000
6 = Riis, 1992
7 = Redfield et al., 2005
8 = Brooks, 1985
9 = Thomson et al., 1999
10 = Mathiesen et al., 2000
11 = Hamann et al., 2005
12 = Hansen & Brooks, 2002
13 = Hansen, 1996
14 = Hansen, 2000
15 = Japsen et al., 2006
16 = Dam et al., 1998
17 = Japsen et al., 2007
18 = Bonow et al., 2006b
19 = Turner et al., 2008
20 = Morais Neto et al., 2008
21 = Peulvast et al., 2008
22 = Magnavita et al., 1994
23 = Saenz et al., 2003
24 = Hackspacher et al., 2004
25 = Cobbold et al., 2001
26 = Gallagher et al., 1994
27 = Gallagher & Brown, 1999
28 = Brown et al., 1990
29 = Raab et al., 2002
30 = Artyushkov & Hofman, 1998
31 = van der Wateren & Dunai, 2001
32 = van der Beek et al., 2002
33 = Brown et al., 2002
34 = Kalaswad et al., 1993
35 = Gunnell et al., 2003
36 = Campanile et al., 2008
37 = Sheth, 2007
38 = Persano et al., 2005
39 = van der Beek & Braun, 1999
40 = Moore et al., 1986
41 = Wellman, 1988
42 = Wellman, 1979

♦ 1 - 3 km total erosion since breakup [20]
♦♦ up to 1.2 km total uplift [30]
♦♦♦ 3 - 5 km total erosion [31]
♦♦♦♦ 4.5 km total erosion [33]

Figure 2.26: Magnitude of tectonic uplift and denudation for each event. Time of events is shown for Myr after breakup at each margin.

2.12.2 Magnitude of the hinterland uplift

Estimates of the magnitude of the tectonic uplift events are always less than 1500 m (Figure 2.26). The magnitude of erosion is much larger; maximum erosion, of up to 4 -5 km, is often observed on the coastal plain whilst much lower values, of up to around 1 km, are measured on the elevated plateaus. On the North Atlantic margins, the proposed Neogene uplift events are thought to have a more domal shape. In some regions, the magnitude of uplift or erosion is simply given as a total since breakup, rather than being separated into individual events. In other cases, depending on the technique used, no magnitude has been given. It should be noted that Figures 2.25 and 2.26 only summarise the available data; if only phases of accelerated erosion are plotted on the chart, it does not mean there has been no tectonic uplift, rather that information cannot be demonstrated certainly from the study.

2.12.3 Distance between the maximum elevation and the ocean-continent transition (OCT)

If the uplift is in any way related to continental breakup and sea-floor spreading, it is important to know the approximate distance between the maximum elevation of the margin, and the OCT and Moho hinge (the location beyond which the crust has been thinned). If there is any pattern, this information may be used to provide some constraint on the uplift mechanism. A gravity inversion, using gravity data from Sandwell & Smith (2009) and bathymetry data from Smith & Sandwell (1997), has been performed for each of the areas to give the Moho depth (Figure 2.27); from this, the location of the OCT and Moho hinge can be determined. A description of the methodology is given in Greenhalgh & Kusznir (2007). The inversion uses the global sediment thickness map of Laske & Masters (1997) to provide a sediment thickness correction. No ice thickness correction has been applied to Greenland. The distance between the Moho hinge and the maximum elevation ranges between 100 – 300 km, and for the OCT the range is 200 – 550 km. There appears to be no correlation between the distance from the Moho hinge and the OCT and the maximum elevation. Osmundsen et al. (2010) suggest instead that a relationship exists between the taper length of a margin and the maximum onshore elevation, and therefore extensional faulting may exert some control on the post-breakup onshore evolution of a rifted margin.

West Greenland

Breakup age = 55 Ma
Reference crustal thickness = 35 km
Distance to maximum elevation from:
Moho hinge = 200 km
OCT = 400 km

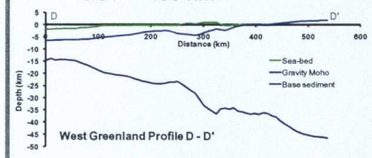

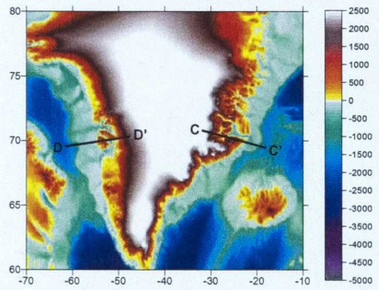

East Greenland

Breakup age = 55 Ma
Reference crustal thickness = 35 km
Distance to maximum elevation from:
Moho hinge = 225 km
OCT = 350 km

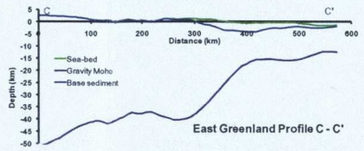

Norway

Breakup age = 55 Ma
Reference crustal thickness = 35 km

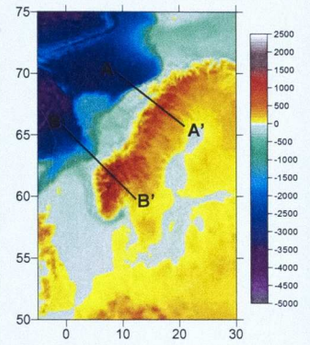

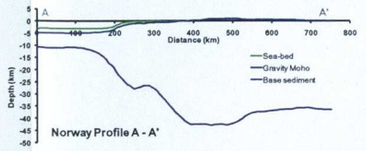

Distance to maximum elevation from:
Moho hinge = 100 km
OCT = 325 km

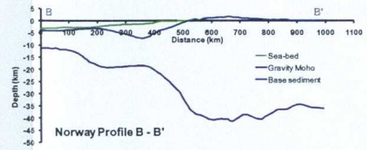

Distance to maximum elevation from:
Moho hinge = 100 km
OCT = 500 km

Brazil

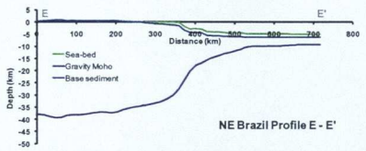

Distance to maximum elevation from:
Moho hinge = 300 km
OCT = 475 km

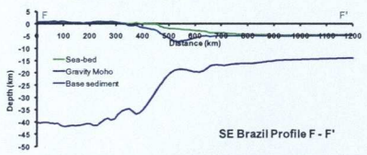

Distance to maximum elevation from:
Moho hinge = 200 km
OCT = 500 km

Breakup age = 110 Ma
Reference crustal thickness = 35 km

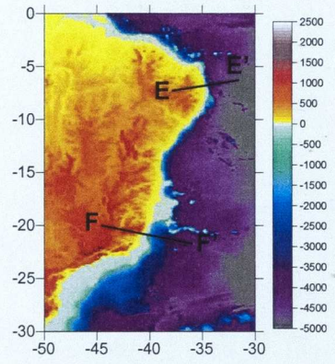

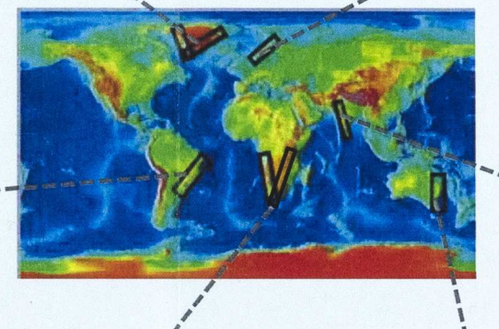

India

Breakup age = 65 Ma
Reference crustal thickness = 35 km
Distance of maximum elevation from:
Moho hinge = 150 km
OCT = 550 km

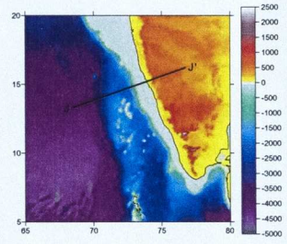

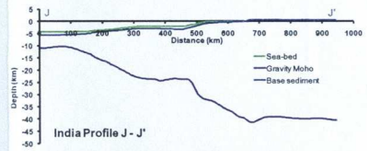

SW Africa

Breakup age = 130 Ma
Reference crustal thickness = 35 km
Distance to maximum elevation from:
Moho hinge = 250 km
OCT = 375 km

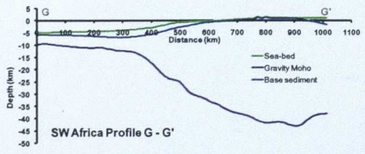

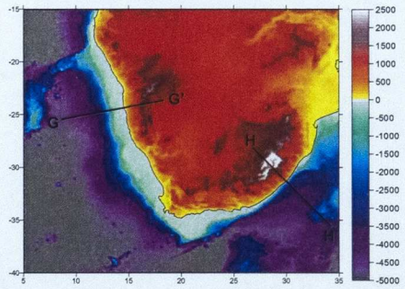

SE Africa

Breakup age = 130 Ma
Reference crustal thickness = 35 km
Distance to maximum elevation from:
Moho hinge = 200 km
OCT = 250 km

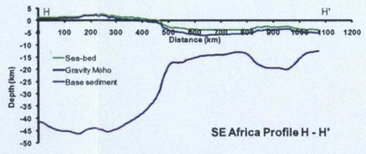

SE Australia

Breakup age = 80 Ma
Reference crustal thickness = 35 km
Distance to maximum elevation from:
Moho hinge = 150 km
OCT = 200 km

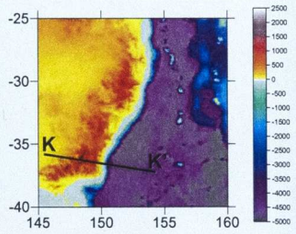

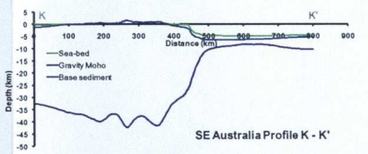

Figure 2.27: Cross sections of the margins discussed in this chapter, from gravity inversion. Distance to Moho hinge and distance to OCT from the maximum elevation are given for each margin.

2.13 Summary

There is strong observational evidence, from geophysics, geology and geomorphology, that uplift of the rifted margins has occurred since continental breakup. However, there remains a lack of consensus on the timing and magnitude of the uplift events. In part, this is due to the different techniques used and their limitations, and also to the scale of the study - whether local or regional. The use of AFT data has given some constraints on the margin's erosional history, but when used alone, fails to distinguish between accelerated erosion associated with uplift or other causes. There is an increasing awareness of both the need to use multiple techniques for the same study and to take an interdisciplinary approach.

Climatic changes, sea-level fluctuations, erosion and flexural isostasy are all important controls on the post-breakup development of the rifted margins, and can lead to significant (apparent) uplift. A climatic component for increased erosion is particularly important at glaciated margins. Nevertheless, for most margins, the need for a tectonic uplift component has been demonstrated. Many mechanisms have been proposed but, as yet, not one can satisfactorily match all of the observations; this will be discussed in more detail in the next chapter. Whilst progress in establishing the uplift history of the rifted margins has certainly been made since 1985, it seems C. F. Pain's statement may still hold some relevance today.

2.14 References

Alvey, A. D. (2010) Using Crustal Thickness & Continental Lithosphere Thinning Factors from Gravity Inversion to Refine Plate Reconstruction Models for the Arctic & North Atlantic, University of Liverpool, Liverpool.

Anell, I., H. Thybo and I. M. Aftemieva (2009), Cenozoic uplift and subsidence in the North Atlantic region: Geological evidence revisited, *Tectonophysics*, vol. 474, no. 1-2, p. 78-105.

Artyushkov, E. V. and A. W. Hofmann (1998), Neotectonic crustal uplift on the continents and its possible mechanisms. The case of Southern Africa, *Surveys in Geophysics*, vol. 19, no. 5, p. 369-415.

Bierman, P. R. and M. Caffee (2001), Slow rates of rock surface erosion and sediment production across the Namib Desert and escarpment, southern Africa, *American Journal of Science*, vol. 301, no. 4-5, p. 326-358.

Bishop, P. (1988), The Eastern Highlands of Australia - the Evolution of an Intraplate Highland Belt, *Progress in Physical Geography*, vol. 12, no. 2, p. 159-182.

Bishop, P. (1998), Griffith Taylor and the SE Australian Highlands: issues of data sources and testability in interpretations of long-term drainage history and landscape evolution, *Australian Geographer*, vol. 29, no. 1, p. 7-29.

Bishop, P. and R. Brown (1992), Denudational Isostatic Rebound of Intraplate Highlands - the Lachlan River Valley, Australia, *Earth Surface Processes and Landforms*, vol. 17, no. 4, p. 345-360.

Bonow, J. M., K. Lidmar-Bergstrom and P. Japsen (2006a), Palaeosurfaces in central West Greenland as reference for identification of tectonic movements and estimation of erosion, *Global and Planetary Change*, vol. 50, no. 3-4, p. 161-183.

Bonow, J. M., P. Japsen, K. Lidmar-Bergstrom, J. A. Chalmers and A. K. Pedersen (2006b), Cenozoic uplift of Nuussuaq and Disko, West Greenland - elevated erosion surfaces as uplift markers of a passive margin, *Geomorphology*, vol. 80, no. 3-4, p. 325-337.

Bonow, J. M., P. Japsen, P. F. Green, P. R. Cobbold, A. J. Pedreira, R. Lilletveit and D. Chiossi (2009), Post-rift landscape development of north-east Brazil, *Geological Survey of Denmark and Greenland Bulletin*, vol. 17, p. 81-84.

Braun, J. and P. van der Beek (2004), Evolution of passive margin escarpments: What can we learn from low-temperature thermochronology?, *Journal of Geophysical Research-Earth Surface*, vol. 109, no. F4, p. F4009.

Brooks, C. K. (1985), Vertical crustal movements in the Tertiary of central East Greenland: a continental margin at a hot-spot, *Zeitschrift Fur Geomorphologie N.F. Suppl. Bd 54*, p. 101-117.

Brown, M. C. (2000), Cenozoic tectonics and landform evolution of the coast and adjacent highlands of southeast New South Wales, *Australian Journal of Earth Sciences*, vol. 47, no. 2, p. 245-257.

Brown, R. W., M. A. Summerfield and A. J. W. Gleadow (2002), Denudational history along a transect across the Drakensberg Escarpment of southern Africa derived from apatite fission track thermochronology, *Journal of Geophysical Research-Solid Earth*, vol. 107, no. B12, p. 2350.

Brown, R. W., D. J. Rust, M. A. Summerfield, A. J. W. Gleadow and M. C. J. Dewit (1990), An Early Cretaceous Phase of Accelerated Erosion on the South-Western Margin of Africa - Evidence from Apatite Fission-Track Analysis and the Offshore Sedimentary Record, *Nuclear Tracks and Radiation Measurements*, vol. 17, no. 3, p. 339-350.

Campanile, D., C. G. Nambiar, P. Bishop, M. Widdowson and R. Brown (2008), Sedimentation record in the Konkan-Kerala Bsin: Implications for the evolution of the Western Ghats and the Western India passive margin, *Basin Research*, vol. 20, p. 3-22.

Chalmers, J. K. (2000), Offshore evidence for Neogene uplift in central West Greenland, *Global and Planetary Change*, vol. 24, no. 3-4, p. 311-318.

Christiansen, F. G., H. C. Larsen, C. Marcussen, K. Hansen, H. Krabbe, L. M. Larsen, S. Piasecki, L. Stemmerik and W. S. Watt (1992), Uplift Study of the Jameson Land Basin, East Greenland, *Norsk Geologisk Tidsskrift*, vol. 72, no. 3, p. 291-294.

Clift, P. D., A. Carter and A. J. Hurford (1996), Constraints on the evolution of the East Greenland Margin: Evidence from detrital apatite in offshore sediments, *Geology*, vol. 24, no. 11, p. 1013-1016.

Cloetingh, S., P. Reemst, H. Kooi and S. Fanavoll (1992), Intraplate Stresses and the Post-Cretaceous Uplift and Subsidence in Northern Atlantic Basins, *Norsk Geologisk Tidsskrift*, vol. 72, no. 3, p. 229-235.

Cobbold, P. R., K. E. Meisling and V. S. Mount (2001), Reactivation of an obliquely rifted margin, Campos and Santos basins, southeastern Brazil, *Aapg Bulletin*, vol. 85, no. 11, p. 1925-1944.

Dam, G., M. Larsen and M. Sonderholm (1998), Sedimentary response to mantle plumes: Implications from Paleocene onshore successions, West and East Greenland, *Geology*, vol. 26, no. 3, p. 207-210.

Doré, A. G. (1992), The Base Tertiary Surface of Southern Norway and the Northern North-Sea, *Norsk Geologisk Tidsskrift*, vol. 72, no. 3, p. 259-265.

Doré, A. G., E. R. Lundin, N. J. Kusznir and C. Pascal (2008) Potential mechanisms for the genesis of Cenozoic domal structures on the NE Atlantic margin: pros, cons and some new ideas, in Johnson, H., A. G. Doré, R. W. Gatliff, R. Holdsworth, E. Lundin and J. D. Ritchie (eds), *The Nature and Origin of Compression in Passive Margins*, The Geological Society of London, vol. Geological Society, London, Special Publications, 306, p. 1-26.

Doré, A. G., J. A. Cartwright, M. S. Stoker, J. P. Turner and N. J. White (2002) Exhumation of the North Atlantic margin: introduction and background, in Doré, A. G., J. A. Cartwright, M. S. Stoker, J. P. Turner and N. J. White (eds), *Exhumation of the North Atlantic Margin: Timing, Mechanisms and Implications for Petroleum Exploration*, Geological Society, London, Special Publications, vol. 196, p. 1-12.

Ebbing, J. (2007), Isostatic density modelling explains the missing root of the Scandes, *Norwegian Journal of Geology*, vol. 87, no. 1-2, p. 13-20.

Ebbing, J. and O. Olesen (2005), The Northern and Southern Scandes - structural differences revealed by an analysis of gravity anomalies, the geoid and regional isostasy, *Tectonophysics*, vol. 411, no. 1-4, p. 73-87.

Eldrett, J. S., I. C. Harding, P. A. Wilson, E. Butler and A. P. Roberts (2007), Continental ice in Greenland during the Eocene and Oligocene, *Nature*, p. 1-4.

Engen, Ø., J. I. Faleide and T. K. Dyreng (2008), Opening of the Fram Strait gateway; a review of plate tectonic constraints, *Tectonophysics*, vol. 450, no. 1-4, p. 51-69.

Evans, D., S. McGiveron, A. E. McNeill, Z. H. Harrison, S. R. Ostmo and J. B. L. Wild (2000), Plio-Pleistocene deposits on the mid-Norwegian margin and their implications for late Cenozoic uplift of the Norwegian mainland, *Global and Planetary Change*, vol. 24, no. 3-4, p. 233-237.

Fleming, A., M. A. Summerfield, J. O. Stone, L. K. Fifield and R. G. Cresswell (1999), Denudation rates for the southern Drakensberg escarpment, SE Africa, derived from in-situ-produced cosmogenic Cl-36: initial results, *Journal of the Geological Society*, vol. 156, p. 209-212.

Gale, S. J. (1992), Long-Term Landscape Evolution in Australia, *Earth Surface Processes and Landforms*, vol. 17, no. 4, p. 323-343.

Gallagher, K. and R. Brown (1999), Denudation and uplift at passive margins: the record on the Atlantic Margin of southern Africa, *Philosophical Transactions of the Royal Society of London Series a-Mathematical Physical and Engineering Sciences*, vol. 357, no. 1753, p. 835-857.

Gallagher, K., C. J. Hawkesworth and M. S. M. Mantovani (1994), The Denudation History of the Onshore Continental-Margin of Se Brazil Inferred from Apatite Fission-Track Data, *Journal of Geophysical Research-Solid Earth*, vol. 99, no. B9, p. 18117-18145.

Gallagher, K., C. J. Hawkesworth and M. S. M. Mantovani (1995), Denudation, Fission-Track Analysis and the Long-Term Evolution of Passive Margin Topography - Application to the Southeast Brazilian Margin, *Journal of South American Earth Sciences*, vol. 8, no. 1, p. 65-77.

Gilchrist, A. R., H. Kooi and C. Beaumont (1994), Post-Gondwana Geomorphic Evolution of Southwestern Africa - Implications for the Controls on Landscape Development from Observations and Numerical Experiments, *Journal of Geophysical Research-Solid Earth*, vol. 99, no. B6, p. 12211-12228.

Greenhalgh, E. E. and N. J. Kusznir (2007), Evidence for thin oceanic crust on the extinct Aegir Ridge, Norwegian Basin, NE Atlantic derived from satellite gravity inversion, *Geophysical Research Letters*, vol. 34, no. 6, p. L06305.

Gunnell, Y. (1998), Passive margin uplifts and their influence on climatic change and weathering patterns of tropical shield regions, *Global and Planetary Change*, vol. 18, no. 1-2, p. 47-57.

Gunnell, Y. and L. Fleitout (1998), Shoulder uplift of the Western Ghats passive margin, India: A denudational model, *Earth Surface Processes and Landforms*, vol. 23, no. 5, p. 391-404.

Gunnell, Y., K. Gallagher, A. Carter, M. Widdowson and A. J. Hurford (2003), Denudation history of the continental margin of western peninsular India since the early Mesozoic - reconciling apatite fission-track data with geomorphology, *Earth and Planetary Science Letters*, vol. 215, no. 1-2, p. 187-201.

Hackspacher, P. C., L. F. B. Ribeiro, M. C. S. Ribeiro, A. H. Fetter, J. C. Hadler, C. E. S. Tello and E. L. Dantas (2004), Consolidation and break-up of the South American platform in southeastern Brazil: Tectonothermal and denudation histories, *Gondwana Research*, vol. 7, no. 1, p. 91-101.

Hamann, N. E., R. C. Whittaker and L. Stemmerik (2005) Geological development of the Northeast Greenland Shelf, in Dore, A. G. and B. A. Vining (eds), *Petroleum Geology: North-West Europe and Global Perspectives - Proceedings of the 6th Petroleum Geology Conference*, p. 887-902.

Hansen, K. (1992), Postorogenic Tectonic and Thermal History of a Rifted Continental-Margin - the Scoresby Sund Area, East Greenland, *Tectonophysics*, vol. 216, no. 3-4, p. 309-326.

Hansen, K. (1996), Thermotectonic evolution of a rifted continental margin: Fission track evidence from the Kangerlussuaq area, SE Greenland, *Terra Nova*, vol. 8, no. 5, p. 458-469.

Hansen, K. (2000), Tracking thermal history in East Greenland: an overview, *Global and Planetary Change*, vol. 24, no. 3-4, p. 303-309.

Hansen, K. and C. K. Brooks (2002), The evolution of the East Greenland margin as revealed from fission-track studies, *Tectonophysics*, vol. 349, no. 1-4, p. 93-111.

Haq, B. U., J. Hardenbol and P. R. Vail (1987), Chronology of Fluctuating Sea Levels since the Triassic, *Science*, vol. 235, no. 4793, p. 1156-1167.

Harbor, D. and Y. Gunnell (2007), Along-strike escarpment heterogeneity of the western ghats: A synthesis of drainage and topography using digital morphometric tools, *Journal of the Geological Society of India*, vol. 70, no. 3, p. 411-426.

Hartley, R., A. B. Watts and J. D. Fairhead (1996), Isostasy of Africa, *Earth and Planetary Science Letters*, vol. 137, no. 1-4, p. 1-18.

Hendriks, B. W. H. and P. A. M. Andriessen (2002) Pattern and timing of the post-Caledonian denudation of nothern Scandinavia constrained by apatite fission-track thermochronology, in Doré, A. G., J. A. Cartwright, M. S. Stoker, J. P. Turner and N. White (eds), *Exhumation of the North Atlantic Margins: Timing, Mechanisms and Implications for Petroleum Exploration*, Geological Society, London, Special Publications, vol. 196, p. 117-137.

Huuse, M. (2002) Cenozoic uplift and denudation of southern Norway: insights from the North Sea Basin, in Doré, A. G., J. A. Cartwright, M. S. Stoker, J. P. Turner and N. White (eds), *Exhumation of the North Atlantic Margin: Timing, Mechanisms and Implications for Petroleum Exploration*, Geological Society, London, Special Publications, vol. 196, p. 209-233.

Janssen, M. E., R. A. Stephenson and S. Cloetingh (1995), Temporal and Spatial Correlations between Changes in Plate Motions and the Evolution of Rifted Basins in Africa, *Geological Society of America Bulletin*, vol. 107, no. 11, p. 1317-1332.

Japsen, P. and J. A. Chalmers (2000), Neogene uplift and tectonics around the North Atlantic: overview, *Global and Planetary Change*, vol. 24, no. 3-4, p. 165-173.

Japsen, P., P. F. Green and J. A. Chalmers (2005), Separation of Palaeogene and Neogene uplift on Nuussuaq, West Greenland, *Journal of the Geological Society*, vol. 162, p. 299-314.

Japsen, P., J. M. Bonow, P. F. Green, J. A. Chalmers and K. Lidmar-Bergstrom (2006), Elevated, passive continental margins: Long-term highs or neogene uplifts? New evidence from West Greenland, *Earth and Planetary Science Letters*, vol. 248, no. 1-2, p. 330-339.

Japsen, P., J. M. Bonow, P. F. Green, J. A. Chalmers and K. Lidmar-Bergstrom (2009), Formation, uplift and dissection of planation surfaces at passive continental margins - a new approach, *Earth Surface Processes and Landforms*, vol. 34, no. 5, p. 683-699.

Kailasam, L. N. (1979), Plateau Uplift in Peninsular India, *Tectonophysics*, vol. 61, no. 1-3, p. 243-269.

Kalaswad, S., M. K. Roden, D. S. Miller and M. Morisawa (1993), Evolution of the Continental-Margin of Western India - New Evidence from Apatite Fission-Track Dating, *Journal of Geology*, vol. 101, no. 5, p. 667-673.

Kohn, B. P., A. J. W. Gleadow, R. W. Brown, K. Gallagher, P. B. O'Sullivan and D. A. Foster (2002), Shaping the Australian crust over the last 300 million years: insights from fission track thermotectonic imaging and denudation studies of key terranes, *Australian Journal of Earth Sciences*, vol. 49, no. 4, p. 697-717.

Lambeck, K. and R. Stephenson (1985), Post-Orogenic Evolution of a Mountain-Range - Southeastern Australian Highlands, *Geophysical Research Letters*, vol. 12, no. 12, p. 801-804.

Laske, G. and G. Masters (1997), A global digital map of sediment thickness, *Eos Transactions, AGU*, vol. 78, p. F483.

Lavier, L. L., M. S. Steckler and F. Brigaud (2001), Climatic and tectonic control on the Cenozoic evolution of the West African margin, *Marine Geology*, vol. 178, no. 1-4, p. 63-80.

Lidmar-Bergstrom, K., C. D. Ollier and J. R. Sulebak (2000), Landforms and uplift history of southern Norway, *Global and Planetary Change*, vol. 24, no. 3-4, p. 211-231.

Lidmar-Bergström, K. and J. O. Näslund (2002) Landforms and uplift in Scandinavia, in Doré, A. G., J. A. Cartwright, M. S. Stoker, J. P. Turner and N. White (eds), *Exhumation of the North Atlantic Margin: Timing, Mechanisms and Implications for Petroleum Exploration*, Geological Society, London, Special Publications, vol. 196, p. 103-116.

Lithgow-Bertelloni, C. and P. G. Silver (1998), Dynamic topography, plate driving forces and the African superswell, *Nature*, vol. 395, no. 6699, p. 269-272.

Lundin, E. and A. G. Doré (2002), Mid-Cenozoic post-breakup deformation in the 'passive' margins bordering the Norwegian-Greenland Sea, *Marine and Petroleum Geology*, vol. 19, no. 1, p. 79-93.

Magnavita, L. P., I. Davison and N. J. Kusznir (1994), Rifting, Erosion, and Uplift History of the Reconcavo-Tucano-Jatoba Rift, Northeast Brazil, *Tectonics*, vol. 13, no. 2, p. 367-388.

Mathiesen, A., T. Bidstrup and F. G. Christiansen (2000), Denudation and uplift history of the Jameson Land basin, East Greenland - constrained from maturity and apatite fission track data, *Global and Planetary Change*, vol. 24, no. 3-4, p. 275-301.

Miller, K. G., M. A. Kominz, J. V. Browning, J. D. Wright, G. S. Mountain, M. E. Katz, P. J. Sugarman, B. S. Cramer, N. Christie-Blick and S. F. Pekar (2005),

The phanerozoic record of global sea-level change, *Science*, vol. 310, no. 5752, p. 1293-1298.

Molnar, P. and P. England (1990), Late Cenozoic Uplift of Mountain-Ranges and Global Climate Change - Chicken or Egg, *Nature*, vol. 346, no. 6279, p. 29-34.

Moore, M. E., A. J. W. Gleadow and J. F. Lovering (1986), Thermal Evolution of Rifted Continental Margins - New Evidence from Fission Tracks in Basement Apatites from Southeastern Australia, *Earth and Planetary Science Letters*, vol. 78, no. 2-3, p. 255-270.

Morais Neto, J. M., K. A. Hegarty, G. D. Karner and F. F. Alkmim (2008), Timing and mechanisms for the generation and modification of the anomalous topography of the Borborema Province, northeastern Brazil, *Marine and Petroleum Geology*, p. 1-17.

Mosar, J., T. H. Torsvik and t. B. team (2002b) Opening of the Norwegian and Greenland Seas: Plate tectonics in Mid Norway since the Late Permian, in Eide, E. A. (ed.), *BATLAS - Mid Norway plate reconstruction atlas with global and Atlantic perspectives*, Geological Survey of Norway, p. 48-59.

Mosar, J., E. A. Eide, P. T. Osmundsen, A. Sommaruga and T. H. Torsvik (2002a), Greenland - Norway separation: A geodynamic model for the North Atlantic, *Norwegian Journal of Geology*, vol. 82, no. 4, p. 281-298.

Moulin, M., D. Aslanian and P. Unternehr (2010), A new starting point for the South and Equatorial Atlantic Ocean, *Earth-Science Reviews*, vol. 98, no. 1-2, p. 1-37.

Muller, R. D., C. Gaina, W. R. Roest and D. L. Hansen (2001), A recipe for microcontinent formation, *Geology*, vol. 29, no. 3, p. 203-206.

Nielsen, S. B., G. E. Paulsen, D. L. Hansen, L. Gemmer, O. R. Clausen, B. H. Jacobsen, N. Balling, M. Huuse and K. Gallagher (2002) Palaeocene initiation of Cenozoic uplift in Norway, in Doré, A. G., J. A. Cartwright, M. S. Stoker, J. P. Turner and N. White (eds), *Exhumation of the North Atlantic Margin: Timing, Mechanisms and Implications for Petroleum Exploration*, Geological Society, London, Special Publication, vol. 196, p. 45-65.

Nielsen, S. B., K. Gallagher, C. Leighton, N. Balling, L. Svenningsen, B. H. Jacobsen, E. Thomsen, O. B. Nielsen, C. Heilmann-Clausen, D. L. Egholm, M. A. Summerfield, O. R. Clausen, J. A. Piotrowski, M. R. Thorsen, M. Huuse, N. Abrahamsen, C. King and H. Lykke-Andersen (2009), The evolution of western Scandinavian topography: A review of Neogene uplift versus the ICE (isostasy-climate-erosion) hypothesis, *Journal of Geodynamics*, vol. 47, no. 2-3, p. 72-95.

Nyblade, A. A. and S. W. Robinson (1994), The African Superswell, *Geophysical Research Letters*, vol. 21, no. 9, p. 765-768.

Nyblade, A. A. and N. H. Sleep (2003), Long lasting epeirogenic uplift from mantle plumes and the origin of the Southern African Plateau, *Geochemistry Geophysics Geosystems*, vol. 4, p. 1102.

Ollier, C. D. (1995), Tectonics and Landscape Evolution in Southeast Australia, *Geomorphology*, vol. 12, no. 1, p. 37-44.

Osmundsen, P. T., T. F. Redfield and J. Ebbing (2010), Crustal thinning and topography at passive continental margins, *Geophysical Research Abstracts*, vol. 12, p. EGU2010-11745-1.

Pain, C. F. (1985), Morphotectonics of the continental margins of Australia, *Zeitschrift Fur Geomorphologie N.F. Suppl. Bd 54*, p. 23-35.

Pandey, O. P., P. K. Agrawal and J. G. Negi (1996), Evidence of low density sub-crustal underplating beneath western continental region of India and adjacent Arabian Sea: Geodynamical considerations, *Journal of Geodynamics*, vol. 21, no. 4, p. 365-377.

Persano, C., F. M. Stuart, P. Bishop and D. N. Barfod (2002), Apatite (U-Th)/He age constraints on the development of the Great Escarpment on the southeastern Australian passive margin, *Earth and Planetary Science Letters*, vol. 200, no. 1-2, p. 79-90.

Persano, C., F. M. Stuart, P. Bishop and T. J. Dempster (2005), Deciphering continental breakup in eastern Australia using low-temperature thermochronometers, *Journal of Geophysical Research-Solid Earth*, vol. 110, no. B12, p. B12405.

Peulvast, J. P. and V. Claudino-Sales (2004), Stepped surfaces and palaeolandforms in the northern Brazilian << Nordeste >>: constraints on models of morphotectonic evolution, *Geomorphology*, vol. 62, no. 1-2, p. 89-122.

Peulvast, J. P., V. Claudino-Sales, F. Betard and Y. Gunnell (2008), Low post-Cenomanian denudation depths across the Brazilian Northeast: Implications for long-term landscape evolution at a transform continental margin, *Global and Planetary Change*, vol. 62, no. 1-2, p. 39-60.

Praeg, D., M. S. Stoker, P. M. Shannon, S. Ceramicola, B. Hjelstuen, J. S. Laberg and A. Mathiesen (2005), Episodic Cenozoic tectonism and the development of the NW European 'passive' continental margin, *Marine and Petroleum Geology*, vol. 22, no. 9-10, p. 1007-1030.

Raab, M. J., R. W. Brown, K. Gallagher, A. Carter and K. Weber (2002), Late Cretaceous reactivation of major crustal shear zones in northern Namibia: constraints from apatite fission track analysis, *Tectonophysics*, vol. 349, no. 1-4, p. 75-92.

Redfield, T. F. (2010), On apatite fission track dating and the Tertiary evolution of West Greenland topography, *Journal of the Geological Society, London*, vol. 167, p. 261-271.

Redfield, T. F., P. T. Osmundsen and B. W. H. Hendriks (2005), The role of fault reactivation and growth in the uplift of western Fennoscandia, *Journal of the Geological Society*, vol. 162, p. 1013-1030.

Riis, F. (1992), Dating and Measuring of Erosion, Uplift and Subsidence in Norway and the Norwegian Shelf in Glacial Periods, *Norsk Geologisk Tidsskrift*, vol. 72, no. 3, p. 325-331.

Riis, F. (1996), Quantification of Cenozoic vertical movements of Scandinavia by correlation of morphological surfaces with offshore data, *Global and Planetary Change*, vol. 12, no. 1-4, p. 331-357.

Riis, F. and W. Fjeldskaar (1992) On the magnitude of the Late Tertiary and Quaternary erosion and its significance for the uplift of Scandinavia and the Barents Sea, in Larsen, R. M., H. Brekke, B. T. Larsen and E. Talleraas (eds), *Structural and Tectonic Modelling and its Application to Petroleum Geology*, NPF Special Publication, vol. 1, p. 163-185.

Roest, W. R. and S. P. Srivastava (1989), Sea-Floor Spreading in the Labrador Sea - a New Reconstruction, *Geology*, vol. 17, no. 11, p. 1000-1003.

Rohrman, M. and P. van der Beek (1996), Cenozoic postrift domal uplift of North Atlantic margins: An asthenospheric diapirism model, *Geology*, vol. 24, no. 10, p. 901-904.

Rohrman, M., P. van der Beek, P. Andriessen and S. Cloetingh (1995), Meso-Cenozoic Morphotectonic Evolution of Southern Norway - Neogene Domal Uplift Inferred from Apatite Fission-Track Thermochronology, *Tectonics*, vol. 14, no. 3, p. 704-718.

Rohrman, M., P. A. van der beek, R. D. van der Hilst and P. Reemst (2002) Timing and mechanism of North Atlantic Cenozoic uplift: evidence for mantle upwelling, in Doré, A. G., J. A. Cartwright, M. S. Stoker, J. P. Turner and N. White (eds), *Exhumation of the North Atlantic Margin: Timing, Mechanisms and Implications for Petroleum Exploration*, Geological Society, London, Special Publications, vol. 196, p. 27-43.

Saenz, C. A. T., P. C. Hackspacher, J. C. Hadler, P. J. Iunes, S. Guedes, L. F. B. Ribeiro and S. R. Paulo (2003), Recognition of Cretaceous, Paleocene, and Neogene tectonic reactivation through apatite fission-track analysis in Precambrian areas of southeast Brazil: association with the opening of the south Atlantic Ocean, *Journal of South American Earth Sciences*, vol. 15, no. 7, p. 765-774.

Sandiford, M., M. Wallace and D. Coblentz (2004), Origin of the in situ stress field in south-eastern Australia, *Basin Research*, vol. 16, no. 3, p. 325-338.

Sandwell, D. T. and W. H. F. Smith (2009), Global marine gravity from retracked Geosat and ERS-1 altimetry: Ridge segmentation versus spreading rate, *Journal of Geophysical Research*, vol. 114, p. B01411.

Seranne, M. and Z. Anka (2005), South Atlantic continental margins of Africa: A comparison of the tectonic vs climate interplay on the evolution of equatorial west Africa and SW Africa margins, *Journal of African Earth Sciences*, vol. 43, no. 1-3, p. 283-300.

Sheth, H. C. (2007) Plume-related regional prevolcanic uplift in the Deccan Traps: Absence of evidence, evidence of absence, in Foulger, G. R. and D. M. Jurdy (eds), *Plates, plumes, and planetary processes*, Geological Society of America Special Paper, vol. 430, p. 785-813.

Smith, W. H. F. and D. T. Sandwell (1997), Global seafloor topography from satellite altimetry and ship depth soundings, *Science*, vol. 277, p. 1957-1962.

Stephenson, R. and K. Lambeck (1985), Erosion-Isostatic Rebound Models for Uplift - an Application to Southeastern Australia, *Geophysical Journal of the Royal Astronomical Society*, vol. 82, no. 1, p. 31-55.

Stuevold, L. M. and O. Eldholm (1996), Cenozoic uplift of Fennoscandia inferred from a study of the mid-Norwegian margin, *Global and Planetary Change*, vol. 12, no. 1-4, p. 359-386.

Summerfield, M. A. (1991), Subaerial Denudation of Passive Margins - Regional Elevation Versus Local Relief Models, *Earth and Planetary Science Letters*, vol. 102, no. 3-4, p. 460-469.

Tenbrink, U. and T. Stern (1992), Rift Flank Uplifts and Hinterland Basins - Comparison of the Transantarctic Mountains with the Great Escarpment of Southern Africa, *Journal of Geophysical Research-Solid Earth*, vol. 97, no. B1, p. 569-585.

Thomson, K., P. F. Green, A. G. Whitham, S. P. Price and J. R. Underhill (1999), New constraints on the thermal history of North-East Greenland from apatite fission-track analysis, *Geological Society of America Bulletin*, vol. 111, no. 7, p. 1054-1068.

Tiwari, P. K., G. Surve and G. Mohan (2006), Crustal constraints on the uplift mechanism of the Western Ghats of India, *Geophysical Journal International*, vol. 167, no. 3, p. 1309-1316.

Torsvik, T. H., S. Rousse, C. Labails and M. A. Smethurst (2009), A new scheme for the opening of the South Atlantic Ocean and the dissection of an Aptian salt basin, *Geophysical Journal International*, vol. 177, no. 3, p. 1315-1333.

Turner, J. P., P. F. Green, S. P. Holford and S. R. Lawrence (2008), Thermal history of the Rio Muni (West Africa)-NE Brazil margins during continental breakup, *Earth and Planetary Science Letters*, vol. 270, no. 3-4, p. 354-367.

van Balen, R. T., P. A. van der Beek and S. A. P. L. Cloetingh (1995), The Effect of Rift Shoulder Erosion on Stratal Patterns at Passive Margins - Implications for Sequence Stratigraphy, *Earth and Planetary Science Letters*, vol. 134, no. 3-4, p. 527-544.

van der Beek, P. and J. Braun (1998), Numerical modelling of landscape evolution on geological time-scales: A parameter analysis and comparison with the south-eastern highlands of Australia, *Basin Research*, vol. 10, no. 1, p. 49-68.

van der Beek, P. and J. Braun (1999), Controls on post-mid-Cretaceous landscape evolution in the southeastern highlands of Australia: Insights from numerical surface process models, *Journal of Geophysical Research-Solid Earth*, vol. 104, no. B3, p. 4945-4966.

van der Beek, P., A. Pulford and J. Braun (2001), Cenozoic landscape development in the Blue Mountains (SE Australia): Lithological and tectonic controls on rifted margin morphology, *Journal of Geology*, vol. 109, no. 1, p. 35-56.

van der Beek, P., M. A. Summerfield, J. Braun, R. W. Brown and A. Fleming (2002), Modeling postbreakup landscape development and denudational history across the southeast African (Drakensberg Escarpment) margin, *Journal of Geophysical Research-Solid Earth*, vol. 107, no. B12, p. 2351.

van der Beek, P. A., J. Braun and K. Lambeck (1999), Post-Palaeozoic uplift history of southeastern Australia revisited: results from a process-based model of landscape evolution, *Australian Journal of Earth Sciences*, vol. 46, p. 157-172.

van der Wateren, F. M. and T. J. Dunai (2001), Late Neogene passive margin denudation history - cosmogenic isotope measurements from the central Namib desert, *Global and Planetary Change*, vol. 30, no. 3-4, p. 271-307.

Wellman, P. (1979), On the Cainozoic uplift of the southeastern Australian highlands, *Australian Journal of Earth Sciences*, vol. 26, no. 1, p. 1-9.

Wellman, P. (1988), Tectonic and Denudational Uplift of Australian and Antarctic Highlands, *Zeitschrift Fur Geomorphologie*, vol. 32, no. 1, p. 17-29.

Whiting, B. M., G. D. Karner and N. W. Driscoll (1994), Flexural and Stratigraphic Development of the West-Indian Continental-Margin, *Journal of Geophysical Research-Solid Earth*, vol. 99, no. B7, p. 13791-13811.

Widdowson, M. (1997) Tertiary palaeosurfaces of the SW Deccan, Western India: implications for passive margin uplift, in Widdowson, M. (ed.), *Palaeosurfaces: Recognition, Reconstruction and Palaeoenvironmental Interpretation*, Geol. Soc. Spec, Pub., vol. 120, p. 221-248.

Widdowson, M. and K. G. Cox (1996), Uplift and erosional history of the Deccan Traps, India: Evidence from laterites and drainage patterns of the Western Ghats and Konkan Coast, *Earth and Planetary Science Letters*, vol. 137, no. 1-4, p. 57-69.

Zachos, J., M. Pagani, L. Sloan, E. Thomas and K. Billups (2001), Trends, rhythms, and aberrations in global climate 65 Ma to present, *Science*, vol. 292, no. 5517, p. 686-693.

Chapter 3

Literature review of postulated uplift mechanisms

3.1 Introduction

In the previous chapter, a number of mechanisms have been mentioned which are considered capable of generating significant rifted margin hinterland uplift. It remains to be established, however, which, if any, of the mechanisms actually contribute to the uplift (Doré et al., 2002; Anell et al., 2009). Any mechanism invoked needs to account for the timing, magnitude and wavelength of the uplift. The lack of consensus regarding the observations of post-breakup uplift makes it difficult to properly test the proposed mechanisms, and therefore the mechanisms which work cannot be easily identified. The postulated mechanisms can be divided into those which cause transient uplift and those which lead to permanent uplift of the continental hinterland. Transient mechanisms are mainly related to thermal mantle anomalies and include mantle diapirism and lithosphere delamination. Other uplift mechanisms include magmatic underplating, which involves addition of material to the crust, intraplate compressive stress, and the flexural isostatic response to erosional and glacial unloading. These are all reviewed in this chapter, with consideration given to the observations that they can match, and their limitations.

3.2 Early geomorphological models

Early 20th Century ideas surrounding hinterland uplift at rifted margins centred around the response to an initial phase of uplift as a geomorphological model termed the "cycle of erosion", referenced most prominently to W. M. Davis (e.g. King, 1953). This is where a region is uplifted and then subjected to erosion and river incision, leading to an increase in relief. The landscape would then be weathered and

reduced to a peneplain. Another early mechanism suggested for the topographic evolution of an uplifted rifted margin was parallel scarp retreat, proposed by W. Penck (see review in King, 1953). This involves the formation of an escarpment at the margin at continental breakup, which then steadily retreated to its present day position (Figure 3.1). King (1953) further developed this theory into a model of cyclic scarp retreat, whereby several erosion surfaces formed as a result of pulses of tectonic uplift and subsequent erosion. However, for south-eastern Africa, the area studied by King (1953), the timing of the hypothesised post-breakup tectonic uplift pulses do not correlate with increases in offshore sedimentation (van der Beek et al., 2002). Recent models, supported by AFT studies, suggest that the escarpment may

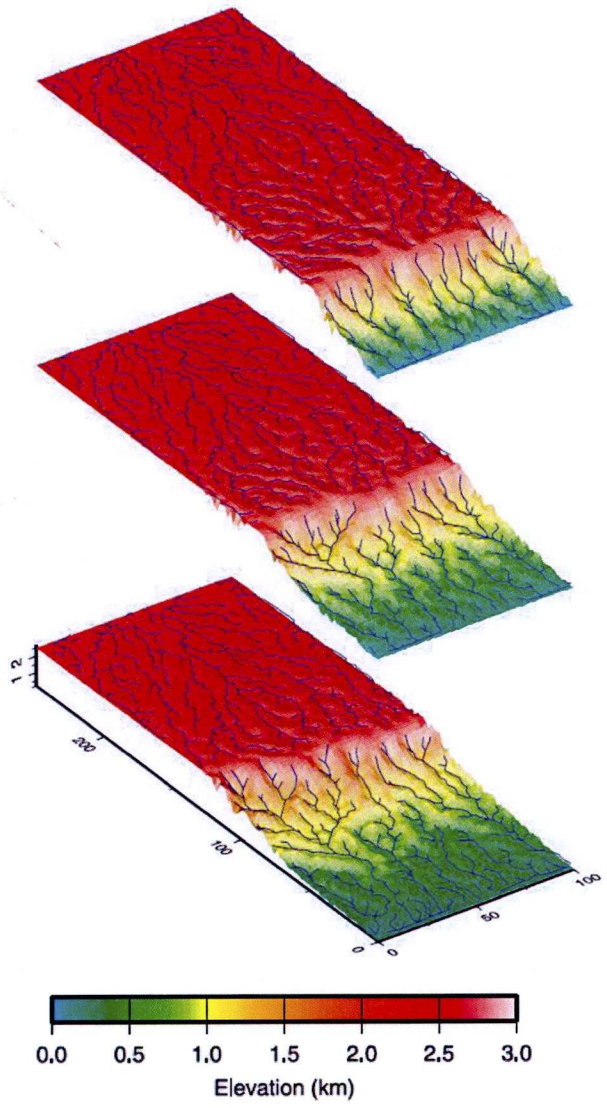

Figure 3.1: Model of escarpment retreat through time from van der Beek et al. (2002). Top = 100 Ma, middle = 60 Ma and bottom = present day.

reach its present-day configuration relatively quickly after breakup (Bierman & Caffee, 2001; Campanile et al., 2008, & references therein), with the escarpment initially forming due to a drop in base level (Braun & van der Beek, 2004). These geomorphological models only consider the response to an uplift event; they do not indicate what mechanism caused the initial uplift.

3.3 Flexural isostatic response to unloading

Unloading of sediments onshore and the offshore loading due to their subsequent deposition leads to tilting and flexural uplift of the continental hinterland. This has been argued by Widdowson (1997) and Campanile et al. (2008) to be the best explanation for the long-term uplift of the western Indian margin. The resulting flexural deflection caused by the erosion of basalts from the coastal plain has the same wavelength as the observed uplift, although it fails to predict the depth to basement offshore (Campanile et al., 2008). It has been proposed that the South-East Australian Highlands were formed by the erosion and isostatic rebound of a Palaeozoic mountain belt (Lambeck & Stephenson, 1985; Stephenson & Lambeck, 1985). However, their assumption that erosion rate is proportional to elevation has attracted some criticism (van der Beek & Braun, 1999), and the palaeotopography in the Late Palaeozoic is not known (Bishop, 1988). Furthermore, a flexural uplift model cannot match the negative Bouguer anomaly observed over the highlands (van der Beek & Braun, 1999). The flexural isostatic response to erosion and glacial unloading is considered a possible explanation for the uplift of Norway (Nielsen et al., 2009; Riis & Fjeldskaar, 1992) but calculations show that a tectonic component of uplift, or alternatively inherited topography at continental breakup, is still required to predict the present-day topography.

3.4 Intraplate compressive stress

It has been proposed that fluctuations in the stress regime of tectonic plates can give rise to significant vertical motions (Cloetingh et al., 1992). Regional compression of the lithosphere may lead to both uplift of the rift flanks and accelerated subsidence of the basins, with displacement rates much greater than

those predicted by thermal subsidence determined from the McKenzie (1978) model. This model can account for the anomalous subsidence of the basins around the North-East Atlantic during the late Neogene, as plate reorganisations in the North Atlantic and the collision of Eurasia and Africa gave an increase in intraplate compressive forces (Cloetingh et al., 1992). A major problem with this model is that the amount of uplift and subsidence predicted by the model is an order of magnitude too small (Japsen & Chalmers, 2000). Also, it is difficult to reconcile the timing of changes in the stress regime and the timing of the uplift of the Norwegian margin (Stuevold & Eldholm, 1996).

3.5 Magmatic underplating

It has been suggested that if rifting is associated with the generation of substantial volumes of melt, much of that melt would be intruded at or near the Moho, leading to a thickening of the crust (Brodie & White, 1994; Cox, 1993). This would initially cause thermal uplift of the surface, which would subside as the intrusion cooled (Nielsen et al., 2002). It would also generate permanent uplift because the melt, whilst denser than the overlying crust, is less dense than the underlying mantle, increasing the buoyancy of the crust. The amount of uplift generated by underplating can be calculated, assuming Airy isostasy, using:

$$H = \left(1 - \frac{\rho_u}{\rho_m}\right) t_u \qquad [3.1]$$

where H = amount of uplift, t_u = thickness of the underplate, ρ_m = density of the mantle and ρ_u = density of the underplate (Brodie & White, 1994). This would predict 0.6 km of surface uplift for a 5 km thick underplate, which would be further amplified by the isostatic response to erosion. The resulting topography predicted by the model depends on the wavelength of the underplating material (Gallagher et al., 1994).

This mechanism has been proposed to have acted at several uplifted rifted margins, including East Greenland (Clift et al., 1996), Norway (Cox, 1993), south-eastern Australia (van der Beek & Braun, 1999), north-eastern Brazil (Magnavita et al., 1994; Peulvast et al., 2008; Morais Neto et al., 2008), and south-eastern Africa (Cox, 1993). However, there are limitations to this mechanism which prevent its

validation as a cause of hinterland uplift. It is difficult to estimate the amount of melt, and its density, which was intruded beneath the crust (Gunnell & Fleitout, 1998) and in some cases, there is a considerable time gap between volcanism and uplift of the continental hinterland.

For southern Norway, magmatic underplating can account for the low Bouguer gravity anomaly that is observed over regions of high topography (Nielsen et al., 2009), and crustal thickness estimates do not discount the possibility of a 6 km thick underplate underlying the crust (Rohrman & van der Beek, 1996). However, the underplate would have been intruded in the Eocene, coincident with continental breakup, and so cannot explain the Neogene uplift of southern Norway (Rohrman & van der Beek, 1996), and the nearest observed Eocene volcanism occurred 300 – 400 km offshore, a sizeable distance from the location of the uplift (Rohrman et al., 2002). Seismic and petrological evidence supports the existence of a magmatic underplate beneath South-East Australia, although the age of its emplacement has not yet been determined (van der Beek & Braun, 1999). For the other rifted margins, seismic and gravity data have not confirmed the existence of a thick underplate underlying the crust, although equally it cannot be ruled out (Morais Neto et al., 2008; van der Beek et al., 2002).

3.6 Transient (plume-related) uplift mechanisms

Transient, or dynamic, mechanisms are those where uplift is generated due to perturbation of the geotherm. Initial uplift occurs due to increased buoyancy, but the deflection is thought to decay according to the timescale of the thermal time constant of the lithosphere (~65 Myr), so transient mechanisms cannot directly explain the present topography of older margins (Gallagher & Brown, 1999). However, the initial uplifted topography would be eroded, leading to sediment deposition offshore and isostatic rebound of the onshore region, which could prolong the high topography (Widdowson & Cox, 1996). The opening of the North Atlantic is contemporaneous with the emplacement of flood basalts (Dam et al., 1998; Clift et al., 1998). A link between this and the Palaeogene uplift has been suggested by several researchers (e.g. Japsen & Chalmers, 2000). Likewise, uplift of North-East Brazil just after continental breakup may have occurred as the South American plate moved over the St Helena and Ascension plumes (Turner et al., 2008). Plume-related

mechanisms include lithosphere delamination and asthenospheric diapirism; these are discussed below, along with mechanisms proposed to explain the African Superswell.

3.6.1 The African Superswell & its possible mechanisms

The African Superswell is the anomalously elevated area consisting of the southern and eastern African plateaus, and a bathymetric swell with an amplitude of ~500 m in the south-eastern Atlantic Ocean (Figure 3.2; Nyblade & Robinson, 1994). These regions show a strong positive residual depth anomaly (Lithgow-Bertelloni & Silver, 1998). Stratigraphic records indicate that it may have been emplaced beneath southern Africa in the Neogene (Seranne & Anka, 2005). It is suggested that the African Superswell is caused, at least partly, by heating of the lithosphere; evidence in support of this includes the long-wavelength geoid high and the high heat flow measurements observed over the region (Nyblade & Robinson, 1994). Furthermore, the low seismic velocities determined at depth in the mantle

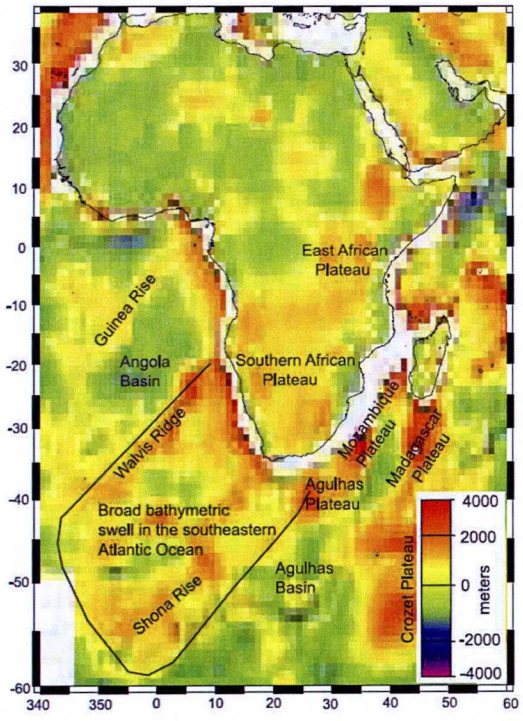

Figure 3.2: Residual depth anomaly for Africa and the south-eastern Atlantic, showing the location of the African Superswell (from Nyblade & Sleep, 2003).

beneath the region suggest that the elevated topography is compensated at depth (Lithgow-Bertelloni & Silver, 1998), whilst seismic tomography shows significant evidence for a lower mantle origin for the anomaly (Ritsema et al., 1999).

Lithgow-Bertelloni & Silver (1998) propose that dynamic topography can explain the African Superswell. In this model, the uplift is due to vertical stresses acting at the base of the lithosphere which are generated by flow in the (deep) mantle, imaged by seismic tomography as a low velocity anomaly. Dynamic topography would account for the geoid anomaly (Lithgow-Bertelloni & Gurnis, 1997). A model whereby uplift is generated by lingering plume tails has also been proposed for southern Africa (Nyblade & Sleep, 2003). This mechanism requires that the plume tails exist for 25-30 Myr, during which time hot material is continually supplied to the base of the lithosphere. Whilst there is some support from the timing of kimberlite eruptions in southern Africa for this model, it cannot generate the observed magnitude of the uplift (Nyblade & Sleep, 2003).

3.6.2 Asthenospheric diapirism

An asthenospheric diapirism model was proposed by Rohrman & van der Beek (1996) to explain the domal uplift of southern Norway. In this model, when hot oceanic asthenosphere, with elevated temperatures due to proximity to the Iceland plume, interacts with cold cratonic lithosphere, a Rayleigh-Taylor instability develops, leading to diapirism (Rohrman & van der Beek, 1996). The stages of this model, applied to southern Norway, are shown in Figure 3.3. When the low-viscosity oceanic asthenosphere impinges at the base of the higher viscosity continental lithosphere, the low-viscosity asthenosphere penetrates the lithosphere forming evenly-spaced diapirs.

Whilst the main uplift associated with diapirism is transient, it may also generate permanent uplift through magmatic underplating (Rohrman & van der Beek, 1996). Domal uplift has also been reported at other North-East Atlantic margins, for example East Greenland (Brooks, 1985). Rohrman & van der Beek (1996) report that this mechanism can explain many of the observations of the post-breakup hinterland uplift and agrees with AFT data for the region. However, Nielsen et al. (2009) question its validity given the assumptions of timing and crustal thickness required in the model.

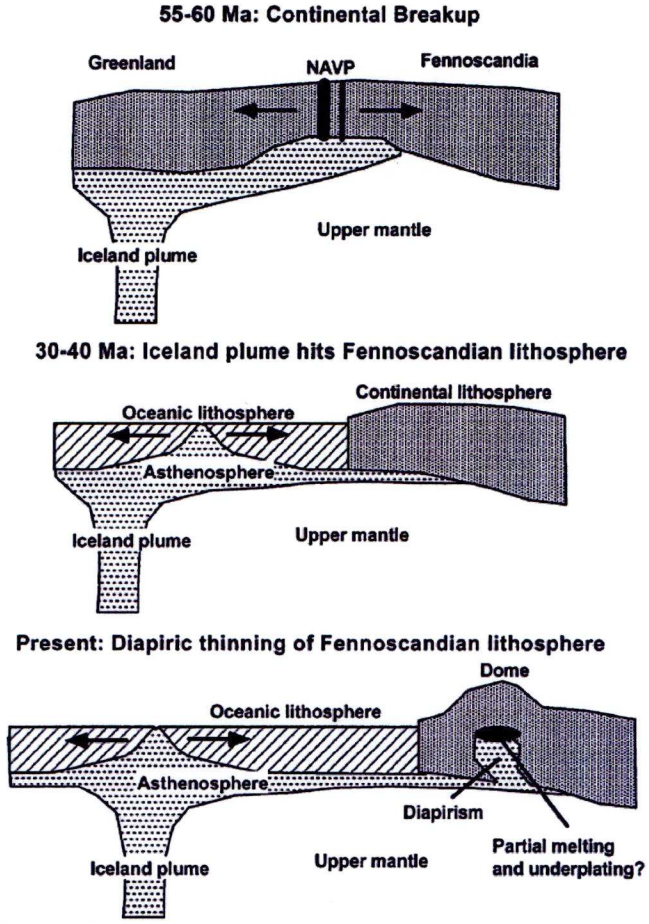

Figure 3.3: Stages of the asthenospheric diapirism model for Norway (from Rohrman & van der Beek, 1996)

3.6.3 Lithosphere delamination

Nielsen et al. (2002) proposed that lithosphere delamination may explain the post-breakup uplift of Norway. Lithosphere delamination occurs when low-viscosity and low-density material convectively removes a small part of the colder overlying mantle (Nielsen et al., 2002; Gunnell & Fleitout, 1998). The delaminated mantle is denser than the overlying lithosphere and therefore when it is replaced by the lower-density material, the buoyancy increases, leading to uplift (Gunnell & Fleitout, 1998). For Norway, Nielsen et al. (2002) suggest that the low-viscosity material is linked to the Iceland plume. There is a question, however, over how much surface uplift this mechanism may actually generate (Gunnell & Fleitout, 1998).

3.7 Summary

Whilst this thesis is examining the hypothesis that deformation to the continental lithosphere during continental breakup and sea-floor spreading initiation may result in significant thermal uplift of the continental hinterland, it is important to review existing proposed models. Various mechanisms, both transient and permanent, which have been proposed to explain post-breakup hinterland uplift have been discussed in this chapter. They can all possibly account for some of the observations of post-breakup rifted margin hinterland uplift, and all have advantages and limitations (Table 3.1). The validity of some mechanisms has been questioned, largely because of the assumptions included in them. However, given the lack of constraints provided by observations, the mechanisms are difficult to validate. Some mechanisms, for example asthenospheric diapirism, have been proposed to explain uplift at a specific location and therefore have limited applicability globally. It seems unlikely that a single mechanism could satisfactorily explain the different uplift

Mechanism	Advantages	Disadvantages
Flexural isostatic response to unloading	Can match wavelength of observed uplift.	Cannot explain observed negative Bouguer anomlies. Tectonic uplift component required to match observed magnitude.
Compressive stress	Can explain accelerated subsidence of marginal basins.	Cannot predict observed magnitude of uplift. Difficult to reconcile timing of changes in stress regime and timing of uplift.
Magmatic underplating	Can account for low Bouguer anomaly. Regionally applicable to areas with large amounts of volcanism at breakup.	Difficult to image and therefore determine existence and/or thickness of underplate.
Asthenospheric diapirism	Can explain domal uplift. Can lead to permanent uplift due to magmatic underplating.	Model requires assumptions of timing and crustal thickness.
Lithosphere delamination		Cannot predict observed magnitude of uplift.

Table 3.1: Main advantages and disadvantages of the mechanisms discussed in this chapter.

histories of all the margins. Erosion and flexural isostasy are almost certain to play a pivotal role in the onshore evolution of a rifted margin, although some contribution of tectonic uplift is required to predict the present-day elevations and initial uplift is required to initiate the erosion process. This review has demonstrated that currently no mechanism, alone or in combination, can provide an adequate description for any uplift event.

3.8 References

Anell, I., H. Thybo and I. M. Aftemieva (2009), Cenozoic uplift and subsidence in the North Atlantic region: Geological evidence revisited, *Tectonophysics*, vol. 474, no. 1-2, p. 78-105.

Bierman, P. R. and M. Caffee (2001), Slow rates of rock surface erosion and sediment production across the Namib Desert and escarpment, southern Africa, *American Journal of Science*, vol. 301, no. 4-5, p. 326-358.

Bishop, P. (1988), The Eastern Highlands of Australia - the Evolution of an Intraplate Highland Belt, *Progress in Physical Geography*, vol. 12, no. 2, p. 159-182.

Braun, J. and P. van der Beek (2004), Evolution of passive margin escarpments: What can we learn from low-temperature thermochronology?, *Journal of Geophysical Research-Earth Surface*, vol. 109, no. F4, p. F4009.

Brodie, J. and N. White (1994), Sedimentary basin inversion caused by igneous underplating: Northwest European continental shelf, *Geology*, vol. 22, p. 147-150.

Brooks, C. K. (1985), Vertical crustal movements in the Tertiary of central East Greenland: a continental margin at a hot-spot, *Zeitschrift Fur Geomorphologie N.F. Suppl. Bd 54*, p. 101-117.

Campanile, D., C. G. Nambiar, P. Bishop, M. Widdowson and R. Brown (2008), Sedimentation record in the Konkan-Kerala Bsin: Implications for the evolution of the Western Ghats and the Western India passive margin, *Basin Research*, vol. 20, p. 3-22.

Clift, P. D., A. Carter and A. J. Hurford (1996), Constraints on the evolution of the East Greenland Margin: Evidence from detrital apatite in offshore sediments, *Geology*, vol. 24, no. 11, p. 1013-1016.

Clift, P. D., A. Carter and A. J. Hurford (1998), The erosional and uplift history of NE Atlantic passive margins: constraints on a passing plume, *Journal of the Geological Society, London*, vol. 155, p. 787-800.

Cloetingh, S., P. Reemst, H. Kooi and S. Fanavoll (1992), Intraplate Stresses and the Post-Cretaceous Uplift and Subsidence in Northern Atlantic Basins, *Norsk Geologisk Tidsskrift*, vol. 72, no. 3, p. 229-235.

Cox, K. G. (1993), Continental Magmatic Underplating, *Philosophical Transactions of the Royal Society A - Mathematical, Physical & Engineering Sciences*, vol. 342, p. 155-166.

Dam, G., M. Larsen and M. Sonderholm (1998), Sedimentary response to mantle plumes: Implications from Paleocene onshore successions, West and East Greenland, *Geology*, vol. 26, no. 3, p. 207-210.

Doré, A. G., J. A. Cartwright, M. S. Stoker, J. P. Turner and N. J. White (2002) Exhumation of the North Atlantic margin: introduction and background, in Doré, A. G., J. A. Cartwright, M. S. Stoker, J. P. Turner and N. J. White (eds), *Exhumation of the North Atlantic Margin: Timing, Mechanisms and Implications for Petroleum Exploration*, Geological Society, London, Special Publications, vol. 196, p. 1-12.

Gallagher, K. and R. Brown (1999), Denudation and uplift at passive margins: the record on the Atlantic Margin of southern Africa, *Philosophical Transactions of the Royal Society of London Series a-Mathematical Physical and Engineering Sciences*, vol. 357, no. 1753, p. 835-857.

Gallagher, K., C. J. Hawkesworth and M. S. M. Mantovani (1994), The Denudation History of the Onshore Continental-Margin of Se Brazil Inferred from Apatite Fission-Track Data, *Journal of Geophysical Research-Solid Earth*, vol. 99, no. B9, p. 18117-18145.

Gunnell, Y. and L. Fleitout (1998), Shoulder uplift of the Western Ghats passive margin, India: A denudational model, *Earth Surface Processes and Landforms*, vol. 23, no. 5, p. 391-404.

Japsen, P. and J. A. Chalmers (2000), Neogene uplift and tectonics around the North Atlantic: overview, *Global and Planetary Change*, vol. 24, no. 3-4, p. 165-173.

King, L. C. (1953), Canons of Landscape Evolution, *Geological Society of America Bulletin*, vol. 64, p. 721-752.

Lambeck, K. and R. Stephenson (1985), Post-Orogenic Evolution of a Mountain-Range - Southeastern Australian Highlands, *Geophysical Research Letters*, vol. 12, no. 12, p. 801-804.

Lithgow-Bertelloni, C. and M. Gurnis (1997), Cenozoic subsidence and uplift of continents from time-varying dynamic topography, *Geology*, vol. 25, no. 8, p. 735-738.

Lithgow-Bertelloni, C. and P. G. Silver (1998), Dynamic topography, plate driving forces and the African superswell, *Nature*, vol. 395, no. 6699, p. 269-272.

Magnavita, L. P., I. Davison and N. J. Kusznir (1994), Rifting, Erosion, and Uplift History of the Reconcavo-Tucano-Jatoba Rift, Northeast Brazil, *Tectonics*, vol. 13, no. 2, p. 367-388.

Mckenzie, D. (1978), Some Remarks on Development of Sedimentary Basins, *Earth and Planetary Science Letters*, vol. 40, no. 1, p. 25-32.

Morais Neto, J. M., K. A. Hegarty, G. D. Karner and F. F. Alkmim (2008), Timing and mechanisms for the generation and modification of the anomalous

topography of the Borborema Province, northeastern Brazil, *Marine and Petroleum Geology*, p. 1-17.

Nielsen, S. B., G. E. Paulsen, D. L. Hansen, L. Gemmer, O. R. Clausen, B. H. Jacobsen, N. Balling, M. Huuse and K. Gallagher (2002) Palaeocene initiation of Cenozoic uplift in Norway, in Doré, A. G., J. A. Cartwright, M. S. Stoker, J. P. Turner and N. White (eds), *Exhumation of the North Atlantic Margin: Timing, Mechanisms and Implications for Petroleum Exploration*, Geological Society, London, Special Publication, vol. 196, p. 45-65.

Nielsen, S. B., K. Gallagher, C. Leighton, N. Balling, L. Svenningsen, B. H. Jacobsen, E. Thomsen, O. B. Nielsen, C. Heilmann-Clausen, D. L. Egholm, M. A. Summerfield, O. R. Clausen, J. A. Piotrowski, M. R. Thorsen, M. Huuse, N. Abrahamsen, C. King and H. Lykke-Andersen (2009), The evolution of western Scandinavian topography: A review of Neogene uplift versus the ICE (isostasy-climate-erosion) hypothesis, *Journal of Geodynamics*, vol. 47, no. 2-3, p. 72-95.

Nyblade, A. A. and S. W. Robinson (1994), The African Superswell, *Geophysical Research Letters*, vol. 21, no. 9, p. 765-768.

Nyblade, A. A. and N. H. Sleep (2003), Long lasting epeirogenic uplift from mantle plumes and the origin of the Southern African Plateau, *Geochemistry Geophysics Geosystems*, vol. 4, p. 1102.

Peulvast, J. P., V. Claudino-Sales, F. Betard and Y. Gunnell (2008), Low post-Cenomanian denudation depths across the Brazilian Northeast: Implications for long-term landscape evolution at a transform continental margin, *Global and Planetary Change*, vol. 62, no. 1-2, p. 39-60.

Riis, F. and W. Fjeldskaar (1992) On the magnitude of the Late Tertiary and Quaternary erosion and its significance for the uplift of Scandinavia and the Barents Sea, in Larsen, R. M., H. Brekke, B. T. Larsen and E. Talleraas (eds), *Structural and Tectonic Modelling and its Application to Petroleum Geology*, NPF Special Publication, vol. 1, p. 163-185.

Ritsema, J., H. J. van Heijst and J. H. Woodhouse (1999), Complex Shear Wave Velocity Structure Imaged Beneath Africa and Iceland, *Science*, vol. 286, no. 5446, p. 1925-1928.

Rohrman, M. and P. van der Beek (1996), Cenozoic postrift domal uplift of North Atlantic margins: An asthenospheric diapirism model, *Geology*, vol. 24, no. 10, p. 901-904.

Rohrman, M., P. A. van der beek, R. D. van der Hilst and P. Reemst (2002) Timing and mechanism of North Atlantic Cenozoic uplift: evidence for mantle upwelling, in Doré, A. G., J. A. Cartwright, M. S. Stoker, J. P. Turner and N. White (eds), *Exhumation of the North Atlantic Margin: Timing, Mechanisms and Implications for Petroleum Exploration*, Geological Society, London, Special Publications, vol. 196, p. 27-43.

Seranne, M. and Z. Anka (2005), South Atlantic continental margins of Africa: A comparison of the tectonic vs climate interplay on the evolution of equatorial west Africa and SW Africa margins, *Journal of African Earth Sciences*, vol. 43, no. 1-3, p. 283-300.

Stephenson, R. and K. Lambeck (1985), Erosion-Isostatic Rebound Models for Uplift - an Application to Southeastern Australia, *Geophysical Journal of the Royal Astronomical Society*, vol. 82, no. 1, p. 31-55.

Stuevold, L. M. and O. Eldholm (1996), Cenozoic uplift of Fennoscandia inferred from a study of the mid-Norwegian margin, *Global and Planetary Change*, vol. 12, no. 1-4, p. 359-386.

Turner, J. P., P. F. Green, S. P. Holford and S. R. Lawrence (2008), Thermal history of the Rio Muni (West Africa)-NE Brazil margins during continental breakup, *Earth and Planetary Science Letters*, vol. 270, no. 3-4, p. 354-367.

van der Beek, P. and J. Braun (1999), Controls on post-mid-Cretaceous landscape evolution in the southeastern highlands of Australia: Insights from numerical surface process models, *Journal of Geophysical Research-Solid Earth*, vol. 104, no. B3, p. 4945-4966.

van der Beek, P., M. A. Summerfield, J. Braun, R. W. Brown and A. Fleming (2002), Modeling postbreakup landscape development and denudational history across the southeast African (Drakensberg Escarpment) margin, *Journal of Geophysical Research-Solid Earth*, vol. 107, no. B12, p. 2351.

Widdowson, M. (1997) Tertiary palaeosurfaces of the SW Deccan, Western India: implications for passive margin uplift, in Widdowson, M. (ed.), *Palaeosurfaces: Recognition, Reconstruction and Palaeoenvironmental Interpretation*, Geol. Soc. Spec, Pub., vol. 120, p. 221-248.

Widdowson, M. and K. G. Cox (1996), Uplift and erosional history of the Deccan Traps, India: Evidence from laterites and drainage patterns of the Western Ghats and Konkan Coast, *Earth and Planetary Science Letters*, vol. 137, no. 1-4, p. 57-69.

Chapter 4

Formulation of the general model for continental lithosphere thinning and sea-floor spreading initiation

4.1 Introduction

The rifted continental margins described in Chapter 2 all have characteristic topography of a coastal plain and elevated plateau, uplifted since continental breakup, separated by a steep coast-facing escarpment, roughly parallel to the coast, extending over hundreds of kilometres. They possess this similar topography despite having different lithologies, structures and drainage patterns, and having experienced different climates since their formation. Given the multitude of geodynamic and geomorphological processes that may have shaped each individual margin, it is reasonable to hypothesise that perhaps different combinations of mechanisms could generate similar uplift patterns. This still, however, leaves the possibility that there could be at least one underlying mechanism acting at every uplifted margin. The most apparent tectonic event which has affected all of these margins is continental rifting and breakup, so could hinterland uplift be a fundamental consequence of the breakup process? A link between continental breakup and hinterland uplift has been proposed before by several authors, for example Ollier (1985). The aim of this project is to investigate whether post-breakup hinterland uplift of volcanic rifted margins could be a result of deformation to the continental lithosphere during continental breakup and sea-floor spreading initiation.

A key, unanswered, question regarding the formation of rifted margins is how the continental lithosphere is thinned prior to breakup. Currently there is no real consensus on what this mechanism is (Davis & Kusznir, 2004; Crosby et al., 2008). Early models of continental breakup invoked extreme extension and depth-uniform thinning of continental lithosphere c.f. the pure shear model of McKenzie (1978), leading to sea-floor spreading initiation. However, several authors have suggested that observations at rifted margins are better explained by models incorporating depth-dependent stretching and thinning (e.g. Royden & Keen, 1980; Davis & Kusznir, 2004; Driscoll & Karner, 1998; Huismans & Beaumont, 2008; Kusznir & Karner, 2007). In consideration of these differing viewpoints, models for continental lithosphere thinning and sea-floor spreading initiation using pure shear, buoyancy-driven upwelling, or a combination of the two are presented in this chapter and their implications for post-breakup hinterland uplift are considered. The sensitivity of the predicted hinterland thermal uplift (from the local, air-loaded isostatic response to geotherm perturbation) to parameters controlling the pure shear and thermal buoyancy driven upwelling flow is also explored.

This chapter, and the subsequent ones, detail the formulation of the model. The program used for the model is original work, with code written in Fortran, and was developed using the key equations presented in this thesis. The flow diagram in Figure 4.1 shows the components of the final model; results from this are presented in Chapter 8.

4.2 Observations and constraints on continental lithosphere thinning and sea-floor spreading initiation at a volcanic rifted margin

4.2.1 Formation of a volcanic rifted margin

Post-breakup uplift of continental hinterlands is mainly observed at volcanic rifted margins; therefore, the processes involved in volcanic rifted margin formation need to be considered in the development of the model. Volcanic rifted margins are characterised by onshore continental flood basalts formed prior to breakup and the presence of a magmatically-thickened crust formed during continental breakup, as shown in Figure 4.2. This crust, which normally has a thickness greater than 20 km, is covered at the margin by subaerially-deposited lava flows that are imaged

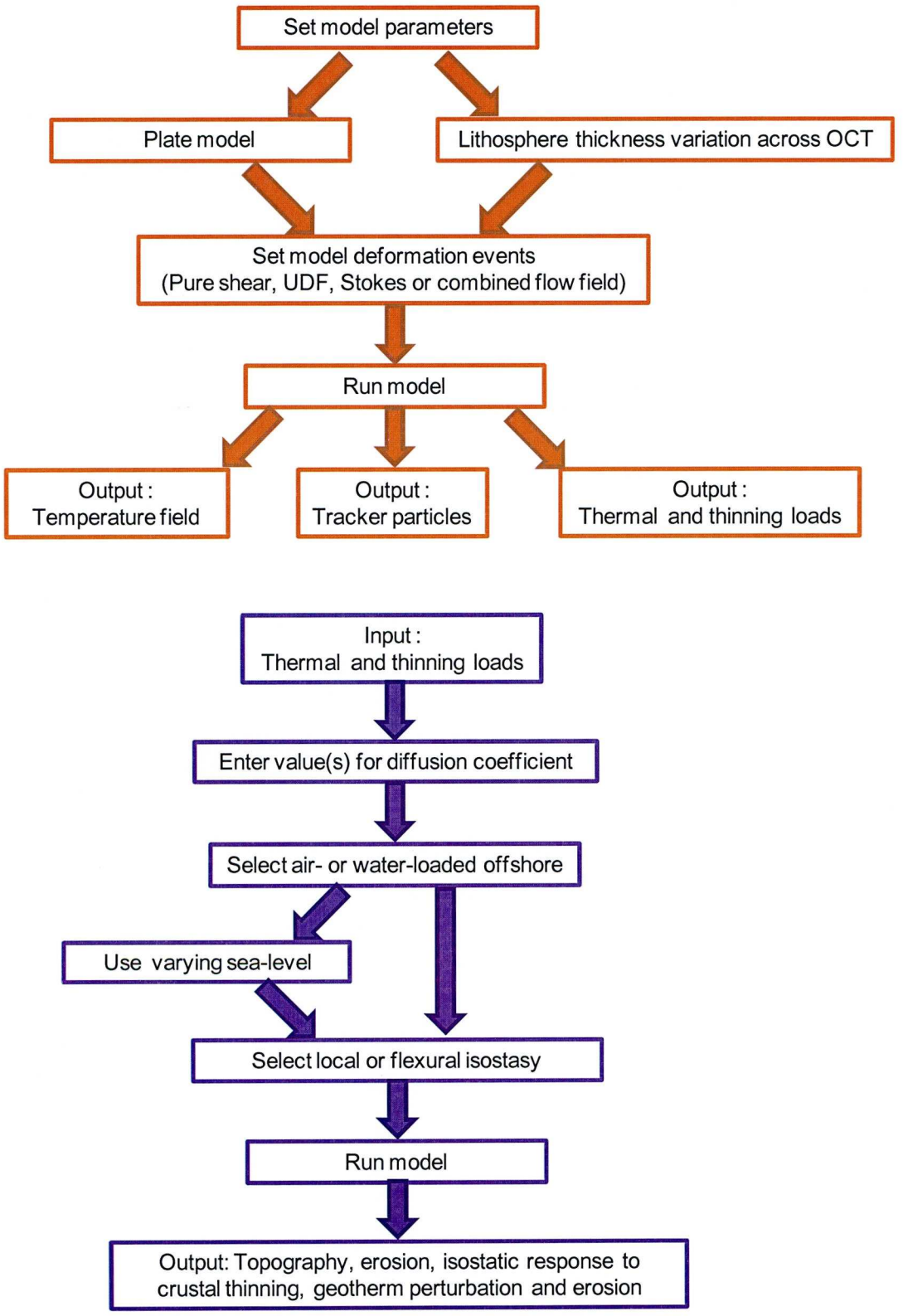

Figure 4.1: Flow diagram for steps in final model, which can be divided into two sections. The top section forma the core part of the code and the bottom section is for the post-processing part. The thermal and thinning loads outputted from the core code are used as the input values for the post-processing code.

seismically as seaward dipping reflector sequences. The lower crust often has zones of high seismic velocity which are usually interpreted as magmatic underplating (Geoffroy, 2005; Callot et al., 2002) although White et al. (2008) interpret these zones as continental crust intruded by sills. A further difference from non-volcanic margins is that extension occurs over a narrow (< 100 km) zone (Callot et al., 2002). Observations suggest that the magmatism associated with volcanic rifted margin formation peaks at continental breakup before decaying relatively quickly to normal levels of oceanic crust generation (Nielsen & Hopper, 2002).

Average oceanic crustal thicknesses are often assumed to be produced by passive plate-driven mantle upwelling, where the upwelling velocity and divergent velocity are roughly equal, and a normal asthenosphere temperature; these conditions cannot generate the much thicker crust observed at volcanic rifted margins. It is thought, therefore, that either anomalously warm asthenosphere temperatures, buoyancy-assisted upwelling or a combination of the two are a requirement for their formation (Holbrook et al., 2001; Nielsen & Hopper, 2004). However, opinions about which of these conditions occurs during the formation of volcanic rifted margins remain divided. On one side is the argument that since, in passive upwelling models, the thickness of oceanic crust is thought to be directly linked to the temperature of the asthenosphere, it is inferred that thick oceanic crust formed after breakup must be due to melting with hotter asthenosphere temperatures (Geoffroy, 2005; Nielsen & Hopper, 2004). A study of two seismic profiles on the North

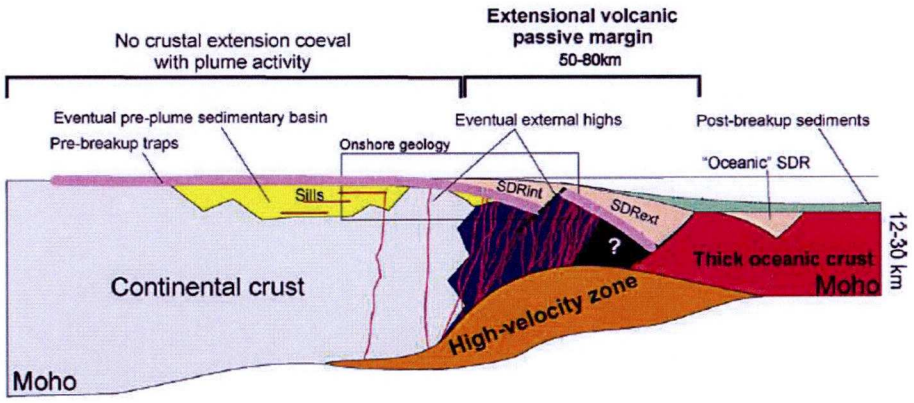

Figure 4.2: Cross section of a volcanic margin from Geoffroy (2005) showing the sub-crustal high-velocity zone, characteristic thick oceanic crust and seaward-dipping reflectors (SDRint and SDRext).

Atlantic margin by White et al. (2008) supports this theory as the measured seismic velocities and thicknesses of igneous crust are consistent with those predicted for a model invoking increased mantle temperatures.

The opposing argument is that buoyancy-assisted upwelling (sometimes called active upwelling), where the upwelling velocity is greater than the divergent velocity, enhances the flux of material through the solidus, resulting in the melting of larger amounts of asthenosphere compared to passive upwelling and thereby producing thick oceanic crust (Nielsen & Hopper, 2002; Korenaga et al., 2002). This is because an increase in buoyancy, coupled with a decrease in mantle viscosity due to the presence of melt, drives transient small-scale mantle convection, causing material beneath the ridge axis to upwell more rapidly (Nielsen & Hopper, 2002; Spiegelman & Reynolds, 1999). Buoyancy-assisted upwelling may be due to thermal buoyancy, melt buoyancy, wet melting and/or mantle depletion (Braun et al., 2000; Nielsen & Hopper, 2004; Fletcher et al., 2009). Convective modelling by Nielsen & Hopper (2002, 2004) shows that buoyant upwelling can occur beneath a mid-ocean ridge without invoking hotter asthenosphere temperatures, although a thermal anomaly at the base of the lithosphere is needed in their model to produce the thick oceanic crust characteristic of volcanic rifted margins. This thermal anomaly would also decrease the viscosity and therefore increase the effect of buoyancy in the upwelling region, and thus further enhance the small-scale convection. An alternative model by Boutilier & Keen (1999) demonstrated that small-scale convection can generate thicker crust at a volcanic margin without the need for an anomalously high mantle temperature.

4.2.2 Magnitude of early sea-floor spreading buoyancy-assisted upwelling

Sea-floor spreading is thought to be characterised by upwelling-divergent flow in the oceanic lithosphere and asthenosphere (e.g. Phipps Morgan, 1987; Kusznir & Karner, 2007; Lachenbruch, 1976). For isoviscous passive mantle upwelling, the ratio of the upwelling velocity, Vz, to the divergent velocity, Vx, is approximately $2/\pi$, determined from isoviscous stream function fluid flow calculations (Phipps Morgan, 1987). If temperature and stress-dependent rheology are considered, a higher Vz/Vx ratio is probably more realistic (Shen & Forsyth, 1992). In a kinematic isoviscous model of sea-floor spreading, a higher Vz/Vx ratio of ~2 predicts observed oceanic crustal thicknesses at slow spreading rates unlike the passive

upwelling velocity ratio (Figure 4.3; Fletcher et al., 2009). Nielsen & Hopper (2002) suggested (from mantle convection models of sea-floor spreading) that for sea-floor spreading initiation with anomalously hot asthenosphere temperatures Vz/Vx is initially large (> 5), because of the thermal buoyancy assisted upwelling, for a short time after continental breakup before decreasing to passive upwelling ratios. This high initial Vz/Vx ratio may, however, just be a consequence of the boundary conditions used at the start of the model (Nielsen & Hopper, 2004), although Holbrook et al. (2001) give similar velocity ratios (Vz/Vx = 4 - 6) for near the North Atlantic hotspot track and Simon et al. (2009) predict up to Vz/Vx = 7 from their models of small-scale mantle convection incorporating a small (50°C) increase in mantle potential temperature. This active upwelling becomes increasingly significant at slower spreading rates (less than 3 cm yr^{-1}), where numerical models of melt generation have shown that the effect of buoyancy increases considerably (Braun et al., 2000). It is thought that there is continuity between pre-breakup and post-breakup processes, therefore it is probable that buoyancy-driven upwelling also plays an important role in thinning the continental lithosphere prior to continental breakup.

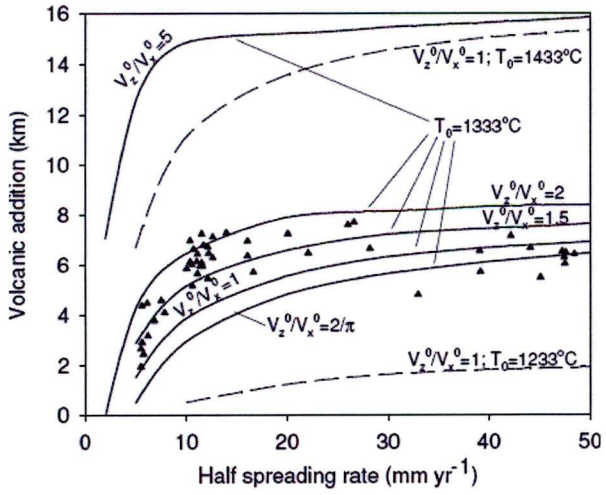

Figure 4.3: Comparison of steady-state volcanic addition predicted by different Vz/Vx ratios and base lithosphere temperatures (from Fletcher et al., 2009). The black triangles are observed seismic oceanic crustal thicknesses. Vz/Vx = 2 with a normal mantle temperature has the best fit to the measured oceanic crustal thickness at slow spreading rates.

4.2.3 Mode of pre-breakup continental lithosphere thinning

Pure shear as a mode of lithosphere thinning and extension was first used by McKenzie (1978) to describe sedimentary basin formation and has since been applied to the formation of rifted margins (e.g. Royden & Keen, 1980; Beaumont et al., 1982). The pure shear model predicts that the magnitude of crustal and lithosphere extension is the same, i.e. stretching and thinning is uniform with depth (Figure 4.4). Isostatic compensation causes passive upwelling of hot asthenospheric material to fill the space generated by thinning of the lithosphere, resulting in a syn-rift change in elevation of the margin.

The McKenzie (1978) pure shear model appears to be a successful mechanism for the formation of intra-continental rift basins, where the upper crust and continental lithosphere have experienced equal amounts of stretching and thinning (Kusznir & Karner, 2007). However, whilst it can explain most general properties of rifted margins, if the initial crustal thickness is greater than ~20 km the model predicts immediate syn-rift subsidence and is therefore not applicable to rift zones that are characterised by an initial elevated topography, for example Labrador, the Red Sea and the East African Rift (Rowley & Sahagian, 1986; Marsden, 1990). The pure shear model also fails to account for varying rheological properties of the lithosphere with depth, which render depth-uniform stretching unlikely (Beaumont et

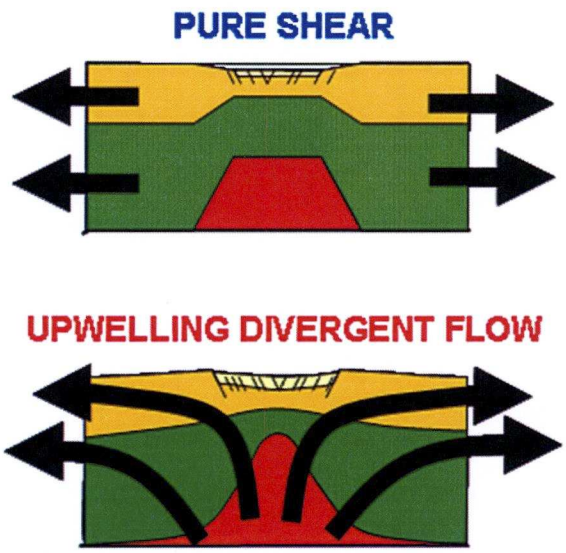

Figure 4.4: Lithosphere thinning by pure shear (depth-uniform) McKenzie (1978) model and by upwelling-divergent flow (from Fletcher et al., 2008).

al., 1982). Furthermore, the application of the McKenzie (1987) model to continent breakup requires much greater extension of the lithosphere than is observed from faulting; pure shear may not, therefore, be the dominant process involved in pre-breakup continental lithosphere thinning leading to sea-floor spreading initiation (Davis & Kusznir, 2004; Kusznir & Karner, 2007).

An early observation of depth-dependent stretching was made by Royden & Keen (1980) who studied the Labrador margin and concluded that the lithosphere there had undergone much more extension than the crust. This was supported by Davis & Kusznir (2004) who showed that this discrepancy in the amount of extension experienced by the lithosphere and crust at rifted margins indicates depth-dependent thinning, and is inconsistent with observations for intra-continental rift basins which support the model of depth-uniform thinning (Figure 4.5). Depth-dependent stretching/thinning, where thinning of the lower crust and lithospheric mantle is much greater than upper crustal fault extension, is observed at both volcanic and non-volcanic conjugate margins, including conjugate margin pairs (Figure 4.6; Davis & Kusznir, 2004). The existence or extent of the observed difference in upper crust and lithosphere thinning factors is, however, still debated. It has been proposed that this extension discrepancy may reflect limitations of seismic imaging of highly deformed rocks (e.g. Crosby et al., 2008) or that the amount of extension in the upper crust is underestimated due to incomplete interpretation of the complex geometries arising in the highly extended crust (Reston, 2009).

Studies of basins which are thought to be/have been propagating rift tips of young oceanic spreading centres, for example the Woodlark Basin (Kusznir & Karner, 2007) and the Faroe-Shetland Basin (Fletcher, 2009), indicate that depth-dependent stretching occurs prior to sea-floor spreading initiation. Pre-breakup continental lithosphere thinning by buoyancy-driven upwelling predicts depth-dependent stretching at both volcanic and non-volcanic margins. This pre-breakup upwelling flow in the continental lithosphere and asthenosphere is driven by thermal and melt buoyancy forces which are induced after the onset of extension in the continental lithosphere (Fletcher et al., 2009; Braun et al., 2000). At continental breakup, continental lithosphere thinning evolves into sea-floor spreading; assuming continuity between these processes, Kusznir & Karner (2007) proposed that pre-breakup continental lithosphere thinning could occur by buoyancy-driven upwelling-divergent flow (Figure 4.4). This flow is like that characteristic of mid-ocean ridges

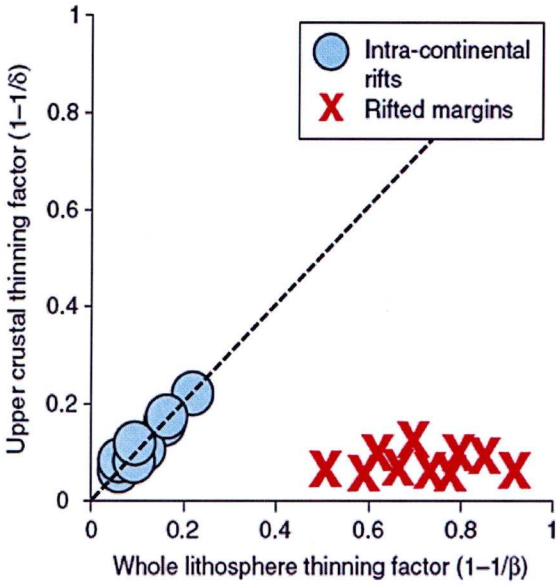

Figure 4.5: Cross-plot of upper crustal thinning factors versus whole lithosphere thinning factors (from Kusznir & Karner, 2007). Values for rifted margins plot in a different region to those for intra-continental rifts.

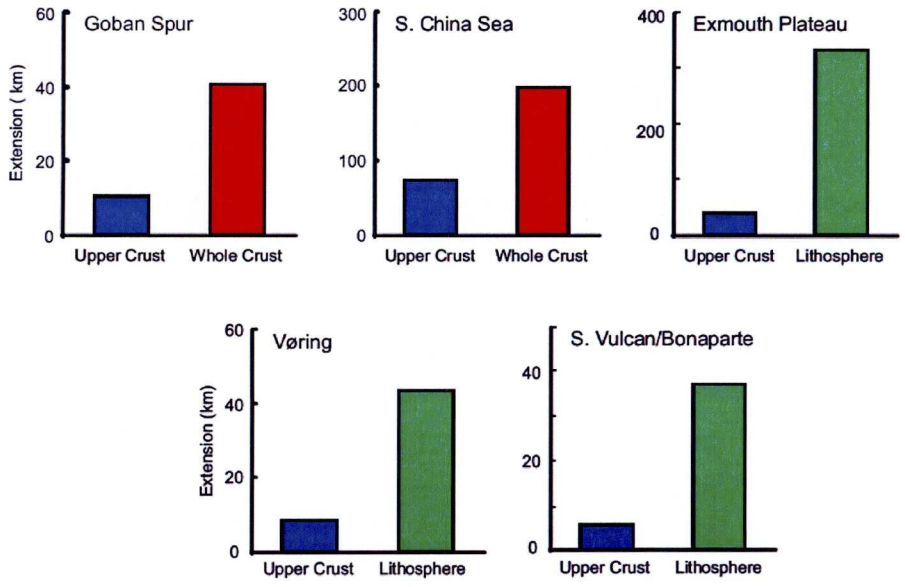

Figure 4.6: Comparison of upper crustal, whole crustal and lithosphere extension for volcanic and non-volcanic margins (from Davis & Kusznir, 2004); all margins show depth-dependent stretching.

but with the horizontal velocity, *Vx*, set to 0; only at the onset of sea-floor spreading does *Vx* becomes finite. The kinematically-defined upwelling-divergent flow is used as an approximation for thermal and melt buoyancy upwelling, with a higher upwelling velocity, *Vz*, being used to represent more energetic upwelling. An alternative method for modelling the buoyancy-driven upwelling is to use Stokes flow, where a fluid sphere rises at a steady velocity through a surrounding fluid of higher viscosity (e.g. Schmeling et al., 1988; Scott, 1992).

Continental lithosphere thinning, prior to the onset of sea-floor spreading, by either pure shear or buoyancy-driven upwelling alone represent end-member models; some contribution from either mechanisms cannot be completely ruled out. The lithosphere at mid-ocean ridges is 10 – 15 km thick, with faults extending to the base of the lithosphere (Cannat, 1996). This layer, which deforms by faulting, can by represented by depth-uniform stretching but observations of depth-dependent stretching at rifted margins point to a mode of lithosphere thinning different from the McKenzie (1978) pure shear model. It is possible that pre-breakup lithosphere thinning occurs by simultaneous pure shear and buoyancy-driven upwelling, where the lithosphere is initially thinned by pure shear, inducing thermal and melt buoyancy which drive the buoyant upwelling.

4.3 Overview of the general model for continental lithosphere thinning and breakup

An overview of the stages involved in the model for continental lithosphere thinning leading to breakup is shown in Figure 4.7; further details for each step are given in the subsequent sections. The model begins with an initially uniformly thick lithosphere (Figure 4.7a). It is assumed that prior to breakup, deformation and thinning of the continental lithosphere occurs by a combination of pure shear and buoyancy-driven upwelling. In this model, continental lithosphere initially thins by pure shear, which is driven by horizontal tensile plate forces (Figure 4.7b). The resulting change to the temperature field and the distribution of crust and lithosphere material creates lateral and vertical density variations, inducing thermal and melt buoyancy (Figure 4.7c). This then drives buoyant upwelling, represented by either propagating upwelling-divergent flow or Stokes flow, within the continental

lithosphere and asthenosphere (Figure 4.7d). Lithosphere thinning then occurs by simultaneous pure shear and buoyancy-driven upwelling (Figure 4.7e), which pushes the material outwards, thickening the lithosphere inland of the region of continental lithosphere thinning. The lithosphere thinning eventually leads to continental breakup (Figure 4.7f) and sea-floor spreading initiation (Figures 4.7g & h).

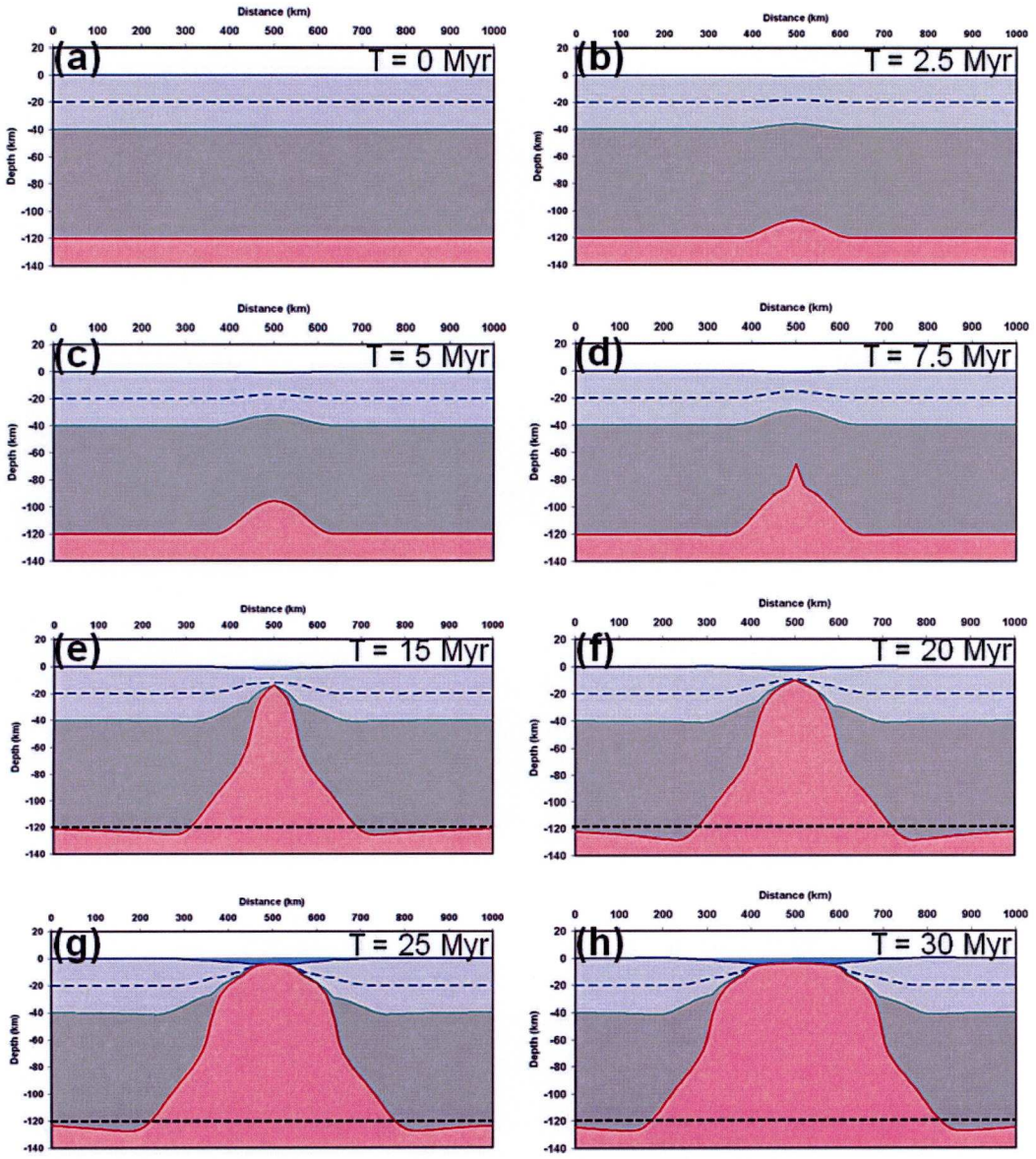

Figure 4.7: Lithosphere cross section through time; (a) initially flat crust and lithosphere, 40 km and 120 km thick respectively; (b, c) rifting by pure shear; (d, e) rifting by combined pure shear and upwelling-divergent flow; (f) continental breakup; (g, h) sea-floor spreading. Dashed line shows original depth of the base of the lithosphere (120 km).

4.4 Model formulation

The deformation field for the continental lithosphere and asthenosphere, whether pure shear, Stokes flow, upwelling-divergent flow or a combination of these, at a given time is described by a flow field. The velocities determined from this flow field are used to drive material and thermal advection.

4.4.1 Initial temperature field and lithosphere configuration

The model assumes an initial lithosphere and Moho depth of 125 km and 35 km respectively (Figure 4.8a). Viscosity and composition are not considered. The initial temperature structure of the continental lithosphere is assumed to be in thermal equilibrium with a surface temperature of 0°C, a base lithosphere temperature of 1300°C at 125 km depth and the temperature in the lithosphere given by a linear geotherm, consistent with the McKenzie (1978) model:

$$T(z) = T_a\left(\frac{z}{a}\right) \qquad [4.1]$$

where T = temperature, T_a = temperature at the base of the lithosphere, z = depth, and a = lithosphere thickness (Figure 4.8b). The surface and base lithosphere boundary conditions are fixed at all times and radiogenic heat production in the lithosphere is neglected.

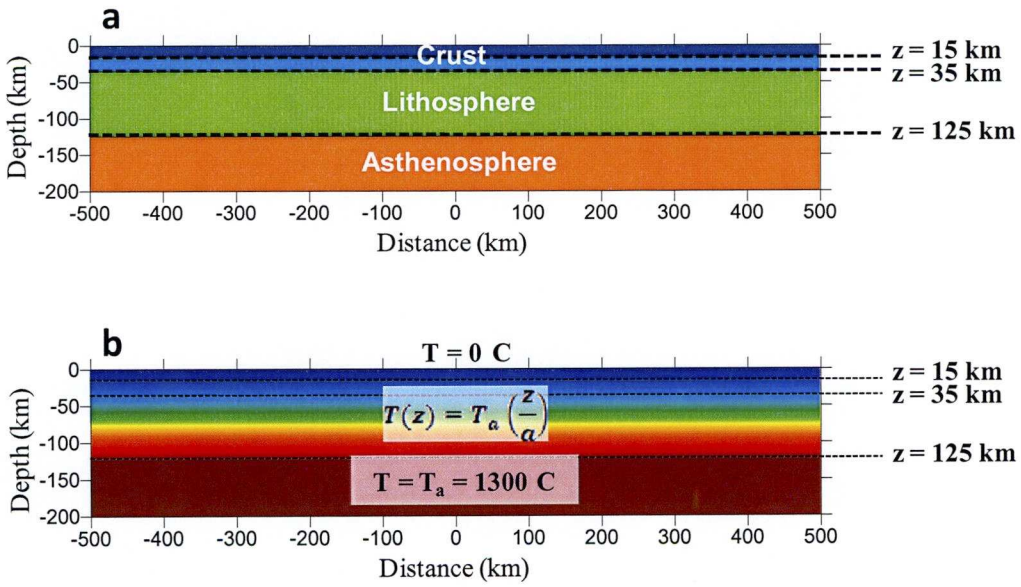

Figure 4.8: a) Initial configuration for the lithosphere used in the model. Dark blue = upper crust and light blue = lower crust. b) Initial configuration for the temperature field.

4.4.2 Coupled diffusion-advection equation

The evolution of the temperature field within the lithosphere and asthenosphere is calculated using a coupled thermal diffusion and advection solution. The governing equation for the variation of temperature in time and space when heat is transferred by diffusion and advection is:

$$\rho_m \sigma \frac{\partial T}{\partial t} = \nabla k \nabla T - \bar{V} \nabla T \qquad [4.2]$$

which, assuming k to be constant, can be expanded in 2D as:

$$\rho_m \sigma \frac{\partial T}{\partial t} = k\left(\frac{\partial^2 T}{\partial x^2} + \frac{\partial^2 T}{\partial z^2}\right) - \left(Vx \frac{\partial T}{\partial x} + Vz \frac{\partial T}{\partial z}\right) \qquad [4.3]$$

where ρ_m = density of the mantle, σ = specific heat capacity, t = time, k = thermal conductivity, Vx = horizontal velocity and Vz = upwelling velocity. The diffusion equation is solved using the explicit finite difference method. It is assumed there is no flow of heat across the lateral boundaries and the temperature is reflected at that boundary ($\partial T/\partial x = 0$). The model is made wide enough so that the assumption about this boundary condition makes little difference to the area of focus. The magnitudes of the Vx and Vz are determined from the flow field from pure shear, upwelling-divergent flow and Stokes flow; these velocities are used to drive the advection of the continental lithosphere and asthenosphere material and the temperature field. The values given in Table 4.1 for the variables have been used for the models presented throughout this thesis, unless otherwise stated.

4.4.3 Calculation of the velocities, Vx and Vz, for the deformation mechanisms

4.4.3.1 Pure shear

The pure shear deformation field is defined by a horizontal strain rate applied, assuming a cosine-squared function, within a fixed half-width zone, with rifting assumed to be symmetrical about the axis (Figure 4.9). The half-extension rate (horizontal velocity), Vx, within this zone (for positive x) is given by:

$$Vx = \int_0^W \dot{\varepsilon}_{xx} \cos^2\left(\frac{\pi x}{W}\right) dx \qquad [4.4]$$

Symbol	Parameter	Value	Units
x	Horizontal co-ordinate		km
z	Vertical co-ordinate		km
Δx	Spacing in x direction	5	km
Δz	Spacing in z direction	5	km
a	Lithosphere thickness	125	km
t	Time		Myrs
Δt	Time step	1000	yrs
ρ_m	Mantle density	3300	kg m^{-3}
ρ_c	Crustal density	2850	kg m^{-3}
ρ_i	Infill density		kg m^{-3}
T	Temperature		°C
T_a	Asthenosphere temperature	1300	°C
q	Heat flux		mW m^{-2}
k	Thermal conductivity	3.0	W m^{-1} $°C^{-1}$
σ	Specific heat capacity	1000	J kg^{-1} K^{-1}
α	Coefficient of thermal expansion	3.28×10^{-5}	K^{-1}
g	Gravitational acceleration	9.81	m s^{-1}
Ψ	Stream function		
Vx	Divergent velocity (half-rate)		cm yr^{-1}
Vz	Upwelling velocity		cm yr^{-1}
W	Pure shear half-width		km
$\dot{\varepsilon}$	Strain rate		s^{-1}
E	Half-extension		km
θ	Wedge angle	10 – 40	°
λ	Viscosity ratio	0.01	
R	Radius of Stokes circle		km
r	radius from centre point		km
ct_0	Initial crustal thickness	35	km
ct	Crustal thickness		km
w	Isostatic response		m
L^{ct}	Load due to crustal thinning		m
L^{th}	Load due to geotherm perturbation		m

Table 4.1: Variables, and their values if applicable, used throughout this thesis.

where W = half-width and $\dot{\mathcal{E}}_{xx}$ = horizontal strain rate. Conservation of volume requires that $\dot{\mathcal{E}}_{xx} + \dot{\mathcal{E}}_{zz} = 0$, therefore the vertical velocity within the zone of extension is:

$$Vz = \int_0^z -\dot{\mathcal{E}}_{xx} dz \qquad [4.5]$$

The solutions to Equations 4.4 and 4.5 are then:

$$Vx = \frac{\dot{\mathcal{E}}_{xx}}{2}\left(x + \frac{W}{\pi} sin\frac{\pi x}{W}\right) \qquad [4.6]$$

$$Vz = -\dot{\mathcal{E}}_{xx} cos^2\left(\frac{\pi x}{2W}\right) z \qquad [4.7]$$

Outside of the zone of pure shear, material moves horizontally at the maximum half-extension rate with $Vx = \dot{\varepsilon}_{xx}W/2$ and $Vz = 0$. The amount of extension, E, (on one margin) is dependent on the maximum horizontal velocity (determined from the strain rate and the width of the pure shear zone) and the duration of rifting:

$$E = \int Vx\, dt \qquad [4.8]$$

McKenzie (1978) assumed that rifting in the pure shear model is instantaneous (no heat is lost by the lithosphere during rifting); Jarvis & McKenzie (1980) showed that, providing extension occurs on a sufficiently short time-scale (< 20 Myr) relative to the thermal time constant of the plate, this assumption is valid. Maximum strain rate values of the order of 10^{-15} s^{-1} have been determined for intra-continental rift basins (Newman & White, 1999), and range from 10^{-16} s^{-1} to just under 10^{-14} s^{-1} for non-volcanic rifted margins (Davis & Kusznir, 2002). Pure shear strain rates are thought to be higher at volcanic rifted margins (Callot et al., 2002), with Lenoir et al. (2003) estimating that the lower boundary for extensional strain rates is $7\pm2\times10^{-15}$ s^{-1}, suggesting that continental lithosphere at volcanic rifted margins is weakened by high thermal gradients.

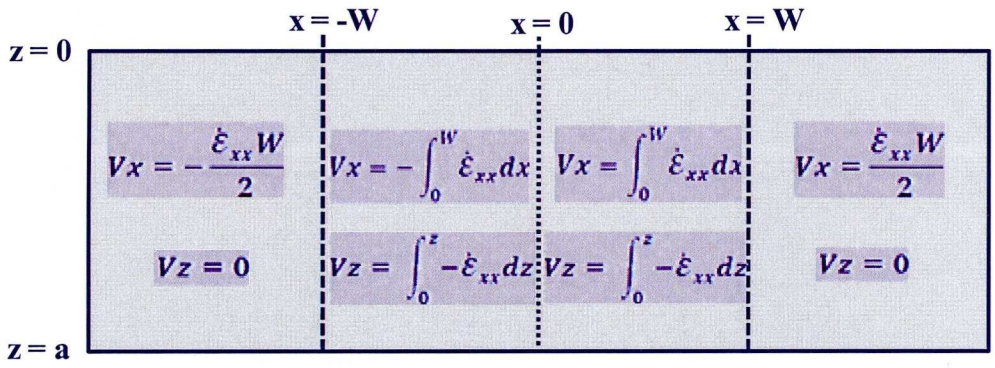

Figure 4.9: 2D pure shear velocity field. x = width and z = depth.

4.4.3.2 Stokes flow

Pre-breakup buoyancy-driven upwelling can be modelled using Stokes flow whereby the thermally buoyant region beneath a mid-ocean ridge is approximated by a buoyant fluid sphere of radius R. The sphere is given a lower viscosity than the surrounding material. Material moves upwards at a prescribed velocity beneath the ridge axis, and then moves out and down to the sides. The flow field in a half-space

to the base of a brittle lid (Figure 4.10) is calculated using the method of images; the flow field is found by summing the original flow field and its mirror image reflected about the base of the brittle lid. A derivation for the governing equations for the Stokes flow velocity field is given by Happel & Brenner (1973). The velocity field inside the fluid sphere, in polar co-ordinates, is:

$$V_r = -\frac{Vz\cos\phi}{2(1+\lambda)}\left[1-\left(\frac{r}{R}\right)^2\right] \quad [4.9]$$

$$V_\phi = \frac{Vz\sin\phi}{2(1+\lambda)}\left[1-2\left(\frac{r}{R}\right)^2\right] \quad [4.10]$$

where V_r and V_ϕ are, respectively, the radial and tangential velocity components, Vz = upwelling velocity (on the ridge axis), λ = the ratio of the interior viscosity (the viscosity of the sphere) to the exterior viscosity (the viscosity of the fluid), R = radius of the sphere and r = radius from the centre of the sphere. The equations for the velocity field exterior to the sphere are:

$$V_r = Vz\cos\phi\left[1-\frac{2+3\lambda}{2(1+\lambda)}\frac{R}{r}+\frac{\lambda}{2(1+\lambda)}\left(\frac{R}{r}\right)^3\right] \quad [4.11]$$

$$V_\phi = -Vz\sin\phi\left[1-\frac{2+3\lambda}{4(1+\lambda)}\frac{R}{r}-\frac{\lambda}{4(1+\lambda)}\left(\frac{R}{r}\right)^3\right] \quad [4.12]$$

For a full derivation of the velocity field in Cartesian co-ordinates see Cooper (2010). This solution assumes free slip along the brittle lid boundary. The radius of the sphere is assumed to grow with time, filling the space generated by thinning of the lithosphere. In the model, the duration of this pre-breakup Stokes flow rifting event is assumed to be dependent on the magnitude of Vz, which determines the time it takes for the flow field to upwell to the surface.

4.4.3.3 Upwelling-divergent flow

Upwelling-divergent flow is used to represent the material and thermal advection of lithosphere and asthenosphere during sea-floor spreading. It has also been applied in a modified form to represent pre-breakup continental lithosphere thinning (Kusznir & Karner, 2007). The upwelling-divergent flow field, where material upwells at the ridge axis and spreads laterally as the plates move apart, is defined kinematically by a horizontal divergence half-rate velocity, Vx, and a vertical

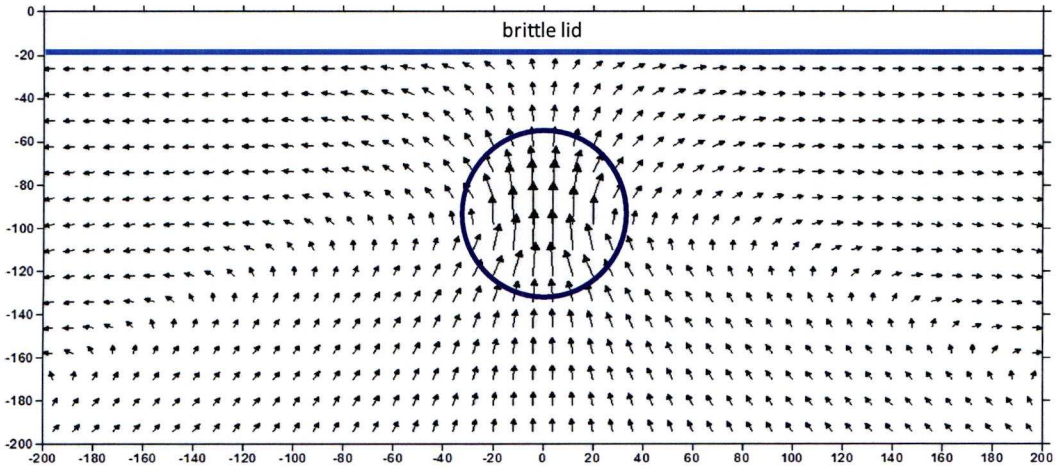

Figure 4.10: Flow field using Stokes flow for a buoyant sphere with a brittle lid (from Cooper, 2010). There is no flow above the brittle lid.

upwelling velocity, *Vz*. The magnitude of *Vx* and *Vz* are determined using the analytical corner flow solution for an isoviscous incompressible fluid (Batchelor, 1967):

$$\Psi = (Ax + Bz) + (Cx + Dz)tan^{-1}\left(\frac{z}{x}\right) \quad [4.13]$$

where Ψ = stream function. The partial derivative of Ψ with respect to x and z gives *Vx* and *Vz* respectively:

$$Vx = \frac{\partial \Psi}{\partial z} \quad [4.14]$$

$$Vz = -\frac{\partial \Psi}{\partial x} \quad [4.15]$$

The solutions of these for a corner flow geometry are given by Turcotte & Schubert (2002):

$$Vx = -B - Dtan^{-1}\left(\frac{z}{x}\right) + (Cx + Dz)\left(\frac{-x}{x^2 + z^2}\right) \quad [4.16]$$

$$Vz = A + Ctan^{-1}\left(\frac{z}{x}\right) + (Cx + Dz)\left(\frac{-z}{x^2 + z^2}\right) \quad [4.17]$$

A, B, C and D are constants and are determined from the boundary conditions, which, for a mid-ocean ridge, are Vx = 0, Vz = Vz_0 for x = 0, z > 0 and Vx = Vx_0, Vz = 0 for x > 0, z = 0, where Vx_0 and Vz_0 are the velocities given along the surface and ridge axis respectively. *Vz* is negative as *z* is taken to be positive downwards.

Substituting these boundary conditions into Equations 4.16 and 4.17 gives the solutions for A, B, C and D as:

$$A = 0$$

$$B = \frac{-Vx_0 \frac{\pi^2}{4} - Vz_0 \frac{\pi}{2}}{\frac{\pi^2}{4} - 1}$$

$$C = \frac{Vx_0 + Vz_0 \frac{\pi}{2}}{\frac{\pi^2}{4} - 1}$$

$$D = \frac{Vz_0 + Vx_0 \frac{\pi}{2}}{\frac{\pi^2}{4} - 1}$$

These constants are then substituted back into the stream function equation (Equation 4.13) and the velocity equations (Equations 4.16 and 4.17) to give the flow lines and magnitude of Vx and Vz at any point in the half-space. The absolute value of the stream function is arbitrary; rather, the physical significance is its derivatives.

Kusznir & Karner (2007) proposed that thinning of the continental lithosphere prior to breakup may occur by a buoyancy-driven dynamically upwelling flow field (Figure 4.11). In this case, the flow field starts from the base of the lithosphere and propagates upwards to the surface before rupturing the continental lithosphere. It is assumed, in the model, that the top of the flow field propagates upwards at the same velocity as Vz_o; therefore the duration of this upward propagation phase is dependent on the magnitude of Vz_o. During the pre-breakup continental lithosphere thinning, the surface boundary condition is set to $Vx_0 = 0$ resulting in little stretching of the upper crust, consistent with observations (Kusznir & Karner, 2007). The horizontal velocity becomes finite at the onset of sea-floor spreading, and the flow field is then calculated in a fixed co-ordinate reference frame.

After the initiation of sea-floor spreading, instead of the typical right-angle corner flow solution for a mid-ocean ridge, the upwelling-divergent flow field can be defined using a wedge geometry (Figure 4.12; Skilbeck, 1975; Spiegelman & Mckenzie, 1987)). This is used to approximate the thickening of the lithosphere due

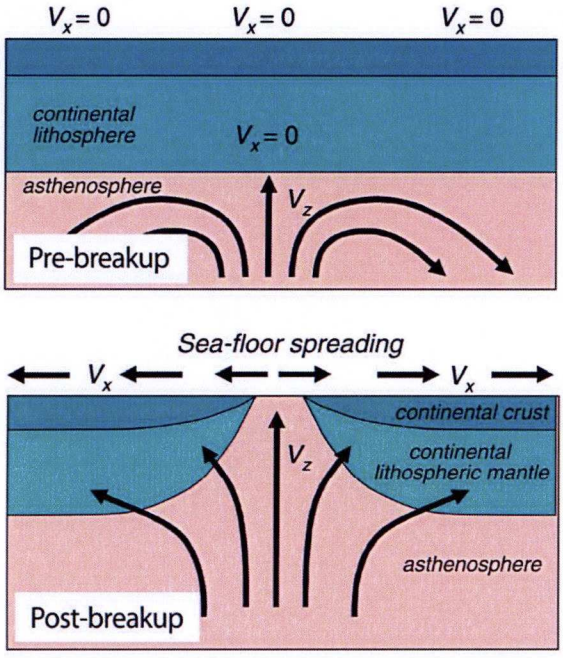

Figure 4.11: Upwelling-divergent flow in the continental lithosphere and asthenosphere with *Vx* and *Vz* defined along the surface and axis respectively. Prior to continental breakup, the flow field propagates upwards from the base of the lithosphere (from Kusznir & Karner, 2007).

to cooling as it moves away from the ridge axis. The stream function constants A, B, C and D are found by substituting the boundary conditions in Figure 4.12 into the velocity equations 4.16 and 4.17 giving:

$$A = Vz_0 - C\frac{\pi}{2} + D$$

$$B = -D\frac{\pi}{2}$$

$$C = \frac{Vx_0 \cos^2\theta - Vz_0\left(-\frac{\pi}{2} + \theta + \sin\theta\cos\theta\right)}{\left(\frac{\pi^2}{4} - \pi\theta + \theta^2 - \sin^2\theta\cos^2\theta - \cos^4\theta\right)}$$

$$D = \frac{-C\cos^2\theta - Vx_0}{\left(-\frac{\pi}{2} + \theta + \sin\theta\cos\theta\right)}$$

Outside of the region confined by the wedge angle, material moves horizontally at the prescribed Vx_0.

An estimation of the wedge angle, θ, is that it is the angle from the ridge to a point where the oceanic lithosphere is 15 – 20 km thick after ~1 Myr of sea-floor spreading (Skilbeck, 1975). The wedge angle is therefore dependent on the spreading

rate and mantle viscosity with a higher wedge angle being formed at slower spreading rates or decreased mantle viscosity (Bown & White, 1994). As the wedge angle increases, the ratio of the upwelling velocity to the divergent velocity (*Vz/Vx*) also increases as using a wedge angle focuses the upwelling flow beneath the mid-ocean ridge. Values used for the wedge angle in previous studies range from 5° - 37°, for a half-spreading rate of 8.5 cm yr^{-1} and 1 cm yr^{-1} respectively (Skilbeck, 1975), and 10 - 40° (Spiegelman & Mckenzie, 1987) to 30° - 60° (Jones et al., 2002). However, as Jones et al. (2002) state, the value cannot be tightly constrained due to its dependence on other model parameters.

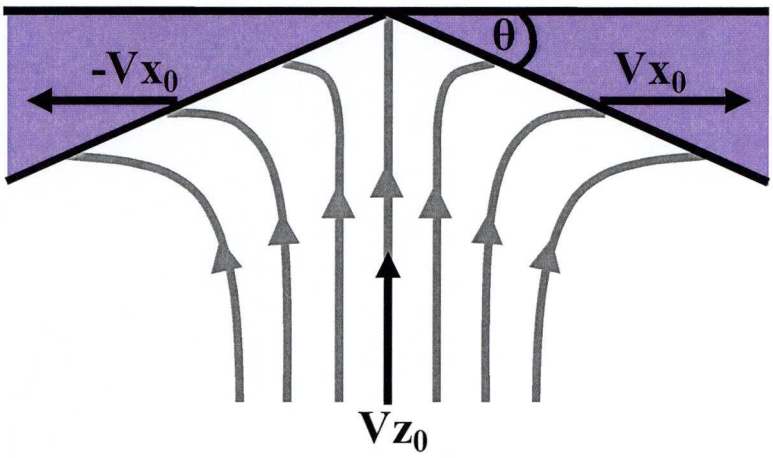

Figure 4.12: Model configuration for a wedge angle geometry

4.4.4 Uplift and subsidence due to crustal thinning and geotherm perturbation

The bathymetry and topography at the rifted margin is determined from the isostatic response to the resulting lithosphere structure and temperature field predicted by the model; initially, local isostasy is assumed. The loads due to crustal thinning and geotherm perturbation are calculated for each column at node (x), at each time step. The crustal thinning load is given by:

$$L^{ct}(x) = -(ct_0 - ct(x))(\rho_m - \rho_c)g \qquad [4.18]$$

where $L^{ct}(x)$ = crustal thinning load for the lithospheric column at co-ordinate x, ct_0 = initial crustal thickness, and $ct(x)$ = current crustal thickness at co-ordinate x (Figure 4.13a). The thermal load due to geotherm perturbation is calculated with respect to the equilibrium geotherm at t = 0 (Figure 4.13c).

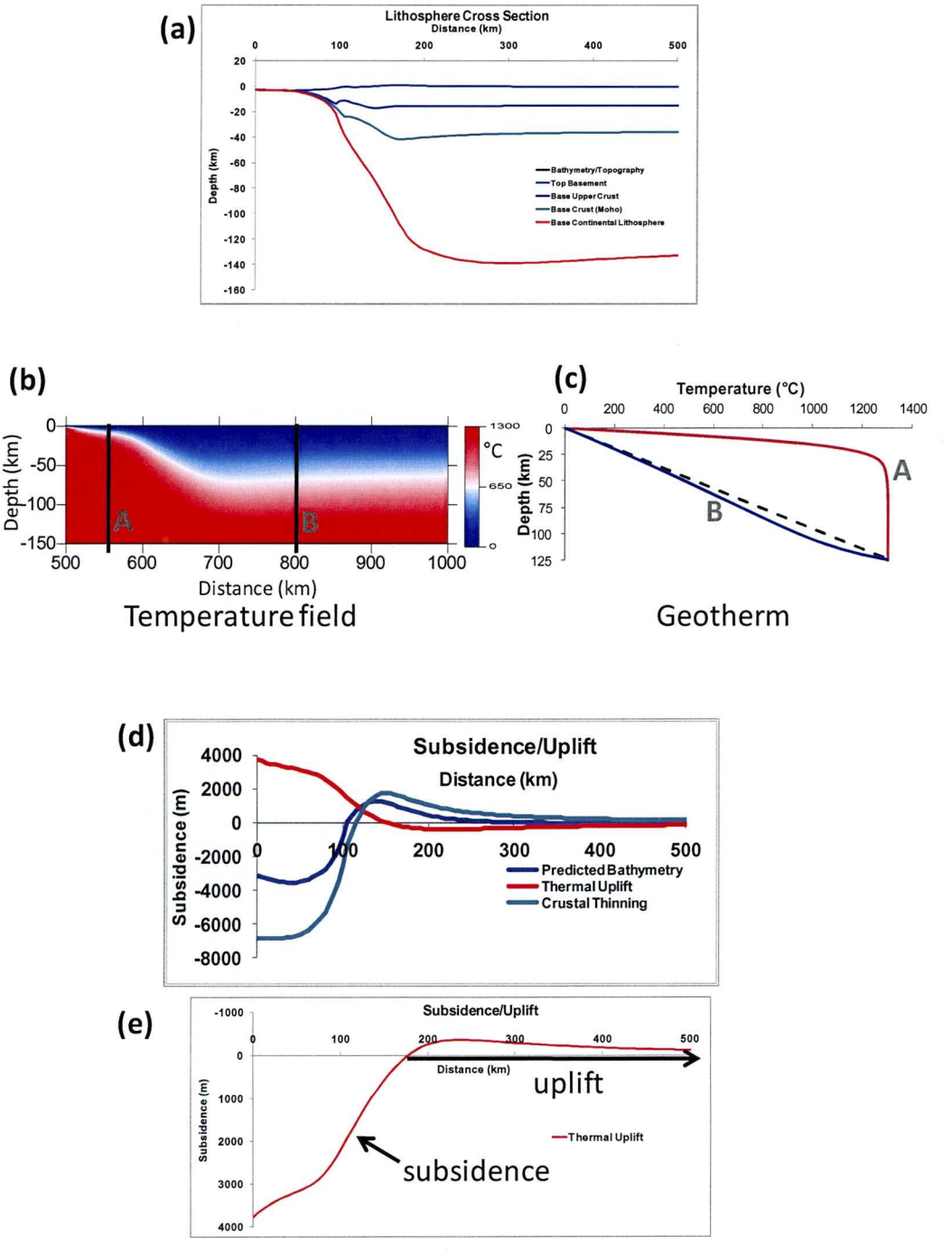

Figure 4.13: Example of the local isostatic response to crustal thinning and geotherm perturbation predicted by the general model. a) Lithosphere cross section with thicker continental lithosphere observed inland of the region of continental lithosphere thinning; b) temperature field and c) corresponding geotherm perturbation. Dashed line is initial linear geotherm, A is raised geotherm over oceanic lithosphere and B is geotherm over cooled, thickened lithosphere. d) Predicted bathymetry, thermal uplift and crustal thinning using local isostasy and e) thermal uplift to time infinity. Model predicts initial syn-rift uplift due to the isostatic response to crustal thickening. As the geotherm re-equilibrates the offshore region will subside whilst the hinterland uplifts.

$$L^{th}(x) = \int_0^{\infty} \rho_m \alpha \Delta T(x) g \qquad [4.19]$$

where α = coefficient of thermal expansion and $\Delta T(x)$ = the difference between the current temperature and initial temperature integrated down the lithospheric column at co-ordinate x. The local isostatic response to the sum of the geotherm perturbation and crustal thinning loads gives the predicted topography/bathymetry of the margin (Figure 4.13d) and is calculated by:

$$w = \frac{L^{ct} + L^{th}}{(\rho_m(1 - \alpha T_a) - \rho_i)g} \qquad [4.20]$$

where ρ_i = surface infill density and w = isostatic response.

At continental breakup the geotherm is elevated over the oceanic and thinned continental lithosphere regions and decreased over the thickened lithosphere of the continental hinterland region (Figure 4.13b & c). Re-equilibration of the geotherm leads to cooling and subsidence of the warmed oceanic and thinned continental margin lithosphere, and warming and a gradual uplift of the continental hinterland. Inverting the isostatic response to the geotherm perturbation then gives the thermal subsidence and uplift to time infinity. The post-breakup thermal uplift of the continental hinterland may be further amplified by the isostatic response to erosion, which is discussed in Chapters 7 and 8.

4.5 Model behaviour

4.5.1 Pre-breakup deformation of the continental lithosphere

As discussed in the previous sections, continental lithosphere thinning prior to breakup may occur by either pure shear, buoyancy-driven upwelling (modelled either by Stokes flow or a propagating upwelling-divergent flow) or combined pure shear and buoyancy-driven upwelling. Figure 4.14 shows examples of the temperature field and lithosphere cross section resulting from continental rifting by pure shear only, with narrow and wide zones of extension. The width of the pure shear zone controls the width of the resulting rifted margin, with a wider zone producing a wider zone of thinning of the crust and lithosphere. Examples of the temperature field and lithosphere cross section through time for continental breakup

by a propagating upwelling-divergent flow are shown in Figure 4.15. These demonstrate that the magnitude of the pre-breakup thinning Vz makes no difference to the predicted lithosphere material deformation, but does affect the temperature field with a higher Vz resulting in a larger thermal anomaly at breakup.

For rifting with simultaneous pure shear and upwelling-divergent flow, a higher upwelling velocity during the combined flow field event means a shorter duration for the event and therefore there is less continental lithosphere thinning by pure shear, producing a narrower margin than for low upwelling velocities (Figure 4.16). An example of the temperature field, flow lines and lithosphere cross section resulting from rifting by combined pure shear and Stokes flow field is shown in Figure 4.17. A lower Vz leads to a wider zone of continental lithosphere thinning as the duration of rifting is longer and therefore the horizontal extension due to pure shear is greater.

The width of the margin is largely controlled by pure shear, with wider zones of lithosphere thinning predicted in the models with the greatest pure shear extension as they have the greatest amount of lateral material advection. The two mechanisms, Stokes flow or propagating upwelling-divergent flow, used to represent the buoyancy-driven upwelling predict significantly different margin geometries, with the Stokes flow generating much greater thinning of the lower crust and upper lithosphere but less thinning of the lower lithosphere compared to the upwelling-divergent flow field (Figures 4.16 & 4.17).

The air-loaded local isostatic response to geotherm perturbation and crustal thinning from these different mechanisms for pre-breakup lithosphere thinning is shown in Figure 4.18, where the blue curve is the predicted topography, and the green and red curves are the isostatic response to crustal thinning and geotherm perturbation respectively. The curves correspond to the time of breakup and after 5 Myr sea-floor spreading; these have been plotted to demonstrate how the predicted topography would evolve. Rift shoulder uplift is observed at breakup in all models except for rifting by a wide zone of pure shear, but is greatest in the upwelling-divergent flow models. The models with upwelling-divergent flow also predict an initial thermal subsidence in the continental hinterland region.

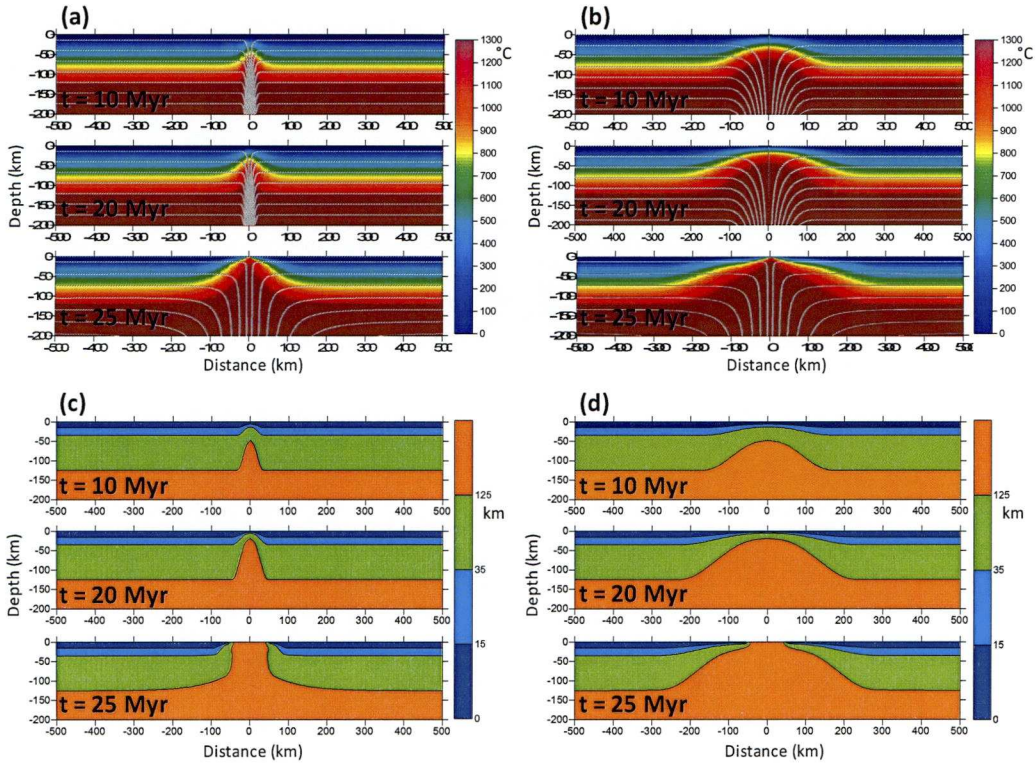

Figure 4.14: Sensitivity of temperature field (top) and lithosphere cross section (bottom) to width of pure shear extension. a) & c) pure shear half-width = 25 km (margin extension = 24 km). b) & d) pure shear half-width = 125 km (margin extension = 119 km). Pure shear event for 20 Myr with strain rate = 3×10^{-15} s^{-1}, followed by 5 Myr of sea-floor spreading with Vx = 1 cm yr^{-1} and Vz = 2 cm yr^{-1}. Figures shown in reference frame of the mid-ocean ridge.

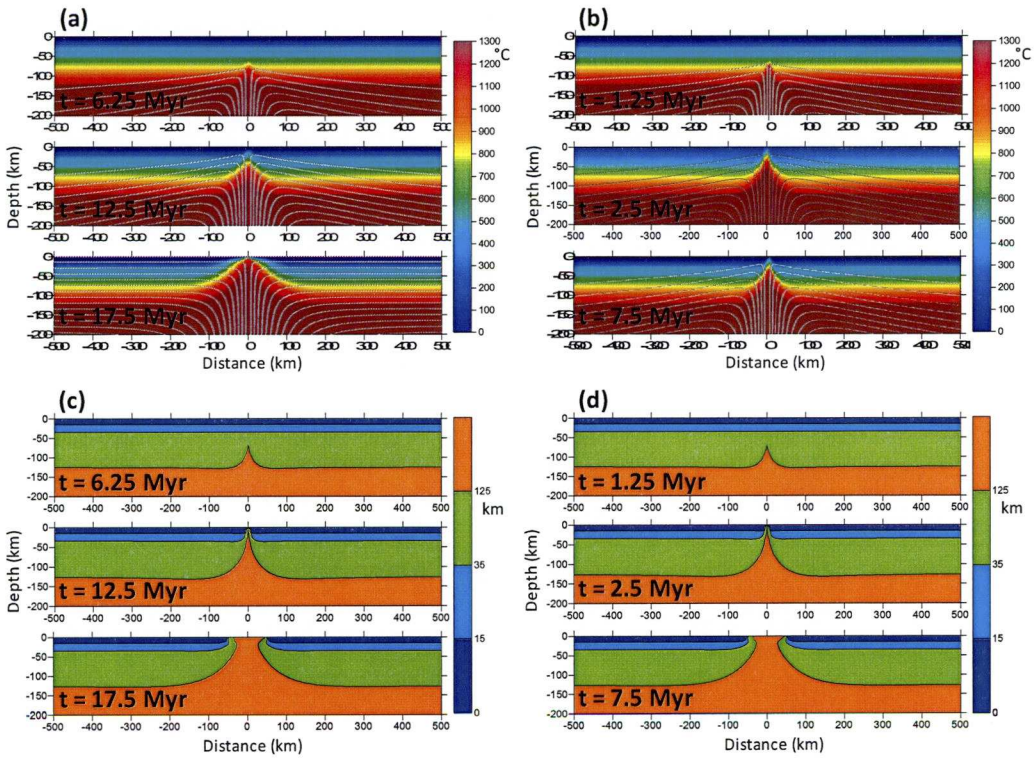

Figure 4.15: Sensitivity of temperature field (top) and lithosphere cross section (bottom) to magnitude of pre-breakup Vz of propagating upwelling-divergent flow. a) & c) pre-breakup Vz = 1 cm yr^{-1} (breakup at 12.5 Myr). b) & d) pre-breakup Vz = 5 cm yr^{-1} (breakup at 2.5 Myr). Continental breakup is followed by 5 Myr of sea-floor spreading with Vx = 1 cm yr^{-1} and Vz = 2 cm yr^{-1}.

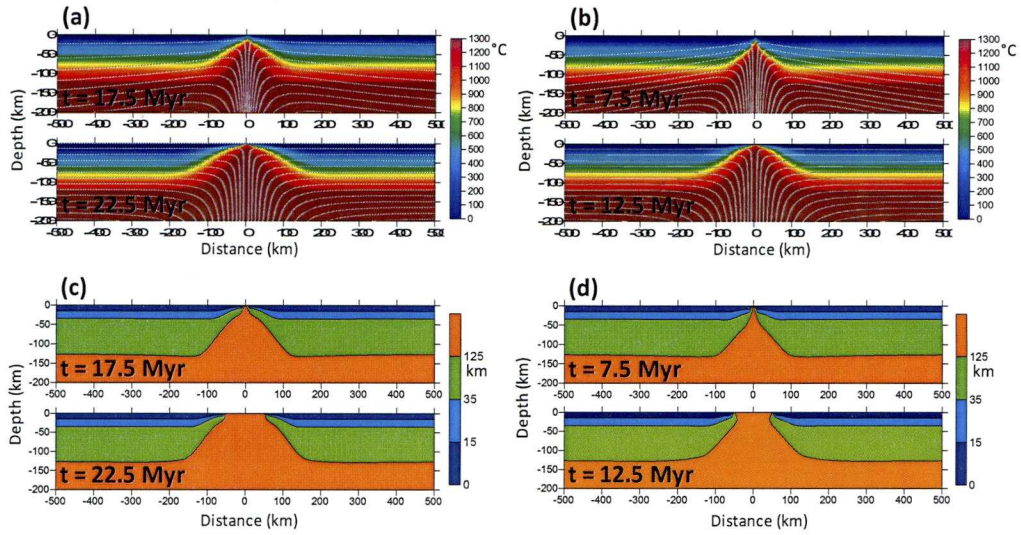

Figure 4.16: Sensitivity of temperature field (top) and lithosphere cross section (bottom) to magnitude of pre-breakup Vz in a combined pure shear and upwelling-divergent flow field. a) & c) pre-breakup Vz = 1 cm yr^{-1}. b) & d) pre-breakup Vz = 5 cm yr^{-1}. Initial rifting for 5 Myr by pure shear alone, then combined flow field followed by 5 Myr of sea-floor spreading with Vx = 1 cm yr^{-1} and Vz = 2 cm yr^{-1}. Both models use $\sigma = 3\times10^{-15}$ s^{-1} and W = 50 km. Plots shown correspond to the time of breakup and after 5 Myr sea-floor spreading.

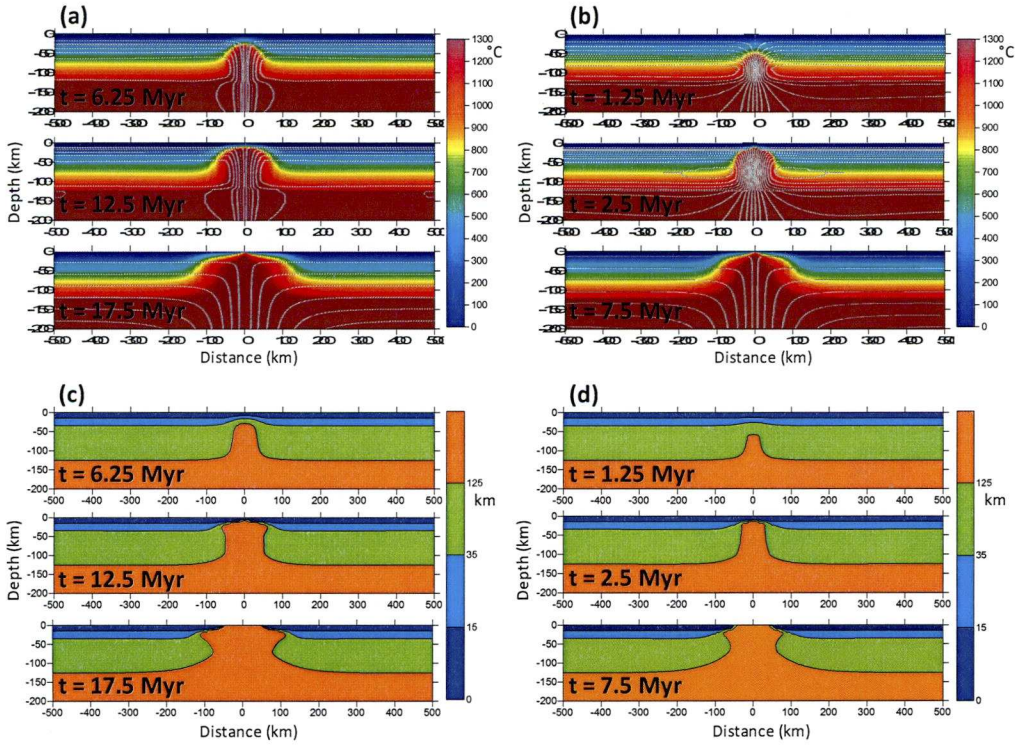

Figure 4.17: Sensitivity of temperature field (top) and lithosphere cross section (bottom) to magnitude of Stokes flow Vz in a combined pure shear and Stokes flow field. a) & c) Vz = 1 cm yr^{-1} (continental breakup at 12.5 Myr). b) & d) Vz = 5 cm yr^{-1} (breakup at 2.5 Myr). In both models, $\sigma = 3\times10^{-15}$ s^{-1}, W = 50 km and $\lambda = 0.01$.

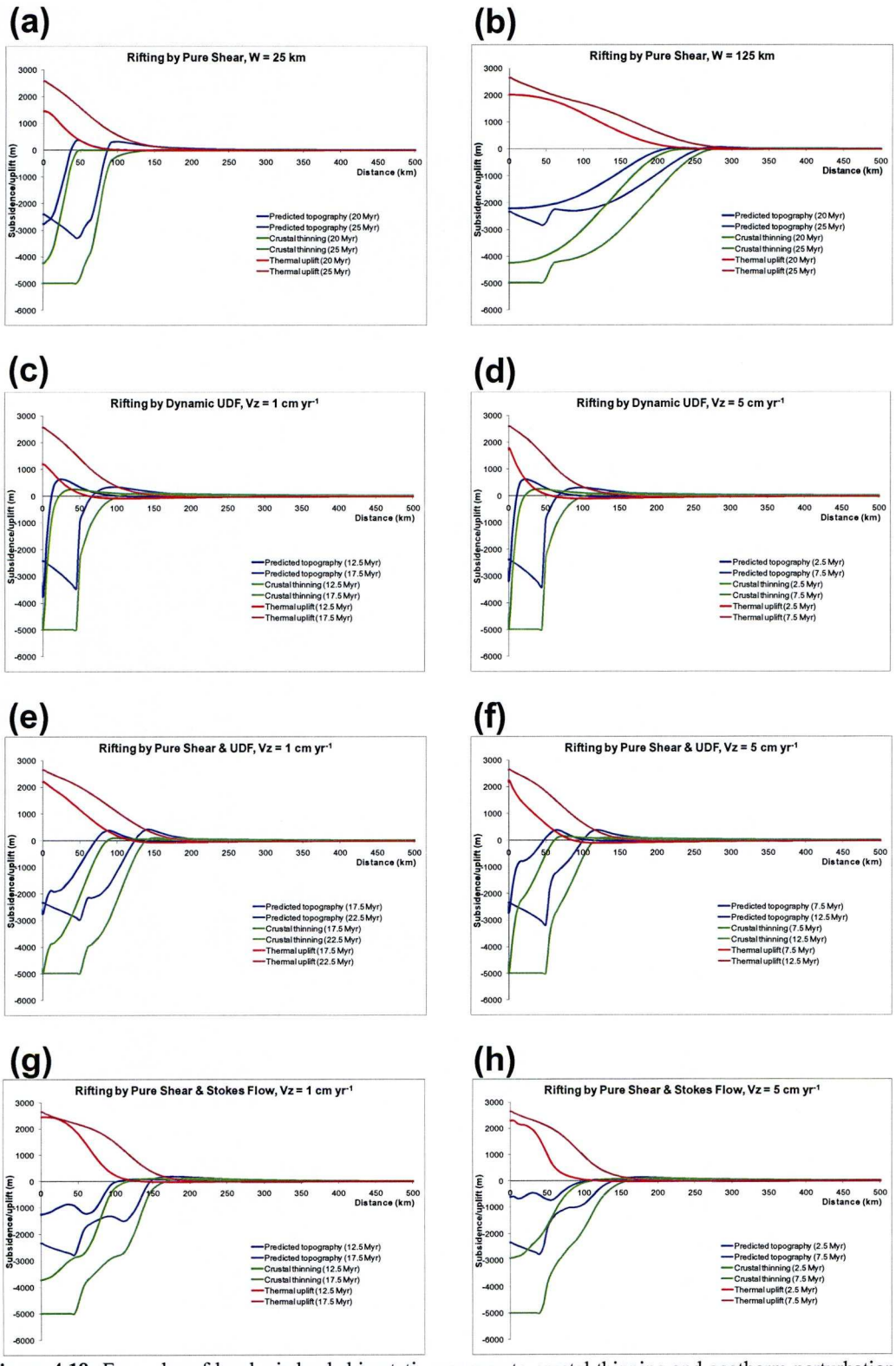

Figure 4.18: Examples of local, air-loaded isostatic response to crustal thinning and geotherm perturbation for pre-breakup parameters. Curves plotted at time of breakup and after 5 Myr of sea-floor spreading with Vx = 1 cm yr^{-1} and Vz = 2 cm yr^{-1}. Rifting by pure shear only with a) W = 25 km (E = 47 km) and b) W = 125 km (E = 237 km); in both models $\sigma = 3\times10^{-15}$ s^{-1}. Rifting by dynamic upwelling divergent flow (UDF) only with c) Vz = 1 cm yr^{-1} and d) Vz = 5 cm yr^{-1}. Rifting by combined pure shear and UDF with e) Vz = 1 cm yr^{-1} and f) Vz = 5 cm yr^{-1}; in both models W = 50 km and $\sigma = 3\times10^{-15}$ s^{-1}, with rifting by pure shear only for 5 Myr prior to the onset of the combined flow field. Rifting by combined pure shear and Stokes flow with g) Vz = 1 cm yr^{-1} and h) Vz = 5 cm yr^{-1}; in both models W = 50 km and $\sigma = 3\times10^{-15}$ s^{-1}. Figures shown in reference frame of mid-ocean ridge.

4.5.2 Post-breakup deformation of the continental lithosphere

Further deformation of the continental lithosphere may occur after continental breakup and the onset of sea-floor spreading, when Vx becomes finite. The effect of increasing the Vz/Vx ratio and spreading rate during early sea-floor spreading on the temperature field and lithosphere cross section is shown in Figure 4.19. At higher Vz/Vx the flow lines show the continental lithosphere and asthenosphere material moves downwards away from the mid-ocean ridge, leading to a thickening of the crust and lithosphere which can be seen in the corresponding lithosphere cross sections. Increasing the half-spreading rate, whilst keeping the Vz/Vx ratio constant, also leads to greater thickening of the continental lithosphere. The temperature field, flow lines and lithosphere cross section for wedge angles of 0°, 10°, 25° and 40° with respective Vx = 8 cm yr^{-1}, 4 cm yr^{-1}, 1.5 cm yr^{-1} and 1 cm yr^{-1} and Vz constant at 8 cm yr^{-1} after 5 Myr sea-floor spreading are plotted in Figure 4.20. A pronounced thickening of the continental lithosphere and crust is observed at higher wedge angles due to the increased velocity ratio (and hence increased buoyant upwelling). The wedge angle also affects the distance over which this thickening of the continental lithosphere is observed; this distance decreases as the wedge angle increases.

The effect of varying the post-breakup parameters of Vz/Vx ratio and Vx on the predicted topography is demonstrated in Figure 4.21. The predicted syn-rift uplift and thermal subsidence of the continental hinterland increases as the Vz/Vx ratio increases. At low Vz/Vx ratios, a higher Vx results in less syn-rift uplift of the margin because the crust and lithosphere are not thinned as much (Figures 4.21a & b). With Vz/Vx = 5 (Figures 4.21e & f) the opposite of this relationship occurs, and also the initial thermal uplift of the continental hinterland is larger with a higher Vx. The representation of pre-breakup buoyancy-driven upwelling affects the syn-rift uplift with the models including upwelling-divergent flow (Figures 4.21e & f) predicting rift shoulder uplift which is greater in magnitude than the models with Stokes flow (Figures 4.21g & h), because the upwelling-divergent flow model causes a greater amount of crustal thinning, although the predicted thermal uplift and subsidence is the same.

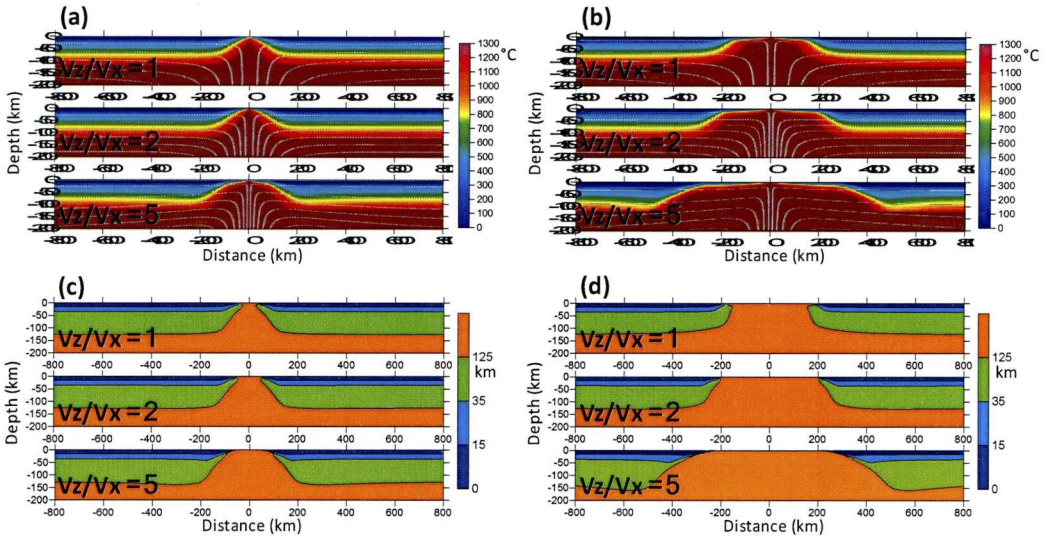

Figure 4.19: Sensitivity of temperature field (top) and lithosphere cross section (bottom) to sea-floor spreading Vz/Vx ratio. a) & c) Vx = 1 cm yr^{-1}; b) & d) Vx = 4 cm yr^{-1}. Pre-breakup rifting initially by pure shear for 10 Myr followed by combined flow field for 2.5 Myr with with $\sigma = 3\times10^{-15}$ s^{-1}, W = 50km and Vz = 5 cm yr^{-1}, then 5 Myr of sea-floor spreading.

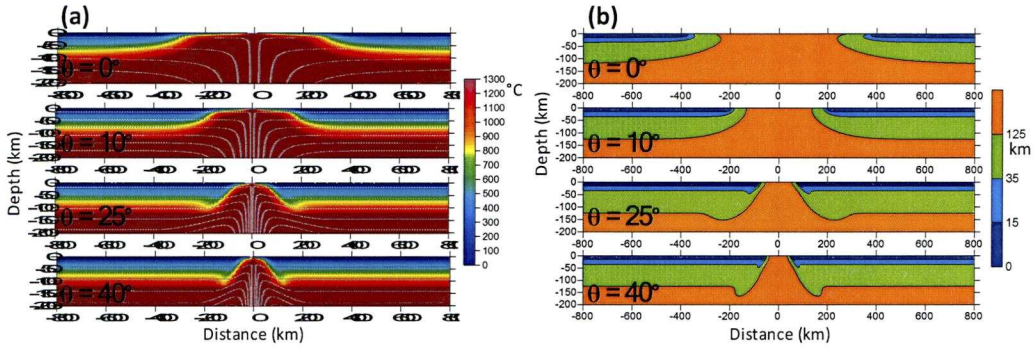

Figure 4.20: Sensitivity of temperature field (left) and lithosphere cross section (right) to wedge angle, after 5 Myr of sea-floor spreading (with a static udf). All with Vz = 8 cm yr^{-1} and Vx corresponding to θ. For θ = 0°, Vx = 8 cm yr^{-1}; for θ = 10°, Vx = 4 cm yr^{-1}; for θ = 25°, Vx = 1.5 cm yr^{-1} and for θ = 40°, Vx = 1 cm yr^{-1}. A pronounced thickening of the lithosphere is observed at higher θ due to increased buoyancy.

4.6 Sensitivity testing of the key model parameters

Post-breakup rifted margin subsidence and hinterland uplift are sensitive to the combined deformation resulting from pure shear and buoyancy-driven upwelling. Key parameters controlling the magnitude of the hinterland uplift include pure shear width, pure shear strain rate, magnitude of the pre-breakup buoyancy-driven upwelling (represented by upwelling-divergent flow or Stokes flow), V_z/V_x during early sea-floor spreading, sea-floor spreading rate (Vx) and the wedge angle.

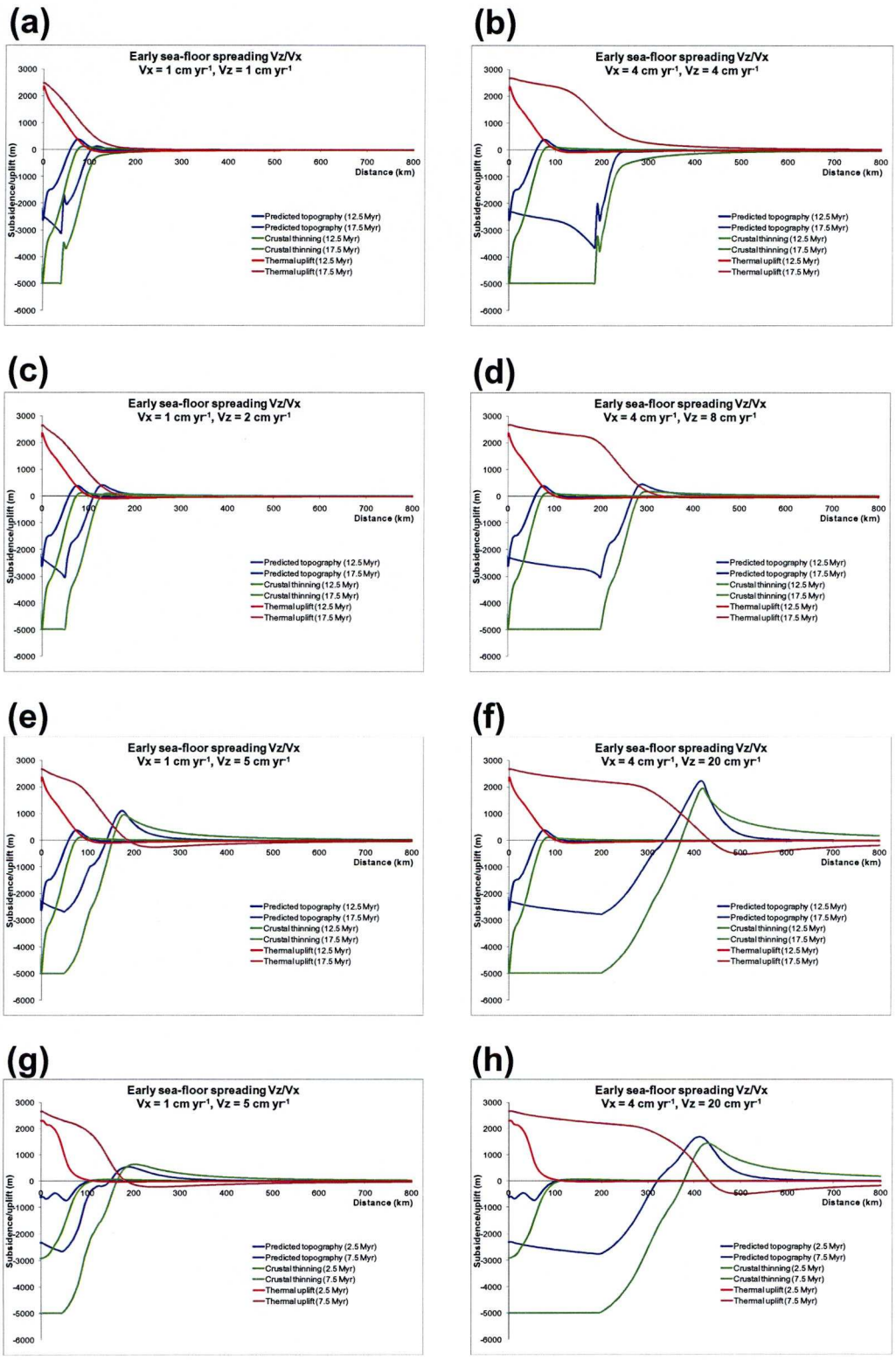

Figure 4.21: Examples of local, air-loaded isostatic response to crustal thinning and geotherm perturbation for post-breakup Vz/Vx ratios. Curves plotted at time of breakup and after 5 Myr of sea-floor spreading. a) Vz/Vx = 1 with Vx = 1 cm yr^{-1}; b) Vz/Vx = 1 with Vx = 4 cm yr^{-1}; c) Vz/Vx = 2 with Vx = 1 cm yr^{-1}; d) Vz/Vx = 2 with Vx = 4 cm yr^{-1}; e) Vz/Vx = 5 with Vx = 1 cm yr^{-1}; f) Vz/Vx = 5 with Vx = 4 cm yr^{-1}. In these models W = 50 km, $\sigma = 3\times10^{-15}$ s^{-1} and pre-breakup Vz = 5 cm yr^{-1}, with rifting by pure shear only for 10 Myr followed by a combined flow field of pure shear and udf for 2.5 Myr. g) Vz/Vx = 5 with Vx = 1 cm yr^{-1}; h) Vz/Vx = 5 with Vx = 4 cm yr^{-1}. For these two models W = 50 km, $\sigma = 3\times10^{-15}$ s^{-1} and pre-breakup Vz = 5 cm yr^{-1} with rifting by combined pure shear and stokes flow for 2.5 Myr. Figures in reference frame of the mid-ocean ridge.

Varying these input parameters demonstrates the effect that each parameter has on the amplitude, wavelength and location of the hinterland uplift. Sensitivity testing (using air-loaded local isostasy) has been carried out to determine the relative importance of the key input parameters and to determine what circumstances may generate the significant amounts of post-breakup uplift as indicated by observations.

4.6.1 Sensitivity of the predicted thermal uplift to pre-breakup parameters

The sensitivity of the predicted thermal uplift at breakup to combined pure shear and upwelling-divergent flow is shown in Figures 4.22a, b & c. Increasing the pure shear strain rate (Figure 4.22a) or the pure shear half-width (Figure 4.22b) leads to a small decrease in the amplitude and wavelength of the predicted thermal uplift but an increase in the distance of the location of maximum uplift from the ocean-continent transition. This is because increasing the strain rate or the width leads to greater extension of the margin and therefore leads to greater thinning of the continental lithosphere. Increasing the magnitude of the pre-breakup upwelling-divergent flow increases both the amplitude and wavelength of the predicted thermal uplift and leads to a decrease in distance to the maximum uplift, as shown in Figure 4.22c. For higher upwelling velocities the duration of the combined pure shear and upwelling-divergent flow field event is shorter, therefore the buoyant upwelling is more dominant than the pure shear component. The sensitivity of the predicted thermal uplift to the parameters in the combined pure shear and Stokes flow field is shown in Figure 4.22d, e & f. Varying the pure shear strain rate and width and the Vz has a negligible effect on the predicted thermal uplift, which is much smaller than predicted by the pre-breakup upwelling-divergent flow field.

4.6.2 Sensitivity of the predicted thermal uplift to post-breakup parameters

A higher Vz/Vx ratio during early sea-floor spreading leads to material upwelling at a faster rate beneath the ridge than the plates are diverging, and so material is pushed downwards, as well as outwards, away from the ridge. This results in a much greater thermal uplift in terms of amplitude and wavelength, but has little effect on the location of maximum uplift (Figure 4.22g). If Vx is increased, but Vz/Vx is kept constant, the magnitude of the thermal uplift, its wavelength, and the distance between the ocean-continent transition and maximum uplift all increase (Figure 4.22h). In Figure 4.22i, the sensitivity of the thermal uplift to the wedge

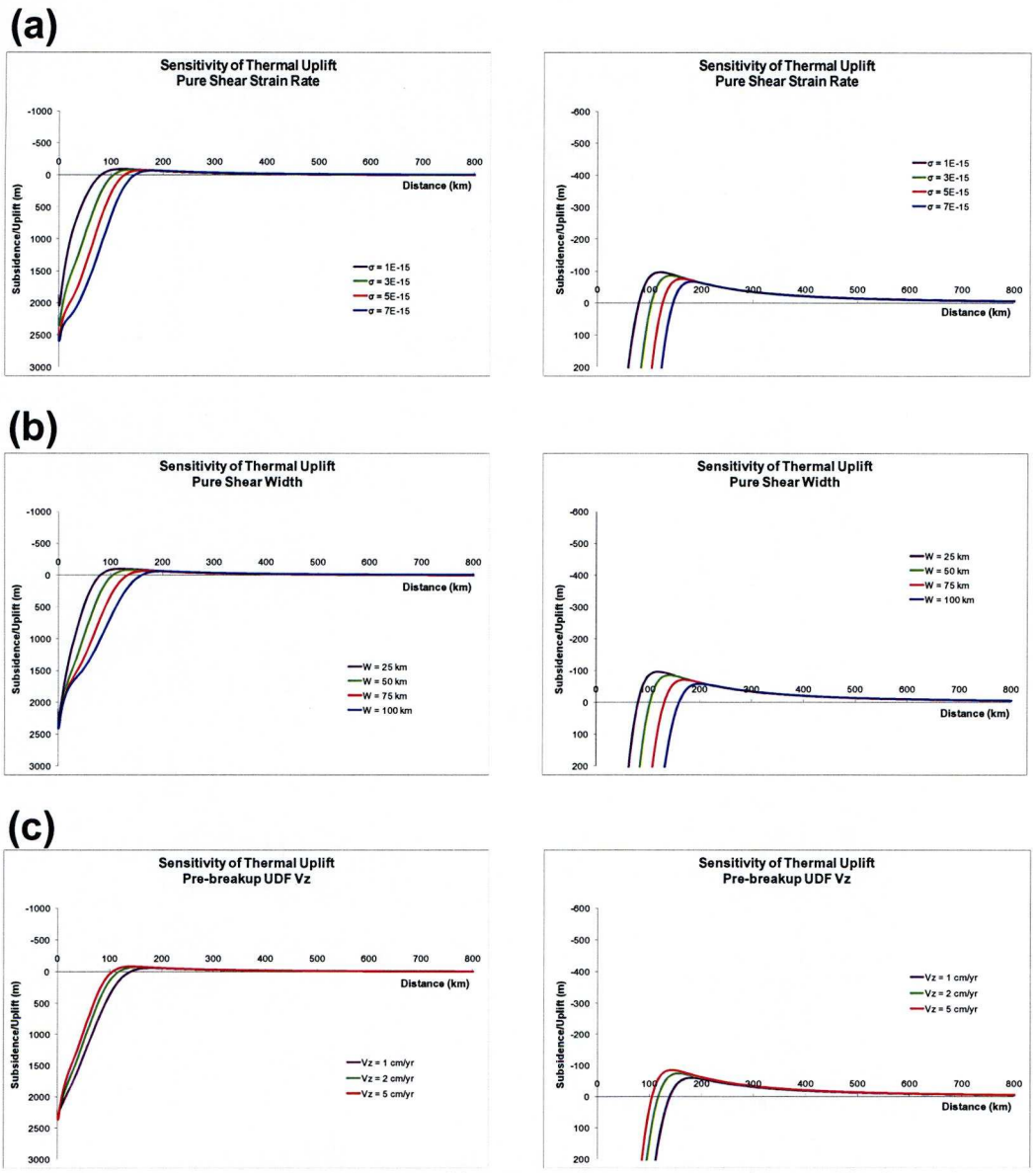

Figure 4.22: Sensitivity of predicted thermal uplift to pre-breakup parameters of the combined pure shear and UDF flow field a) pure shear strain rate, b) pure shear width and c) magnitude of the pre-breakup Vz. Left hand side shows whole margin and right hand side shows a close-up along the y-axis. All models have rifting by pure shear for 10 Myr followed by combined flow field with the duration dependent on the magnitude of Vz. Values of $\sigma = 3\times10^{-15}$ s^{-1}, W = 50 km and Vz = 5 cm yr^{-1} have been used unless otherwise stated. Figures in reference frame of the mid-ocean ridge.

(d)

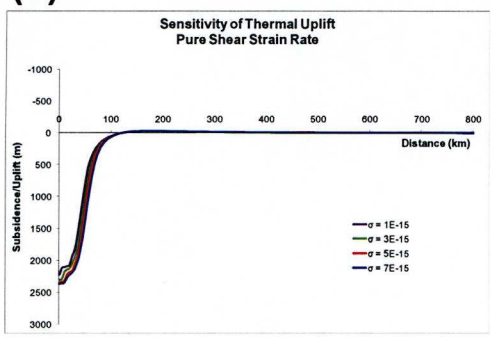

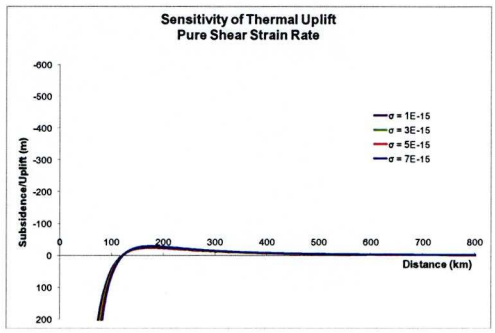

(e)

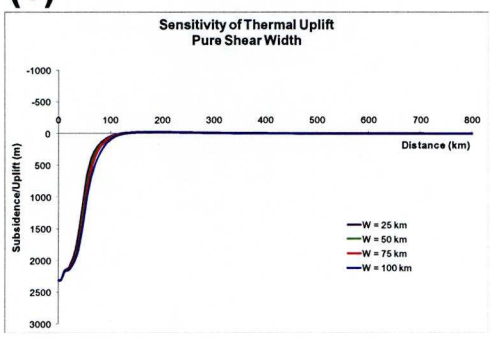

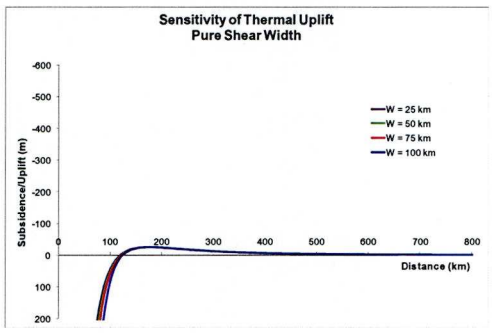

(f)

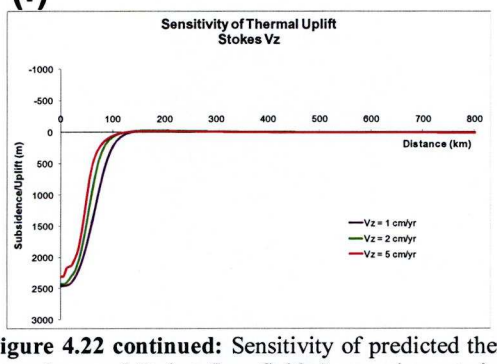

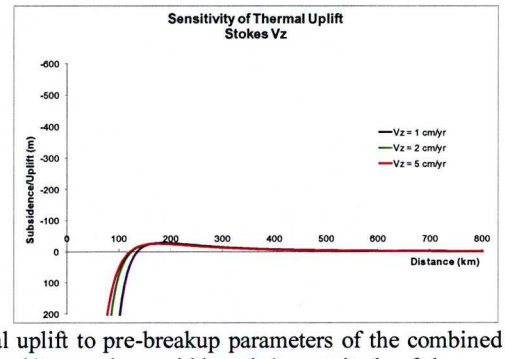

Figure 4.22 continued: Sensitivity of predicted thermal uplift to pre-breakup parameters of the combined pure shear and Stokes flow field a) pure shear strain rate, b) pure shear width and c) magnitude of the pre-breakup Vz. Left hand side shows whole margin and right hand side shows a close-up along the y-axis. All models have the combined flow field with the duration dependent on the magnitude of Vz. Values of $\sigma = 3\times10^{-15}$ s^{-1}, W = 50 km and Vz = 5 cm yr^{-1} have been used unless otherwise stated.

(g)

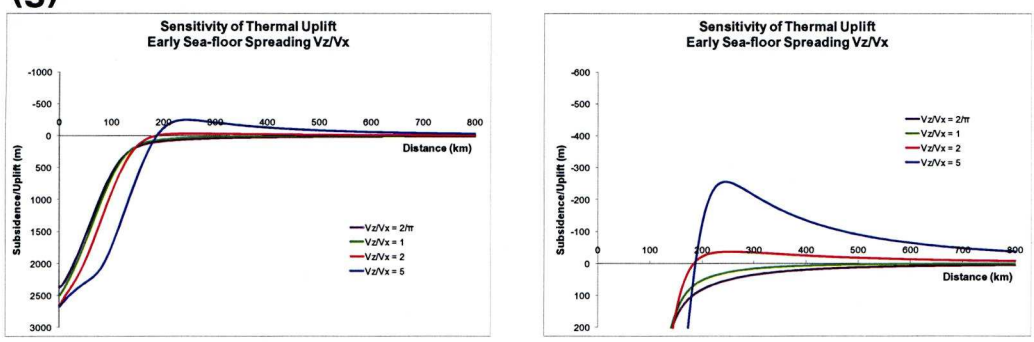

(h)

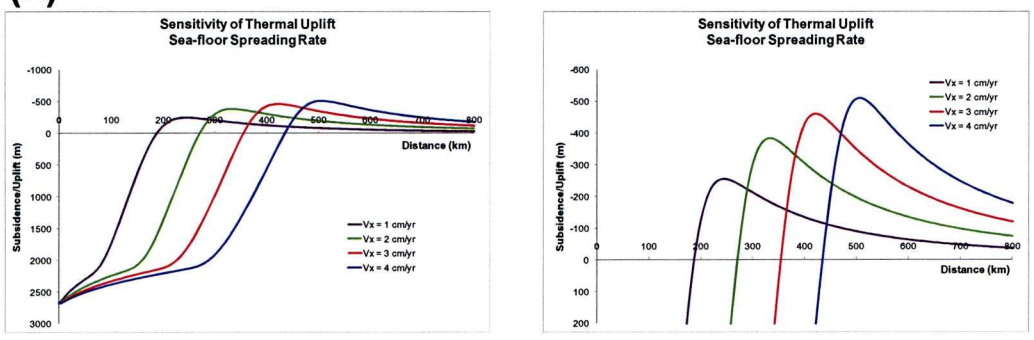

(i)

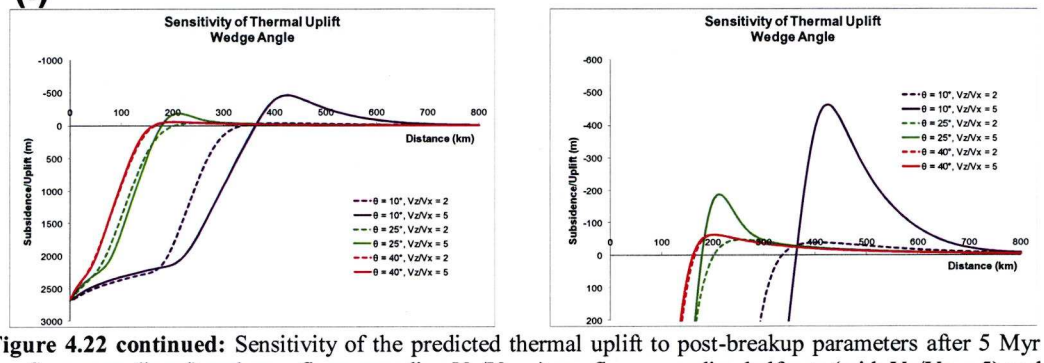

Figure 4.22 continued: Sensitivity of the predicted thermal uplift to post-breakup parameters after 5 Myr sea-floor spreading d) early sea-floor spreading Vz/Vx, e) sea-floor spreading half-rate (with Vz/Vx = 5) and f) wedge angle. Values used for pre-breakup lithosphere thinning with pure shear and UDF as before.

angle is shown. At a low Vz/Vx the amplitude of the predicted thermal uplift increases slightly with increasing wedge angle whereas for a higher Vz/Vx the thermal uplift increases dramatically with decreasing wedge angle. This may, at least in part, be due to the limitations of using a plate model with a fixed basal temperature at 125 km depth. The magnitude of the wedge angle also provides a control on the wavelength of the predicted uplift with the wavelength decreasing as the wedge angle increases.

4.7 Summary

In this chapter, models for continental lithosphere thinning and breakup have been presented, considering both pre- and post-breakup processes. Continental lithosphere thinning by simultaneous pure shear and upwelling-divergent flow, and simultaneous pure shear and Stokes flow predict differing temperature field and lithosphere cross sections. Rifting involving Stokes flow leads to greater thinning of the lower crust, but little thickening of the continental lithosphere in the hinterland unlike with rifting by upwelling-divergent flow; this is due to the assumption of free slip along the brittle lid boundary. It has been shown that continental lithosphere can continue to be deformed after breakup and significant thickening of the continental lithosphere can occur in the hinterland regions due to buoyant upwelling beneath the young mid-ocean ridge.

The local, air-loaded isostatic response to these models has also been explored. Both pre-and post-breakup processes may generate thermal uplift, with more thermal uplift predicted by the pre-breakup upwelling-divergent flow model than by the Stokes flow model. The post-breakup parameters of Vz/Vx ratio and spreading rate are the dominant controls on the predicted hinterland thermal uplift. Improvements to this model, including a variation in lithosphere thickness across the OCT and flexural isostasy are discussed in the next two chapters.

4.8 References

Batchelor, G. K. (1967) *An introduction to fluid dynamics*, Cambridge U.P.

Beaumont, C., C. E. Keen and R. Boutilier (1982), On the Evolution of Rifted Continental Margins - Comparison of Models and Observations for the Nova-Scotian Margin, *Geophysical Journal of the Royal Astronomical Society*, vol. 70, no. 3, p. 667-715.

Boutilier, R. R. and C. E. Keen (1999), Small-scale convection and divergent plate boundaries, *Journal of Geophysical Research-Solid Earth*, vol. 104, no. B4, p. 7389-7403.

Bown, J. W. and R. S. White (1994), Variation with Spreading Rate of Oceanic Crustal Thickness and Geochemistry, *Earth and Planetary Science Letters*, vol. 121, no. 3-4, p. 435-449.

Braun, M. G., G. Hirth and E. M. Parmentier (2000), The effects of deep damp melting on mantle flow and melt generation beneath mid-ocean ridges, *Earth and Planetary Science Letters*, vol. 176, no. 3-4, p. 339-356.

Callot, J. P., L. Geoffroy and J. P. Brun (2002), Development of volcanic passive margins: Three-dimensional laboratory models, *Tectonics*, vol. 21, no. 6, p. 1052.

Cannat, M. (1996), How thick is the magmatic crust at slow spreading oceanic ridges?, *Journal of Geophysical Research-Solid Earth*, vol. 101, no. B2, p. 2847-2857.

Cooper, C. (2010) Anomalous bathymetry and mass heterogeneity at the conjugate Iberia and Newfoundland rifted margins, *PhD Thesis*, University of Liverpool.

Crosby, A., N. White, G. Edwards and D. J. Shillington (2008), Evolution of the Newfoundland-Iberia conjugate rifted margins, *Earth and Planetary Science Letters*, vol. 273, no. 1-2, p. 214-226.

Davis, M. and N. Kusznir (2002), Are buoyancy forces important during the formation of rifted margins?, *Geophysical Journal International*, vol. 149, no. 2, p. 524-533.

Davis, M. and N. Kusznir (2004), Depth-dependent lithospheric stretching at rifted continental margins, *Rheology and Deformation of the Lithosphere at Continental Margins*, vol. 352, p. 92-137.

Driscoll, N. W. and G. D. Karner (1998), Lower crustal extension across the Northern Carnarvon basin, Australia: Evidence for an eastward dipping detachment, *Journal of Geophysical Research-Solid Earth*, vol. 103, no. B3, p. 4975-4991.

Fletcher, R. (2009) Mechanisms of Continental Lithosphere Thinning and Rifted Margin Formation, *PhD Thesis*, University of Liverpool.

Fletcher, R., N. Kusznir and M. Cheadle (2009), Melt initiation and mantle exhumation at the Iberian rifted margin: Comparison of pure-shear and upwelling-divergent flow models of continental breakup, *Comptes Rendus Geoscience*, vol. 341, no. 5, p. 394-405.

Geoffroy, L. (2005), Volcanic passive margins, *Comptes Rendus Geoscience*, vol. 337, no. 16, p. 1395-1408.

Happel, J. and H. Brenner (1973) *Low Reynods Number Hydrodynamics*, Second revised edition. edn, Noordhoff International Publishing, [S.l.].

Holbrook, W. S., H. C. Larsen, J. Korenaga, T. Dahl-Jensen, I. D. Reid, P. B. Kelemen, J. R. Hopper, G. M. Kent, D. Lizarralde, S. Bernstein and R. S. Detrick (2001), Mantle thermal structure and active upwelling during continental breakup in the North Atlantic, *Earth and Planetary Science Letters*, vol. 190, no. 3-4, p. 251-266.

Huismans, R. S. and C. Beaumont (2008), Complex rifted continental margins explained by dynamical models of depth-dependent lithospheric extension, *Geology*, vol. 36, no. 2, p. 163-166.

Jarvis, G. T. and D. P. Mckenzie (1980), Sedimentary Basin Formation with Finite Extension Rates, *Earth and Planetary Science Letters*, vol. 48, no. 1, p. 42-52.

Jones, S. M., N. White and J. Maclennan (2002), V-shaped ridges around Iceland: Implications for spatial and temporal patterns of mantle convection, *Geochemistry Geophysics Geosystems*, vol. 3, p. 1059.

Korenaga, J., P. B. Kelemen and W. S. Holbrook (2002), Methods for resolving the origin of large igneous provinces from crustal seismology, *Journal of Geophysical Research-Solid Earth*, vol. 107, no. B9, p. 2178.

Kusznir, N. J. and G. D. Karner (2007) Continental lithospheric thinning and breakup in response to upwelling divergent mantle flow: application to the Woodlark, Newfoundland and Iberia margins, in Karner, G. D., G. Manatschal and L. M. Pinheiro (eds), *Imaging, Mapping and Modelling Continental Lithosphere Extension and Breakup*, Geological Society, London, Special Publications, vol. 282, p. 389-419.

Lachenbruch, A. H. (1976), Dynamics of a Passive Spreading Center, *Journal of Geophysical Research*, vol. 81, no. 11, p. 1883-1902.

Lenoir, X., G. Feraud and L. Geoffroy (2003), High-rate flexure of the East Greenland volcanic margin: constraints from Ar-40/Ar-39 dating of basaltic dykes, *Earth and Planetary Science Letters*, vol. 214, no. 3-4, p. 515-528.

Marsden, G. (1990) Numerical Modelling of Continental Lithosphere Extension Leading to Sedimentary Basin Formation, *PhD Thesis*, University of Liverpool.

Mckenzie, D. (1978), Some Remarks on Development of Sedimentary Basins, *Earth and Planetary Science Letters*, vol. 40, no. 1, p. 25-32.

Newman, R. and N. White (1999), The dynamics of extensional sedimentary basins: constraints from subsidence inversion, *Philosophical Transactions of the Royal Society of London Series a-Mathematical Physical and Engineering Sciences*, vol. 357, no. 1753, p. 805-830.

Nielsen, T. K. and J. R. Hopper (2002), Formation of volcanic rifted margins: Are temperature anomalies required?, *Geophysical Research Letters*, vol. 29, no. 21, p. 2022.

Nielsen, T. K. and J. R. Hopper (2004), From rift to drift: Mantle melting during continental breakup, *Geochemistry Geophysics Geosystems*, vol. 5, p. Q07003.

Ollier, C. D. (1985), Morphotectonics of passive continental margins: introduction, *Zeitschrift fur Geomorphologie, Supplementband*, vol. 54, p. 1-9.

Phipps Morgan, J. (1987), Melt Migration beneath Mid-Ocean Spreading Centers, *Geophysical Research Letters*, vol. 14, no. 12, p. 1238-1241.

Reston, T. J. (2009), The extension discrepancy and syn-rift subsidence deficit at rifted margins, *Petroleum Geoscience*, vol. 15, no. 3, p. 217-237.

Rowley, D. B. and D. Sahagian (1986), Depth-Dependent Stretching - a Different Approach, *Geology*, vol. 14, no. 1, p. 32-35.

Royden, L. and C. E. Keen (1980), Rifting Process and Thermal Evolution of the Continental-Margin of Eastern Canada Determined from Subsidence Curves, *Earth and Planetary Science Letters*, vol. 51, no. 2, p. 343-361.

Schmeling, H., A. R. Cruden and G. Marquart (1988), Finite Deformation in and around a Fluid Sphere Moving through a Viscous Medium - Implications for Diapiric Ascent, *Tectonophysics*, vol. 149, no. 1-2, p. 17-34.

Scott, D. R. (1992), Small-scale convection and mantle melting beneath mid-ocean ridges, *Mantle Flow and Melt Generation at Mid-ocean Ridges*, vol. Geophysical Monograph Series 71, p. 311-326.

Shen, Y. and D. W. Forsyth (1992), The Effects of Temperature-Dependent and Pressure-Dependent Viscosity on 3-Dimensional Passive Flow of the Mantle beneath a Ridge-Transform System, *Journal of Geophysical Research-Solid Earth*, vol. 97, no. B13, p. 19717-19728.

Simon, K., R. S. Huismans and C. Beaumont (2009), Dynamical modelling of lithospheric extension and small-scale convection: implications for magmatism during the formation of volcanic rifted margins, *Geophysical Journal International*, vol. 176, no. 1, p. 327-350.

Skilbeck, J. N. (1975), In the fluid dynamics of ridge crests, *Notes on the 1975 Summer Study Program in Geophysical Fluid Dynamics at the Woods Hole Oceanographic Institution 2*, vol. Woods Hole Ocean Inst. Ref No. 75-58, p. 113-122.

Spiegelman, M. and D. Mckenzie (1987), Simple 2-D Models for Melt Extraction at Midocean Ridges and Island Arcs, *Earth and Planetary Science Letters*, vol. 83, no. 1-4, p. 137-152.

Spiegelman, M. and J. R. Reynolds (1999), Combined dynamic and geochemical evidence for convergent melt flow beneath the East Pacific Rise, *Nature*, vol. 402, no. 6759, p. 282-285.

Turcotte, D. L. and G. Schubert (2002) *Geodynamics*, 2nd edn, Cambridge University Press, Cambridge.

White, R. S., L. K. Smith, A. W. Roberts, P. A. F. Christie, N. J. Kusznir and i. Team (2008), Lower-crustal intrusion on the North Atlantic continental margin, *Nature*, vol. 452, no. 7186, p. 460-U6.

Chapter 5

Variation in lithosphere thickness and its effect on the geotherm perturbation

5.1 Introduction

The magnitude of post-breakup thermal uplift predicted by the model is dependent on the geotherm perturbation, and therefore on the initial thermal state of the lithosphere. In the general model for continental breakup and sea-floor spreading presented in Chapter 4, the initial temperature field and its evolution were calculated using the thermal plate model. This assumes a lithosphere thickness of 125 km and a constant base temperature of 1300°C, values determined by Parsons & Sclater (1977) for oceanic lithosphere. However, continental lithosphere thickness often exceeds 125 km (Jaupart & Mareschal, 1999; Artemieva, 2009), leading to a juxtaposition of thin oceanic lithosphere against thicker continental lithosphere at the ocean-continent transition. The effect of increasing the lithosphere thickness and imposing a step change in lithosphere thickness across the ocean-continent transition on the geotherm perturbation is examined in this chapter.

5.2 Effect of increasing the continental lithosphere thickness

The thermal plate model, which assumes a lithosphere of constant thickness with a constant basal temperature, and predicts increasing thickness of the lithosphere away from the mid-ocean ridge, is considered an adequate approximation for the thermal evolution of oceanic lithosphere younger than 70 Ma (Parsons & Mckenzie, 1978). The thermal evolution of continental lithosphere is much less

constrained (Leroy et al., 2008), largely because of the complexities arising from the age distribution, radiogenic heat productivity, varying conductivity and variations in lithosphere thickness. The base of the continental lithosphere can be defined as the depth to a constant isotherm, commonly taken to be 1300°C (Artemieva, 2009). Above this boundary, heat transfer occurs predominantly by conduction, and below it, by convection. Estimates of cratonic lithosphere thicknesses based on this definition range between 140 – 350 km, although most values are less than 250 km (Artemieva & Mooney, 2002).

Figure 5.1 shows the temperature field after 5 Myr of sea-floor spreading for lithosphere thicknesses of 100, 125, 150, 175 and 200 km, assuming a constant base temperature of 1300°C and, initially, a linear geotherm. The corresponding

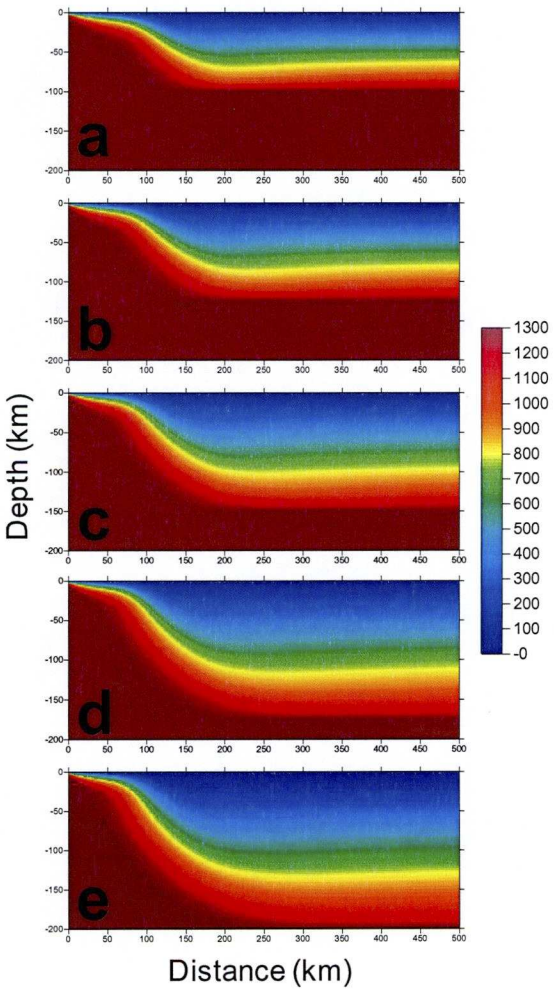

Figure 5.1: Temperature field after 5 Myr sea-floor spreading, with Vz/Vx = 5, for lithosphere thickness a) 100 km, b) 125 km, c) 150 km, d) 175 km, and e) 200 km. Pre-breakup continental lithosphere thinning modelled assuming a combined pure shear and upwelling-divergent flow field. Figures are in reference frame of the mid-ocean ridge.

topography and isostatic response to the geotherm perturbation is shown in Figure 5.2. The height of the predicted topography increases with increasing continental lithosphere thickness, as does the geotherm perturbation in the hinterland region. Therefore, a greater amount of thermal uplift for larger lithosphere thicknesses is predicted as the geotherm re-equilibrates.

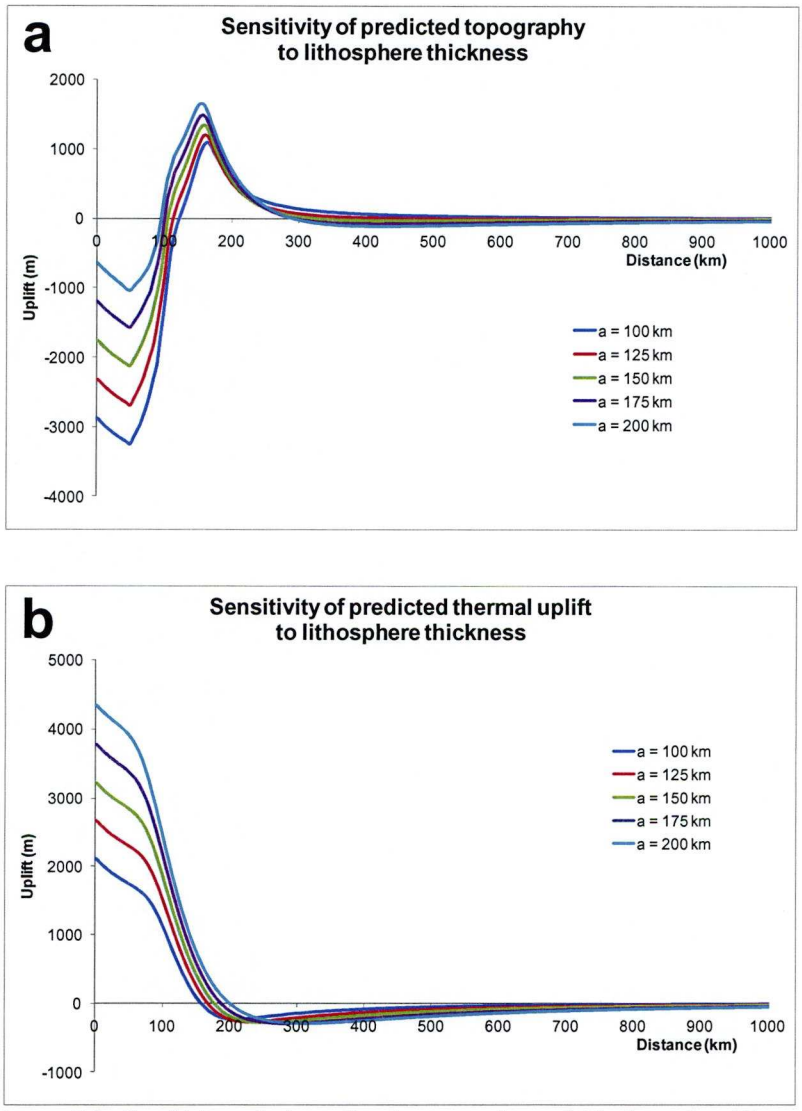

Figure 5.2: Sensitivity of a) predicted topography and b) thermal uplift to lithosphere thickness. Model is shown after 5 Myr sea-floor spreading (Vz/Vx = 5), with pre-breakup continental lithosphere thinning by a combined pure shear and upwelling-divergent flow field. Figures shown in reference frame of the mid-ocean ridge.

5.3 Variation in lithosphere thickness across the OCT

The assumption of a lithosphere thickness as large as 200 km across the whole model predicts an unrealistic thermal anomaly for oceanic regions (Figure 5.2b). A maximum oceanic lithosphere thickness of 125 km is often assumed, from agreement between the observed bathymetry and heat flow, and that predicted by the thermal plate model (Parsons & Sclater, 1977). Several studies have indicated that the ocean-continent transition may be associated with a step change in lithosphere thickness (Leroy et al., 2008; Lucazeau et al., 2008; Sandiford & Egholm, 2008; Fernandez et al., 2005), although this transition is poorly understood (Scheck-Wenderoth & Maystrenko, 2008). The juxtaposition of warm oceanic lithosphere and thinned continental lithosphere against cold, thick, cratonic lithosphere may cause a lateral variation in temperature across the rifted margin, leading to heating of the continental lithosphere adjacent to the margin. This has been shown to significantly affect the thermal subsidence and uplift of a margin (Leroy et al., 2008, & references therein), and may drive small-scale convection processes at the edge of the continent (Lucazeau et al., 2008).

A step change in lithosphere thickness at the ocean-continent transition has been included in the general model. The lithosphere thickness is initially assumed to be constant in the model, as per the plate model, but once the lithosphere has thinned to a prescribed thickness, the new lithosphere thickness boundary condition is imposed. The lithosphere thickness between the two regions is assumed to increase linearly. The resulting temperature field is shown in Figure 5.3, and the difference between the predicted temperature and that from assuming a constant lithosphere thickness is also plotted. The sensitivity of the predicted topography and the local isostatic response to the geotherm perturbation is shown in Figure 5.4. A thermal anomaly is observed over the transition region, with the step boundary condition predicting warmer temperatures than the plate model. The anomaly has an elongated shape which is parallel to the gradient of the linear transition between the oceanic and continental lithosphere, and its magnitude and width increases as the step increases. The anomaly is greatest near to the base of the lithosphere, although a small temperature difference can still be observed close to the surface.

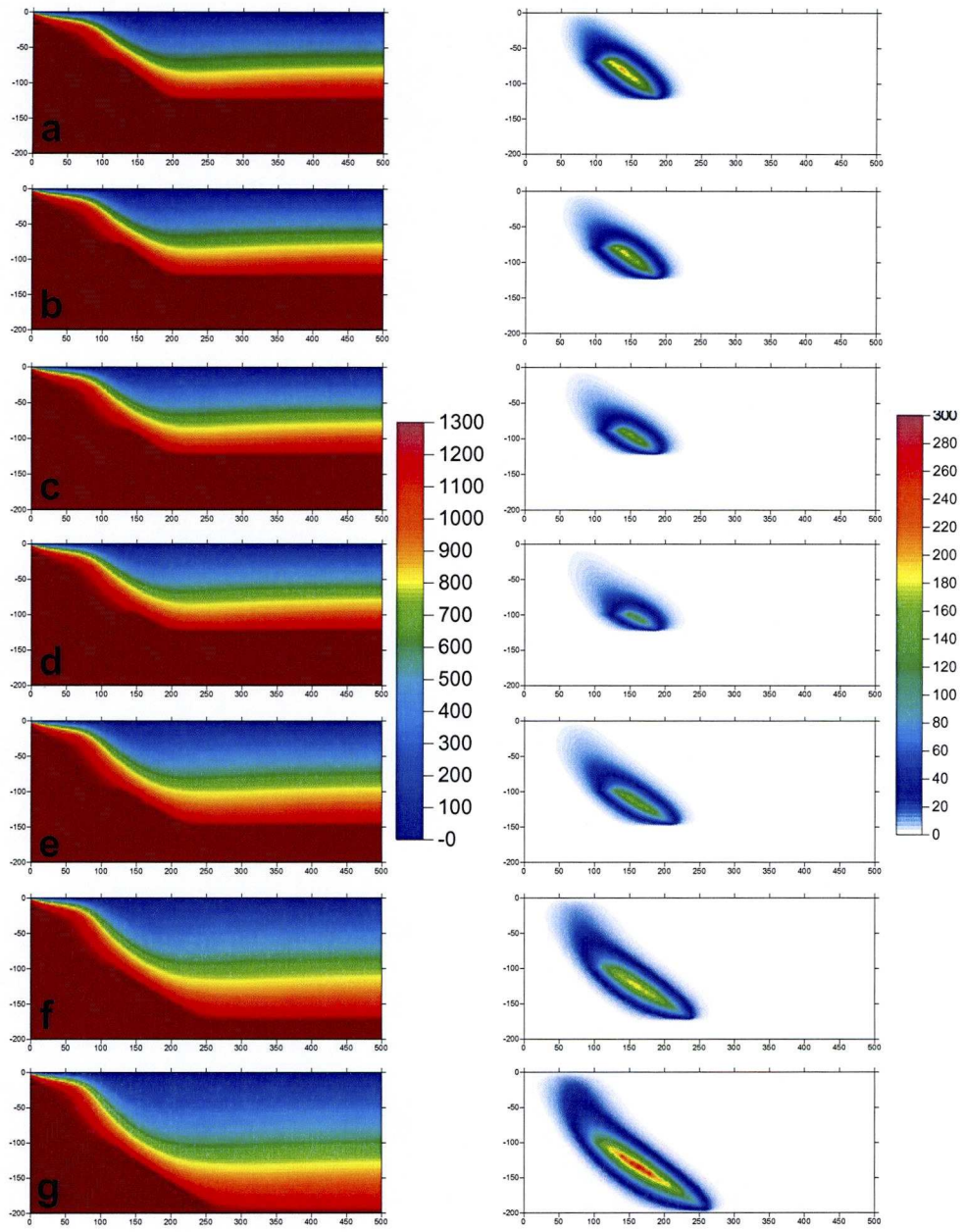

Figure 5.3: Temperature field for lithosphere thickness variation across the OCT. Right hand side shows the temperature difference for when the continental lithosphere thickness is assumed across the whole section. Oceanic and continental lithosphere thicknesses are, respectively, a) 70 km & 125 km; b) 80 km & 125 km; c) 90 km & 125 km; d) 100 km & 125 km; e) 100 km & 150 km; f) 100 km & 175 km; g) 100 km & 200 km. Figures shown in reference frame of the mid-ocean ridge.

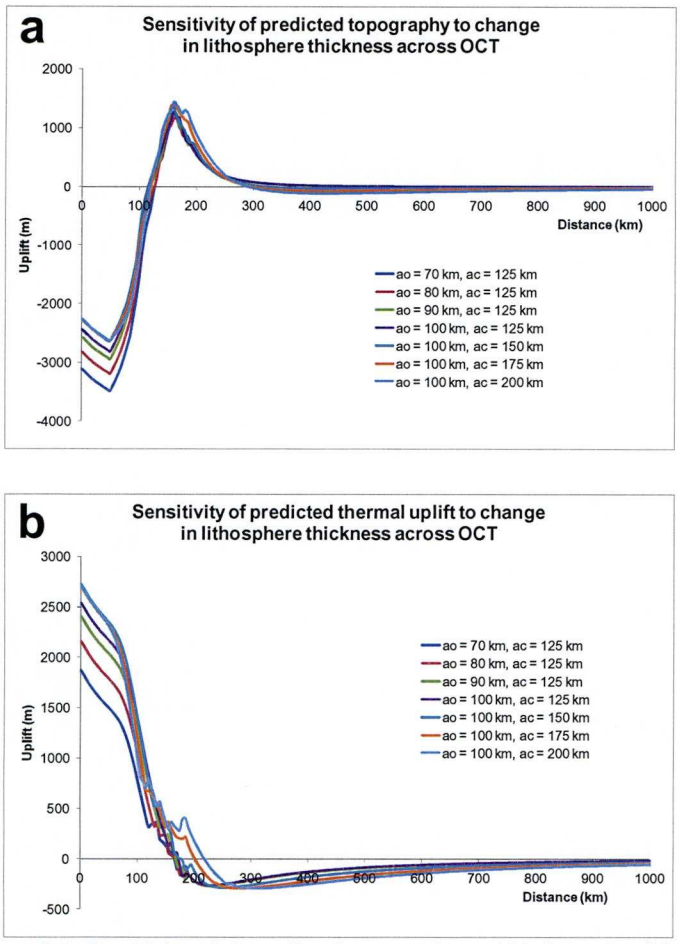

Figure 5.4: Sensitivity of a) predicted topography and b) thermal uplift to step change in lithosphere thickness across the OCT. ao = oceanic lithosphere thickness and ac = continental lithosphere thickness.

Applying a step change in lithosphere thickness at the OCT predicts a more realistic thermal anomaly for oceanic regions (Figure 5.4). The perturbation depends on the difference between the oceanic and continental lithosphere thicknesses, and on the actual values used for the thicknesses. More thermal uplift at the OCT is predicted for larger continental lithosphere thicknesses. The predicted geotherm perturbation over the transition region does not give a smooth curve like that of the oceanic and continental regions, due to the spacing used in the model (5 km) and the limitations of using a fixed-grid finite difference method.

The difference in the predicted temperature field, topography, and geotherm perturbation between using a constant lithosphere thickness across the section and

assuming a step change in lithosphere thickness across the OCT is shown in Figure 5.5, for up to 50 Myr of sea-floor spreading. In this model, thicknesses of 100 km and 175 km are used for the oceanic and continental lithosphere respectively. Varying the lithosphere thickness across the OCT leads to a persistent thermal anomaly in that region, which increases with time due to the continuing lateral heat flow from the warmer thinned continental and oceanic lithosphere into the adjacent thick continental lithosphere. It also predicts higher topography in the hinterland region. Upper crustal radiogenic heat production and varying conductivity within the lithosphere is neglected in the model. Including radiogenic heat productivity would give elevated temperatures in the continental lithosphere compared to the oceanic lithosphere at shallower depths (Sandiford & Egholm, 2008). This would lead to lateral heat transfer from the continent to the oceanic lithosphere, cooling the upper crust adjacent to the margin.

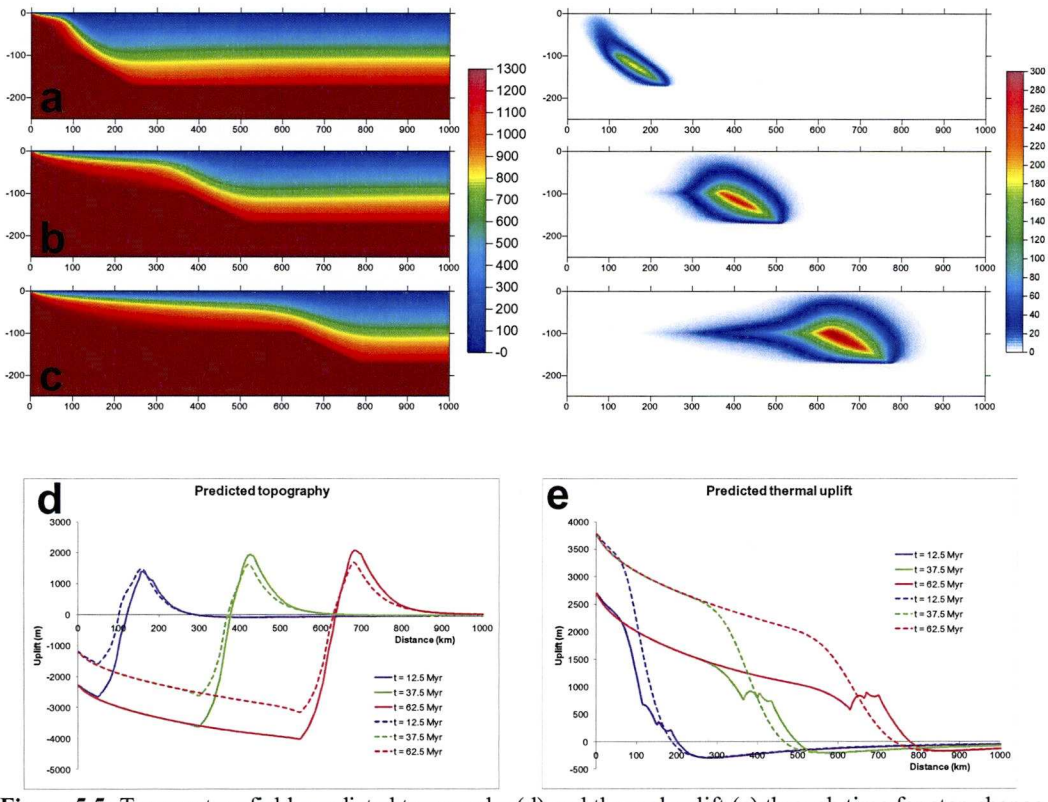

Figure 5.5: Temperature field, predicted topography (d) and thermal uplift (e) through time for step change in lithosphere thickness across the OCT, with oceanic lithosphere thickness = 100 km and continental lithosphere thickness = 175 km. Temperature field and temperature difference a) after 5 Myr sea-floor spreading with Vz/Vx = 5, b) after 25 Myr sea-floor spreading with Vz/Vx = 2, and c) after 50 Myr sea-floor spreading with Vz/Vx = 2. In d) and e) solid lines are for model with variation in lithosphere thickness across the OCT and dashed lines are for model assuming constant lithosphere thickness = 175 km. Figures are in reference frame of the mid-ocean ridge.

5.4 Summary

In this chapter, the effect of increasing the lithosphere thickness and imposing a step change in the lithosphere thickness across the OCT on the temperature field and resulting geotherm perturbation has been explored. Increasing the lithosphere thickness leads to greater thermal uplift of the continental hinterland. Varying the lithosphere thickness across the OCT leads to a persistent thermal anomaly at the margin and predicts higher topography, compared to that predicted when a constant lithosphere thickness is assumed. This suggests that it is important to consider lithosphere structure in the thermal evolution of a rifted margin, as this affects the geotherm re-equilibration and hence thermal uplift of the continental hinterland.

5.5 References

Artemieva, I. M. (2009), The continental lithosphere: Reconciling thermal, seismic, and petrologic data, *Lithos*, vol. 109, p. 23-46.

Artemieva, I. M. and W. D. Mooney (2002), On the relations between cratonic lithosphere thickness, plate motions, and basal drag *Tectonophysics*, vol. 358, p. 211-231.

Fernandez, M., C. Ayala, M. Torne, J. Verges, M. Gomez and R. Karpuz (2005), Lithospheric structure of the Mid-Norwegian margin: comparison between the More and Voring margins, *Journal of the Geological Society*, vol. 162, p. 1005-1012.

Jaupart, C. and J. C. Mareschal (1999), The thermal structure and thickness of continental roots, *Lithos*, vol. 48, p. 93-114.

Leroy, M., F. Gueydan and O. Dauteuil (2008), Uplift and strength evolution of passive margins inferred from 2-D conductive modelling, *Geophysical Journal International*, vol. 172, p. 464-476.

Lucazeau, F., S. Leroy, A. Bonneville, B. Goutorbe, F. Rolandone, E. D'Acrement, L. Watremez, D. Dusunur, P. Tuchais, P. Huchon, N. Bellahsen and K. Al-Toubi (2008), Persistant thermal activity at the Eastern Gulf of Aden after continental break-up, *Nature Geoscience*, vol. 359, p. 854-858.

Parsons, B. and J. G. Sclater (1977), An analysis of the variation of ocean floor bathymetry and heat flow with age, *Journal of Geophysical Research*, vol. 82, p. 803-827.

Parsons, B. and D. Mckenzie (1978), Mantle Convection and the Thermal Structure of the Plates, *Journal of Geophysical Research*, vol. 83, no. B9, p. 4485-4496.

Sandiford, M. and D. L. Egholm (2008), Enhanced intraplate seismicity along continental margins: Some causes and consequences, *Tectonophysics*, vol. 457, p. 197-208.

Scheck-Wenderoth, M. and Y. Maystrenko (2008), How warm are passive continental margins? A 3-D lithospheric-scale study from the Norwegian margin, *Geology*, vol. 36, no. 5, p. 419-422.

Chapter 6

Flexural isostasy and eustatic sea-level changes

6.1 Introduction

The general model for continental breakup and sea-floor spreading initiation presented in Chapter 4 assumed air-loaded local isostatic compensation and a constant bathymetry. However, as discussed in Chapters 2 and 3, flexural isostasy exerts a fundamental control on the topographic evolution of a rifted margin (e.g. Campanile et al., 2008). Variations in sea-level also play an important role, as a drop in sea-level gives an apparent surface uplift and alters the erosional base level (Huuse, 2002). In this chapter, the general model is further developed by the incorporation of flexural isostasy, water-loaded subsidence, and eustatic sea-level changes.

6.2 Flexural isostasy

For Airy isostasy, when a load is applied to the lithosphere, a response is only generated immediately below the load, i.e. it is locally compensated. If the lithosphere has a finite flexural strength, then the applied load will be supported by a regional displacement of the lithosphere. The resulting deflection of an elastic plate overlying a viscous mantle is described by (Watts, 2001):

$$D\frac{d^4y}{dx^4} + (\rho_m - \rho_i)yg = 0 \qquad [6.1]$$

where x is the horizontal co-ordinate, y is the vertical deflection, g is the acceleration due to gravity, and ρ_m and ρ_i are, respectively, the mantle density and infill density.

D, the flexural rigidity, characterises the flexural strength of the lithosphere and is given by:

$$D = \frac{ETe^3}{12(1-\nu^2)} \quad [6.2]$$

where E is Young's modulus, ν is Poisson's ratio and Te is the elastic thickness of the plate. Values of 100 GPa and 0.25 are used for E and ν respectively. The deflection of the lithosphere is strongly dependent on Te, and also on the width and amplitude of the applied load. Although it is assumed to be constant in this model, in reality the Young's modulus may vary laterally and would therefore also be an important control on the flexural rigidity (S. Wienecke, personal communication, 2010). If the lithosphere has zero flexural rigidity ($D = 0$), the Airy isostatic response is predicted.

Estimates for the elastic thickness of the lithosphere are varied; for oceanic lithosphere they range from 2 – 50 km (Watts & Burov, 2003) and for continental lithosphere, 5 – 110 km (Burov & Diament, 1995). The elastic thickness of oceanic lithosphere is determined by the depth to a specific isotherm, between 450 – 600°C and, as such, it will increase with time, due to cooling of the oceanic lithosphere as it moves away from the mid-ocean ridge (Burov & Diament, 1995). The elastic thickness of continental lithosphere, thought only partly to be controlled by its thermal state, is much harder to constrain, leading to the much larger range of Te estimates. However, it is thought that rifts are characterised by a low elastic thickness, due to the thermal weakening of the lithosphere during the rifting event (Watts & Burov, 2003).

The air-loaded flexural isostatic response to crustal thinning and geotherm perturbation during continental breakup and sea-floor spreading initiation is shown in Figure 6.1, for Te = 0.1, 5 and 30 km. The response when Te = 0.1 km is approximately equal to the Airy isostatic response. As Te increases, the maximum amplitude of the deflection decreases but its wavelength increases (Figure 6.2). It also leads to an increase in the distance between the ocean-continent transition and the location of the maximum topography (Figures 6.1 & 6.2).

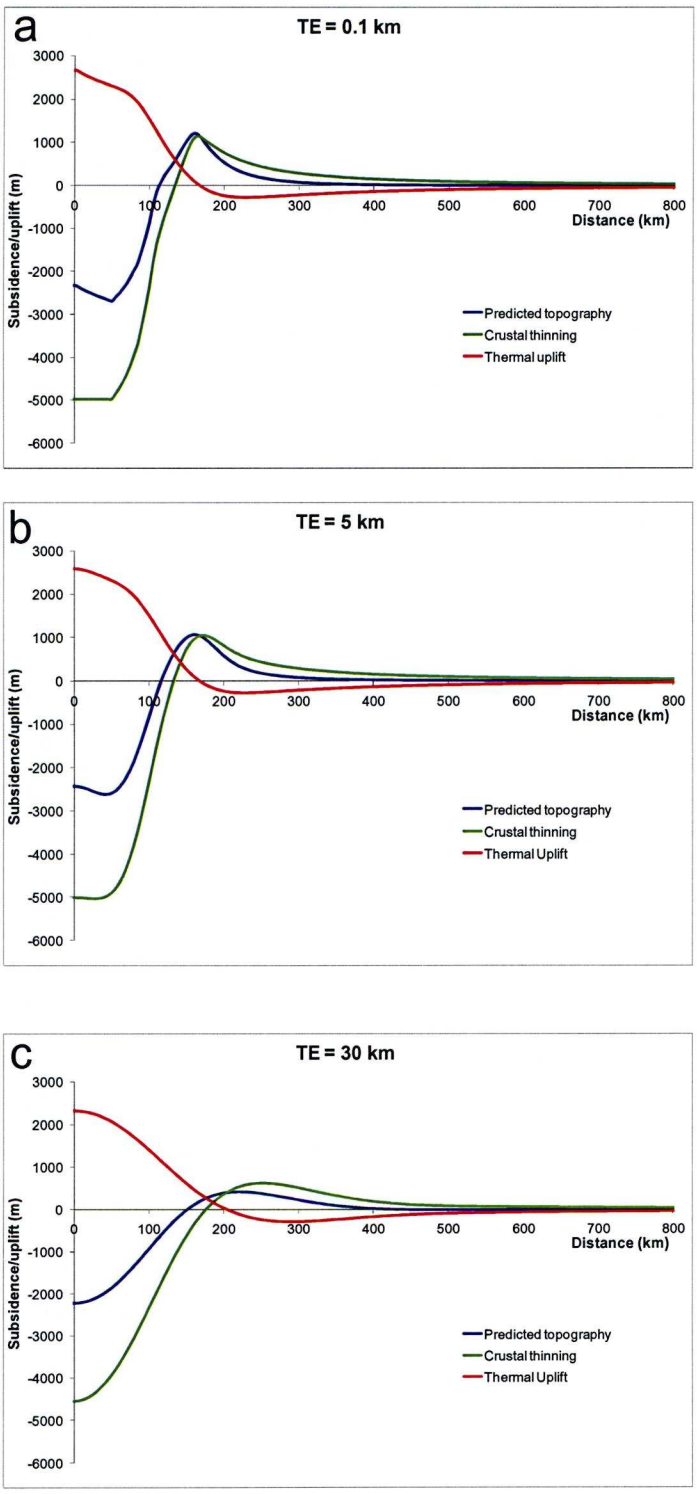

Figure 6.1: Flexural isostatic response to crustal thinning and geotherm perturbation, and the resulting topography for a) Te = 0.1 km, b) Te = 5 km and c) Te = 30 km. Model shown at 12.5 Myr, after 5 Myr sea-floor spreading following continental breakup by a combined pure shear and upwelling-divergent flow. Figures in reference frame of the mid-ocean ridge.

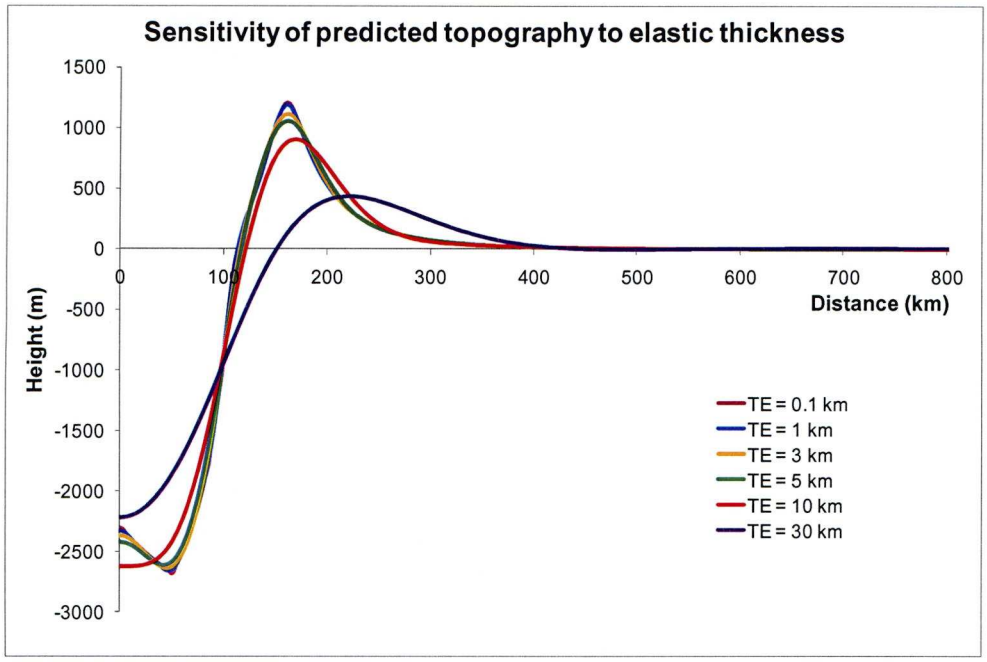

Figure 6.2: Sensitivity of predicted topography to the elastic thickness of the lithosphere

6.3 Water-loaded subsidence

Up to now, all of the models presented in this thesis have assumed an air-loaded isostatic response. A more physically realistic approach is to assume that regions below sea-level are water-loaded, with the depth of water determined by the bathymetry. In this case, ρ_i in Equation 6.1 becomes ρ_w, for which a value of 1000 kg m^{-3} is used. The predicted topography when water-loaded subsidence is included in the model is shown in Figure 6.3, and compared to the air-loaded response. The deflection due to water-loading increases the depth of the basin, and the flexural coupling also leads to a slight uplift of the continental hinterland. This effect is particularly observable at higher elastic thicknesses, for example when Te = 10 km, the maximum height for the water-loaded response is 25 m higher than the air-loaded response (Figure 6.3b).

6.4 Sea-level changes

Eustatic sea-level changes are included in the model by using a digitised version of the Haq et al. (1987) sea-level curve, provided as supplementary material to

Miller et al. (2005). The curve is interpolated to give a value at each time step in the model, and the topography is then corrected according to this value to give the predicted height relative to sea-level. The resulting variation to the predicted topography with time is shown in Figure 6.4. For the model presented in this chapter, the start time is 12.5 Ma, when sea-level was ~95 m higher than today. As sea-level falls, an apparent rise in the topography is observed, such that the hinterland region of the model, assumed initially to be at sea-level, stands at +95 m at the end of the model. The sensitivity of the model to elastic thickness is also considered (Figure 6.5) because changes in sea-level alter the amount of water-loading offshore, and therefore the deflection onshore would also vary slightly.

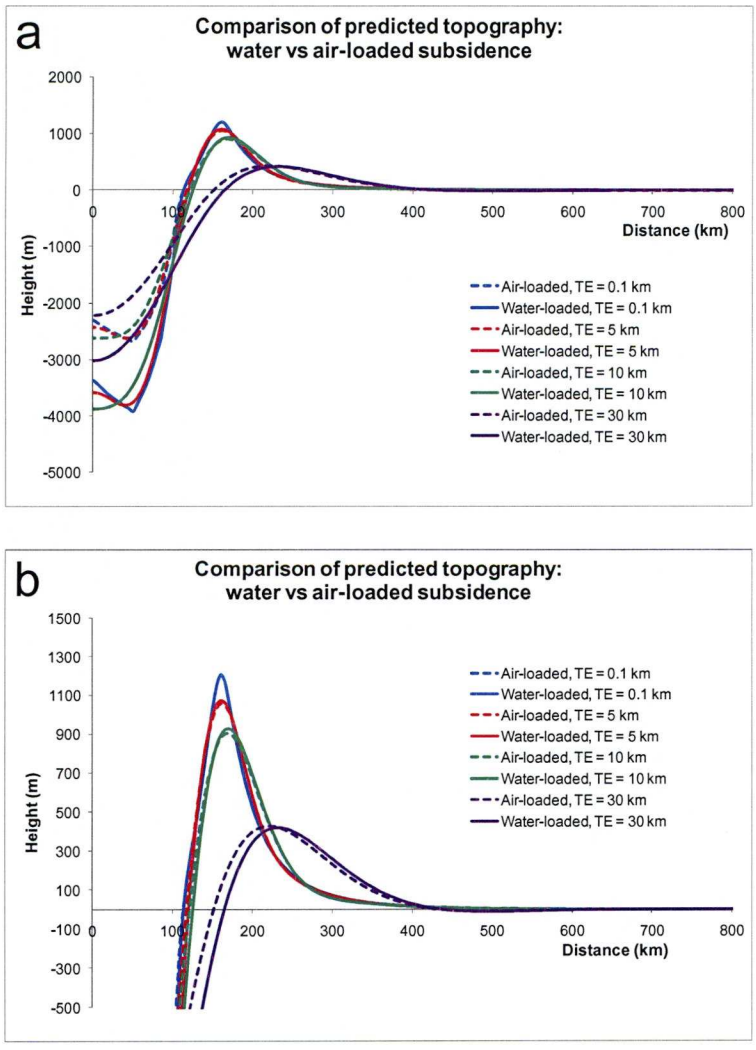

Figure 6.3: Comparison of predicted topography with air-loaded (dashed lines) and water-loaded (solid lines) subsidence offshore. b) is a close-up of a) to show the onshore region more clearly. Figures shown in reference frame of the mid-ocean ridge.

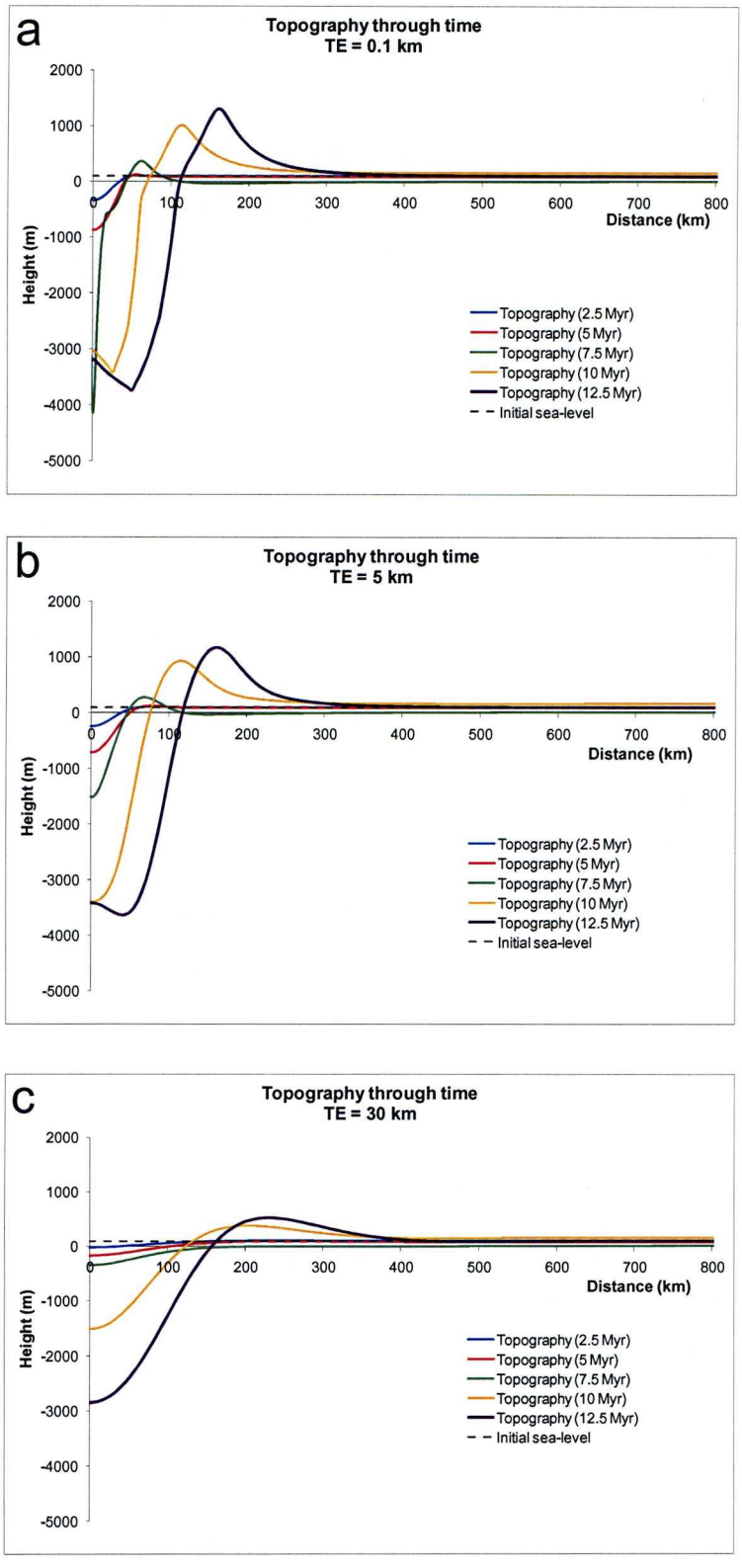

Figure 6.4: Topography through time with sea-level variation according to the global sea-level curve of Haq et al. (1987). a) Te = 0.1 km, b) Te = 5 km and c) Te = 30 km. Figures shown in reference frame of the mid-ocean ridge.

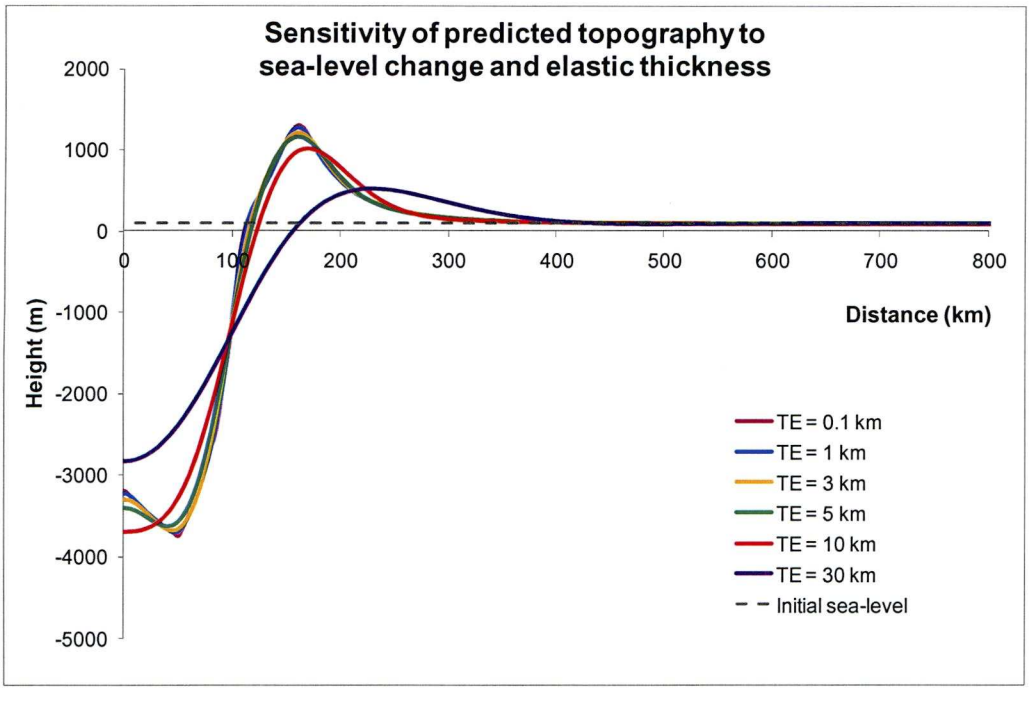

Figure 6.5: Sensitivity of predicted topography with model including sea-level changes to Te.

6.5 Pre-existing topography

The palaeobathymetry at continental breakup is often poorly constrained, but several margins – southern Africa (van der Beek et al., 2002), western India (Widdowson, 1997), Norway (Nielsen et al., 2009) and south-eastern Australia (Stephenson & Lambeck, 1985) – are thought to possibly have been above sea-level. Therefore, an option to define the initial topography relative to sea-level has been included in the model (Figure 6.6). Previous numerical modelling studies have demonstrated that the pre-breakup topography strongly affects the development of the margin (van der Beek et al., 2002).

6.6 Summary

In this chapter, the general model presented in chapter 4 has been developed further by considering flexural isostasy, water-loaded subsidence and sea-level variations. Flexural isostasy controls the amplitude and wavelength of the predicted hinterland uplift, and leads to coupling between the onshore and offshore deflection

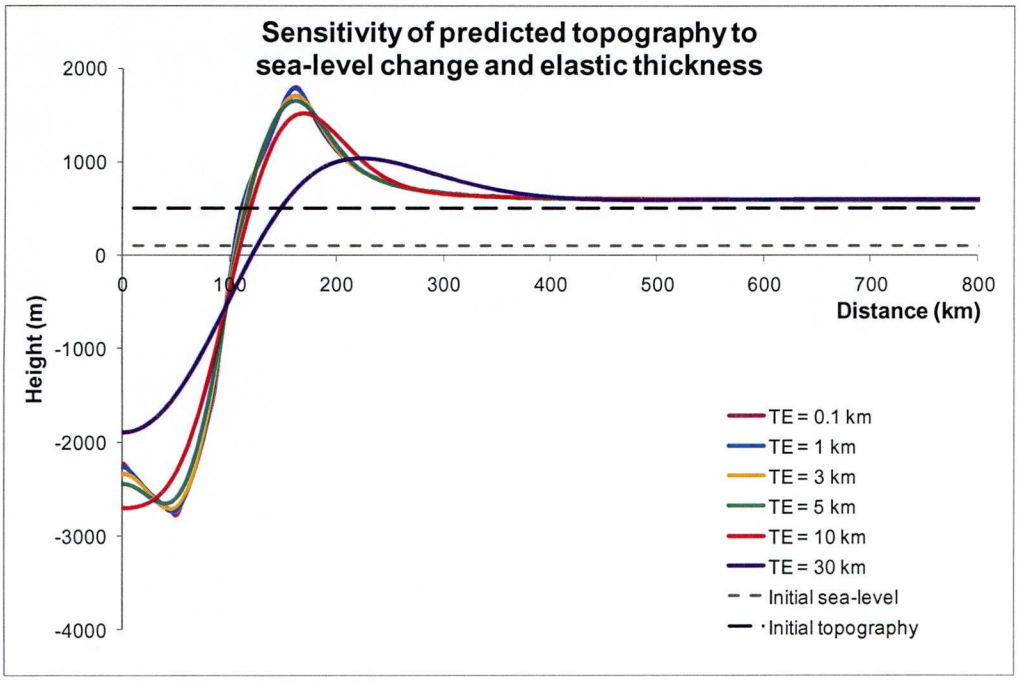

Figure 6.6: Sensitivity of predicted topography to Te, for model including sea-level changes and initial topography = 500 m.

if water-loaded subsidence is assumed offshore. Eustatic sea-level changes are also likely to play a considerable role in the evolution of a rifted margin, and can lead to an apparent surface uplift if sea-level falls. These factors will become more important when erosion is incorporated into the model in Chapter 8.

6.7 References

Burov, E. B. and M. Diament (1995), The effective elastic thickness (Te) of continental lithosphere: What does it really mean?, *Journal of Geophysical Research*, vol. 100, no. B3, p. 3905-3927.

Campanile, D., C. G. Nambiar, P. Bishop, M. Widdowson and R. Brown (2008), Sedimentation record in the Konkan-Kerala Bsin: Implications for the evolution of the Western Ghats and the Western India passive margin, *Basin Research*, vol. 20, p. 3-22.

Haq, B. U., J. Hardenbol and P. R. Vail (1987), Chronology of Fluctuating Sea Levels since the Triassic, *Science*, vol. 235, no. 4793, p. 1156-1167.

Huuse, M. (2002) Cenozoic uplift and denudation of southern Norway: insights from the North Sea Basin, in Doré, A. G., J. A. Cartwright, M. S. Stoker, J. P.

Turner and N. White (eds), *Exhumation of the North Atlantic Margin: Timing, Mechanisms and Implications for Petroleum Exploration*, Geological Society, London, Special Publications, vol. 196, p. 209-233.

Miller, K. G., M. A. Kominz, J. V. Browning, J. D. Wright, G. S. Mountain, M. E. Katz, P. J. Sugarman, B. S. Cramer, N. Christie-Blick and S. F. Pekar (2005), The phanerozoic record of global sea-level change, *Science*, vol. 310, no. 5752, p. 1293-1298.

Nielsen, S. B., K. Gallagher, C. Leighton, N. Balling, L. Svenningsen, B. H. Jacobsen, E. Thomsen, O. B. Nielsen, C. Heilmann-Clausen, D. L. Egholm, M. A. Summerfield, O. R. Clausen, J. A. Piotrowski, M. R. Thorsen, M. Huuse, N. Abrahamsen, C. King and H. Lykke-Andersen (2009), The evolution of western Scandinavian topography: A review of Neogene uplift versus the ICE (isostasy-climate-erosion) hypothesis, *Journal of Geodynamics*, vol. 47, no. 2-3, p. 72-95.

Stephenson, R. and K. Lambeck (1985), Erosion-Isostatic Rebound Models for Uplift - an Application to Southeastern Australia, *Geophysical Journal of the Royal Astronomical Society*, vol. 82, no. 1, p. 31-55.

van der Beek, P., M. A. Summerfield, J. Braun, R. W. Brown and A. Fleming (2002), Modeling postbreakup landscape development and denudational history across the southeast African (Drakensberg Escarpment) margin, *Journal of Geophysical Research-Solid Earth*, vol. 107, no. B12, p. 2351.

Watts, A. B. (2001) *Isostasy and Flexure of the Lithosphere*, Cambridge University Press.

Watts, A. B. and E. B. Burov (2003), Lithospheric strength and its relationship to the elastic and seismogenic layer thickness, *Earth and Planetary Science Letters*, vol. 213, p. 113-131.

Widdowson, M. (1997) Tertiary palaeosurfaces of the SW Deccan, Western India: implications for passive margin uplift, in Widdowson, M. (ed.), *Palaeosurfaces: Recognition, Reconstruction and Palaeoenvironmental Interpretation*, Geol. Soc. Spec, Pub., vol. 120, p. 221-248.

Chapter 7

Erosion of a box profile using the diffusion equation

7.1 Introduction

The previous chapters have focussed largely on the geodynamic processes which have possibly contributed to the development of the uplifted rifted margins discussed in this thesis. However, the topography at these rifted margins is certain to also have been shaped, if not dominated, by denudational processes. Furthermore, the flexural response to onshore denudational unloading and offshore loading due to sediment deposition can give rise to significant topographic effects. It is therefore essential that this is considered in a model of the onshore evolution of a rifted margin.

It was first recognised by Culling (1960) that the diffusion equation, discussed previously in Chapter 4 in relation to heat transfer in the lithosphere, could be used to describe long-term erosional processes. It has subsequently been utilised effectively in many landscape development studies, e.g. Sinclair et al. (1991), Flemings & Jordan (1989), Braun & Sambridge (1997), Kooi & Beaumont (1994), Kooi & Beaumont (1996), Chase (1992) and Willett et al. (2001), to approximate long-term, short- and long-range processes including small-scale hillslope evolution (weathering and creep), erosion of mountain belts, and fluvial and deltaic processes in depositional settings. This chapter is an introduction to modelling sediment transport and deposition along a box profile using the diffusion equation; this will be incorporated into the model for continental lithosphere thinning and breakup in the subsequent chapters.

7.2 Diffusion as a model for landscape development

Erosion, sediment transport, and deposition can be modelled using the diffusion equation. It is assumed that the rate of down slope transport of mass (the degree of erosion and deposition) is linearly proportional to the surface gradient at that point (Equation 7.1; Culling, 1960).

$$q_s = -\mathrm{K}\frac{\partial h}{\partial x} \qquad [7.1]$$

where q_s = sediment flux, K = the diffusion coefficient, h = height of topography and x = horizontal position. The time-dependent evolution of a topographic profile, assuming that volume is conserved, is given by:

$$\frac{\partial h}{\partial t} = \frac{\partial}{\partial x}\left(\mathrm{K}\frac{\partial h}{\partial x}\right) \qquad [7.2]$$

where $\partial h / \partial t$ = the change in height with time, i.e. the amount of erosion and t = time. This is, like the heat transfer equation, solved using the finite difference approximation. Providing K is constant along the profile, this can be simplified to:

$$\frac{\partial h}{\partial t} = \mathrm{K}\frac{\partial^2 h}{\partial x^2} \qquad [7.3]$$

This is similar to the thermal diffusion equation (Equation 4.3) and can be used in the same way. Equilibrium topography is achieved when the gradient of the slope becomes zero. An assumption implicit in the model is that there is a constant supply of regolith which is produced prior to transportation. The flexural response to the resulting erosional unloading and depositional loading is also calculated and, along with the amount of erosion, added to the previous height to give the resulting topography, h_{new}, i.e.

$$h_{new} = h + \Delta h + \frac{\Delta h \rho_c}{(\rho_m - \rho_c) + Dk^4} \qquad [7.4]$$

where Δh is the change in height. The effect of compaction of the deposited sediments is not considered.

Whilst the diffusion equation is a good mathematical approximation of the general behaviour of hillslope transport (Burbank & Anderson, 2001), it does not directly account for other geomorphological processes which play an important role in topographic evolution, including landslides, slumping and river incision. A further

limitation of the diffusion equation is that it does not include an advection term, which is ideally required to model fluvial transport (Godard et al., 2004). However, given the long time period covered by the model, the diffusion equation can be considered a valid approximation for short-range transport processes as they all depend on the local surface gradient (Kooi & Beaumont, 1994). It has been shown that there is a positive relationship between denudation rate and topographic relief (Flemings & Jordan, 1989; Pinet & Souriau, 1988; Summerfield, 1991; Sinclair et al., 1991). In fact, relief is thought to be the dominant control on long-term denudation rates (Pinet & Souriau, 1988), whereas environmental factors are important on shorter timescales (Sinclair et al., 1991).

7.3 Value of the diffusion coefficient, K

The diffusion coefficient, K, which has units of $m^2\ yr^{-1}$, represents the mobility of the erodible surface (Culling, 1960), and may be thought as the volumetric transport rate at unit gradient (Martin & Church, 1997). Factors controlling K include source rock lithology, climatic fluctuations, the drainage network, and vegetational cover (Flemings & Jordan, 1989; Sinclair et al., 1991). Higher values of K are used when modelling regions with humid climates or rocks which are easily eroded. Likewise, K is much higher for studies of fluvial and deltaic systems compared to studies of creep and scarp degradation; values for K range, from previous studies, from $10^{-4} - 10^{-2}\ m^2\ yr^{-1}$ to $10^{4} - 10^{5}\ m^2\ yr^{-1}$ (Table 7.1; Flemings & Jordan, 1989; Martin & Church, 1997). In some studies, it is assumed that all slope processes, including creep and landsliding, and fluvial processes can be represented by a single value of K; in such studies, a much higher value of K is used than in studies considering only creep (Martin & Church, 1997).

7.4 Evolution of a box profile through time

In this section, the erosion and deposition, the corresponding flexural response, and the resulting topography are presented for a box profile, with sediment transport modelled using the diffusion equation. This is undertaken to illustrate and test the model on a simple profile, in order to gain an understanding of the general behaviour

Study	K (m^2 yr^{-1})	Notes
van der Beek et al. (2001)	0.001	creep (basement/sandstones)
van der Beek et al. (2002)	$10^{-3} - 10^{-2}$	creep
van der Beek et al. (2001)	0.1	creep (shales/sediments)
Gilchrist et al. (1994)	0.1 – 0.5	creep (bedrock)
Kooi & Beaumont (1994)	0.5	creep (bedrock)
van Balen et al. (1995)	1	creep (basement)
van Balen et al. (1995)	5	creep (sediments)
Kooi & Beaumont (1994)	5	creep (sediment)
Gilchrist et al. (1994)	5 – 10	creep (sediment (arid/humid))
Moretti & Turcotte (1985)	18	
Sinclair et al. (1991)	500	
Flemings & Jordan (1989)	$10^2 - 10^3$	mountain belt
Avouac & Burov (1996)	$10^3 - 10^4$	
Flemings & Jordan (1989)	10^4	sedimentary basin

Table 7.1: Values for K from published studies of landscape development.

of the model. The diffusion coefficient is prescribed to be either constant along the profile, varying with height or varying laterally (using Equation 7.2). The sensitivity of the predicted topography to the magnitude of K and the elastic thickness is also considered.

7.4.1 Constant diffusion coefficient

Figure 7.1a shows the evolution of a topographic box profile through time, for K = 100 m^2 yr^{-1} along the profile, when only sediment transport is considered (the flexural response to erosion and sediment deposition is not included). The sediment is transported from the elevated region and is deposited symmetrically either side of the box, decreasing the topographic relief. The steep sides of the box experience a greater amount of erosion than the initially horizontal centre (Figure 7.1b); this is particularly the case early on in the model because as the topography erodes with time, the rate of erosion decreases. The sensitivity of the predicted topography to the magnitude of K is shown in Figure 7.1c. As K increases, representing greater efficiency of the diffusion process, the reduction of the topography is much quicker.

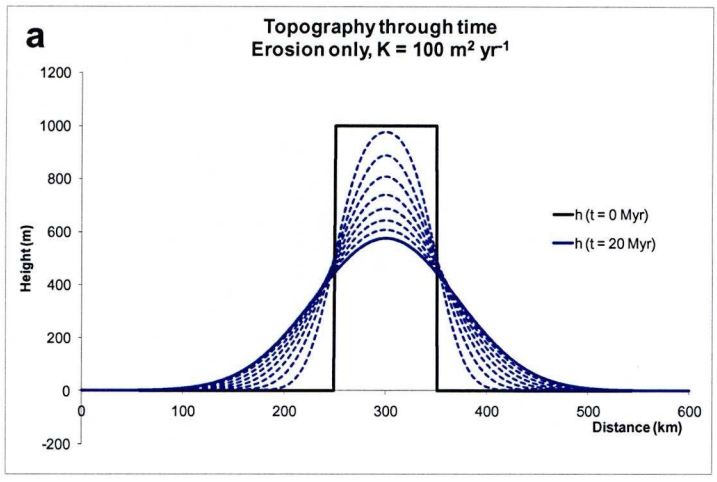

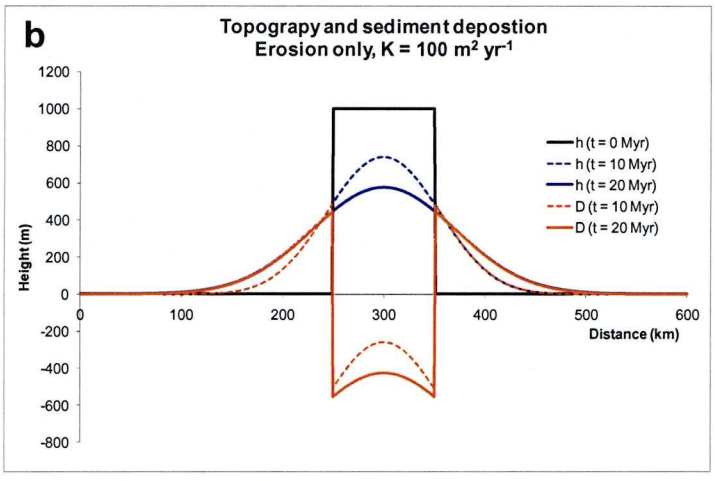

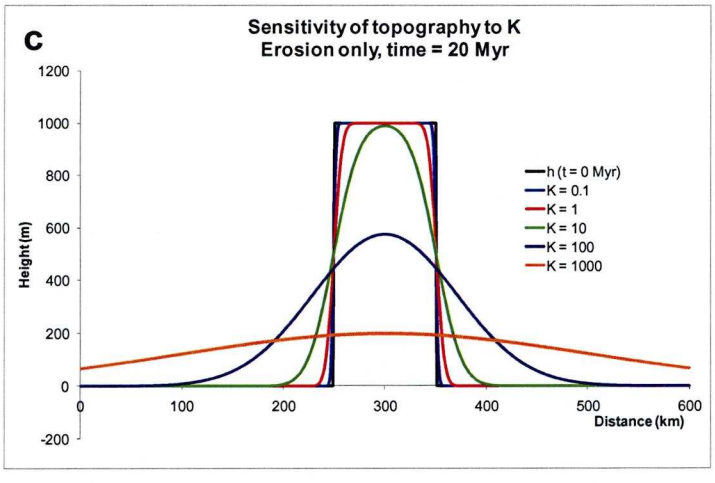

Figure 7.1: Erosion of a box profile with K = 100 m^2 yr^{-1} along the profile (the flexural response to denudational unloading is neglected). a) Topography through time. Dashed lines are shown at 2.5 Myr intervals. b) Topography and sediment deposition (erosion is negative) at 10 & 20 Myr. c) Sensitivity of the predicted topography to *K*. *h* = topography and *D* = deposition.

The flexural response to the erosion and sediment deposition has also been considered (Figures 7.2 & 7.3). Figures 7.2a and 7.2b show the amount of erosion and deposition, and the corresponding flexural response for elastic thicknesses of 0.01 km (equivalent to local isostasy) and 5 km respectively. The lithosphere rebounds in response to erosional unloading, thereby compensating for much of the change in height from the erosion, and increasing the amount of material that can be eroded (Campanile et al., 2008). In areas of deposition, the lithosphere subsides in response to sediment loading; this can lead to tilting of the topography, thus further enhancing the uplift due to the flexural rebound in response to erosion (Avouac & Burov, 1996). Figures 7.3a & b illustrate this, such that in certain conditions, the maximum elevation can increase due to the coupling effect of erosional unloading and tectonic uplift. The sensitivity of the topography to *Te* is shown in Figure 7.3c; the predicted topography when the flexural response to erosion is neglected is also plotted for comparison. This graph demonstrates the above point that isostatic rebound acts to restore the topography, with flexurally weak lithosphere resulting in a greater amount of surface uplift.

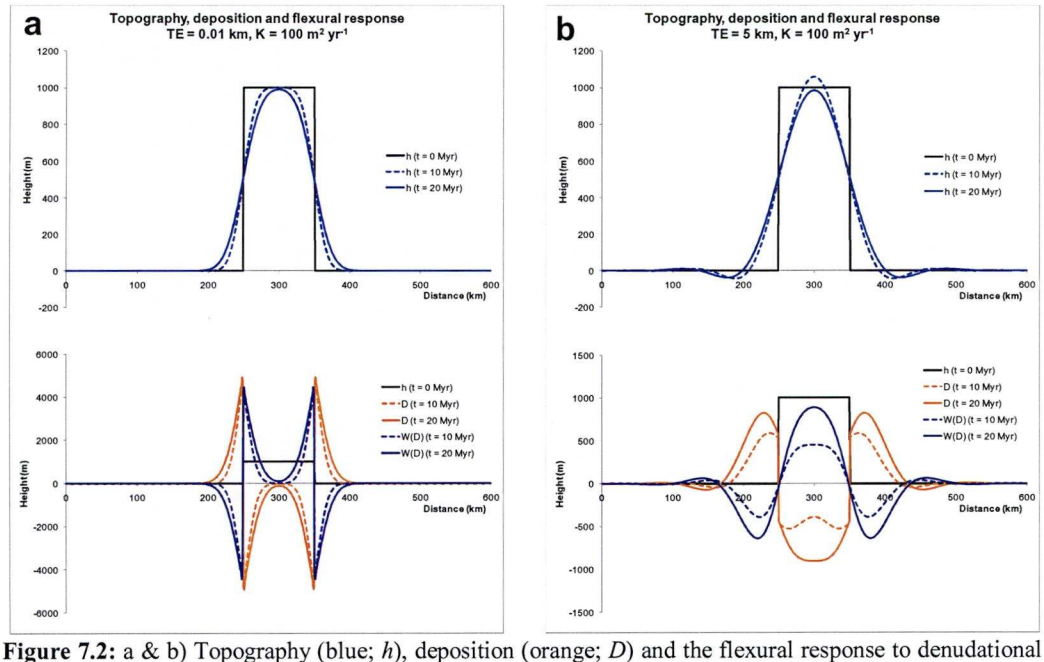

Figure 7.2: a & b) Topography (blue; *h*), deposition (orange; *D*) and the flexural response to denudational unloading (purple; *W(D)*) with Te = 0.01 km and Te = 5 km respectively (K = 100 m^2 yr^{-1}). For a very low *Te*, much a greater amount of topography than the initial height is eroded due to exhumation.

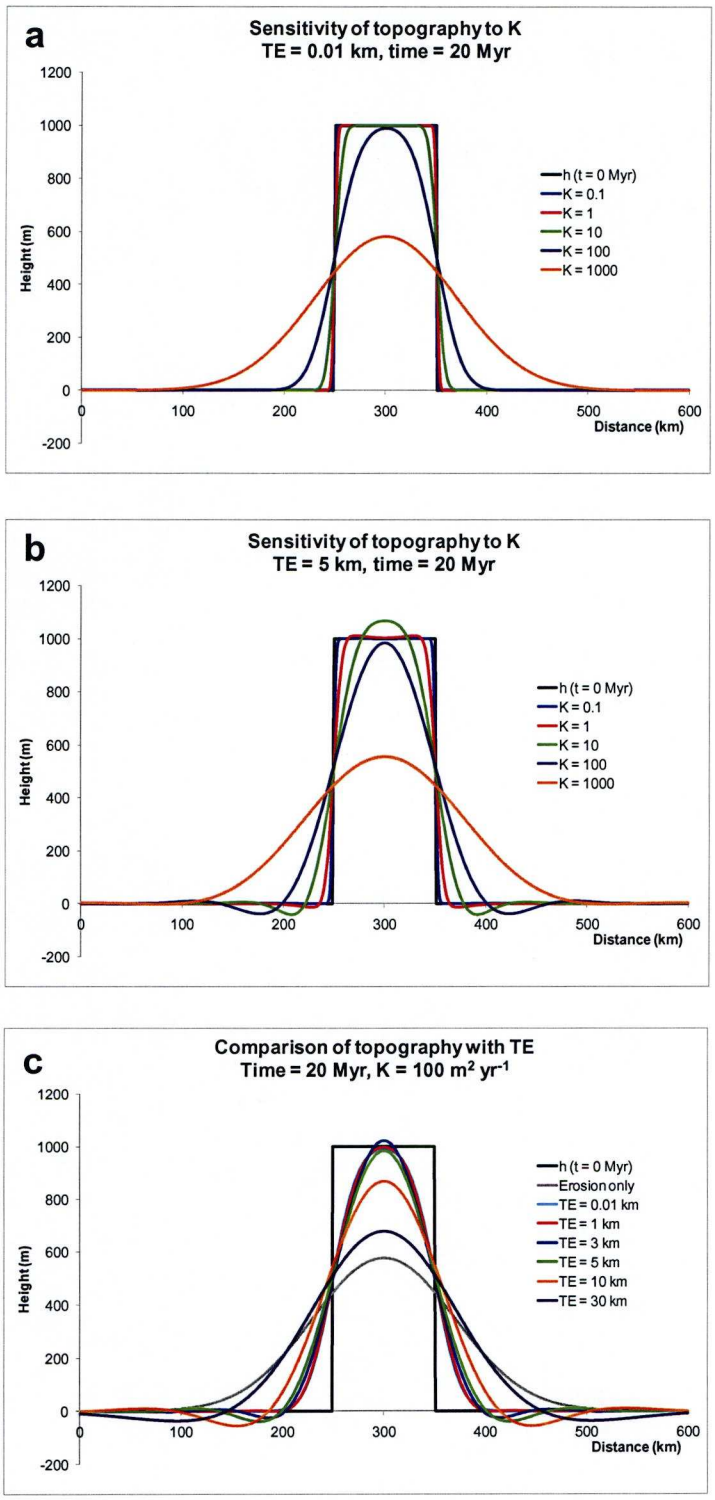

Figure 7.3: Sensitivity of predicted topography to: a) varying K, with Te = 0.01 km; b) varying K, with Te = 5 km; c) varying Te, with $K = 100$ m^2 yr^{-1}.

7.4.2 Height-dependent diffusion coefficient

A height-dependent diffusion coefficient is considered here because in some locations, precipitation, and hence denudation, may increase with height. Figures 7.4 and 7.5 show two models where K is higher above a given elevation than below it, calculated using Equation 7.2. The resulting topography after 20 Myr is presented for both the air- and water-loaded flexural response for regions which are below zero (Figure 7.4). Including water-loaded subsidence has the effect of increasing the bathymetry in these regions. The amount of erosion and sediment deposition is shown in Figures 7.5a & 7.5b. The greatest amount of deposition occurs on the downslope sides of the points where the topographic curve intersects the boundary line. By using a higher K above a certain height in the model, a plateau may start to form (Figure 7.5b) because the material at lower elevations experiences a lower rate of transportation.

For marine environments, the linear relationship assumed in the diffusion equation between sediment flux and slope may not be appropriate for modelling sediment transport because wave energy decreases with depth. Following Kaufman et al. (1991), the diffusion coefficient for regions below sea-level can be improved by employing a diffusion coefficient which decays exponentially with water depth, to represent the wave base i.e.:

$$K = K_w e^{-Cwd} \qquad [7.5]$$

where K_w = the diffusion coefficient at sea-level, C = the depth decay constant and wd = water depth. This equation tends to zero, so a minimum value of K is defined in the model to still allow some transport of sediment at depth. Other processes which occur below sea-level, such as gravity flows at the shelf edge and the transport of huge volumes of material far offshore are not accounted for in this equation, and are therefore not considered in the model.

The resulting topography using this equation with K_w = 1000 m^2 yr^{-1} and C = 0.05 is shown in Figure 7.6. A suitable range for C = 0 – 0.1 (Kaufman et al., 1991), with C = 0 giving a constant K with depth. K decays more rapidly, and therefore the lateral transport of sediment is less efficient with depth as C increases. The sensitivity of the predicted topography to the depth decay constant and elastic thickness is shown in Figure 7.7. The application of Equation 7.5 in the model results in the development of a prograding shelf-like topography at shallow water

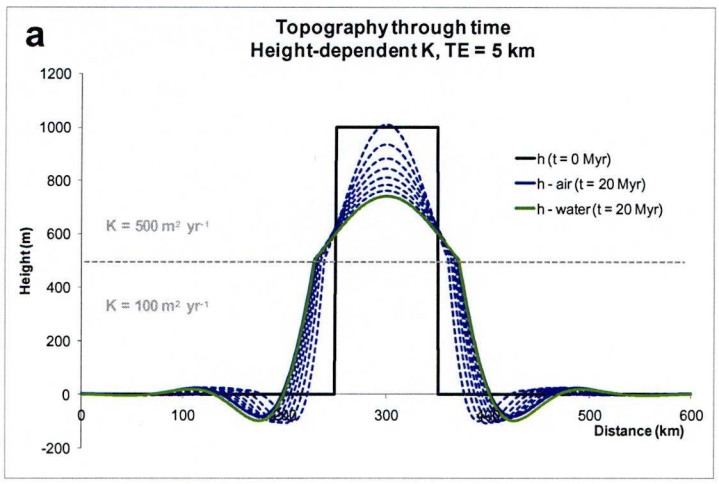

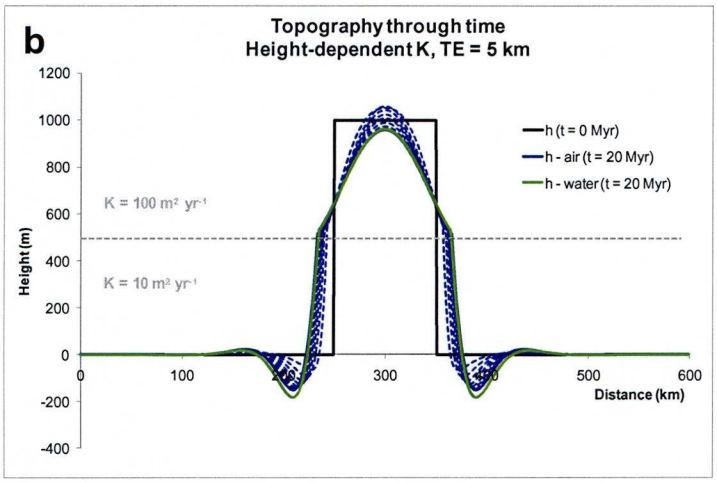

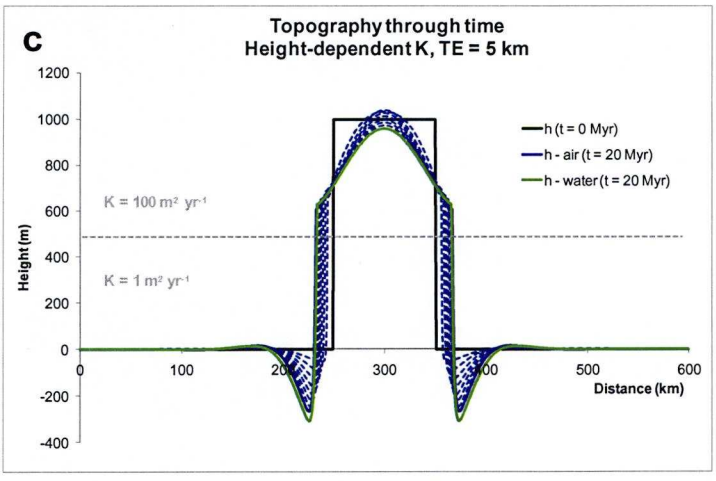

Figure 7.4: Topography through time for a height-dependent *K*. a) K = 500 m^2 yr^{-1} above & K = 100 m^2 yr^{-1} below the line, b) K = 100 m^2 yr^{-1} above & K = 100 m^2 yr^{-1} below the line, c) K = 100 m^2 yr^{-1} above & K = 1 m^2 yr^{-1} below the line. Air-loaded (blue curves at 2.5 Myr intervals) and water-loaded response (green) are shown. Grey dashed line representing the boundary at which K changes is at 500 m

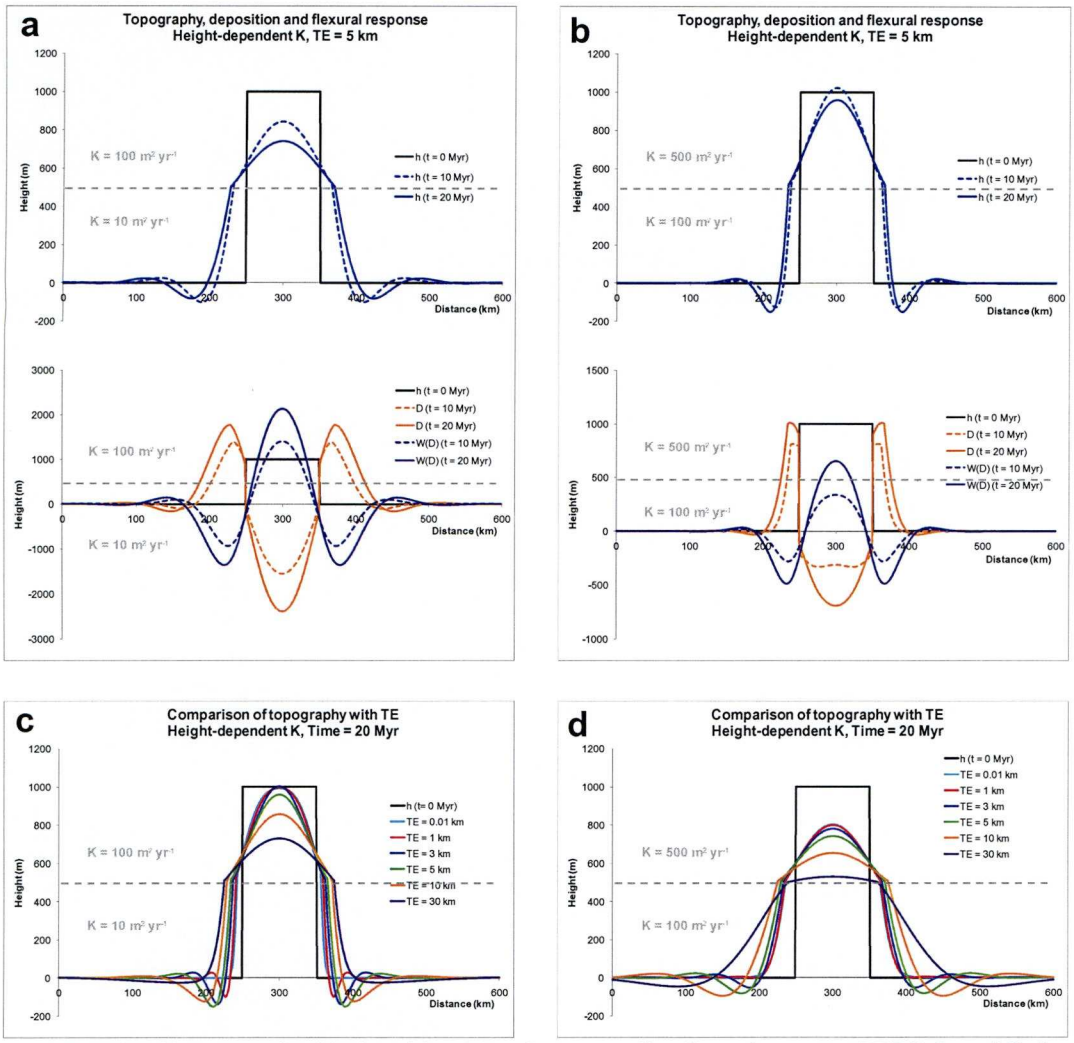

Figure 7.5: a) & b) Topography (h), deposition (D) and corresponding flexural response (W(D)) for a diffusion coefficient which varies with height, shown at 10 & 20 Myr. c) & d) sensitivity of the predicted topography to elastic thickness. Grey dashed line, at +500 m, represents the height where K changes. c) & d)

depths (Figure 7.6a). The length of this shelf increases with increasing *Te* (Figure 7.7a), but decreases with increasing *C* (Figure 7.7b).

7.4.3 Laterally-varying diffusion coefficient

The diffusion coefficient can also be assumed to vary laterally; this could be, for example, to approximate variations in lithology. In the case of a box profile, if the outer regions are more erodible than the inner region, the maximum elevation along the profile will increase, even as the mean elevation decreases due to erosion (Figures 7.8, 7.9 & 7.10). This is due to coupling between erosional unloading,

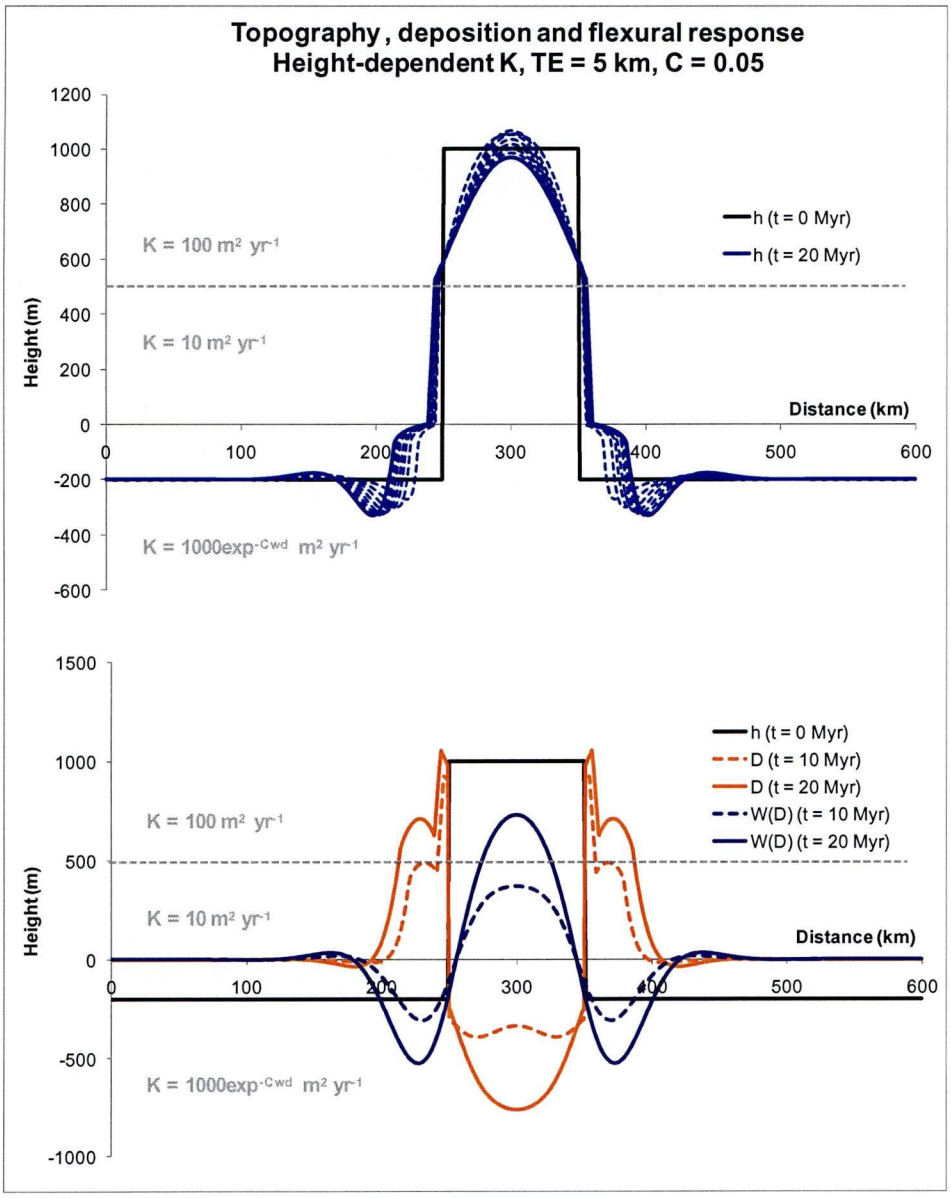

Figure 7.6: Topography (h), deposition (D) and the flexural response ($W(D)$) for a model with a diffusion coefficient which decays exponentially with water depth, using a decay constant (C) = 0.05 and Te = 5 km. Grey dashed line at 500 m is the elevation at which the diffusion coefficient changes. The exponentially decaying coefficient applies below 0 m.

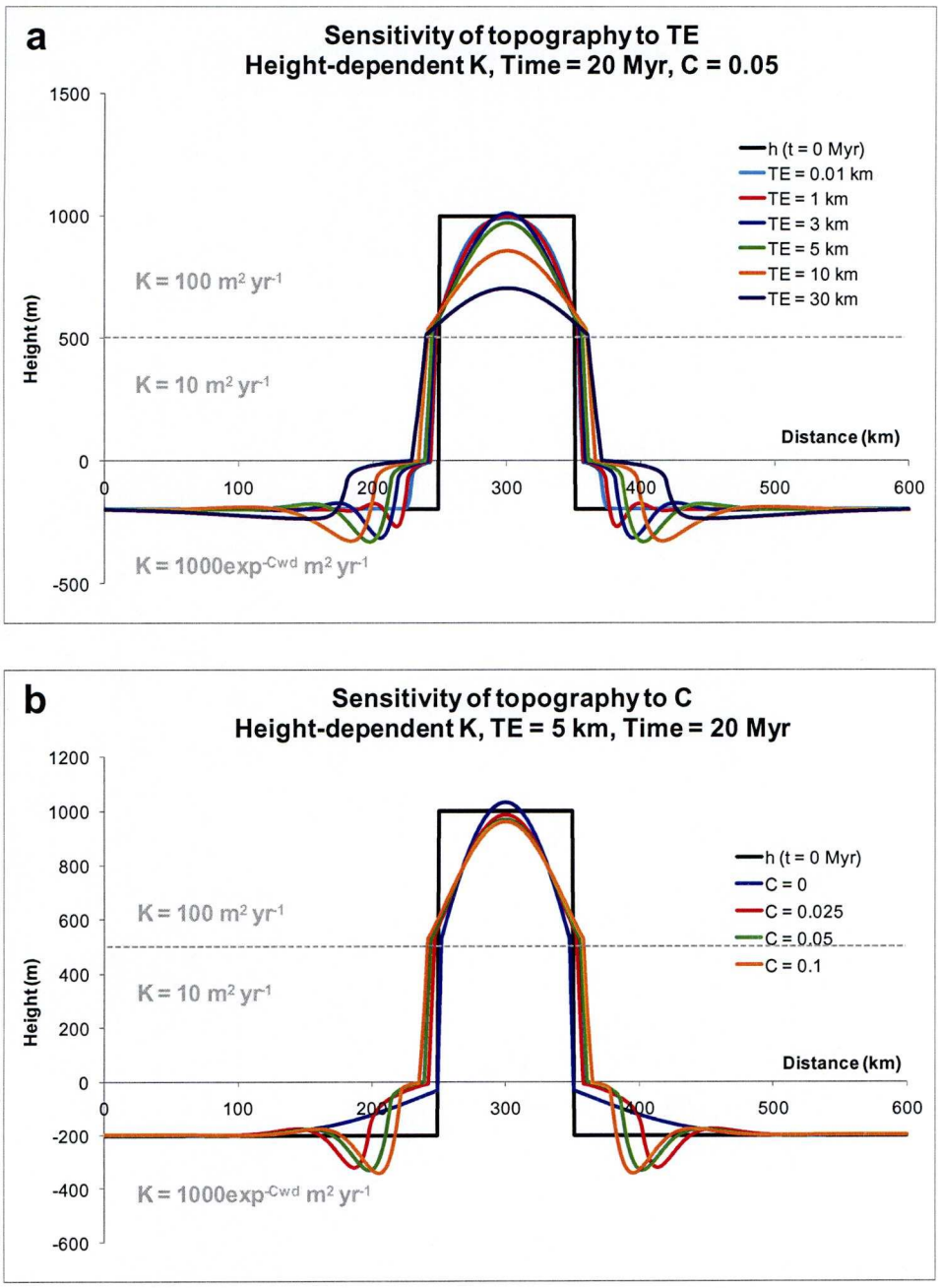

Figure 7.7: Sensitivity of predicted topography from model with a diffusion coefficient which decays exponentially with water depth to a) elastic thickness and b) depth decay constant.

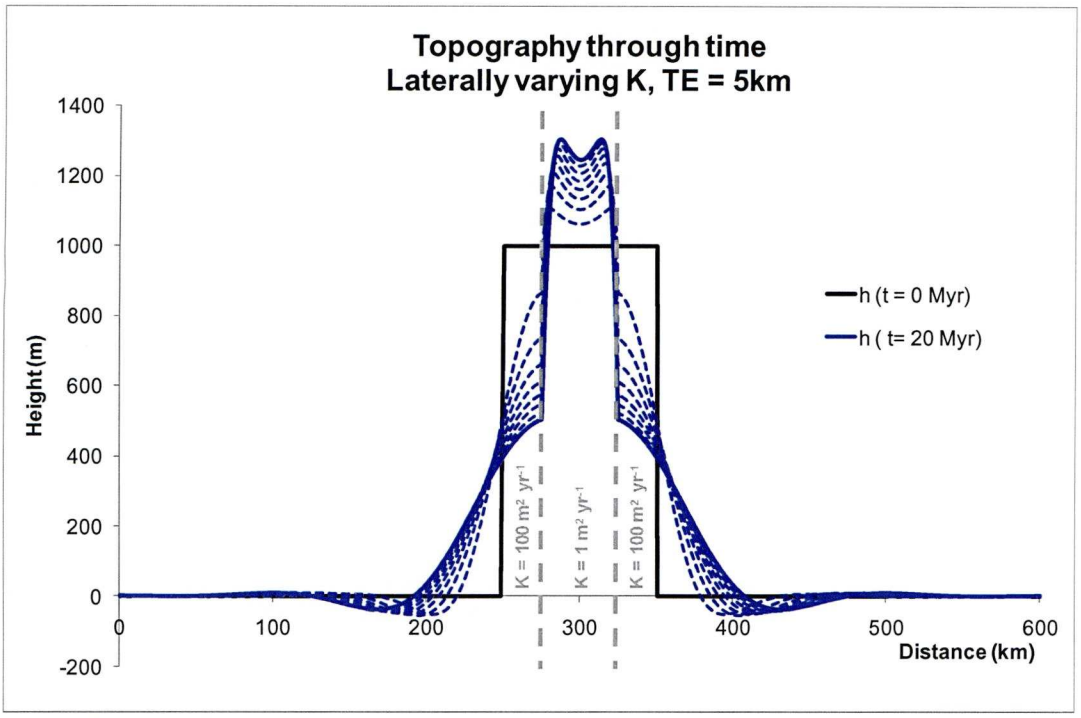

Figure 7.8: Topography through time for a laterally-varying diffusion coefficient (shown at 2.5 Myr intervals). The grey dashed boundary lines are at 275 km and 325 km.

sediment deposition and the flexural response to these processes (e.g. Molnar & England, 1990). The magnitude of this effect is very dependent on the elastic thickness, and is greater for lower elastic thicknesses.

7.5 Eustatic sea-level changes

The predicted hinterland topography is also sensitive to variations in eustatic sea-level, due to the flexural response to offshore water-loading and perhaps to changes in the diffusion coefficient, depending on how it is prescribed in the model. The box profile of 1 km height is corrected to the initial sea-level of the model; in the results presented here, the model is started at 20 Ma when, sea-level was ~ 65 m above the present level (Haq et al., 1987). Water-loading subsidence is assumed for regions below 0 m. The model is then run for 20 Myr, with the sea-level height varying with time according to the sea-level curve of Haq et al. (1987) until the present-day is reached. Figures 7.11, 7.12, and 7.13 show the predicted topography when sea-level changes through time, assuming a constant diffusion coefficient of

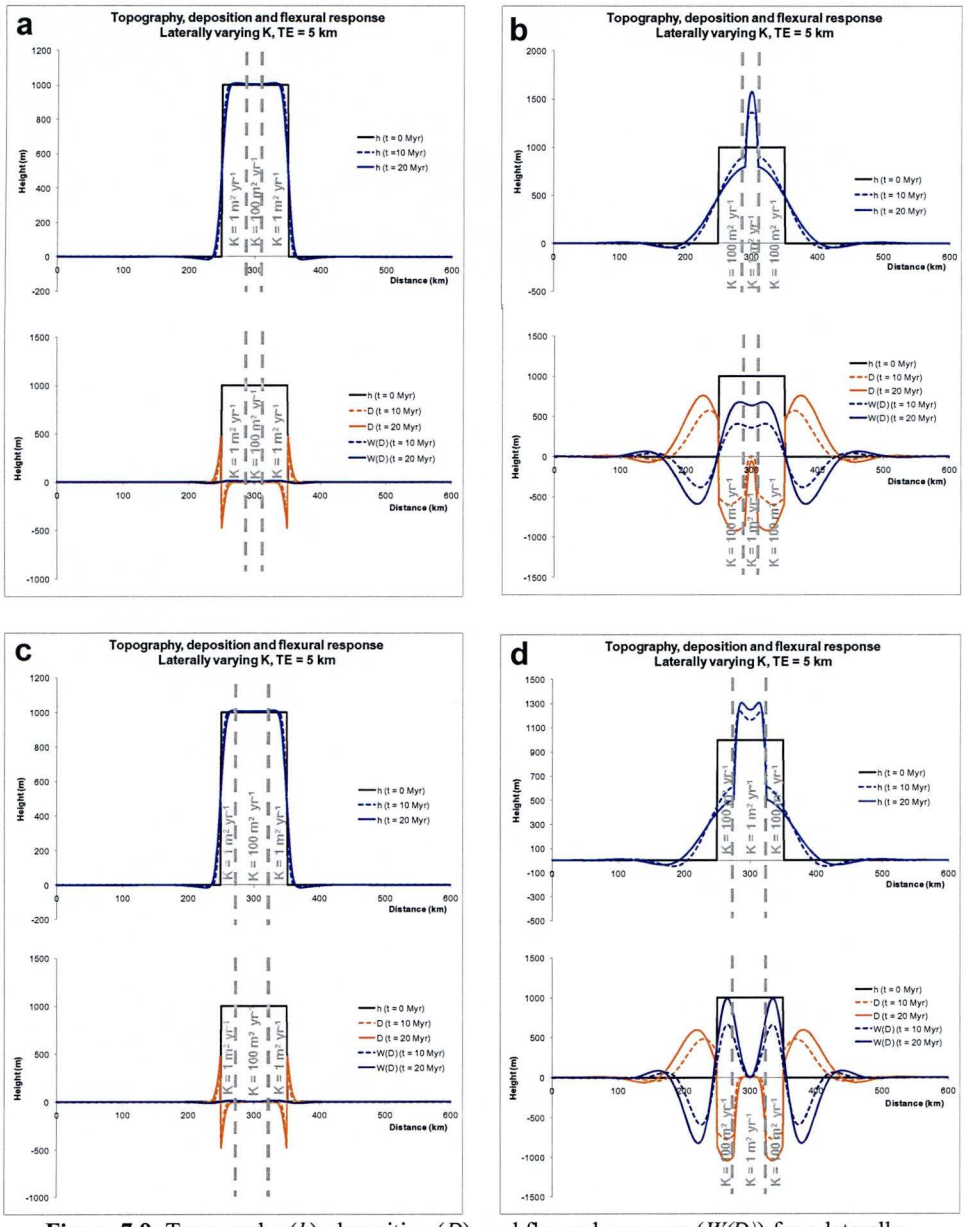

Figure 7.9: Topography (*h*), deposition (*D*), and flexural response (*W(D)*) for a laterally-varying diffusion coefficient, and varying width. Grey dashed line represents the distance at which the diffusion coefficient changes. a & b) grey dashed lines at 290 km and 310 km. c & d) grey dashed lines at 275 km and 325 km.

K = 100 m^2 yr^{-1}. A lowering of sea-level leads to an apparent rise in the maximum elevation of the profile (Figure 7.11), although, for Te = 5 km, there is very little difference in the shape and magnitude of the predicted topography when a constant sea-level is assumed (Figure 7.2b). In Figures 7.14, 7.15 & 7.16, a diffusion coefficient to approximate the wave base below sea-level (Equation 7.5) is applied.

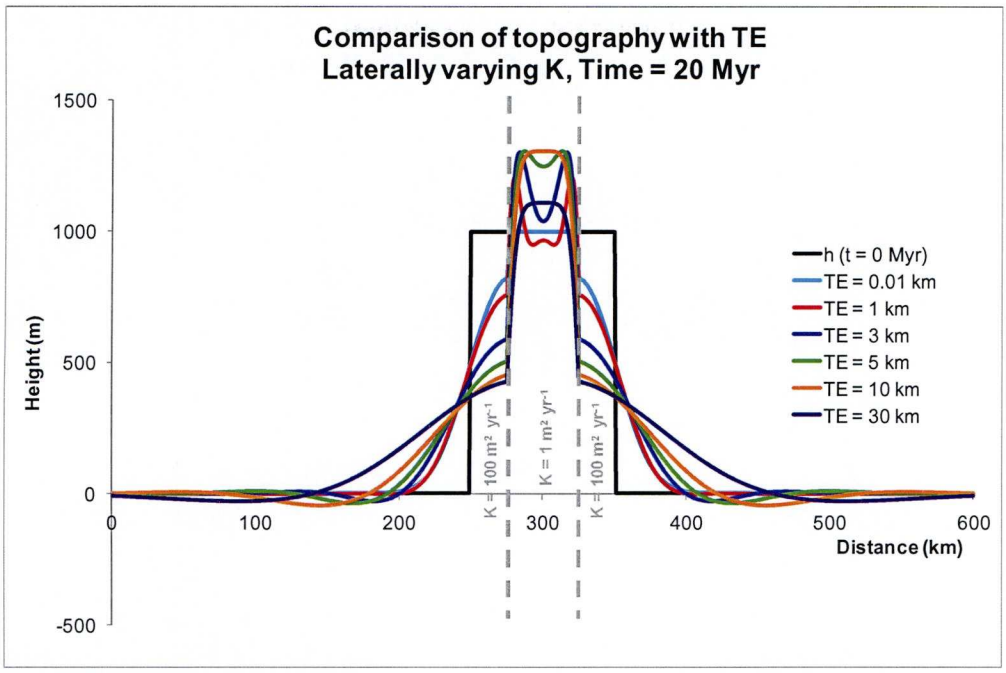

Figure 7.10: Sensitivity of the predicted topography with a laterally-varying diffusion coefficient to elastic thickness. Grey dashed lines at 275 km and 325 km.

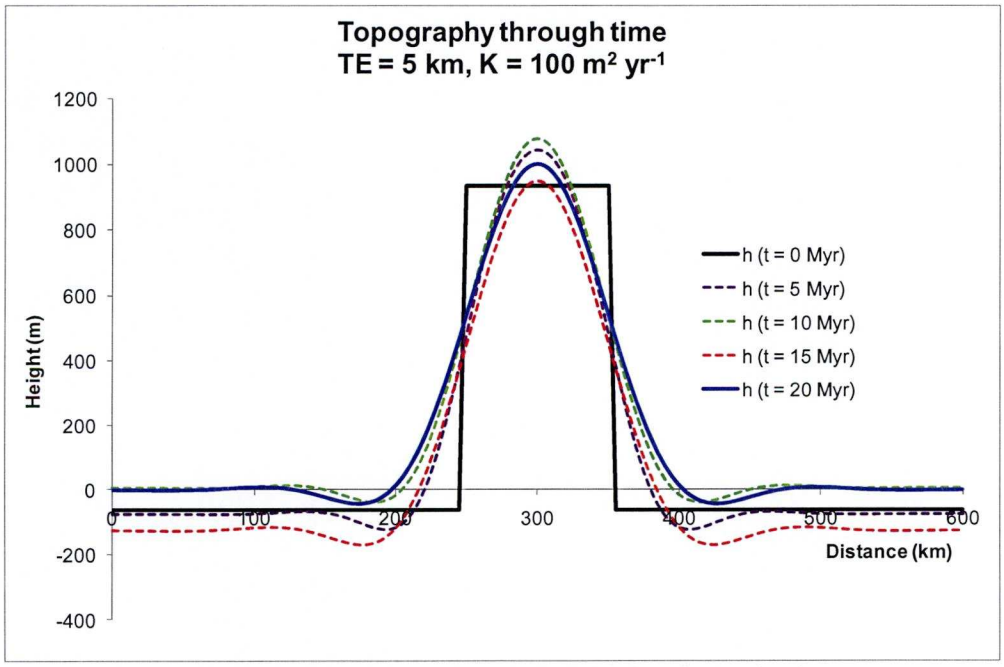

Figure 7.11: Topography through time with changing sea-level.

At low elastic thicknesses, a small step in the topography of the basins, which form to the sides of the box, develops. The resulting wavelength and depth of the basins are very dependent on the elastic thickness and depth decay constant (Figure 7.16).

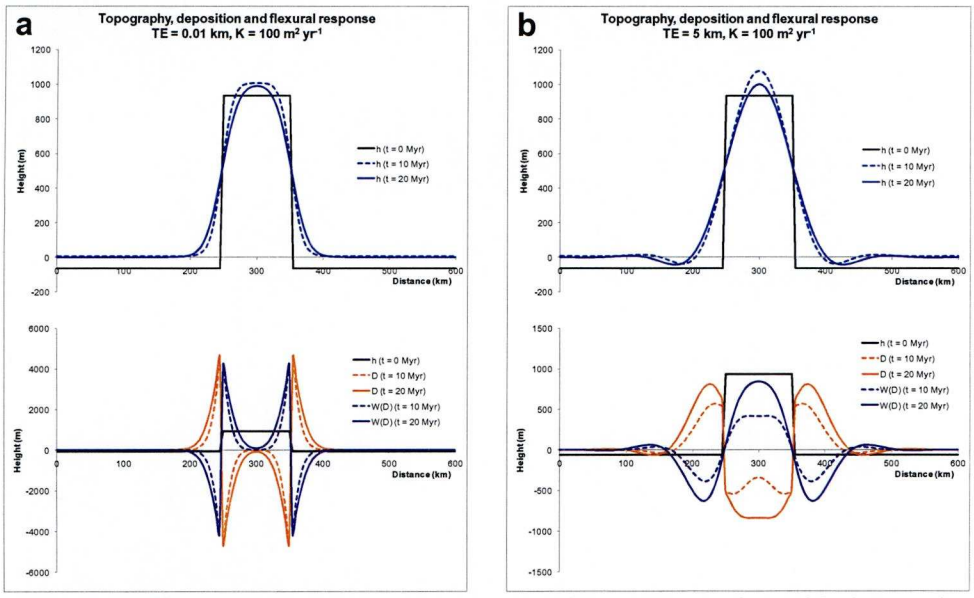

Figure 7.12: Topography, deposition and corresponding flexural response for model where sea-level varies through time. a) TE = 0.01 km & b) TE = 5 km.

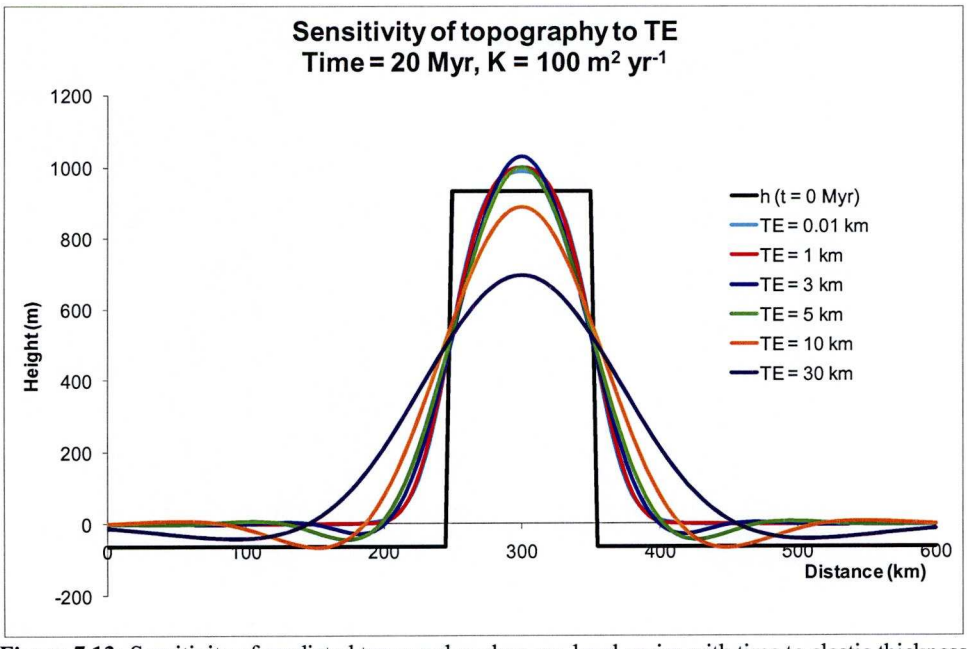

Figure 7.13: Sensitivity of predicted topography when sea-level varies with time to elastic thickness

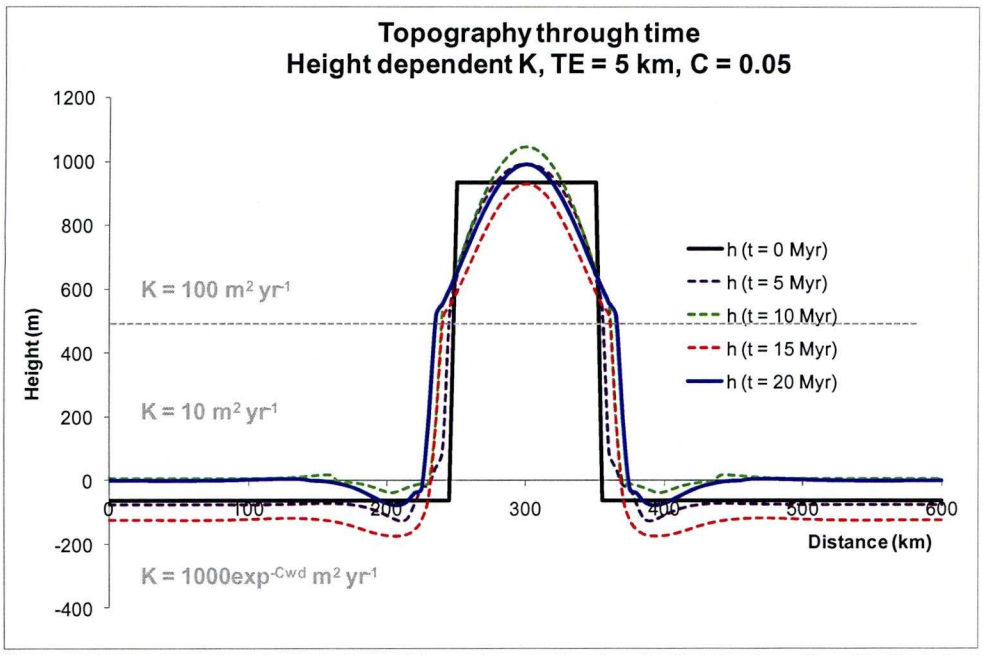

Figure 7.14: Topography through time with varying sea-level and a height-dependent K. Grey dashed line representing the elevation where K changes is at 500 m, and an exponentially decreasing K applies below sea-level.

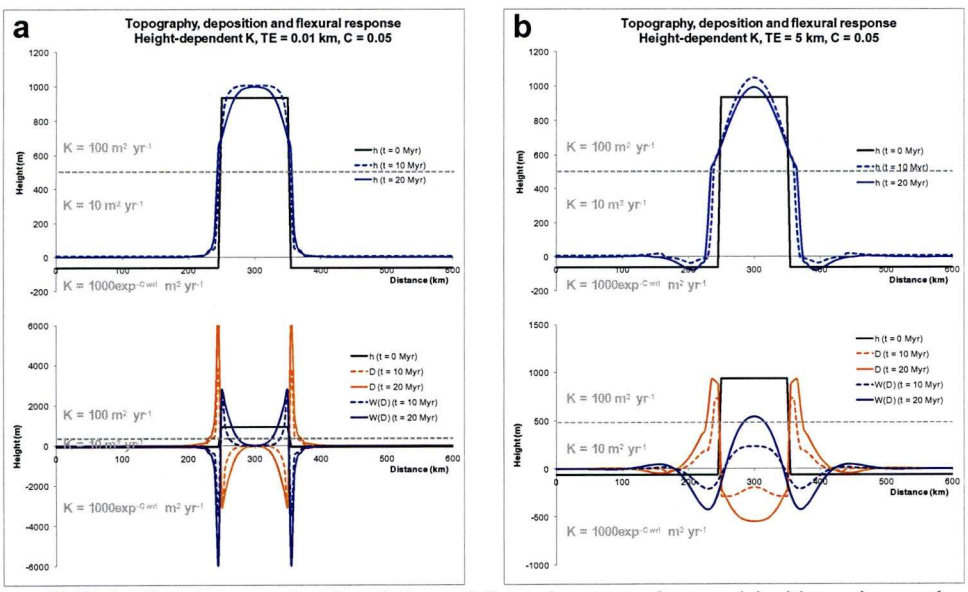

Figure 7.15: Predicted topography, denudation and flexural response for a model with varying sea-level and a height-dependent K.

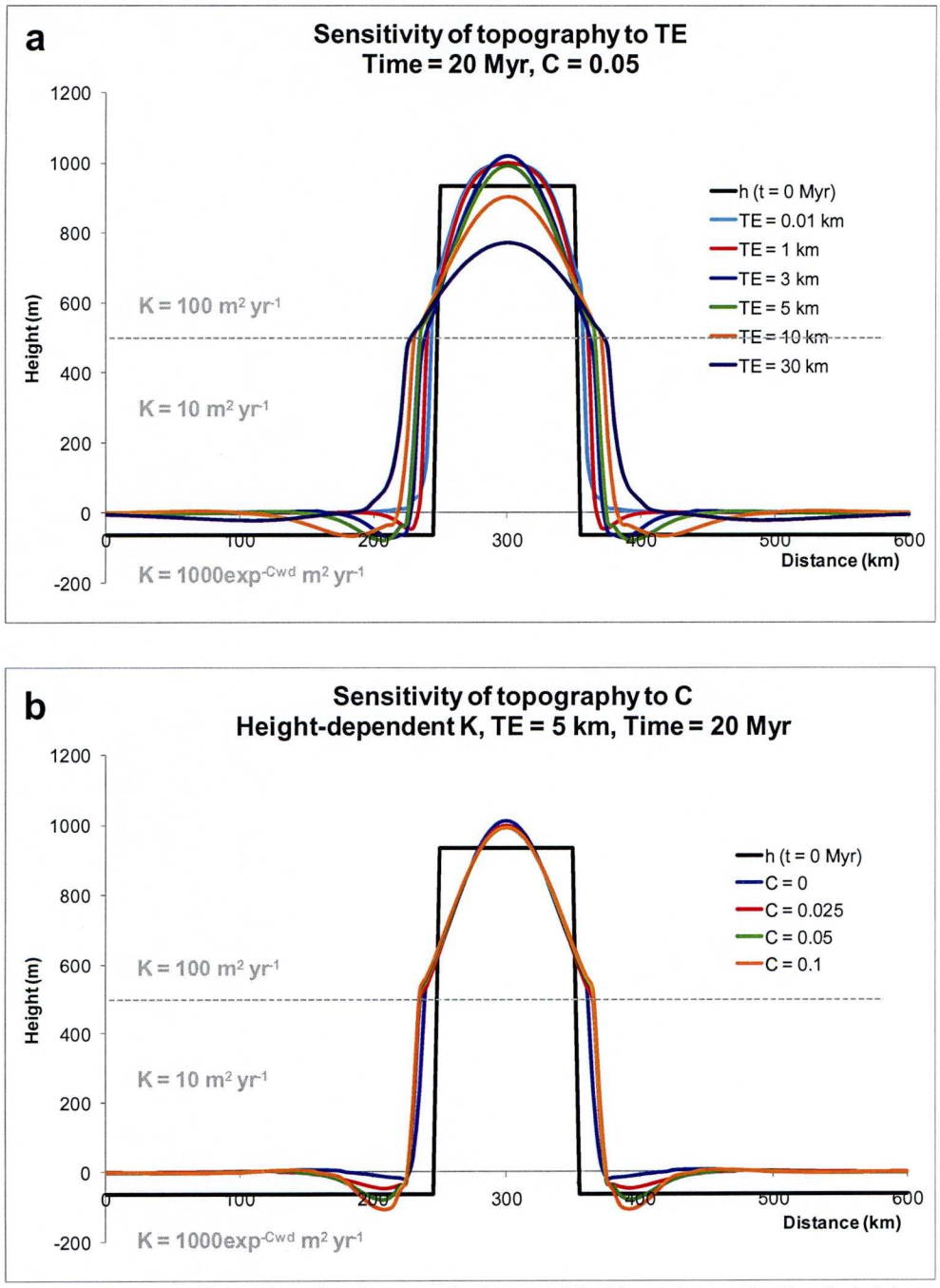

Figure 7.16: Sensitivity of predicted topography for a model with varying sea-level and a height dependent K to a) elastic thickness and b) depth decay constant.

7.6 Summary

In this chapter, the diffusion equation has been applied to model erosion, sediment transport and deposition along a box profile. Several models have been presented for where the diffusion coefficient is either constant, height-dependent or laterally-varying. The effect of eustatic sea-level changes has also been considered. Sediment transport becomes more efficient with increasing K, resulting in increased erosion of the topography, and applying a K to approximate the wave base can result in the development of a shelf topography below sea-level. It has also been shown that the flexural response to erosional unloading and sediment deposition is an important control on the resulting topography, and that the coupling effect between these processes can cause the maximum elevation of the topography to increase, even though the mean elevation along the profile is decreasing due to erosion.

7.7 References

Avouac, J. P. and E. B. Burov (1996), Erosion as a driving mechanism of intracontinental mountain growth, *Journal of Geophysical Research-Solid Earth*, vol. 101, no. B8, p. 17747-17769.

Braun, J. and M. Sambridge (1997), Modelling landscape evolution on geological time scales: A new method based on irregular spatial discretization, *Basin Research*, vol. 9, no. 1, p. 27-52.

Burbank, D. W. and R. S. Anderson (2001) *Tectonic geomorphology*, Blackwell Science, Oxford.

Campanile, D., C. G. Nambiar, P. Bishop, M. Widdowson and R. Brown (2008), Sedimentation record in the Konkan-Kerala Bsin: Implications for the evolution of the Western Ghats and the Western India passive margin, *Basin Research*, vol. 20, p. 3-22.

Chase, C. G. (1992), Fluvial Landsculpting and the Fractal Dimension of Topography, *Geomorphology*, vol. 5, no. 1-2, p. 39-57.

Culling, W. E. H. (1960), Analytical Theory of Erosion, *Journal of Geology*, vol. 68, no. 3, p. 336-344.

Flemings, P. B. and T. E. Jordan (1989), A Synthetic Stratigraphic Model of Foreland Basin Development, *Journal of Geophysical Research-Solid Earth and Planets*, vol. 94, no. B4, p. 3851-3866.

Gilchrist, A. R., H. Kooi and C. Beaumont (1994), Post-Gondwana Geomorphic Evolution of Southwestern Africa - Implications for the Controls on Landscape Development from Observations and Numerical Experiments, *Journal of Geophysical Research-Solid Earth*, vol. 99, no. B6, p. 12211-12228.

Godard, V., R. Cattin and J. Lave (2004), Numerical modeling of mountain building: Interplay between erosion law and crustal rheology, *Geophysical Research Letters*, vol. 31, no. 23, p. L23607.

Haq, B. U., J. Hardenbol and P. R. Vail (1987), Chronology of Fluctuating Sea Levels since the Triassic, *Science*, vol. 235, no. 4793, p. 1156-1167.

Kaufman, P., J. P. Grotzinger and D. S. McCormick (1991), Depth-dependent diffusion algorithm for simulation of sedimentation in shallow marine depositional systems, *Kansas Geological Survey Bulletin*, vol. 233, p. 489-508.

Kooi, H. and C. Beaumont (1994), Escarpment Evolution on High-Elevation Rifted Margins - Insights Derived from a Surface Processes Model That Combines Diffusion, Advection, and Reaction, *Journal of Geophysical Research-Solid Earth*, vol. 99, no. B6, p. 12191-12209.

Kooi, H. and C. Beaumont (1996), Large-scale geomorphology: Classical concepts reconciled and integrated with contemporary ideas via a surface processes model, *Journal of Geophysical Research-Solid Earth*, vol. 101, no. B2, p. 3361-3386.

Martin, Y. and M. Church (1997), Diffusion in landscape development models: On the nature of basic transport relations, *Earth Surface Processes and Landforms*, vol. 22, no. 3, p. 273-279.

Molnar, P. and P. England (1990), Late Cenozoic Uplift of Mountain-Ranges and Global Climate Change - Chicken or Egg, *Nature*, vol. 346, no. 6279, p. 29-34.

Moretti, I. and D. L. Turcotte (1985), A Model for Erosion, Sedimentation, and Flexure with Application to New-Caledonia, *Journal of Geodynamics*, vol. 3, no. 1-2, p. 155-168.

Pinet, P. and M. Souriau (1988), Continental Erosion and Large-Scale Relief, *Tectonics*, vol. 7, no. 3, p. 563-582.

Sinclair, H. D., B. J. Coakley, P. A. Allen and A. B. Watts (1991), Simulation of Foreland Basin Stratigraphy Using a Diffusion-Model of Mountain Belt Uplift and Erosion - an Example from the Central Alps, Switzerland, *Tectonics*, vol. 10, no. 3, p. 599-620.

Summerfield, M. A. (1991), Subaerial Denudation of Passive Margins - Regional Elevation Versus Local Relief Models, *Earth and Planetary Science Letters*, vol. 102, no. 3-4, p. 460-469.

van der Beek, P., A. Pulford and J. Braun (2001), Cenozoic landscape development in the Blue Mountains (SE Australia): Lithological and tectonic controls on rifted margin morphology, *Journal of Geology*, vol. 109, no. 1, p. 35-56.

van der Beek, P., M. A. Summerfield, J. Braun, R. W. Brown and A. Fleming (2002), Modeling postbreakup landscape development and denudational history across the southeast African (Drakensberg Escarpment) margin, *Journal of Geophysical Research-Solid Earth*, vol. 107, no. B12, p. 2351.

Vanbalen, R. T., P. A. Vanderbeek and S. A. P. L. Cloetingh (1995), The Effect of Rift Shoulder Erosion on Stratal Patterns at Passive Margins - Implications

for Sequence Stratigraphy, *Earth and Planetary Science Letters*, vol. 134, no. 3-4, p. 527-544.

Willett, S. D., R. Slingerland and N. Hovius (2001), Uplift, shortening, and steady-state topography in active mountain belts, *American Journal of Science*, vol. 301, no. 4-5, p. 455-485.

Chapter 8

Coupled geodynamic and surface process model for continental lithosphere thinning and sea-floor spreading

8.1 Introduction

It has been demonstrated that surface processes play a fundamental role in the onshore development of rifted margins (van der Beek et al., 2002, & references therein). Sediment loading offshore and erosional unloading onshore can lead to tilting, and therefore uplift of the margin (Avouac & Burov, 1996; Campanile et al., 2008). Furthermore, knowledge of the erosional history of a margin is important in order to correctly interpret the offshore sedimentary record. To this end, the sediment diffusion model discussed in Chapter 7 has been incorporated into the geodynamic model for continental lithosphere thinning and sea-floor spreading initiation developed in Chapters 4, 5 and 6. The model is tested to determine whether significant hinterland uplift can be generated and maintained. Examples of the model are shown for when the diffusion coefficient is constant along the profile, varies laterally or varies with height. The sensitivity of the predicted topography and sediment erosion/deposition to elastic thickness is also considered.

8.2 Incorporation of sediment diffusion into the geodynamic model

The diffusion equation for sediment transport presented in Chapter 7 (Equation 7.2; Culling, 1960) is incorporated into the model by considering the change in height due to erosion and the advection of the sediment erosion/deposition history, such that:

$$\frac{\partial E}{\partial t} = K\nabla^2 h - \bar{V}\nabla E \qquad [8.1]$$

where h = topography, t = time, K = diffusion coefficient, V = velocity, and E = the erosion history. The topography is then determined from the flexural isostatic response to the sum of the loads due to crustal thinning, geotherm perturbation and sediment deposition, plus the erosion history. In the model, erosion is assumed to start contemporaneous with the onset of sea-floor spreading.

8.3 Results from coupled geodynamic and surface process model

The predicted topography and sediment deposition are presented below for three schematic geodynamic models: a thermal plate model with a lithosphere thickness of 125 km and pre-breakup continental lithosphere thinning by combined pure shear and upwelling-divergent flow (Model 1), a thermal plate model with a lithosphere thickness of 125 km and pre-breakup continental lithosphere thinning by combined pure shear and Stokes flow (Model 2), and a model with a lateral variation in lithosphere thickness across the ocean-continent transition (Model 3). In Model 3, pre-breakup continental lithosphere thinning occurs by combined pure shear and upwelling-divergent flow, and thicknesses of 100 km and 175 km are used for the oceanic lithosphere and continental lithosphere respectively.

The input parameters used for the events in all of these models are as follows:

1)	Pure shear	$\dot{\varepsilon} = 2\times10^{-15}$ s^{-1}, $W = 50$ km	t = 10 Myr
2)	Pure shear & UDF or Stokes flow	$\dot{\varepsilon} = 2\times10^{-15}$ s^{-1}, $W = 50$ km $Vz = 5$ cm yr^{-1}	t = 2.5 Myr
3)	Sea-floor spreading with high Vz/Vx	$Vx = 1$ cm yr^{-1}, $Vz = 5$ cm yr^{-1}	t = 5 Myr
4)	Sea-floor spreading	$Vx = 1$ cm yr^{-1}, $Vz = 2$ cm yr^{-1}	t = 127.5 Myr

The temperature field and lithosphere structure through time, up to a total model run time of 145 Myr, for models 1, 2 and 3 is shown in Figures 8.1, 8.2 and 8.3 respectively. Results are presented in the reference frame of the continent to focus on the evolution of the continental hinterland region. As discussed in Chapter 4, the buoyancy-driven upwelling during continental lithosphere thinning and early sea-floor spreading leads to a permanent thickening of the continental lithosphere inboard of the region of localised continental lithosphere thinning. In all the models, the temperature field at t = 145 Myr (Figures 8.1f, 8.2f and 8.3f), has nearly reached equilibrium since the margin is sufficiently far from the mid-ocean ridge, and its associated thermal anomaly, by that time. The predicted topography and deposition when erosion is included in Model 1 is shown in Figures 8.4 through to 8.8; these figures are discussed in the following sections. All models include flexural isostasy and water-loaded subsidence offshore.

8.3.1 Thermal plate model (Model 1) with constant diffusion coefficient

Erosion has been included in Model 1 assuming a constant diffusion coefficient across the profile with K = 100 m^2 yr^{-1}. The resulting topography and sediment deposition are shown in Figure 8.4a, 8.4b & 8.4c for Te = 5 km. The sensitivity of the topography and deposition to elastic thickness is also shown (Figures 8.4d & 8.4e). By 145 Myr, the contribution of the thermal uplift due to geotherm perturbation to the predicted topography is very small (Figure 8.4a). The elevation is maintained through time, as the flexural isostatic response to erosion compensates for the height change. Furthermore, the elevation of the hinterland region is observed to increase through time, mainly due to thermal uplift as the geotherm re-equilibrates. Figure 8.4b also shows the lateral migration of the coastline, and the location of maximum elevation through time. In agreements with observations of erosion at uplifted rifted margins (Campanile et al., 2008; Brown et al., 2002; Gilchrist et al., 1994; Hackspacher et al., 2004), the maximum erosion occurs at the coast and escarpment, with the sediments being deposited offshore, adjacent to the margin. Increasing the elastic thickness increases the wavelength of the uplift (Figure 8.4d), and greatly decreases the amount of predicted erosion/deposition (Figure 8.4e).

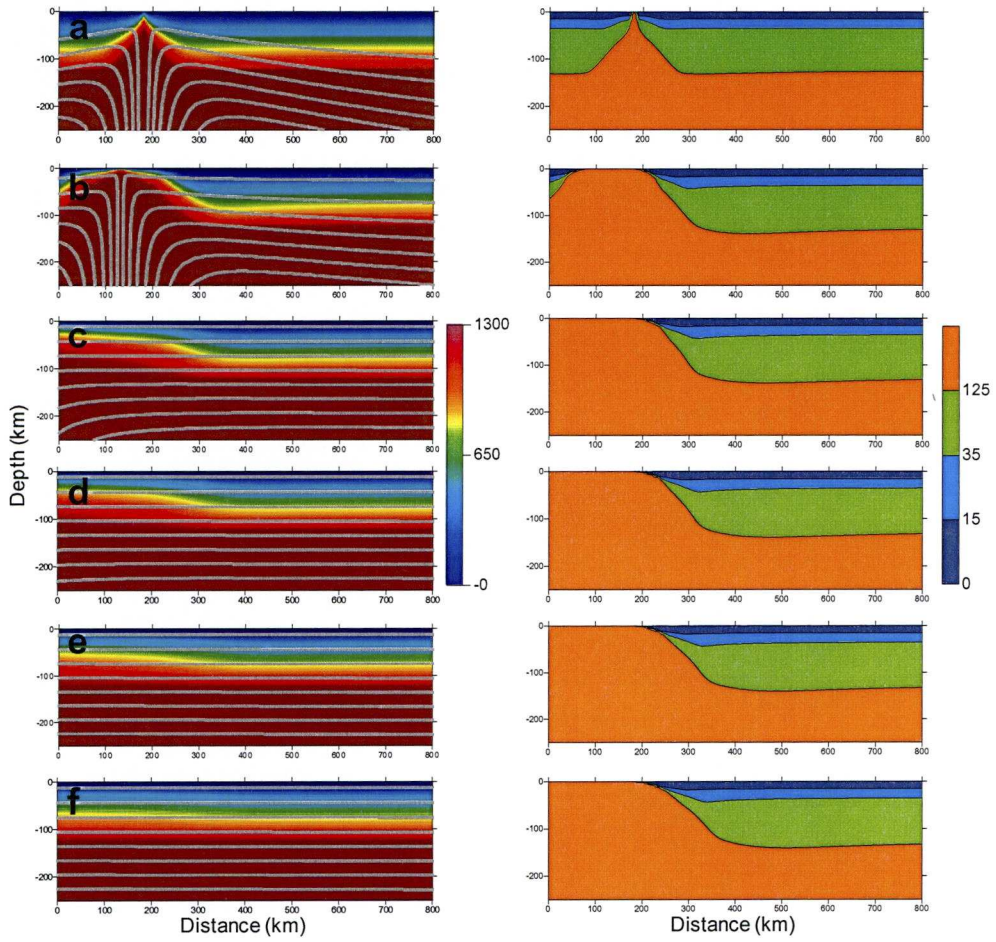

Figure 8.1: Temperature and flow lines (left) and lithosphere cross section (right) through time for Model 1 – see text for parameters. a) t = 12.5 Myr (breakup); b) t = 17.5 Myr (end of early sea-floor spreading); c) t = 50 Myr; d) = 70 Myr; e) = 100 Myr; f) = 145 Myr. Figures are shown in reference frame of the continent.

8.3.2 Thermal plate model (Model 1) with a laterally-varying diffusion coefficient

Figure 8.5 shows the resulting topography and deposition when a laterally-varying diffusion coefficient is applied in the model. For this model, $K = 100$ m^2 yr^{-1} except in the region between 375 – 425 km, where $K = 1$ m^2 yr^{-1}. Less erosion occurs in this region, and therefore the topography is higher than the surrounding areas which are more erodible (Figure 8.5b). This effect is more noticeable as the elastic thickness increases (Figures 8.5d & 8.5 e).

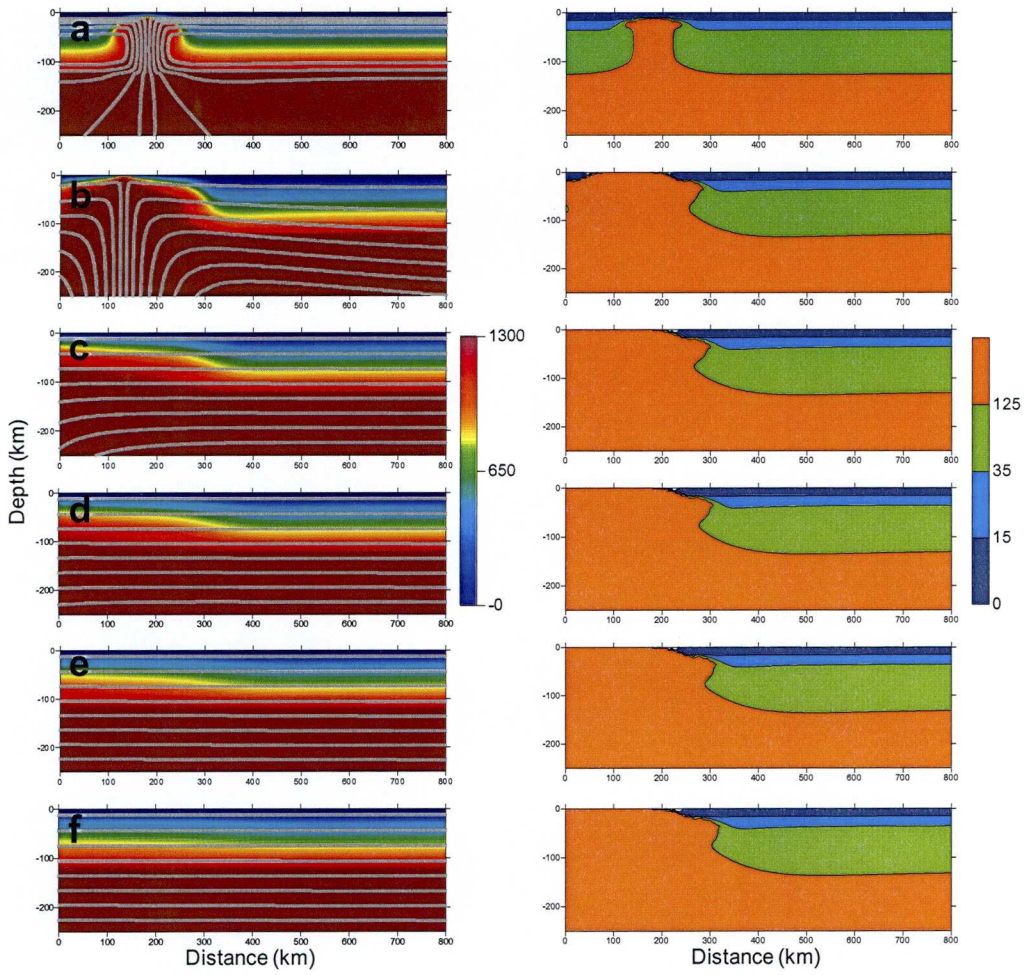

Figure 8.2: Temperature and flow lines (left) and lithosphere cross section (right) through time for Model 2 – see text for parameters. a) t = 12.5 Myr (breakup); b) t = 17.5 Myr (end of early sea-floor spreading); c) t = 50 Myr; d) = 70 Myr; e) = 100 Myr; f) = 145 Myr.

8.3.3 Thermal plate model (Model 1) with a height-dependent diffusion coefficient

The model has also been run with a diffusion coefficient which varies with height (Figure 8.6). In this case, K = 100 m^2 yr^{-1} above a height of 500 m, and K = 10 m^2 yr^{-1} below it. Since the higher topography is eroded quicker than that below it, a plateau begins to form at the height where the diffusion coefficient changes (Figure 8.6b). The wavelength and maximum elevation of this plateau is dependent on the elastic thickness, with the topography decreasing and the wavelength increasing with increasing elastic thickness (Figure 8.6d).

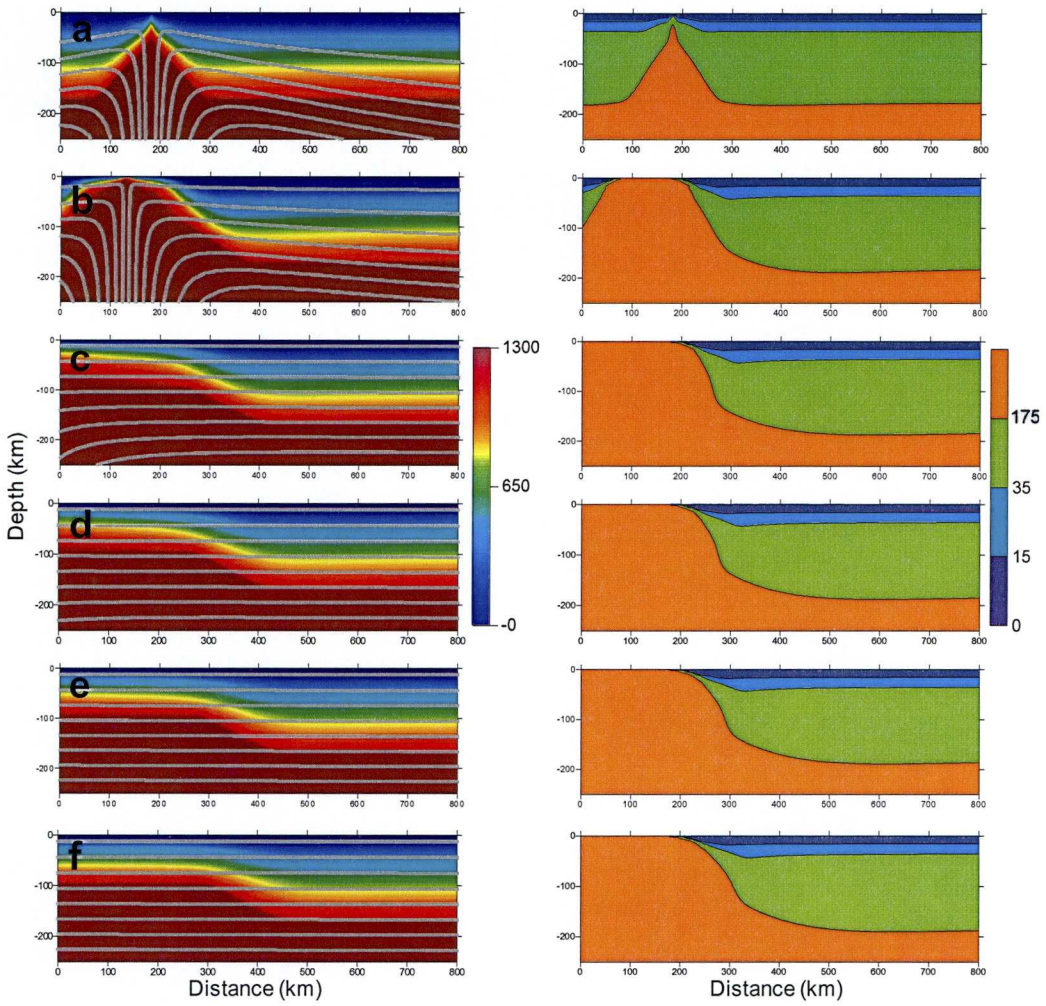

Figure 8.3: Temperature and flow lines (left) and lithosphere cross section (right) through time for Model 3 – see text for parameters. a) t = 12.5 Myr (breakup); b) t = 17.5 Myr (end of early sea-floor spreading); c) t = 50 Myr; d) = 70 Myr; e) = 100 Myr; f) = 145 Myr.

8.3.4 Thermal plate model (Model 1) with a height-dependent diffusion coefficient and a marine diffusion coefficient

The predicted topography and erosion/deposition for a model where the diffusion coefficient, for regions below sea-level, decays exponentially with water depth, is shown in Figure 8.7. The diffusion coefficient used above sea-level is the same as in section 8.3.3, and for below sea-level K_w = 1000 and C = 0.05. Including the marine diffusion coefficient leads to the development of a step in the topography at shallow water depths immediately adjacent to the onshore region. The width of this step increases with increasing elastic thickness (Figure 8.7d).

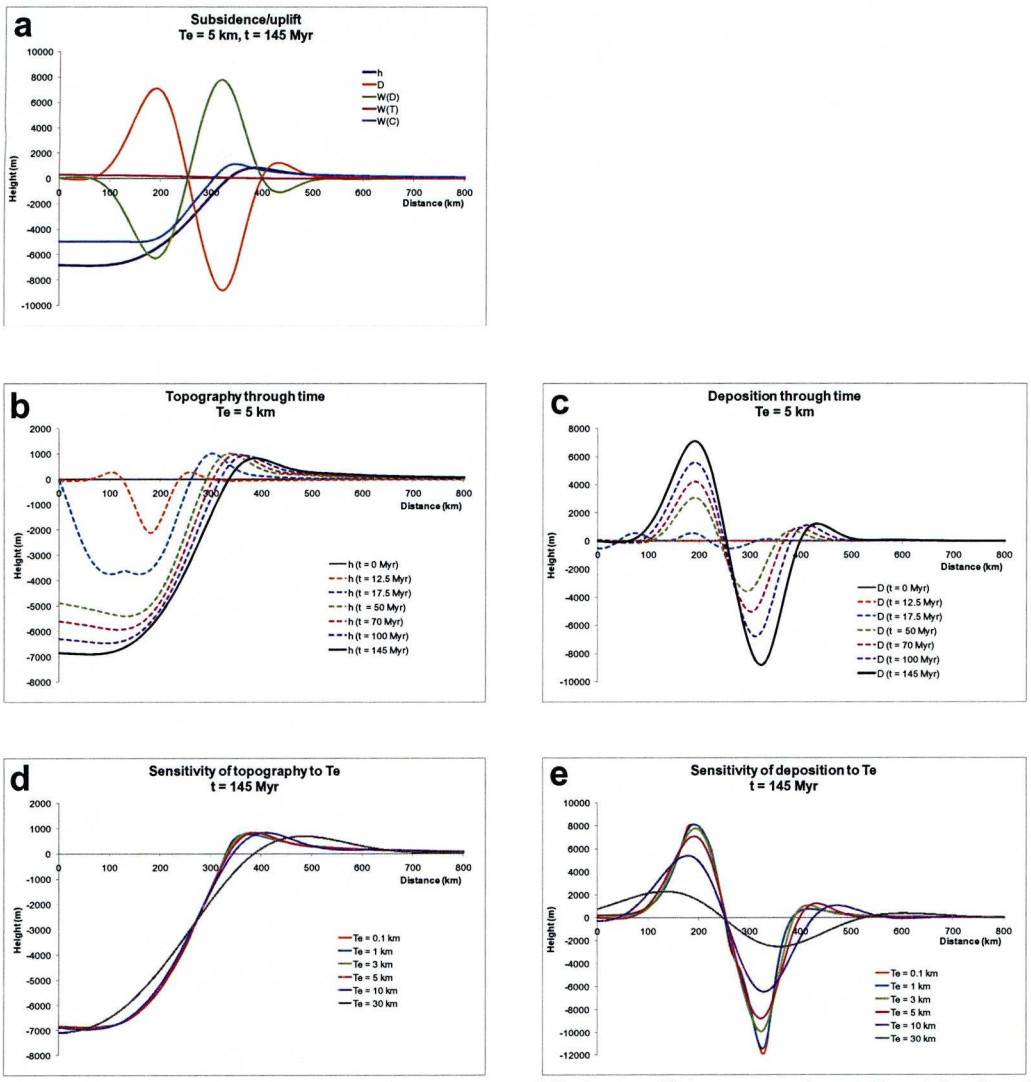

Figure 8.4: Model 1 with erosion assuming a constant diffusion coefficient across the profile. a) Predicted topography, deposition, and flexural response to deposition, geotherm perturbation and crustal thinning for Te = 5 km after 145 Myr. b) Topography through time for Te = 5 km. c) Deposition through time for Te = 5 km. d) Sensitivity of the predicted topography to elastic thickness, at t = 145 Myr. e) Sensitivity of deposition to elastic thickness at t = 145 Myr. K = 100 m^2 yr^{-1}. h = topography, D = deposition (erosion is negative), *W(D)* = flexural isostatic response to erosion, *W(T)* = flexural isostatic response to geotherm perturbation, and *W(C)* = flexural isostatic response to crustal thinning.

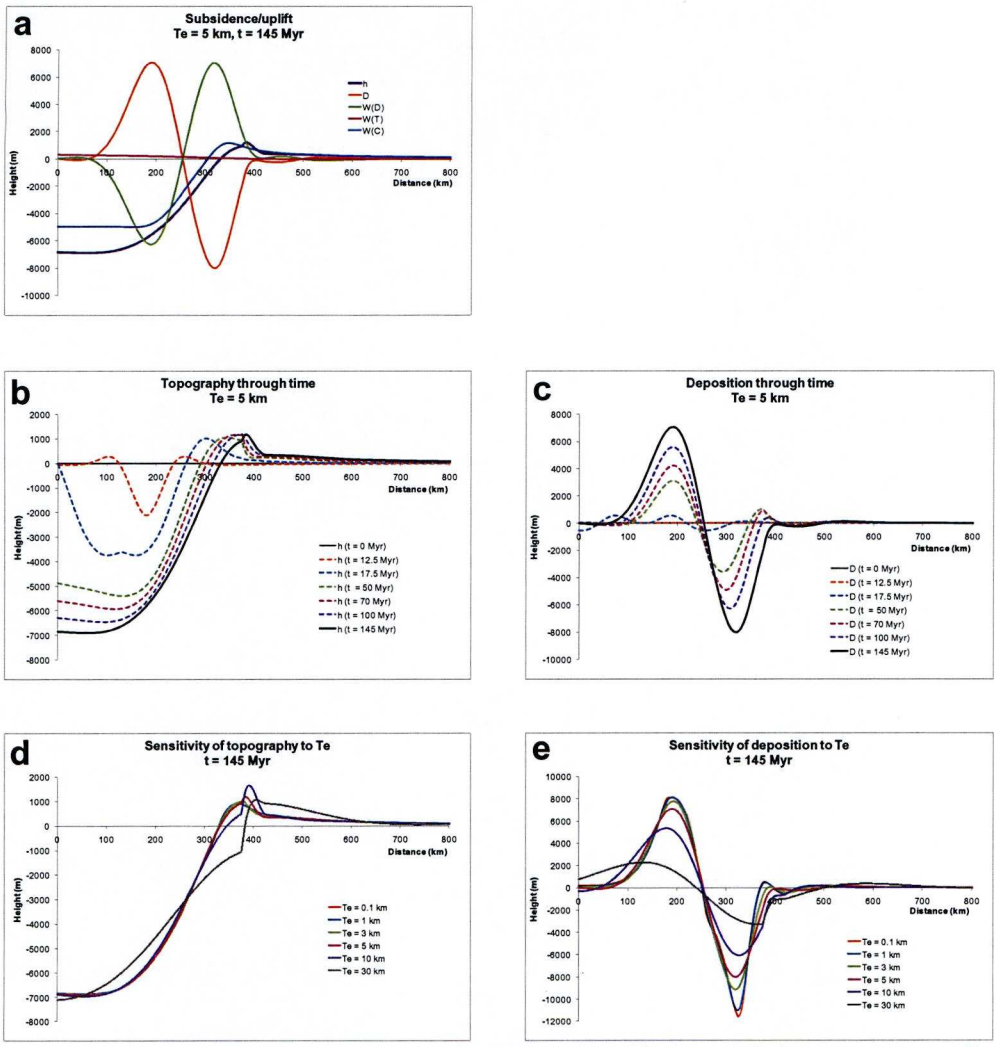

Figure 8.5: Model 1 with erosion assuming a laterally-varying diffusion coefficient across the profile. a) Predicted topography, deposition, and flexural response to deposition, geotherm perturbation and crustal thinning for Te = 5 km after 145 Myr. b) Topography through time for Te = 5 km. c) Deposition through time for Te = 5 km. d) Sensitivity of the predicted topography to elastic thickness, at t = 145 Myr. e) Sensitivity of deposition to elastic thickness at t = 145 Myr. $K = 1$ m^2 yr^{-1} between 375 – 425 km and $K = 100$ m^2 yr^{-1} everywhere else.

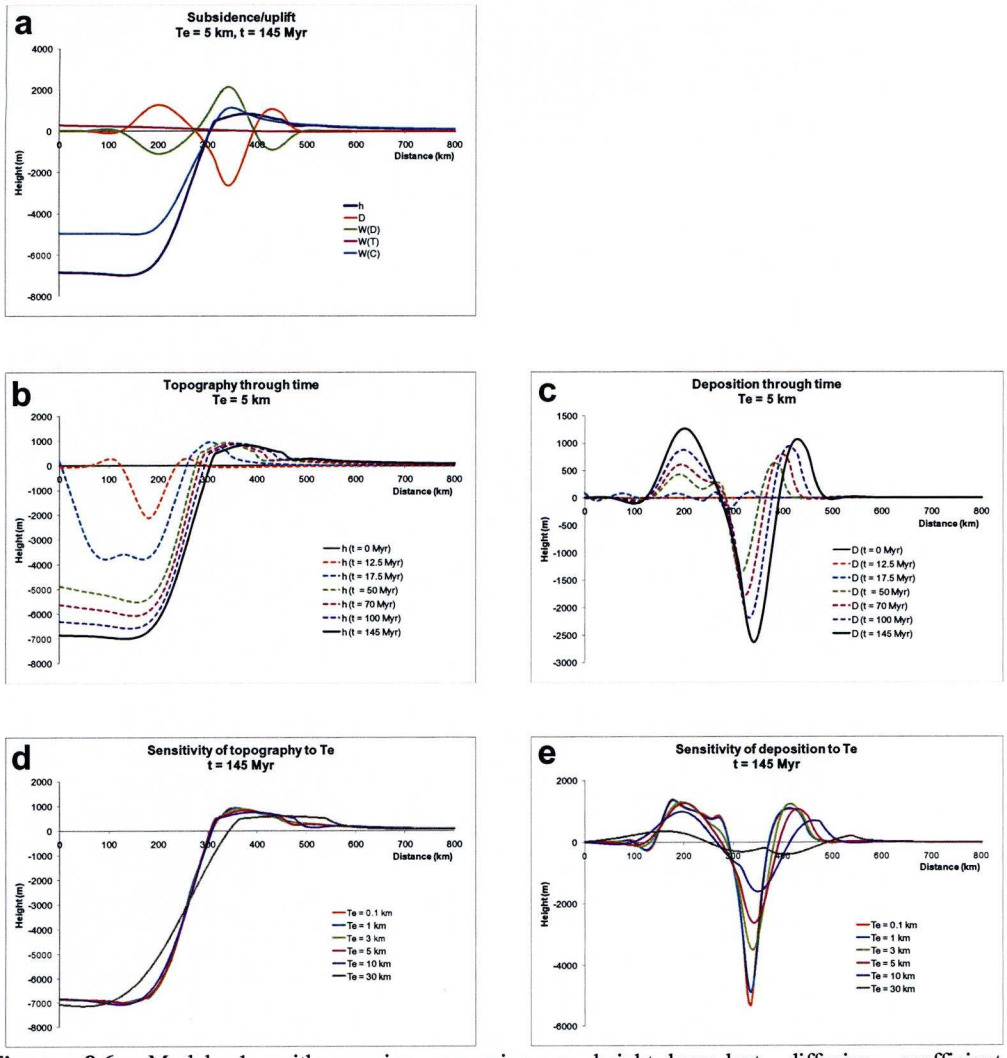

Figure 8.6: Model 1 with erosion assuming a height-dependent diffusion coefficient. a) Predicted topography, deposition, and flexural response to deposition, geotherm perturbation and crustal thinning for Te = 5 km after 145 Myr. b) Topography through time for Te = 5 km. c) Deposition through time for Te = 5 km. d) Sensitivity of the predicted topography to elastic thickness, at t = 145 Myr. e) Sensitivity of deposition to elastic thickness at t = 145 Myr. K = 100 m^2 yr^{-1} above 500 m and K = 10 m^2 yr^{-1} below 500 m.

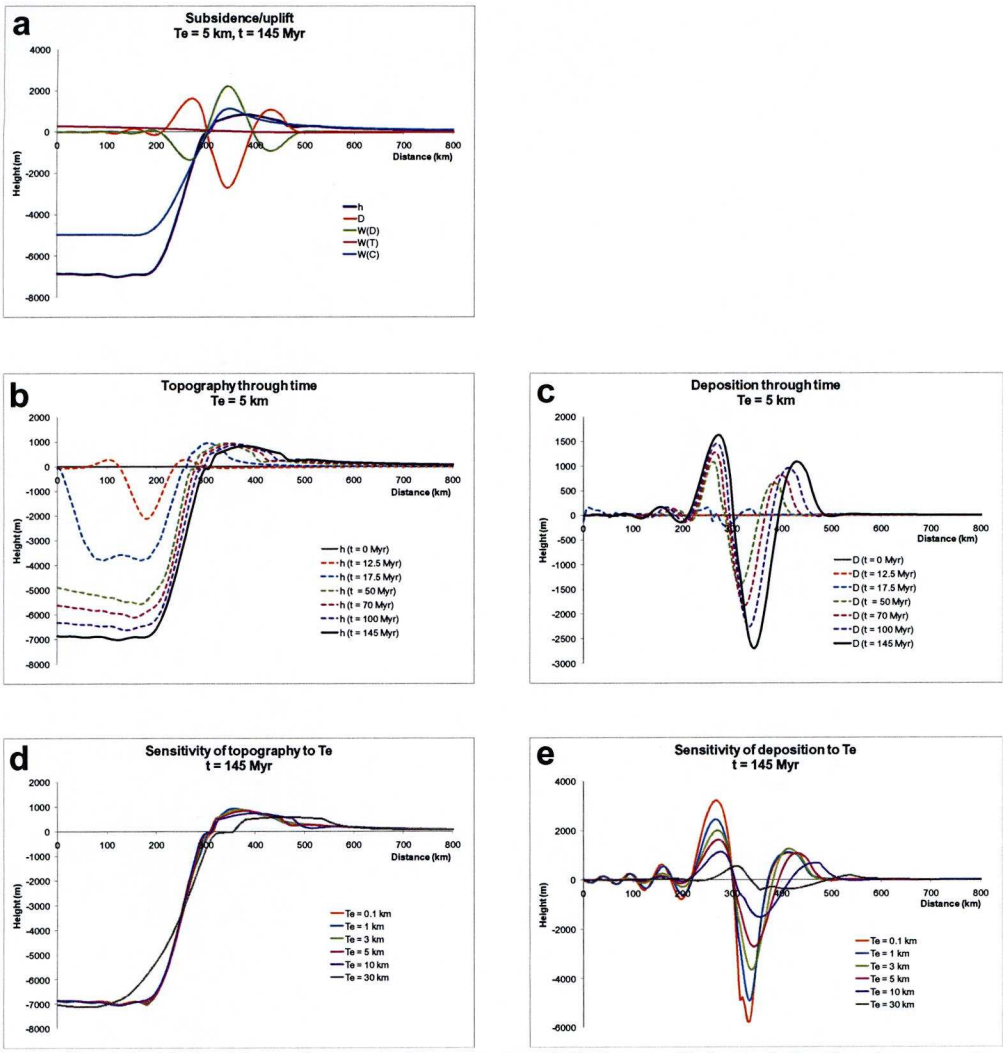

Figure 8.7: Model 1 with erosion assuming a marine diffusion coefficient. a) Predicted topography, deposition, and flexural response to deposition, geotherm perturbation and crustal thinning for Te = 5 km after 145 Myr. b) Topography through time for Te = 5 km. c) Deposition through time for Te = 5 km. d) Sensitivity of the predicted topography to elastic thickness, at t = 145 Myr. e) Sensitivity of deposition to elastic thickness at t = 145 Myr. Below sea-level, K decays exponentially, with $K_w = 1000$ m^2 yr^{-1} and $C = 0.05$. Above sea-level, $K = 100$ m^2 yr^{-1} above 500 m and $K = 10$ m^2 yr^{-1} below 500 m.

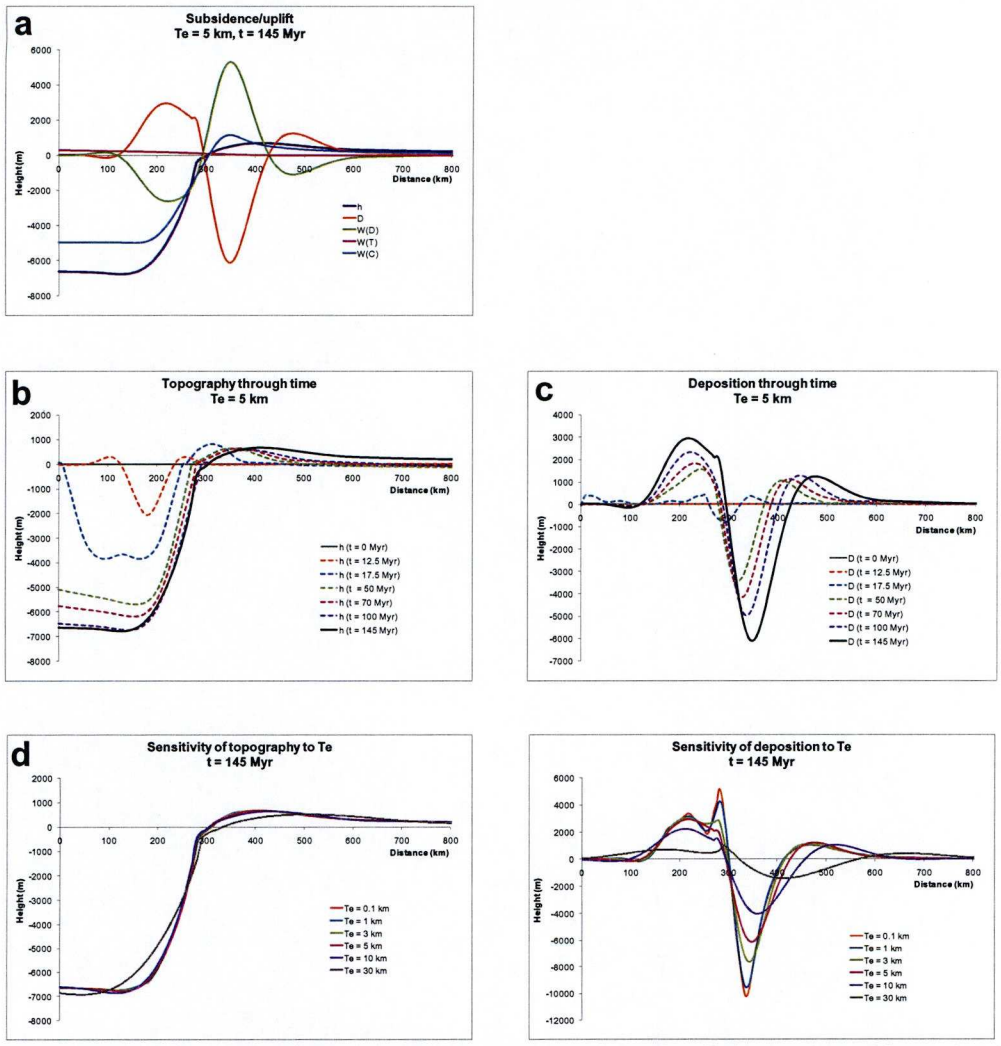

Figure 8.8: Model 1 with erosion assuming a marine diffusion coefficient and eustatic sea-level changes. a) Predicted topography, deposition, and flexural response to deposition, geotherm perturbation and crustal thinning for Te = 5 km after 145 Myr. b) Topography through time for Te = 5 km. c) Deposition through time for Te = 5 km. d) Sensitivity of the predicted topography to elastic thickness, at t = 145 Myr. e) Sensitivity of deposition to elastic thickness at t = 145 Myr. Below sea-level, K decays exponentially, with $K_w = 1000$ m^2 yr^{-1} and $C = 0.05$. Above sea-level, $K = 100$ m^2 yr^{-1} above 500 m and $K = 10$ m^2 yr^{-1} below 500 m.

8.3.5 Thermal plate model (Model 1) with a marine diffusion coefficient and eustatic sea-level changes

It is also possible to include eustatic sea-level changes in the model (Figure 8.8), with sea-level varying through time according to the sea-level curve of Haq et al. (1987). The diffusion coefficients used in the model presented in Figure 8.8 are the same as for section 8.3.4, and the initial topography is set to the same height as the sea-level at that time. In the case of this model, which is started at 145 Ma, the initial sea-level is +120 m. The fall in sea-level to its present-day level gives an apparent uplift by this amount along the whole profile, and is particularly noticeable in the continental hinterland region (Figure 8.8b).

8.3.6 Thermal plate model with Stokes flow (Model 2) with a marine diffusion coefficient and eustatic sea-level changes

The post-process parameters used for section 8.3.5 (Figure 8.8) of a height-dependent and marine diffusion coefficient are applied to Model 2, and the results are presented in Figure 8.9, for Te = 5 km. The same general behaviour as in the previous models is observed. Significant uplift of the hinterland region is predicted, which is up to ~550 m in some locations along the profile, although a considerable part of that is due to the fall in sea-level.

8.3.7 Lithosphere thickness variation across the OCT (Model 3) with a marine diffusion coefficient and eustatic sea-level changes

Again, the same post-processing parameters as before are applied to Model 3, and the same general behaviour is also observed (Figure 8.10). In this model, although the maximum elevation remains reasonably constant throughout the time of normal sea-floor spreading (when Vz/Vx = 2), the location of maximum elevation moves continent-ward by ~100 km (Figure 8.10b). Therefore, the hinterland region experienced an uplift of over 1100 m since 127.5 Ma, occurring after the end of the early sea-floor spreading phase associated with thermal buoyancy driven upwelling at 17.5 Myr into the model.

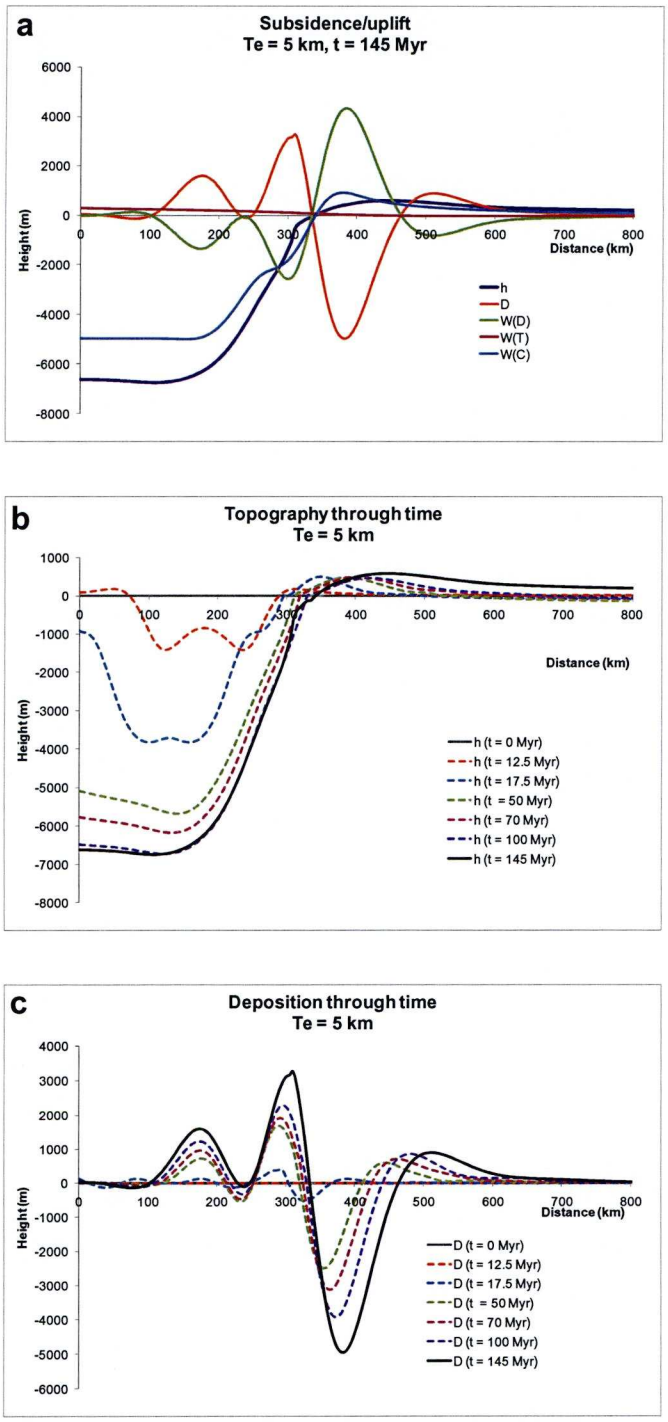

Figure 8.9: Model 2 with erosion assuming a marine diffusion coefficient and eustatic sea-level changes. a) Predicted topography, deposition, and flexural response to deposition, geotherm perturbation and crustal thinning for Te = 5 km after 145 Myr. b) Topography through time for Te = 5 km. c) Deposition through time for Te = 5 km. Below sea-level, K decays exponentially, with $K_w = 1000$ m^2 yr^{-1} and $C = 0.05$. Above sea-level, $K = 100$ m^2 yr^{-1} above 500 m and $K = 10$ m^2 yr^{-1} below 500 m.

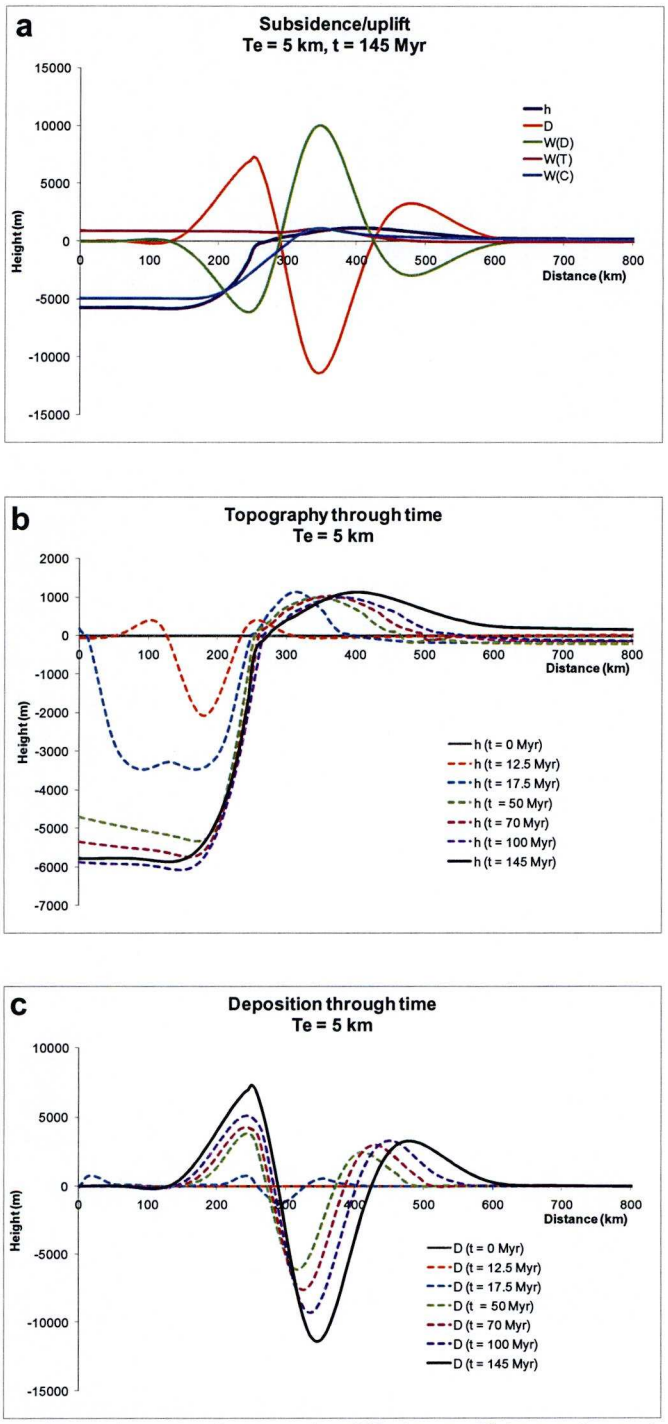

Figure 8.10: Model 3 with erosion assuming a marine diffusion coefficient and eustatic sea-level changes. a) Predicted topography, deposition, and flexural response to deposition, geotherm perturbation and crustal thinning for Te = 5 km after 145 Myr. b) Topography through time for Te = 5 km. c) Deposition through time for Te = 5 km. Below sea-level, K decays exponentially, with $K_w = 1000$ m^2 yr^{-1} and $C = 0.05$. Above sea-level, $K = 100$ m^2 yr^{-1} above 500 m and $K = 10$ m^2 yr^{-1} below 500 m.

8.4 Comparison of models

The schematic models presented in section 8.3 (Figures 8.4 – 8.10) show that erosion and the flexural isostatic response to erosional unloading are an important control on the predicted topography. The topography at 145 Myr, the maximum run time of the model, predicted for the thermal plate model (Model 1) for the different methods of prescribing the diffusion coefficient is compared in Figure 8.11. The topography is strongly dependent on how the diffusion coefficient is defined. Including erosion, sediment transport, and deposition in the model predicts a

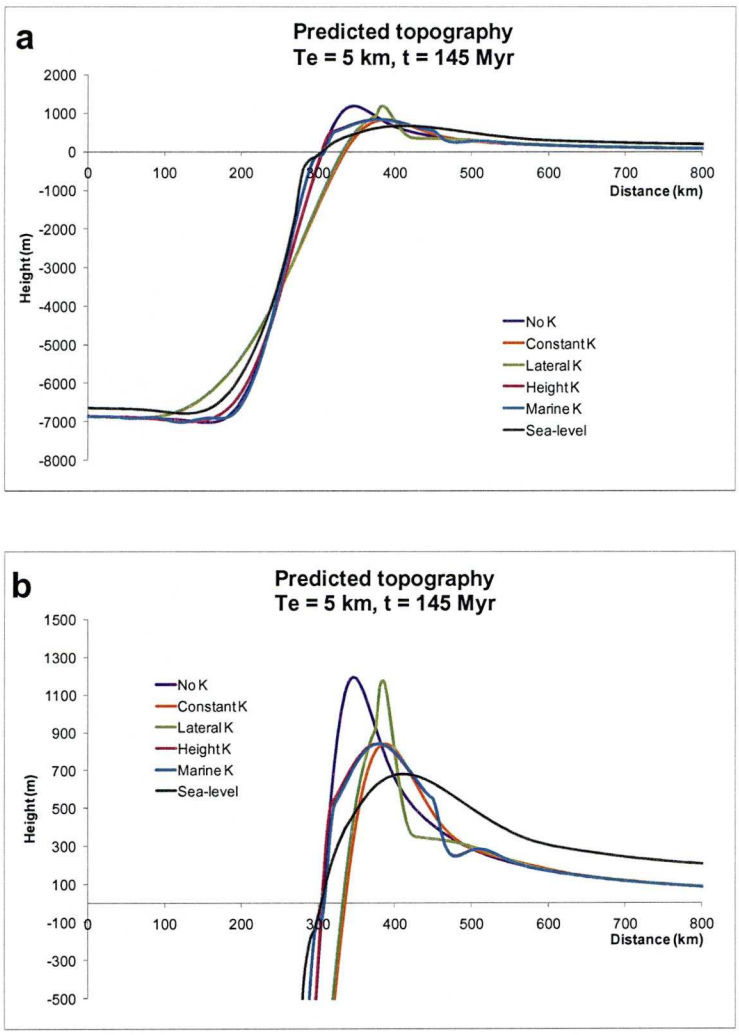

Figure 8.11: Comparison of the predicted topography for the different methods of prescribing the diffusion coefficient, applied to Model 1. Topography shown for Te = 5 km at t = 145 Myr. b) is a close-up of the onshore region of a). Lines shown for no erosion (purple), constant K (orange), laterally-varying K (green), height-dependent K (red), height-dependent with marine K (blue), and height-dependent with marine K and eustatic sea-level changes (grey).

continent-ward movement of the escarpment if K is sufficiently large enough. It also leads to a reduction in the maximum amplitude of the topography, except when a region of low diffusivity, i.e. more resistant lithology, is bounded by a region of high diffusivity. If the diffusion coefficient varies with height, a broad plateau may develop, and the inclusion of a diffusion coefficient which decays exponentially with water depth leads to the development of a shelf-like topography at shallow water depths.

The topography and deposition predicted by the geodynamic models 1, 2 and 3, with erosion by a height-dependent and marine diffusion coefficient, and eustatic sea-level changes is compared in Figure 8.12. The highest topography is predicted by Model 3, with the change in lithosphere thickness across the OCT. This is because of the larger geotherm perturbation associated with the thicker continental lithosphere and the lateral heat flow from the warm oceanic lithosphere to the cooler continental lithosphere at the margin. This effect gives at least 100 m more thermal uplift of the hinterland, if the geotherm fully re-equilibrates, than the plate model (Figure 8.13a), and persistent thermal uplift at the OCT (Figure 8.13b). The topography predicted by the model with pre-breakup buoyancy-driven upwelling represented by Stokes flow (Model 2) is smaller in amplitude and wavelength than that represented by upwelling-divergent flow (Model 1), and the distance between the location of maximum elevation and the ocean-continent transition is increased. The most denudation is predicted for Model 3, as this has the highest topography and therefore more material can be eroded.

8.5 Summary

In this chapter, a schematic geodynamic and surface process model of continental breakup and sea-floor spreading initiation, combined from the models developed in the previous four chapters, has been presented. Significant uplift of the continental hinterland is observed in the models, and the elevated topography persists even after ~130 Myr of sea-floor spreading. Incorporating erosion, and the corresponding flexural isostatic response, shows that surface processes are a fundamental component of the evolution of a rifted margin, and largely control the shape and amplitude of the observed topography. The resulting topography is

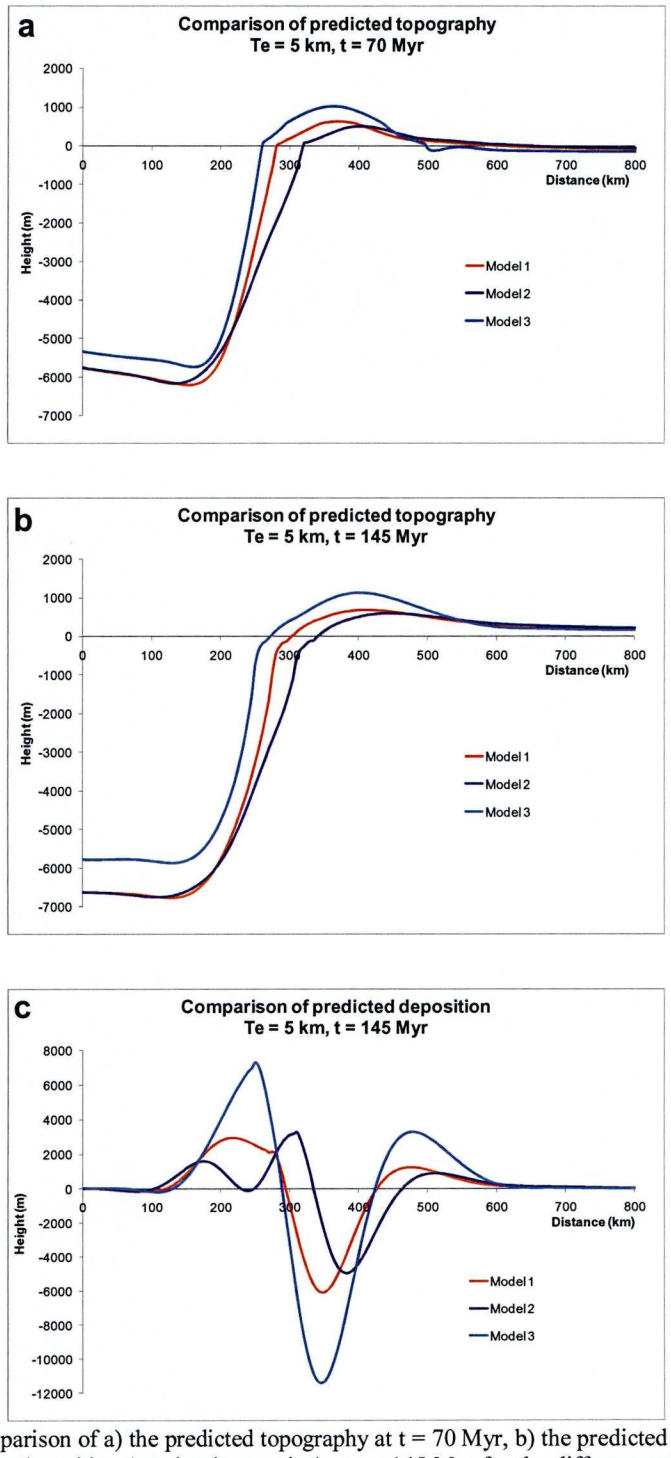

Figure 8.12: Comparison of a) the predicted topography at t = 70 Myr, b) the predicted topography at t = 145 Myr and c) the deposition (erosion is negative) at t = 145 Myr for the different geodynamic models discussed in this chapter. Model 1 = thermal plate model with upwelling-divergent flow, Model 2 = thermal plate model with Stokes flow and Model 3 = model with a step change in lithosphere thickness across the OCT. Erosion is assumed to occur with a height-dependent and marine diffusion coefficient, and sea-level changes are included.

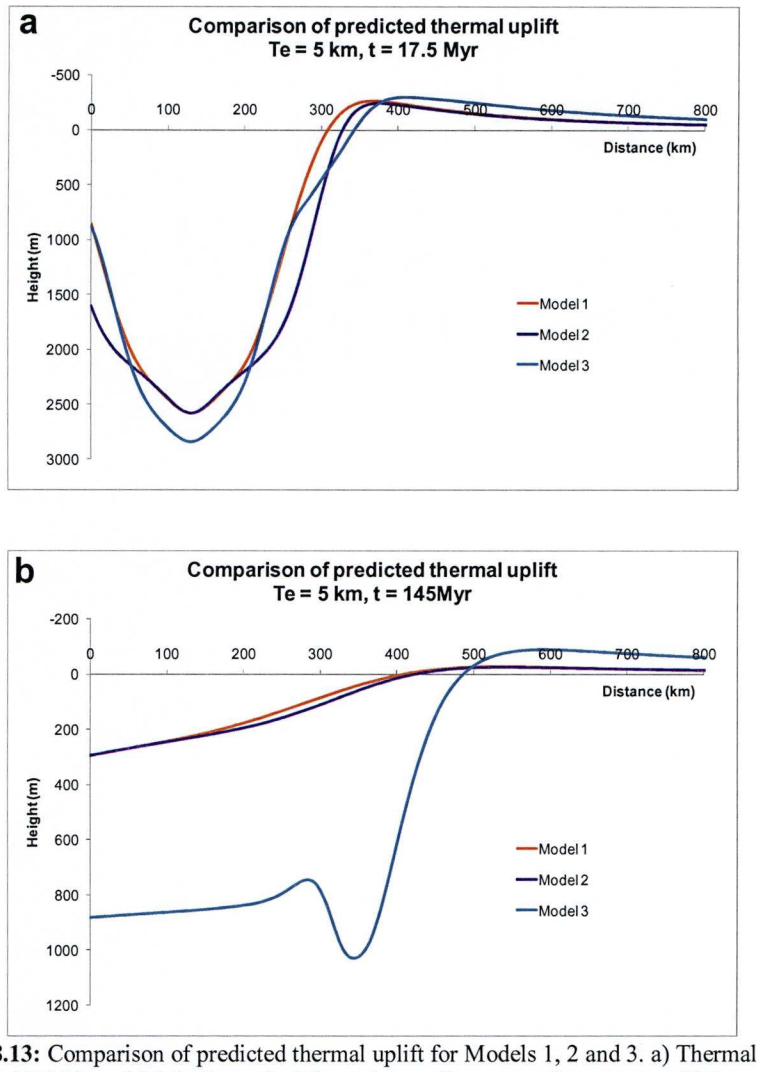

Figure 8.13: Comparison of predicted thermal uplift for Models 1, 2 and 3. a) Thermal uplift shown at 17.5 Myr which is the end of the early sea-floor spreading events with buoyancy-driven upwelling, and corresponds to maximum geotherm perturbation. b) Thermal uplift at 145 Myr (the end of the model).

strongly dependent on the magnitude of the diffusion coefficient, and therefore lithology and climate. It is also important to consider sea-level changes, as a fall in sea-level equates to topographic uplift, echoing the point made by Huuse (2002). It has been demonstrated that the predicted uplift is dependent on the thermal structure of the lithosphere, and on the mode of pre-breakup continental lithosphere thinning. As shown in Chapter 6, the elastic thickness is a key parameter, and controls the wavelength of the predicted topography.

8.6 References

Avouac, J. P. and E. B. Burov (1996), Erosion as a driving mechanism of intracontinental mountain growth, *Journal of Geophysical Research-Solid Earth*, vol. 101, no. B8, p. 17747-17769.

Brown, R. W., M. A. Summerfield and A. J. W. Gleadow (2002), Denudational history along a transect across the Drakensberg Escarpment of southern Africa derived from apatite fission track thermochronology, *Journal of Geophysical Research-Solid Earth*, vol. 107, no. B12, p. 2350.

Campanile, D., C. G. Nambiar, P. Bishop, M. Widdowson and R. Brown (2008), Sedimentation record in the Konkan-Kerala Bsin: Implications for the evolution of the Western Ghats and the Western India passive margin, *Basin Research*, vol. 20, p. 3-22.

Culling, W. E. H. (1960), Analytical Theory of Erosion, *Journal of Geology*, vol. 68, no. 3, p. 336-344.

Gilchrist, A. R., H. Kooi and C. Beaumont (1994), Post-Gondwana Geomorphic Evolution of Southwestern Africa - Implications for the Controls on Landscape Development from Observations and Numerical Experiments, *Journal of Geophysical Research-Solid Earth*, vol. 99, no. B6, p. 12211-12228.

Hackspacher, P. C., L. F. B. Ribeiro, M. C. S. Ribeiro, A. H. Fetter, J. C. Hadler, C. E. S. Tello and E. L. Dantas (2004), Consolidation and break-up of the South American platform in southeastern Brazil: Tectonothermal and denudation histories, *Gondwana Research*, vol. 7, no. 1, p. 91-101.

Haq, B. U., J. Hardenbol and P. R. Vail (1987), Chronology of Fluctuating Sea Levels since the Triassic, *Science*, vol. 235, no. 4793, p. 1156-1167.

Huuse, M. (2002) Cenozoic uplift and denudation of southern Norway: insights from the North Sea Basin, in Doré, A. G., J. A. Cartwright, M. S. Stoker, J. P. Turner and N. White (eds), *Exhumation of the North Atlantic Margin: Timing, Mechanisms and Implications for Petroleum Exploration*, Geological Society, London, Special Publications, vol. 196, p. 209-233.

van der Beek, P., M. A. Summerfield, J. Braun, R. W. Brown and A. Fleming (2002), Modeling postbreakup landscape development and denudational history across the southeast African (Drakensberg Escarpment) margin, *Journal of Geophysical Research-Solid Earth*, vol. 107, no. B12, p. 2351.

Chapter 9

Discussion and summary

9.1 Introduction

The aims of this thesis were to test the hypothesis that deformation to continental lithosphere during continental breakup and sea-floor spreading initiation could result in post-breakup hinterland uplift of rifted margins, and to consider the effect of erosion, sediment transport and deposition, and flexural isostasy on the onshore evolution of a rifted margin. A geodynamic model for continental breakup and sea-floor spreading initiation coupled with erosion has been developed in this thesis, with much consideration given to the sensitivity of the model predictions to the input parameters. The model predicts syn-rift uplift due to the isostatic response to crustal thinning and, post-breakup, a gradual thermal uplift of the continental hinterland. In this chapter, the key findings from the modelling work are summarised and discussed in relation to the observations of post-breakup hinterland uplift detailed in Chapter 2. Suggestions for further model development and testing are also given.

9.2 Model sensitivities

Sensitivity of the predicted thermal uplift and topography to the key model input parameters has been undertaken in order to gain a thorough understanding of the general model behaviour. For the geodynamic model, the key parameters are the pure shear width, pure shear strain rate, pre-breakup upwelling velocity, and the post-breakup ratio of the upwelling velocity to divergent velocity (Vz/Vx). The pure shear width controls the width of the rifted margin, with a wider zone of thinning resulting in a wider margin. It has little effect on the predicted amplitude or wavelength of the thermal uplift, but has some control on its location. The duration

of the pre-breakup buoyancy-driven upwelling, assumed to be dependent on the velocity of the upwelling, effects the width of the margin and the predicted thermal uplift. Increasing the Vz increases the amplitude of wavelength of the predicted thermal uplift. The representation of the pre-breakup buoyancy-driven upwelling, whether by upwelling-divergent or Stokes flow, is also important. The upwelling divergent flow predicts much greater thermal uplift than the Stokes flow because of the free-slip boundary condition assumed in the Stokes flow model.

Post-breakup, the dominant control on the predicted thermal uplift is the Vz/Vx ratio during early sea-floor spreading. At high Vz/Vx ratios, the continental lithosphere material is pushed downwards away from the ridge, leading to a pronounced thickening of the continental lithosphere under the hinterland, and hence greater perturbation of the lithosphere geotherm. Increasing the spreading rate, Vx, whilst keeping the Vz/Vx ratio constant, enhances the thickening of the continental lithosphere and hence the magnitude of the thermal uplift. It also increases the distance between the OCT and the maximum elevation onshore. Including a wedge angle may also increase the predicted thermal uplift, although its use is limited due to the boundary conditions assumed in the thermal plate model.

Including a step change in lithosphere thickness greatly increases the predicted thermal uplift, and leads to a persistent positive thermal anomaly where thin, warm, oceanic lithosphere is juxtaposed against thick, cold, continental lithosphere. The magnitude of this anomaly depends on the difference in thickness between the oceanic lithosphere and the continental lithosphere. Flexural isostasy is also a dominant control on the wavelength and amplitude of the predicted topography and thermal uplift.

The shape of predicted topography is largely controlled by erosion and the flexural response to denudational unloading and offshore sediment deposition. A higher diffusion coefficient means more efficient sediment transport, and hence greater erosion. The diffusion coefficient depends on the climate and lithology of a location, thus they are controlling factors for the shape of the topography. The coupling effect between flexural isostasy and sediment loading can lead to the maximum elevation of the profile increasing whilst the mean elevation decreases. Including a diffusion coefficient which decays exponentially with water depth for regions below sea-level leads to the development of a shelf topography at shallow water depths. The width of this shelf is controlled by the depth decay constant and

the elastic thickness. Sea-level changes give apparent uplift or subsidence of the profile (Molnar & England, 1990) and therefore control the erosional base level.

9.3 Model predictions and comparison to observations

The theoretical model presented in Chapter 8 shows that deformation to continental lithosphere during continental breakup and sea-floor spreading initiation, due to buoyancy-driven upwelling, generates significant uplift of a rifted margin. The model predicts the characteristic topography – that of a steep escarpment and an asymmetrical elevated plateau – that is observed at the uplifted rifted margins. Whilst the input parameters are not defined for application to a specific location, the predictions of the model can be compared to the key observations of post-breakup uplift – timing, magnitude, and location - discussed in Chapter 2 and summarised in Table 9.1. The values predicted by the models in Chapter 8 at 70 Myr (55 Myr sea-floor spreading) and 145 Myr (130 Myr sea-floor spreading) are shown in Table 9.2 and Table 9.3 respectively. Proposed timings of uplift events are not given in Table 9.1 due to the lack of consensus in the observations.

9.3.1 Timing of the uplift

The model predicts syn-rift uplift due to crustal thinning and a gradual post-rift thermal uplift of the hinterland as the continental lithosphere geotherm re-equilibrates. Distinct uplift events are reported for the Norwegian margin, in the Palaeocene and the Neogene (Riis, 1996), two Neogene uplift events are reported for West Greenland (Japsen et al., 2006). The model cannot account for this observed increase in uplift ~25 Myr after continental breakup. It may, however, be more appropriate to the western Indian and south-eastern Australian margins, where there is little evidence for a major uplift event post-dating continental breakup (Kalaswad et al., 1993; Stephenson & Lambeck, 1985).

9.3.2 Magnitude of the driving uplift

The driving uplift for the model is the thermal uplift. The flexural isostatic response to erosion emphasises the original uplift, although it is not a driving uplift mechanism – material needs to exist to be eroded in the first place. The magnitude of

Location	Mean Elevation (metres)	Wavelength (kilometres)	Magnitude of Uplift (metres)	Magnitude of Erosion (metres)	Distance of Maximum Elevation from OCT (kilometres)
Norway	1200	200 (North) 400 (South)	2000 – 3000	1500 - 2500	325 (North) 500 (South)
East Greenland	2000		2500	4000	350
West Greenland			2000 – 3000		400
North-East Brazil	1000		600	3000	475
South-East Brazil	1000	600		2500 – 4000	500
South-West Africa	1000		1200	3000 – 5000	375
South-East Africa	1000			4500	250
West India	900	400	1000	2000 – 4000	550
South-East Australia	1000	300	1500	1500 - 2500	200

Table 9.1: Summary of key observations of the uplifted rifted margins discussed in Chapter 2

Model	Maximum Topography (metres)	Wavelength Topography (kilometres)	Magnitude Thermal Uplift (metres)	Wavelength Thermal Uplift (kilometres)	Magnitude of Erosion (metres)	Distance of Maximum Elevation from OCT (kilometres)
Model 1 No Erosion	1200	300	175	400		165
Model 1 Constant K	1000	230	175	400	5050	185
Model 1 Lateral K	1180	200	175	400	4860	200
Model 1 Height K	920	300	175	400	1830	185
Model 1 Marine K	920	300	175	400	1560	185
Model 1 Sea-level	640	250	175	400	4150	205
Model 2 Sea-level	500	230	160	325	3130	210
Model 3 Sea-level	1020	250	135	500	7630	200

Table 9.2: Key values predicted by the models presented in Chapter 8 after 55 Myr sea-floor spreading

Model	Maximum Topography (metres)	Wavelength Topography (kilometres)	Magnitude Thermal Uplift (metres)	Wavelength Thermal Uplift (kilometres)	Magnitude of Erosion (metres)	Distance of Maximum Elevation from OCT (kilometres)
Model 1 No Erosion	1200	300	230	350		180
Model 1 Constant K	840	200	230	350	8700	220
Model 1 Lateral K	1180	200	230	350	7970	220
Model 1 Height K	840	300	230	350	2630	210
Model 1 Marine K	840	300	230	350	2680	215
Model 1 Sea-level	680	500	230	350	6100	245
Model 2 Sea-level	590	500	215	325	4960	255
Model 3 Sea-level	1125	600	210	500	11300	235

Table 9.3: Key values predicted by the models presented in Chapter 8 after 130 Myr sea-floor spreading

the thermal uplift is dependent on the parameters discussed in section 9.2, and can be up to a few hundred metres. The parameters used for the schematic model in Chapter 8 predict a total driving uplift of ~ 300 m if the geotherm is allowed to completely re-equilibrate. The tectonic uplift of Norway is thought to be 1 – 1.5 km (Riis, 1996; Lidmar-Bergstrom et al., 2000). Similar magnitudes of tectonic uplift have been proposed for East Greenland (Mathiesen et al., 2000) and West Greenland (Bonow et al., 2006). Approximately 600 m of uplift has been reported for NE Brazil (Magnavita et al., 1994). The model is therefore unable to match the full magnitude of the driving uplift.

The model has more success in matching the observed topography and its wavelength. The predicted topography is higher than the magnitude of the thermal uplift because the syn-rift uplift due the isostatic response to crustal thinning is maintained due to the isostatic response to erosion. The schematic model predicts elevations of 1 km or under. This is in reasonable agreement with the mean elevation of Norway (1200 m; Lidmar-Bergström & Näslund, 2002), India (600 - 900 m; Tiwari et al., 2006) and South-East Australia (600 - 1000 m; van der Beek & Braun, 1999). There is also plenty of scope for the model variables to be tuned to give an even better agreement between the observed and predicted topography.

9.3.3 Magnitude of denudation

The greatest magnitude of denudation is predicted at the coast, with much less predicted for the elevated hinterland; this observation is matched by the model. Southern Norway is thought to have experienced 1.5 – 2.5 km denudation (Rohrman et al., 1995), and for East Greenland values of 4 km at the coast and 2 km on the hinterland are given (Hansen & Brooks, 2002). For south-western Africa, values of 3 – 5 km at the coast and 1 km in the hinterland have been estimated (van der Wateren & Dunai, 2001). Up to 2 - 4 km of denudation has been reported for the coastal plain of West India (Campanile et al., 2008), and less than 1 km of denudation on the elevated plateau (Gunnell et al., 2003). The magnitude of denudation predicted by the model depends on the magnitude of the diffusion coefficient and how it varies along the profile. Whilst the amount of denudation predicted in the schematic models of Chapter 8 generally exceeds the observed amount of denudation, this can easily be rectified by using a lower diffusion coefficient.

9.3.4 Escarpment formation

AFT studies suggest that the escarpment separating the coastal plain from the elevated plateau forms relatively quickly after continental breakup, and then retreats rapidly to its present-day position (Braun & van der Beek, 2004; Bierman & Caffee, 2001; Campanile et al., 2008). For the model presented in this thesis, an escarpment develops contemporaneous with the syn-rift uplift, and if the diffusion coefficient for erosion is sufficiently large, it migrates 50 – 100 km inland from its initiation position at breakup. This lateral migration is constant through time, and so does not match the observations or rapid scarp retreat, although river incision is not considered in the model which is likely to have a considerable effect on the initial development of the escarpment.

9.3.5 Distance between the OCT and location of maximum elevation

The distances from the OCT to the location of maximum elevation at the margins predicted by the gravity inversion (Figure 2.27; Chapter 2) range from 200 – 550 km. No obvious pattern between the margins was observed. However, this information would be useful as a constraint if the model was applied to a particular margin. The wavelength of the observed uplift is several hundred kilometres, e.g. for south-east Australia it is approximately 300 km (Wellman, 1979). The schematic model predicts a wavelength of the uplift of a few hundred kilometres and a distance between the OCT and maximum elevation of ~ 200 km. These values are heavily dependent on the elastic thickness, and to a lesser extent on the amount of pure shear included in the model. Again, the model input parameters can be adapted to give a better agreement to the observations for a particular location.

9.4 Suggestions for further model development

There are several adaptations that could be made to the model which would give a better determination of the geotherm perturbation and topographic evolution at a rifted margin. It was shown in Chapters 5 and 8 that the initial thermal structure of the lithosphere is very important, therefore the model would benefit from the inclusion of radiogenic heat productivity in the upper crust and varying conductivity

in the lithosphere; this would provide a more realistic continental geotherm. The magnitude of the geotherm perturbation was limited for some models, for example the models incorporating a wedge angle, due to using a fixed-grid finite difference approximation, with a constant basal temperature at a fixed depth. This could be overcome either by applying a moving boundary condition, like that used by Manglik et al. (1995), or by using finite elements. The use of the finite element method would also allow for temperature and stress-dependent rheology. Furthermore, the use of stress-dependent rheology would enable compressive stress to be considered in the model. The tectonic model could also be further improved by considering asymmetry in the breakup process, which is observed at conjugate margins (Ranero & Pérez-Gussinyé, 2010).

The elastic thickness provides a strong control on the wavelength of the predicted thermal uplift and topography. The model presented here assumes a constant elastic thickness through time and along the profile. However, elastic thickness is likely to vary in both time and space (Watts, 2001), and so this should be incorporated into the model. If the model is to be applied to a particular margin, then a realistic crustal configuration should be used. Also, several improvements could be made to the surface process part of the model, for example accounting for river incision and including a drainage divide which is thought to exert a fundamental control on the location of the escarpment (Kooi & Beaumont, 1994). Sediment blanketing at the margin should also be explored, since that would keep the geotherm in that region elevated for longer, and so would affect the timing and the magnitude of the predicted thermal uplift.

This thesis has focussed on post-breakup uplift at magma-rich rifted margins, where Leroy et al. (2008) have observed that the mean topography is two – three times that of magma-poor rifted margins. The thermal uplift in the model is a result of buoyancy-assisted upwelling both prior to continental breakup and during the first few million years of sea-floor spreading. This could be an explanation for the observed difference in mean topography at the different margin types, as the magnitude of buoyancy-assisted upwelling at a magma-poor margin would be much less than that at a magma-rich margin. However, whilst there may be little surface expression of hinterland uplift at magma-poor rifted margins, they may still have experienced exhumation. This has not been considered at all for this thesis, but it would be an interesting study and help to further establish the differences in the

mode of continental lithosphere thinning at magma-poor and magma-rich rifted margins.

It is hypothesised that several mechanisms act in combination to produce the observed post-breakup hinterland uplift. Some of these mechanisms could be incorporated into the model to test what effect, if any, they might have. Magmatic underplating (Cox, 1993; Brodie & White, 1994) would be one example as that is based on isostasy, which is already included in the model. The uncertainties surrounding the amount and scale of the underplating (White et al., 2008; Morais Neto et al., 2008) would need to be acknowledged through rigorous sensitivity testing. Transient mechanisms involving thermal perturbation could be included by increasing the asthenosphere temperature for a period of time and/or assuming buoyant upwelling. Whilst this would not lead to permant uplift, it would lead to more erosion, and therefore prolong the elevated topography due to the flexural response to the erosional unloading (Widdowson & Cox, 1996).

There are several ways the model could be tested to see if it is applicable to any location. Firstly, the final crustal thickness predicted by the geodynamic model could be calibrated against seismic data. It would also be possible to calibrate the model against the observed gravity anomaly and bathymetry. The magnitude of erosion could be calibrated by comparing that predicted by the model to the volume of sediment deposited offshore. However, this volume could easily be underestimated if not all of the eroded material remained in the basin. Likewise, it could be overestimated if there was more than one source of material deposited in the basin (Jones et al., 2002). The thermal history predicted by the model could be compared to AFT data, although this should also be used with caution as the thermal history determined from AFT data is based on a model itself (Redfield, 2010).

9.5 Summary

A geodynamic model for continental lithosphere thinning and sea-floor spreading initiation coupled with erosion and flexural isostasy has been presented in this thesis. The literature review (Chapter 2) shows that post-breakup uplift has been experienced by many, mainly volcanic, rifted margins. There is often little consensus on the observations of timing and magnitude of the uplift, making it difficult to

validate and test the proposed mechanisms. It is likely, however, that post-breakup uplift is due to the superposition of several mechanisms, including those which cause driving uplift and those, e.g. the flexural isostatic response to erosion, which are a response to the original uplift and merely amplify it, although this effect can be considerable.

Results show that buoyancy-driven upwelling during continental breakup and early sea-floor spreading can generate significant thermal uplift of the continental hinterland, of the order of a few hundred metres. The elevated topography generated at breakup is maintained over millions of years, during which time the continental hinterland is observed to rise gradually. The main parameters controlling the magnitude of the predicted thermal uplift are the magnitude of the buoyancy-driven upwelling (Chapter 4), the thermal state of the lithosphere (Chapter 5) and the elastic thickness (Chapter 6).

Erosion has been shown to play a fundamental control in shaping the topography, and is dependent on the magnitude of the diffusion coefficient and how it varies across the profile. This suggests that climate and lithology are important factors in the onshore evolution of a rifted margin. If the diffusion coefficient varies with height, then a broad plateau may be formed (Chapter 8). Whilst the mechanism for generating post-breakup hinterland uplift presented here cannot successfully match the observations of timing and magnitude of uplift events, it can match the shape and the wavelength of the uplift, and predicts elevated topography even after 130 Myr sea-floor spreading. Therefore, this mechanism may at least be a contributing factor in the post-breakup uplift of rifted margin continental hinterlands. Further model development would greatly benefit from improved data, and a consensus on the uplift history of a margin, in order to assess the validity of the model.

9.6 References

Bierman, P. R. and M. Caffee (2001), Slow rates of rock surface erosion and sediment production across the Namib Desert and escarpment, southern Africa, *American Journal of Science*, vol. 301, no. 4-5, p. 326-358.

Bonow, J. M., P. Japsen, K. Lidmar-Bergstrom, J. A. Chalmers and A. K. Pedersen (2006), Cenozoic uplift of Nuussuaq and Disko, West Greenland - elevated

erosion surfaces as uplift markers of a passive margin, *Geomorphology*, vol. 80, no. 3-4, p. 325-337.

Braun, J. and P. van der Beek (2004), Evolution of passive margin escarpments: What can we learn from low-temperature thermochronology?, *Journal of Geophysical Research-Earth Surface*, vol. 109, no. F4, p. F4009.

Brodie, J. and N. White (1994), Sedimentary basin inversion caused by igneous underplating: Northwest European continental shelf, *Geology*, vol. 22, p. 147-150.

Campanile, D., C. G. Nambiar, P. Bishop, M. Widdowson and R. Brown (2008), Sedimentation record in the Konkan-Kerala Bsin: Implications for the evolution of the Western Ghats and the Western India passive margin, *Basin Research*, vol. 20, p. 3-22.

Cox, K. G. (1993), Continental Magmatic Underplating, *Philosophical Transactions of the Royal Society A - Mathematical, Physical & Engineering Sciences*, vol. 342, p. 155-166.

Gunnell, Y., K. Gallagher, A. Carter, M. Widdowson and A. J. Hurford (2003), Denudation history of the continental margin of western peninsular India since the early Mesozoic - reconciling apatite fission-track data with geomorphology, *Earth and Planetary Science Letters*, vol. 215, no. 1-2, p. 187-201.

Hansen, K. and C. K. Brooks (2002), The evolution of the East Greenland margin as revealed from fission-track studies, *Tectonophysics*, vol. 349, no. 1-4, p. 93-111.

Japsen, P., J. M. Bonow, P. F. Green, J. A. Chalmers and K. Lidmar-Bergstrom (2006), Elevated, passive continental margins: Long-term highs or neogene uplifts? New evidence from West Greenland, *Earth and Planetary Science Letters*, vol. 248, no. 1-2, p. 330-339.

Jones, S. M., N. White, B. J. Clarke, E. Rowley and K. Gallagher (2002) Present and Past Influence of the Iceland Plume on Sedimentation, in Doré, A. G., J. A. Cartwright, M. S. Stoker, J. P. Turner and N. White (eds), *Exhumation of the North Atlantic Margin: Timing, Mechanisms and Implications for Petroleum Exploration*, Geological Society London Special Publication, vol. 196, p. 13-27.

Kalaswad, S., M. K. Roden, D. S. Miller and M. Morisawa (1993), Evolution of the Continental-Margin of Western India - New Evidence from Apatite Fission-Track Dating, *Journal of Geology*, vol. 101, no. 5, p. 667-673.

Kooi, H. and C. Beaumont (1994), Escarpment Evolution on High-Elevation Rifted Margins - Insights Derived from a Surface Processes Model That Combines Diffusion, Advection, and Reaction, *Journal of Geophysical Research-Solid Earth*, vol. 99, no. B6, p. 12191-12209.

Leroy, M., F. Gueydan and O. Dauteuil (2008), Uplift and strength evolution of passive margins inferred from 2-D conductive modelling, *Geophysical Journal International*, vol. 172, p. 464-476.

Lidmar-Bergstrom, K., C. D. Ollier and J. R. Sulebak (2000), Landforms and uplift history of southern Norway, *Global and Planetary Change*, vol. 24, no. 3-4, p. 211-231.

Lidmar-Bergström, K. and J. O. Näslund (2002) Landforms and uplift in Scandinavia, in Doré, A. G., J. A. Cartwright, M. S. Stoker, J. P. Turner and N. White (eds), *Exhumation of the North Atlantic Margin: Timing, Mechanisms and Implications for Petroleum Exploration*, Geological Society, London, Special Publications, vol. 196, p. 103-116.

Magnavita, L. P., I. Davison and N. J. Kusznir (1994), Rifting, Erosion, and Uplift History of the Reconcavo-Tucano-Jatoba Rift, Northeast Brazil, *Tectonics*, vol. 13, no. 2, p. 367-388.

Manglik, A., A. O. Gliko and R. N. Singh (1995), Movement of the lithosphere-asthenosphere interface in response to erosion of thickened continental lithosphere: a moving boundary approach, *Geophysical Journal International*, vol. 122, p. 479-488.

Mathiesen, A., T. Bidstrup and F. G. Christiansen (2000), Denudation and uplift history of the Jameson Land basin, East Greenland - constrained from maturity and apatite fission track data, *Global and Planetary Change*, vol. 24, no. 3-4, p. 275-301.

Molnar, P. and P. England (1990), Late Cenozoic Uplift of Mountain-Ranges and Global Climate Change - Chicken or Egg, *Nature*, vol. 346, no. 6279, p. 29-34.

Morais Neto, J. M., K. A. Hegarty, G. D. Karner and F. F. Alkmim (2008), Timing and mechanisms for the generation and modification of the anomalous topography of the Borborema Province, northeastern Brazil, *Marine and Petroleum Geology*, p. 1-17.

Ranero, C. R. and M. Pérez-Gussinyé (2010), Sequential faulting explains the asymmetry and extension discrepancy of conjugate margins, *Nature*, vol. 468, no. 7321, p. 294-U180.

Redfield, T. F. (2010), On apatite fission track dating and the Tertiary evolution of West Greenland topography, *Journal of the Geological Society, London*, vol. 167, p. 261-271.

Riis, F. (1996), Quantification of Cenozoic vertical movements of Scandinavia by correlation of morphological surfaces with offshore data, *Global and Planetary Change*, vol. 12, no. 1-4, p. 331-357.

Rohrman, M., P. van der Beek, P. Andriessen and S. Cloetingh (1995), Meso-Cenozoic Morphotectonic Evolution of Southern Norway - Neogene Domal Uplift Inferred from Apatite Fission-Track Thermochronology, *Tectonics*, vol. 14, no. 3, p. 704-718.

Stephenson, R. and K. Lambeck (1985), Erosion-Isostatic Rebound Models for Uplift - an Application to Southeastern Australia, *Geophysical Journal of the Royal Astronomical Society*, vol. 82, no. 1, p. 31-55.

Tiwari, P. K., G. Surve and G. Mohan (2006), Crustal constraints on the uplift mechanism of the Western Ghats of India, *Geophysical Journal International*, vol. 167, no. 3, p. 1309-1316.

van der Beek, P. and J. Braun (1999), Controls on post-mid-Cretaceous landscape evolution in the southeastern highlands of Australia: Insights from numerical surface process models, *Journal of Geophysical Research-Solid Earth*, vol. 104, no. B3, p. 4945-4966.

van der Wateren, F. M. and T. J. Dunai (2001), Late Neogene passive margin denudation history - cosmogenic isotope measurements from the central Namib desert, *Global and Planetary Change*, vol. 30, no. 3-4, p. 271-307.

Watts, A. B. (2001) *Isostasy and Flexure of the Lithosphere*, Cambridge University Press.

Wellman, P. (1979), On the Cainozoic uplift of the southeastern Australian highlands, *Australian Journal of Earth Sciences*, vol. 26, no. 1, p. 1-9.

White, R. S., L. K. Smith, A. W. Roberts, P. A. F. Christie, N. J. Kusznir and i. Team (2008), Lower-crustal intrusion on the North Atlantic continental margin, *Nature*, vol. 452, no. 7186, p. 460-U6.

Widdowson, M. and K. G. Cox (1996), Uplift and erosional history of the Deccan Traps, India: Evidence from laterites and drainage patterns of the Western Ghats and Konkan Coast, *Earth and Planetary Science Letters*, vol. 137, no. 1-4, p. 57-69.